AL.2.1994-93
c.2

AOSTRA TECHNICAL PUBLICATION SERIES #12

ELECTROKINETIC TRANSPORT PHENOMENA

JACOB H. MASLIYAH

National Library
of Canada

Bibliothèque nationale
du Canada

CANADIANA

MAY 25 1994

AOSTRA TECHNICAL PUBLICATION SERIES #12

ELECTROKINETIC TRANSPORT PHENOMENA

JACOB H. MASLIYAH
DEPARTMENT OF CHEMICAL ENGINEERING
UNIVERSITY OF ALBERTA

Alberta
OIL SANDS TECHNOLOGY
AND RESEARCH AUTHORITY

Digitized by the Internet Archive
in 2015

https://archive.org/details/electrokinetictr00masl

OTHER PUBLICATIONS IN THE AOSTRA TECHNICAL PUBLICATION SERIES

1. Syncrude Analytical Methods For Oil Sand and Bitumen Processing
2. The Thermodynamic and Transport Properties of Bitumens and Heavy Oils
3. Aquathermolysis: A Synopsis of Work on the Chemical Reaction Between Water (Steam) and Heavy Oil Sands During Simulated Steam Stimulation
4. Oil Sands Composition and Behaviour Research
5. A Review of Analytical Methods For Bitumens and Heavy Oils
6. AOSTRA Technical Handbook on Oil Sands, Bitumens and Heavy Oils
7. Resource Characterization of the McMurray/Wabiskaw Deposit in the Athabasca Central Region of Northeastern Alberta
8. Resource Characterization of the McMurray/Wabiskaw Deposit in the Athabasca South Region of Northeastern Alberta
9. Resource Characterization of the McMurray/Wabiskaw Deposit in the Athabasca West Region of Northeastern Alberta
10. Resource Characterization of the McMurray/Wabiskaw Deposit in the Athabasca Oil Sands Area: A synthesis *
11. Syncrude Analytical Methods Manual For Bitumen Upgrading
12. Electrokinetic Transport Phenomena
13. AOSTRA Mini-Frac Manual
14. The Alberta Oil Sands: Industrial Procedures For Extraction, and Some Recent Fundamental Research*
15. The Chemistry of Alberta's Oil Sands Bitumens and Heavy Oils*

* To be published at a future date.

ELECTROKINETIC TRANSPORT PHENOMENA

Copyright 1994 by AOSTRA. All rights reserved. Printed in Canada. No part of this publication may be reproduced, stored in a retrieval system, or transmitted, in any form or by any means, electronic, mechanical, photocopying, recording, or otherwise, without the prior permission of the publisher.

ISBN 0-7732-1381-3

PUBLISHED BY

ALBERTA OIL SANDS TECHNOLOGY AND RESEARCH AUTHORITY
500 HIGHFIELD PLACE
10010 – 106 STREET
EDMONTON, ALBERTA, CANADA
T5J 3L8

PUBLISHER'S NOTE

AOSTRA TECHNICAL PUBLICATION SERIES #12

AOSTRA is pleased to publish this twelfth book in a series of special publications by industry and academic authors. Like its predecessors, this publication is designed to make available, research results, analytical procedures, and engineering data on the properties and behaviour of Alberta petroleum resources that may otherwise not be available to the public.

Richard Luhning

Richard W. Luhning
Vice Chairman and Executive Director
Alberta Oil Sands Technology and Research Authority

The Alberta Oil Sands Technology and Research Authority (AOSTRA) makes no warranty, express or implied, nor assumes any legal liability or responsibility for the accuracy, completeness, or usefulness of any information, apparatus, product, or process disclosed in this publication, or represents that its use would not infringe on privately owned rights. Reference herein to any specific commercial product, process, or service by trade name, trademark, manufacturer, or otherwise, does not necessarily constitute or imply its endorsement, recommendation, or favoring by AOSTRA. The views and opinions of authors expressed herein do not necessarily reflect those of AOSTRA.

In memory of my parents Heskel Haim and Naima Masliyah

To my family Odette, Tamara, Ruth, and Daniel

and to my mentor and friend Dr. Norman Epstein

PREFACE

Electrokinetic transport phenomena have many applications in the industrial sphere and in biological systems. Due to the presence of charge on surfaces in contact with electrolyte solutions, colloidal particles migrate in an electric field, liquids can be made to flow in narrow capillaries under an electric potential gradient, colloidal suspensions can exhibit markedly different rheological behaviour in the presence of electrolytes, and colloidal particle deposition and coagulation can be controlled by altering the relative magnitudes of the electric repulsive and London–van der Waals attractive forces.

Although the subjects of fluid mechanics and heat and mass transfer are taught quite extensively in North American universities, the subject of electrokinetic transport has received much less attention. I was first introduced to electrokinetics through the visits of Dr. Sam Levine to Edmonton, and became seriously involved as I recognized its importance to the recovery of bitumen from Alberta's vast oil sands reserves. This book is an outgrowth of graduate lecture notes on electrokinetics offered at the Chemical Engineering Department, University of Alberta. In recent years several excellent texts have been published on the general subject of colloids, including *Physicochemical Hydrodynamics* by R. Probstein (Butterworths); *Colloidal Dispersions* by W. Russel, D. Saville and W. Schowalter, Cambridge University Press; and *Colloidal Hydrodynamics* by T. van de Ven, Academic Press. Interestingly, all the three texts were published in 1989. I have depended heavily on these texts in organizing the present book.

In this book, I attempted to bring together the salient features of electrokinetic transport phenomena in such a manner that the book can serve as a stepping stone for further learning and study. By and large, I tried to make the book self-contained, useful to both senior undergraduate and graduate students, as well as engineers involved in the area of transport phenomena.

I would like to thank the University of Alberta for giving me a McCalla Research Professorship which enabled me to initiate the writing of the book. The generous use of Alberta Research Council (ARC) facilities helped me very much in retrieving the necessary scientific papers and made my job much easier. To this end many thanks are due to Dr. Eddy Isaacs of ARC for the many discussions and his encouragement. I would also like to thank my many friends and colleagues at Syncrude Canada Ltd. who have been an inspiration to me and who kept me reminded of the many applications of electrokinetic transport phenomena in the oil sands industry.

I owe much appreciation to Ms. Rachel Recto and Ms. Diane Teppan who put the time and dedication into typesetting the book through its many versions and to Dr. Janis Watkin and Mr. Conrad Gietz who corrected my awkward sentence structure. My thanks are extended to Dr. Tadeusz Dabros for his many helpful suggestions and for checking the text.

Continued financial support from the Natural Sciences and Engineering Research Council of Canada has helped me greatly in pursuing my research interests and in developing this book.

Finally, I would like to thank the Alberta Oil Sands Technology and Research Authority for agreeing to publish this book and for making it affordable to the readers.

Jacob H. Masliyah
Edmonton, Alberta, Canada
1994

TABLE OF CONTENTS

CHAPTER 1 UNITS AND PHYSICAL CONSTANTS

1.1 BASIC UNITS 1
1.2 PHYSICAL CONSTANTS 2
1.3 FREQUENTLY USED FUNCTIONS 2
1.4 VECTOR OPERATORS 3
1.5 REFERENCES 4

CHAPTER 2 DEFINITION OF THE COLLOIDAL STATE AND IMPLICATIONS

2.1 COLLOIDAL PHENOMENA 5
2.2 STABILIZATION OF COLLOIDS 12
2.3 PREPARATION OF COLLOIDAL SYSTEMS 14
2.3.1 Dispersion Methods 14
2.3.2 Condensation Methods 15
2.4 PURIFICATION OF SOLS 17
2.5 NOMENCLATURE 19
2.6 REFERENCES 20

CHAPTER 3 ELECTROSTATICS

3.1 BASIC ELECTROSTATICS IN VACUUM 21
3.2 ELECTRICAL CLASSIFICATION OF MATERIALS 28
3.3 MAXWELL'S EQUATIONS IN A DIELECTRIC 29
3.4 BOLTZMANN'S PROBABILITY LAW 33
3.5 ORIGIN OF INTERFACIAL CHARGE 34
3.6 POTENTIAL DISTRIBUTION NEAR AN INTERFACE 35
3.6.1 Mathematical Analysis of Double Layer for a Flat Surface: Gouy–Chapman Model 37
3.6.2 Diffuse Electric Double Layer Around a Sphere 45
3.6.3 Surface Charge Density and Potential 46
3.7 SURFACE POTENTIAL MODELS 48
3.7.1 Model I 48
3.7.2 Model II 49
3.8 FORCE BETWEEN TWO CHARGED BODIES 52
3.9 DERJAGUIN APPROXIMATION 57
3.10 ELECTROSTATIC POTENTIAL ENERGY 60
3.11 ZETA POTENTIAL 61
3.12 SUMMARY OF GOUY–CHAPMAN MODEL 64
3.13 FORMS OF VARIOUS NOTATIONS 65
3.14 NOMENCLATURE 66
3.15 REFERENCES 68

CHAPTER 4 TRANSPORT EQUATIONS IN ELECTROLYTIC SOLUTIONS

4.1 SINGLE-COMPONENT SYSTEM: NO ELECTRIC FORCE 71
4.2 MULTICOMPONENT SYSTEM: ELECTROLYTIC SOLUTIONS 73
4.2.1 Momentum Equations 73
4.2.2 Convection-Diffusion-Migration Equation 74
4.2.3 Boltzmann Distribution 79
4.2.4 Conservation of Ionic Mass 81
4.2.5 Current Density 81
4.2.6 Conservation of Charge 88
4.2.7 Example: Evaluation of Current Density 88
4.3 SUMMARY OF GOVERNING EQUATIONS 89
4.4 NOMENCLATURE 95
4.5 REFERENCES 97

CHAPTER 5 ELECTROKINETIC PHENOMENA

5.1 ELECTROOSMOSIS 99
5.2 ELECTROPHORESIS 100
5.3 STREAMING POTENTIAL 100
5.4 SEDIMENTATION POTENTIAL 101
5.5 REFERENCES 101

CHAPTER 6 ELECTROOSMOSIS AND STREAMING POTENTIAL PHENOMENA

6.1 ELECTROOSMOSIS IN A CIRCULAR CHARGED CAPILLARY 103
6.2 CURRENT FLOW IN ELECTROOSMOSIS 114
6.3 STREAMING POTENTIAL ANALYSIS 117
6.4 ELECTROVISCOUS EFFECT 117
6.5 HIGH SURFACE POTENTIAL 119
6.6 NOMENCLATURE 121
6.7 REFERENCES 122

CHAPTER 7 ELECTROPHORESIS

7.1 ELECTROPHORESIS 125
7.2 LARGE DEBYE LENGTH, $\kappa a \ll 1$ 125
7.3 SMALL DEBYE LENGTH, $\kappa a \gg 1$ 129
7.4 IMPROVED SOLUTIONS: ARBITRARY DEBYE LENGTH 132
7.4.1 Henry's Solution 133
7.4.2 Effect of Particle Conductivity and Shape 140
7.4.3 Alternate Forms of the Electrophoresis Velocities 142

7.5 NUMERICAL SOLUTIONS: HIGH SURFACE POTENTIAL 145
7.6 ELECTRIC FORCE ON A CHARGED PARTICLE IN AN ELECTRIC FIELD 148
7.7 EFFECT OF PARTICLE CONCENTRATION ON THE ELECTROPHORETIC MOBILITIES: SPHERICAL PARTICLES 150
7.8 EFFECT OF PARTICLE CONCENTRATION ON THE ELECTROPHORETIC MOBILITIES: CIRCULAR CYLINDERS NORMAL TO THE ELECTRICAL FIELD 156
7.9 NOMENCLATURE 159
7.10 REFERENCES 161

CHAPTER 8 SEDIMENTATION POTENTIAL

8.1 SEDIMENTATION POTENTIAL 165
8.2 SEDIMENTATION POTENTIAL FOR A MULTIPARTICLE SYSTEM (A SEDIMENTING SUSPENSION): EXTENSION 168
8.3 NOMENCLATURE 170
8.4 REFERENCES 171

CHAPTER 9 DISPERSION FORCES

9.1 DISPERSION FORCES BETWEEN BODIES IN VACUUM 173
9.2 EFFECTS OF INTERVENING MEDIUM 180
9.3 POTENTIAL ENERGY CURVES AND DLVO THEORY 182
9.4 SCHULZE-HARDY RULE 186
9.5 VERIFICATION OF THE DLVO THEORY 189
9.6 NOMENCLATURE 192
9.7 REFERENCES 193

CHAPTER 10 COAGULATION OF PARTICLES

10.1 GENERAL 197
10.2 PARTICLE–PARTICLE FLOCCULATION 198
10.2.1 Brownian Motion 198
10.2.2 Collision Frequency 202
10.2.3 Brownian Coagulation: Without a Field Force, the Smoluchowski Solution 203
10.2.4 Brownian Coagulation: Effect of a Field Force 209
10.2.5 Coagulation Due to Shear in the Absence of Brownian Motion: The Smoluchowski Solution 219
10.2.6 Coagulation Due to Shear in the Absence of Brownian Motion: With Hydrodynamic and Field Forces 223
10.3 NOMENCLATURE 236
10.4 REFERENCES 239

CHAPTER 11 DEPOSITION OF COLLOIDAL PARTICLES

11.1 GENERAL 243
11.2 CLASSICAL DEPOSITION MECHANISMS 245
11.2.1 Brownian Diffusion: Classical Convection-Diffusion Transport 245
11.2.2 Interception Deposition 245
11.2.3 Inertial Deposition 249
11.3 EULERIAN APPROACH 252
11.3.1 Deposition Due to Brownian Diffusion Without External Forces: Spherical Collector 253
11.3.2 Deposition Due to Brownian Diffusion With External Forces: Stagnation Flow 257
11.4 LAGRANGIAN APPROACH 271
11.4.1 Particle Collisions on a Spherical Collector: With the Presence of External Forces 271
11.5 RELATIONSHIP BETWEEN DEPOSITION EFFICIENCY AND SHERWOOD NUMBER 285
11.6 EXPERIMENTAL VERIFICATIONS 286
11.7 SUMMARY OF DIMENSIONLESS GROUPS 295
11.7.1 Dimensionless Groups in the Flux Equation 295
11.7.2 Dimensionless Groups in the Trajectory Equation 297
11.8 NOMENCLATURE 298
11.9 REFERENCES 301

CHAPTER 12 ELECTROKINETIC APPLICATIONS

12.1 GENERAL 305
12.2 ELECTROKINETIC SALT REJECTION IN POROUS MEDIA 305
12.3 ELECTROOSMOTIC CONTROL OF HAZARDOUS WASTES 309
12.4 IONTOPHORETIC DELIVERY OF DRUGS 312
12.5 FLOTATION OF OIL DROPLETS AND FINE PARTICLES 314
12.6 RHEOLOGY OF COLLOIDAL SYSTEMS 316
12.6.1 Historical Background 317
12.6.2 Hard Sphere Model 319
12.6.3 Electroviscous Effects 321
12.7 BITUMEN EXTRACTION FROM OIL SANDS 327
12.7.1 Initiation of Bitumen Displacement from Sand Grains 328
12.7.2 Surface Ionization Models 333
12.7.3 Bitumen Recovery 337
12.8 NOMENCLATURE 339
12.9 REFERENCES 342

AUTHOR INDEX 347

SUBJECT INDEX 355

UNITS AND PHYSICAL CONSTANTS 1

1.1 BASIC UNITS

The International Metric system (SI from the French, Système Internationale d'Unités) is given below.

Quantity	Name	Symbol
Mass	kilogram	kg
Length	metre	m
Time	second	s
Temperature	kelvin	K
Amount of substance	mole	mol
Electric current	ampere	A
Luminous intensity	candela	cd

The units derived from the above set of units are given below.

Quantity	Name	Symbol	Definition
Force	newton	N	$\mathrm{kg\ m\ s^{-2}}$
Pressure	pascal	Pa	$\mathrm{N\ m^{-2} = kg\ m^{-1}\ s^{-2}}$
Energy	joule	J	$\mathrm{N\ m = kg\ m^{2}\ s^{-2}}$
Power	watt	W	$\mathrm{J\ s^{-1} = kg\ m^{2}\ s^{-3}}$
Electric charge	coulomb	C	$\mathrm{A\ s}$
Electric potential difference	volt	V	$\mathrm{J\ C^{-1} = kg\ m^{2}\ s^{-3}\ A^{-1}}$
Electric resistance	ohm	Ω	$\mathrm{V\ A^{-1} = kg\ m^{2}\ s^{-3}\ A^{-2}}$
Electric conductance	siemens	S	$\mathrm{A\ V^{-1} = kg^{-1}\ m^{-2}\ s^{3}\ A^{2}}$
Electric capacitance	farad	F	$\mathrm{C\ V^{-1} = kg^{-1}\ m^{-2}\ s^{4}\ A^{2}}$
Frequency	hertz	Hz	$\mathrm{s^{-1}}$

Adapted from Russel *et al.* (1989) and Probstein (1989)

The commonly used scale factors for the basic units are:

Factor	Prefix	Symbol	Factor	Prefix	Symbol
10^{-1}	deci	d	10	deca	da
10^{-2}	centi	c	10^{2}	hecto	h
10^{-3}	milli	m	10^{3}	kilo	k
10^{-6}	micro	μ	10^{6}	mega	M
10^{-9}	nano	n	10^{9}	giga	G
10^{-12}	pico	p	10^{12}	tera	T

1.2 PHYSICAL CONSTANTS

The commonly used physical constants are:

Quantity	Symbol	Value	SI Units
Avogadro number	N_a	6.022×10^{23}	mol^{-1}
Boltzmann constant	k	1.381×10^{-23}	J K^{-1}
Elementary charge	e	1.602×10^{-19}	C
Faraday constant	F	9.648×10^{4}	C mol^{-1}
Gas constant	R	8.314	$\text{J K}^{-1}\text{ mol}^{-1}$
Permittivity of vacuum	ε_o	8.854×10^{-12}	$\text{C V}^{-1}\text{ m}^{-1}$ or $\text{C}^2/\text{N m}^2$
Planck constant	$2\pi h$	6.626×10^{-34}	J s
Standard acceleration of gravity	g	9.8066	m s^{-2}
Standard atmosphere	p_o	1.013×10^{5}	Pa
Speed of light in vacuum	c	2.9979×10^{8}	m/s
Zero of Celsius scale	T_o	273.15	K
kT/e at 298.16 K		25.69×10^{-3}	V
1 molar solution	M	1	mol/dm^3 or kmol/m^3
1 litre	L	1.0000028×10^{-3}	m^3

Adapted from Hiemenz (1986), Russel *et al.* (1989), and Probstein (1989)

1.3 FREQUENTLY USED FUNCTIONS

$$\exp(x) = 1 + x + \frac{x^2}{2!} + \frac{x^3}{3!} + \dots \qquad -\infty < x < \infty$$

$$ln\,(1 + x) = x - \frac{x^2}{2} + \frac{x^3}{3} - \frac{x^4}{4} + \dots \qquad -1 < x \leq 1$$

$$\sinh(x) = \frac{1}{2}\left[\exp(x) - \exp(-x)\right]$$

$$= x + \frac{x^3}{3!} + \frac{x^5}{5!} + \frac{x^7}{7!} + \dots \qquad -\infty < x < \infty$$

$$\cosh(x) = \frac{1}{2}\left[\exp(x) + \exp(-x)\right]$$

$$= 1 + \frac{x^2}{2!} + \frac{x^4}{4!} + \frac{x^6}{6!} + \dots \qquad -\infty < x < \infty$$

$$\tanh(x) = \sinh(x) / \cosh(x)$$

$$= x - \frac{x^3}{3} + \frac{2x^5}{16} - \frac{17x^7}{315} + \dots \qquad |x| < \frac{\pi}{2}$$

$\cosh^2(x) = 1 + \sinh^2(x)$

$\sinh(x) \cong \cosh(x)$ $\qquad x \rightarrow \infty$

$\tanh(x) \rightarrow 1$ $\qquad x \rightarrow \infty$

1.4 VECTOR OPERATORS

ψ is a scalar and $\vec{u}$ is a vector, Bird *et al.* (1960).

Rectangular (Cartesian) coordinates (x, y, z):

$$\vec{\nabla}\psi = \vec{i}_x \frac{\partial \psi}{\partial x} + \vec{i}_y \frac{\partial \psi}{\partial y} + \vec{i}_z \frac{\partial \psi}{\partial z} \qquad \text{(A)}$$

$$\nabla^2 \psi = \frac{\partial^2 \psi}{\partial x^2} + \frac{\partial^2 \psi}{\partial y^2} + \frac{\partial^2 \psi}{\partial z^2} \qquad \text{(B)}$$

$$\vec{\nabla} \cdot \vec{u} = \frac{\partial u_x}{\partial x} + \frac{\partial u_y}{\partial y} + \frac{\partial u_z}{\partial z} \qquad \text{(C)}$$

Cylindrical coordinates (r, θ, z):

$$\vec{\nabla}\psi = \vec{i}_r \frac{\partial \psi}{\partial r} + \vec{i}_\theta \frac{1}{r} \frac{\partial \psi}{\partial \theta} + \vec{i}_z \frac{\partial \psi}{\partial z} \qquad \text{(A)}$$

$$\nabla^2 \psi = \frac{\partial^2 \psi}{\partial r^2} + \frac{1}{r}\frac{\partial \psi}{\partial r} + \frac{1}{r^2}\frac{\partial^2 \psi}{\partial \theta^2} + \frac{\partial^2 \psi}{\partial z^2} \qquad \text{(B)}$$

$$\vec{\nabla} \cdot \vec{u} = \frac{1}{\mathrm{r}}\frac{\partial}{\partial r}(\mathrm{ru_r}) + \frac{1}{\mathrm{r}}\frac{\partial}{\partial \theta} u_\theta + \frac{\partial}{\partial z} u_z \qquad \text{(C)}$$

Spherical coordinates (r, θ, ϕ):

$$\vec{\nabla}\psi = \vec{i}_r \frac{\partial \psi}{\partial r} + \vec{\mathrm{i}}_\theta \frac{1}{r}\frac{\partial \psi}{\partial \theta} + \vec{i}_\phi \frac{1}{r \sin\theta}\frac{\partial \psi}{\partial \phi} \qquad \text{(D)}$$

$$\nabla^2 \psi = \frac{1}{r^2}\frac{\partial}{\partial r}\left(r^2 \frac{\partial \psi}{\partial r}\right) + \frac{1}{r^2 \sin\theta}\frac{\partial}{\partial \theta}\left(\sin\theta \frac{\partial \psi}{\partial \theta}\right) + \frac{1}{r^2 \sin^2\theta}\frac{\partial^2 \psi}{\partial \phi^2} \qquad \text{(H)}$$

$$\vec{\nabla} \cdot \vec{u} = \frac{1}{r^2}\frac{\partial}{\partial r}\left(r^2 u_r\right) + \frac{1}{r \sin\theta}\frac{\partial}{\partial \theta}\left(u_\theta \sin\theta\right) + \frac{1}{r \sin\theta}\frac{\partial u_\phi}{\partial \phi} \qquad \text{(I)}$$

1.5 REFERENCES

Bird, R.B., Stewart, W.E., and Lightfoot, E.N. (1960), *Transport Phenomena*, John Wiley and Sons, New York.

Hiemenz, P.C. (1986), *Principles of Colloid and Surface Chemistry*, 2nd ed., Marcel Dekker, Inc., New York.

Probstein, R.F. (1989), *Physicochemical Hydrodynamics*, Butterworths, Boston.

Russel, W.B., Saville, D.A., and Schowalter, W.R. (1989), *Colloidal Dispersions*, Cambridge University Press, Cambridge.

DEFINITION OF THE COLLOIDAL STATE AND IMPLICATIONS

2

2.1 COLLOIDAL PHENOMENA

The colloidal phenomenon is concerned with small particles or with systems where the ratio of surface area to volume is very large. In this context, colloidal phenomenon deals with particles having a size range from 10^{-9} m (= 1 nm) to 10^{-5} m (= 10 μm). Some examples of colloidal systems are outlined in Table 2-1 and typical particle sizes for some colloidal systems are given in Table 2-2. It becomes clear from Table 2-1 that colloidal systems consist of a dispersed phase distributed in a dispersion medium or a continuous phase. The interaction between the components of the two phases gives rise to the properties of a colloidal system. By and large, the factors which contribute most to the overall nature of a colloidal system are:

- Particle size and shape
- Surface properties, both chemical and physical
- Continuous phase chemical and physical properties
- Particle–particle interactions
- Particle–continuous phase interactions

The various forces that enter into the interactions are:

- Electric repulsive or attractive force
- Attractive London–van der Waals force
- Brownian force
- Viscous force
- Inertial force
- Gravitational force
- Surface tension

The electric force between two particles can be derived from Coulomb's law and it is of the order $\varepsilon\varepsilon_o\psi_s^2$ where ε is the dielectric constant of the continuous phase and ε_o is the permittivity of the vacuum. For air $\varepsilon \approx 1.0$. The surface potential is given by ψ_s.

Table 2-1. Some typical dispersions

Examples	Class	Nature of the dispersed phase	Nature of the continuous phase
Disperse systems			
Fog, mist, tobacco smoke, aerosol sprays	Liquid aerosol or aerosol of liquid particles[a]	Liquid	Gas
Industrial smokes	Solid aerosol or aerosol of solid particles[a]	Solid	Gas
Milk, butter, mayonnaise, asphalt, pharmaceutical creams	Emulsions	Liquid	Liquid
Inorganic colloids (gold, silver iodide, sulphur, metallic hydroxides, *etc.*), paints[b]	Sols or colloidal suspensions	Solid	Liquid
Clay slurries, toothpaste, muds, polymer lattices	When very concentrated called a paste	Solid	Liquid
Opal, pearl, stained glass, pigmented plastics	Solid suspension or dispersion	Solid	Solid
Froths, foams	Foam[c]	Gas	Liquid
Meerschaum, expanded plastics	Solid foam	Gas	Solid
Microporous oxides, silica gel, porous glass, microporous carbons, zeolites	Xerogels[d]		
Macromolecular colloids			
Jellies, glue	Gels	Macromolecules	Solvent
Association colloids			
Soap/water, detergent/water, dye solutions	–	Micelles	Solvent

continued ...

Table 2-1 continued

Examples	Class	Nature of the dispersed phase	Nature of the continuous phase
Biocolloids			
Blood		Corpuscles	Serum
Bone		Hydroxy-apatite	Collagen
Muscle, cell membranes		Protein structures, thin films of lecithin, *etc.*	
Three-phase colloidal systems (multiple colloids)		Coexisting phases	
Oil-bearing rock	Porous rock	Oil	Water
Capillary condensed vapours	Porous solid	Liquid	Vapour
Frost heaving	Porous rock or soil	Ice	Water
Mineral flotation	Mineral	Water	Air bubbles or oil droplets
Double emulsions	Oil	Aqueous phase	Water

(Everett, 1988)

[a] Preferred nomenclature according to IUPAC recommendations.

[b] Many modern paints are more complex, containing both dispersed pigment and emulsion droplets.

[c] In a foam it is usually the thickness of the film of dispersion medium which is of colloidal dimensions, although the dispersed phase may also be finely divided.

[d] In some cases both phases are continuous, forming interpenetrating networks both of which have colloidal dimensions.

The London–van der Waals forces on the atomic scale yield the force between macroscopic bodies known as the dispersion force which is of the order A/a. Here A is the Hamaker constant which is a function of the properties of both the dispersed and continuous phases. The characteristic length of the particle is given by a.

The thermal energy of the molecules manifests itself as a Brownian force of order kT/a. Here k is Boltzmann's constant and T is the absolute temperature.

The fluid (continuous phase) viscosity gives rise to a viscous force of the order μUa where μ is the continuous phase viscosity and U is the particle velocity through the continuous phase. Due to bulk particles movement, an inertial force comes into play which is of the order ρa^2U^2 where ρ is the continuous medium density.

Table 2-2. Typical particle sizes

µm				
10^2				
			Sand	Pulverized coal
10^1		↑		
			Silt	Red blood cells
10^0	Mist and fog			Paint pigment
			Clay	Lattices
10^{-1}		↓		
				Coiled macromolecules
			Colloidal silica	Carbon black
10^{-2}				
			Colloid gold	Micelles
10^{-3}				

(Russel *et al.*, 1989)

The gravitational body force on a particle is of the order $a^3 g \Delta\rho$ where g is the acceleration due to gravity and $\Delta\rho$ is the density difference between the particle and the continuous phase.

Surface tension arises from the interaction between the two phases represented by the particle and the continuous phase. This force is of the order γa where γ is the surface tension of the particle and the medium.

Table 2-3 gives the order of magnitude values for the relative significance of the forces cited above (Russel *et al.*, 1989). For the particular values chosen, it is clear that the ratio of inertial to viscous forces is not important and that the ratio of the repulsive electric force to the Brownian force is fairly high. This would indicate a stable colloidal system. However, it should be recognized that the electrical and attractive forces between particles are greatly influenced by the separation distance between the particles. Consequently, the analysis cannot be considered as being complete.

Table 2-3 shows that the ratio of the various forces contains the particle dimension which can vary from 10^{-8} to 10^{-5} m and consequently can affect the nature of the interactions. As the surface to volume ratio is of order $1/a$, it becomes clear that for very small particles, the surface to volume ratio for a colloidal particle can be significantly large and a high percentage of the molecules for such a particle lie within or close to the region of inhomogeneity associated with the particle/medium interface. These molecules have

Table 2-3. Magnitudes of the characteristic forces: $T = 300$ K, $a = 1$ μm, $\mu = 10^{-3}$ Pa s, $U = 1 \times 10^{-6}$ m/s, $\rho = 10^3$ kg/m^3, $\Delta\rho/\rho = 10^{-2}$, $g = 10$ m/s^2, $A = 10^{-20}$ J, $\psi_s = 0.05$ V, $\varepsilon = 10^2$, $\gamma = 0.1$ N/m, $\varepsilon_o = 8.85 \times 10^{-12}$ C/Vm, $k = 1.381 \times 10^{-23}$ J/K

electrical force / Brownian force	$\dfrac{\varepsilon\varepsilon_o \psi_s^2}{kT/a}$	$\approx 10^3$
attractive force / Brownian force	$\dfrac{A/a}{kT/a}$	≈ 1
Brownian force / viscous force	$\dfrac{kT/a}{\mu U a}$	≈ 1
gravitational force / viscous force	$\dfrac{a^3 g \Delta\rho}{\mu U a}$	$\approx 10^{-1}$
inertial force / viscous force	$\dfrac{\rho a^2 U^2}{\mu U a}$	$\approx 10^{-6}$
surface tension / gravitational force	$\dfrac{\gamma a}{a^3 g \Delta\rho}$	$\approx 10^9$

(Adapted from Russel *et al.*, 1989)

properties different from those in the bulk phases more distant from the interface. It is no longer possible to describe a colloidal system (dispersed and continuous phases) simply in terms of the sum of contributions from molecules in the bulk phases, calculated as if both phases had the same properties as they would have in the individual bulk state. A significant and a dominating contribution comes from the molecules residing at the interface. This is why surface chemistry plays an important role in colloid science and why colloidal properties begin to become important as the particle decreases in size, say below 10 μm (Everett, 1988).

The following example demonstrates how the ratio of the number of the "surface molecules" to the total molecules increases with the decreasing ratio of the particle size to the molecule size.

Consider a particle in the shape of a cube having a side length of L. Assume that the particle material is made up of molecules having the shape of a cube whose side length is S. The total number of molecules N_t contained in the particle is given by

$$N_t = \left(\frac{L}{S}\right)^3 \tag{2-1}$$

The number of surface particles is given by

$$N_s = 2\left(\frac{L}{S}\right)^2 + 2\left(\frac{L}{S} - 2\right)\left(\frac{L}{S}\right) + 2\left(\frac{L}{S} - 2\right)^2 \qquad \text{for } L/S \geq 2 \tag{2-2}$$

Figure 2-1 shows the subdivision of the particle. The ratio of the number of surface molecules to the total number of molecules is then given by

$$\frac{N_s}{N_t} = 6\left(\frac{S}{L}\right) - 12\left(\frac{S}{L}\right)^2 + 8\left(\frac{S}{L}\right)^3 \tag{2-3}$$

For the case of $S/L << 1$, Eq. (2-3) gives

$$\frac{N_s}{N_t} = 6\left(\frac{S}{L}\right) \tag{2-4}$$

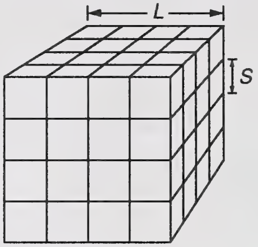

Figure 2-1. Subdivision of a cube by its molecules.

For $L = 10$ nm and $S = 0.3$ nm, Eq. (2-3) gives $N_s/N_t = 0.17$. This indicates that 17% of the molecules reside on the particle surface, *i.e.*, on the interface of the particle and the medium. Such a high percentage would indicate that the properties of the molecules at the interface are important in describing the behaviour of a colloidal particle. Figure 2-2 gives the variation of N_s/N_t with S/L.

Another example is that of a particle straddling an interface. It illustrates the significance of the particle size. Consider a cube of side length L and a density ρ_p straddling the interface of air and water. The water density is ρ_w and the air density is ρ_a. Figure 2-3 shows such a particle.

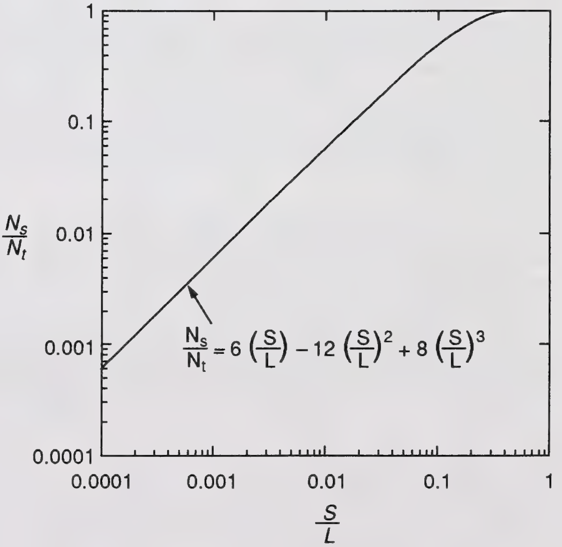

Figure 2-2. Ratio of surface to total molecules as a function of size ratio.

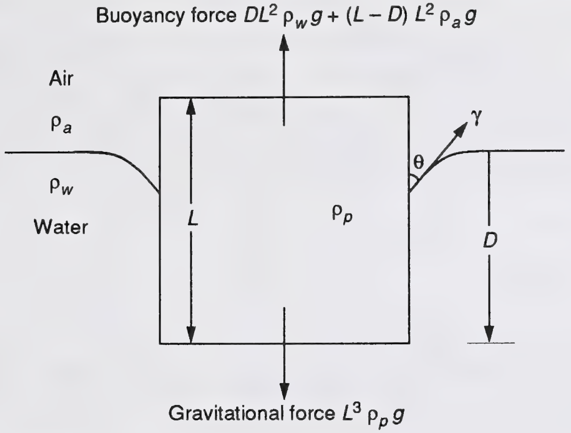
Buoyancy force $DL^2 \rho_w g + (L - D) L^2 \rho_a g$
Air
ρ_a
ρ_w
Water
L
ρ_p
θ
γ
D
Gravitational force $L^3 \rho_p g$

Figure 2-3. Straddling of a particle at an air/water interface.

Assuming a downward force is positive, the forces acting on the cube are given by

Surface tension $-4L\gamma \cos\theta$
Gravitation $L^3\rho_p g$
Buoyancy $-DL^2\rho_w g - (L-D)L^2\rho_a g$

At equilibrium, the sum of all forces is zero, hence

$$L^3\rho_p g - 4L\gamma\cos\theta - DL^2\rho_w g - (L-D)L^2\rho_a g = 0 \tag{2-5}$$

D is the submerged length and θ is the static contact angle which is related to the surface tensions of the particle–air, particle–water and water–air. As $\rho_a/\rho_w \ll 1$, Eq. (2-5) leads to

$$\frac{D}{L} = \frac{\rho_p}{\rho_w} - \frac{4\gamma\cos\theta}{L^2\rho_w g} \tag{2-6}$$

and

$$\frac{D}{L} = \frac{\rho_p}{\rho_w} - \frac{4\cos\theta}{Bo} \tag{2-7}$$

where

$$\frac{\rho_w g L^2}{\gamma} = \frac{\text{gravitational force}}{\text{surface tension}} = Bo$$

Bo is the Bond number. For given physical properties ρ_p, ρ_w, γ and $\cos\theta$, and constant g, the Bond number → 0 as the particle dimension $L \rightarrow 0$.

For $0 < D/L < 1$, the particle floats on the surface. (D/L) value is a balance between (ρ_p/ρ_w) and $4\cos\theta/Bo$. For a large particle, *Bo* is large and Eq. (2-7) leads to $D/L \approx \rho_p/\rho_w > 1$. This is the situation where the particle sinks into the water. This criterion is only related to the density ratio. For the case of a very small particle, *i.e.*, $L \rightarrow 0$ and $Bo \rightarrow 0$, Eq. (2-7) gives

$$\frac{D}{L} \approx -\frac{4\cos\theta}{Bo} \tag{2-8}$$

A negative (D/L) value signifies that a small particle will always float on the water surface irrespective of the density ratio. This is shown in Figure 2-4. Consequently, it is clear that the particle size has a major role in determining its behaviour.

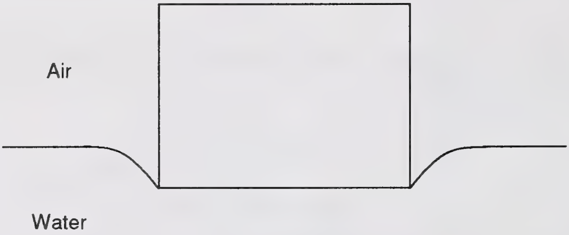

Figure 2-4. A floating particle having a small Bond number.

2.2 STABILIZATION OF COLLOIDS

Colloidal particles can be stabilized against coagulation (or flocculation) by electrostatic repulsion due to the presence of ions near their surfaces or by steric effects arising from polymer chains being attached to the surface of the particles. The properties of a colloidal system, *i.e.*, its rheology, shear stability, and stability to added electrolyte or polymers are much affected by the nature of the stabilizing mechanism (Walbridge, 1987).

Colloidal particles can be stabilized by the electrostatic forces that arise as a result of a charged particle surface and the presence of an associated diffuse atmosphere (double layer) of counterions. Surface charge can arise from different causes, *e.g.*, surface ionization and physically adsorbed ionized surfactant groups. Electrostatic stabilization plays a dominant role in aqueous systems. Electrostatically stabilized particles can be flocculated by the addition of an electrolyte and by shear. Figure 2-5 shows the effect of electrolyte addition on the total interaction potential energy ϕ of a colloidal particle. A positive value of the derivative of the interaction potential energy with respect to the separation distance indicates an attractive force. Figure 2-5 shows that increasing the electrolyte concentration changes the shape of the interaction potential energy leading to a weak repulsive force and a possible attractive force at a large separation distance between the particles.

A colloidal dispersion can be stabilized in either an aqueous or nonaqueous continuous phase by solvated polymeric moieties adsorbed on the colloidal particle surface. The polymeric chains attached to the surface can be regarded as a barrier around each particle, preventing their close approach to each other. For sterically stable colloidal systems, the continuous phase (medium) must be a good solvent to the attached polymer with nearly complete surface coverage as shown in Figure 2-6a.

The total potential energy for sterically stabilized particles is shown in Figure 2-7. Sterically stabilized colloidal particles are usually very stable over a wide range of particle size and shear rate, and at high dispersed phase concentrations. They can be flocculated by changing the solvency of the continuous phase or by desorbing the attached polymeric moieties. In practice, molecular weights above 1000 are desirable (Walbridge, 1987).

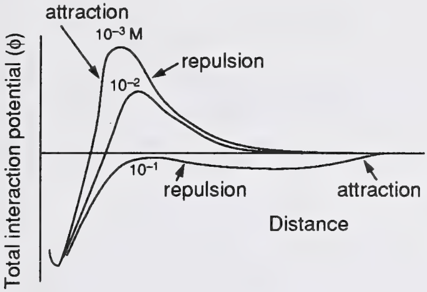

Figure 2-5. Variation of the total potential at different electrolyte molarity for charge-stabilized particles.

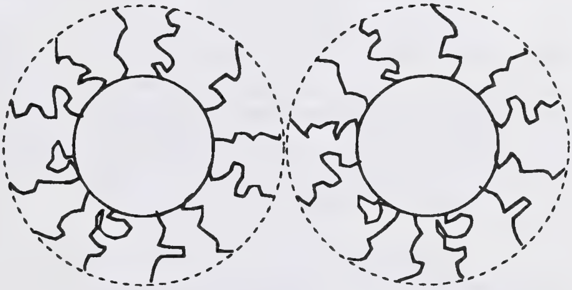

Figure 2-6a. Highly sterically stabilized colloidal particles (polymer is in a good solvent).

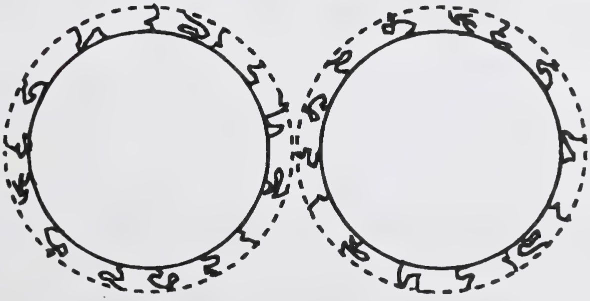

Figure 2-6b. Poorly sterically stabilized colloidal particles (polymer is in a poor solvent).

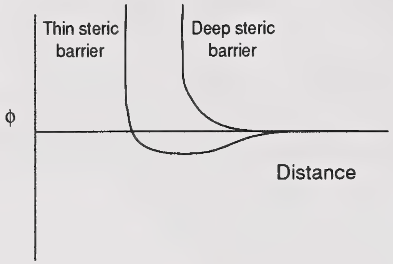

Figure 2-7. Variation of total interaction potential energy for sterically stabilized particles.

2.3 PREPARATION OF COLLOIDAL SYSTEMS

There are two fundamentally different ways in which colloidal dispersions can be made: either by breaking down (splitting) bulk coarse matter to colloidal dimensions or by building up molecular aggregates to colloidal size. The first method is referred to as the dispersion method and the second is referred to as the condensation or nucleation method.

2.3.1 Dispersion Methods

Energy changes are associated with the breakup of a coarse particle. The free energy change associated with creating a new surface area A is given by

$$\Delta G = \gamma A \tag{2-9}$$

where γ is the solids material surface tension and ΔG is the change in Gibbs free energy due to the creation of new surface area. ΔG is then the work required to create the new surface area and it is directly related to γ and A (Everett, 1988).

The diameter of particles obtained in the grinding or milling of a solid, either in a mortar or in a ball mill, is about 1 to 5 μm. The size of the colloidal particles can be reduced by grinding the solids in a liquid having a low surface tension. A further decrease in size can be achieved by the addition of a surface-active electrolyte to the grinding medium. These electrolytes, such as soaps or long chain alkylaryl-sulphonates, are adsorbed on the particle surfaces and hence tend to stabilize the dispersion of the colloidal particles. Particle sizes of the order of 0.1 μm can be achieved by wet milling (Jirgensons and Straumanis, 1962).

Formation of emulsions by the “breaking down” of one liquid in the presence of another can be achieved either by simple stirring or by applying a high shear to the two liquid phases. Colloidal mills or high speed homogenizers are commonly used to prepare liquid-in-liquid dispersion, *i.e.*, an emulsion. The success of an emulsification process depends, to a large extent, on the interfacial tension between the two liquid phases and on the stabilizing forces present. Emulsifying agents, *i.e.*, agents that lower interfacial tension, are usually required for successful emulsification.

In addition to the mechanical approach used in the breaking up of solids or liquids, ultrasonic waves can be used for the breaking up of solids and in the emulsification process. The velocity of sound v is related to the wavelength λ and the frequency f by

$$v = f\lambda \tag{2-10}$$

Ultrasonic vibrations can be easily generated in the range of 25 kHz–2 MHz with commercially available equipment. An oscillating quartz disk is able to produce very high intensity ultrasonic vibrations of up to 10^5 W/m^2. This intensity is about 10^{10} of that produced by a loud radio. Such an energy level can disintegrate coarse particles and form emulsions (Jirgensons and Straumanis, 1962). It is interesting to note that with proper particle size and vibration frequency, the reverse processes of solids agglomeration or demulsification can occur.

2.3.2 Condensation Methods

Colloidal particles can be made by combining small molecules into larger units. This can be achieved either by a decrease in solubility or through chemical methods. The chart below illustrates the types of condensation methods used in the making of a colloidal system (or a sol).

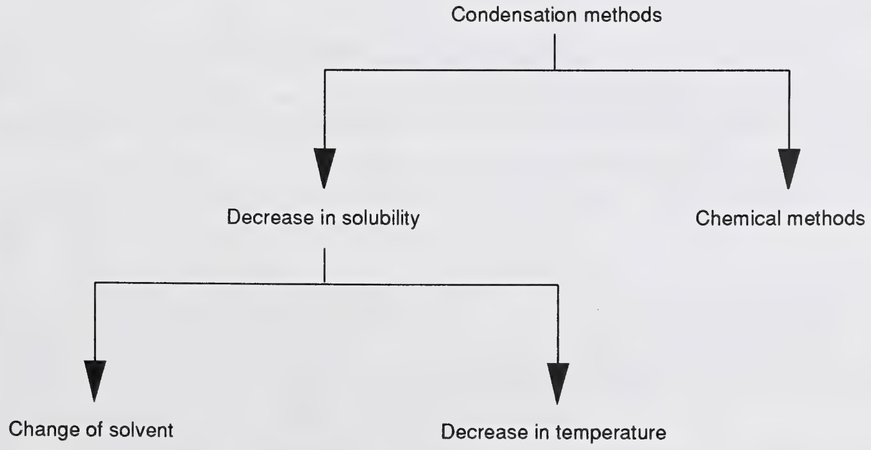

A simple way to prepare a colloidal system is to pour a true micromolecular solution of a solute into another liquid in which the solute is practically insoluble. A sulphur sol can be prepared in this way by decreasing the sulphur solubility due to a change of the solvent. Sulphur is dissolved in alcohol and then the solution is diluted with water in which the sulphur is much less soluble. Various hydrosols of resins and fats are prepared similarly.

Instead of reducing solubility by changing the solvent, one can decrease the temperature. A sol of ice in pentane can be prepared by cooling pentane that contains traces of water.

Chemical methods provide excellent means for preparing colloidal systems. The basic idea is to perform a chemical reaction in which an insoluble or practically insoluble substance is formed so that the solid remains dispersed as small particles. For example, sols of hydroxides can be prepared by hydrolysis. Specifically, colloidal ferric hydroxide is prepared by the hydrolysis of ferric chloride at the boiling point:

$$\mathrm{Fe\,Cl_3} + 3\mathrm{H_2O} \rightarrow \mathrm{Fe\,(OH)_3} + 3\mathrm{HCl}$$

Methods for preparation and characterization of monodisperse metal hydrous oxide sols are given by Matijevic (1976). Monodisperse silica spheres can be prepared using techniques advanced by Stöber *et al.* (1968), van Blaaderen and Vrij (1993), and Nyffenegger *et al.* (1993). Some recipes for the preparation of some simple sols are given below (Everett, 1988).

Gold Sol

Add 1 cm^3 of a 1% solution of gold chloride ($HAuCl_4 \cdot 3H_2O$) to 100 cm^3 of distilled water, bring to the boil and add 2.5 cm^3 of 1% sodium citrate solution. Keep the solution just boiling. After a few minutes observe the appearance of a blue coloration, followed shortly by the formation of a ruby-red gold sol.

Sulphur Sol

Rapidly mix equal amounts of 0.004 mol dm^{-3} sodium thiosulphate solution and 0.004 mol dm^{-3} hydrochloric acid. The mixture becomes cloudy after a few minutes and then develops to an opaque white dispersion of colloidal sulphur.

Silver Bromide Sol

Mix equal amounts of 0.020 mol dm^{-3} sodium bromide solution and 0.018 mol dm^{-3} silver nitrate solution. A colloidal dispersion of silver bromide is formed immediately. A silver iodide sol may be prepared in a similar manner.

Ferric Hydroxide Sol

Add 2 cm^3 of a 30% solution of ferric chloride slowly, with stirring, to 500 cm^3 of boiling distilled water. A clear reddish-brown dispersion of ferric hydroxide is formed.

Polymer Dispersions

Polymer dispersions can be prepared by emulsion polymerization, dispersion polymerization, and suspension polymerization (Walbridge, 1987).

In emulsion polymerization, a monomer is emulsified in a non-solvent (usually water) in the presence of a surfactant. A water-soluble initiator is added. Particles of polymer form and grow in the aqueous continuous phase. Production of the particles proceeds until the monomer is used up.

In dispersion polymerization, monomer, initiator, stabilizer, and solvent initially form a homogeneous solution. Polymer precipitates when the solubility limit is exceeded. Polymer particles continue to grow until the monomer is used up.

In suspension polymerization, the monomer is emulsified in the medium using a surfactant. The initiator is often dissolved within the monomer droplet. The droplet is gradually converted into the insoluble particles, but no new particles are formed. The size distribution of the dispersion becomes that of the original monomer.

In most of the processes involving preparation of a colloidal system, the formation of the sols passes through nucleation and growth stages. Control of such stages would determine the size of the colloidal particles and their size distribution.

2.4 PURIFICATION OF SOLS

In the last section, we dealt with methods of making colloidal systems of solids or of immiscible liquids in either an aqueous or non-aqueous continuous phase.

Prepared sols of solid particles that are insoluble in water or in a solvent usually contain some contamination having low molecular weight. The contaminants can be removed by various methods such as dialysis, ultrafiltration, and electrodialysis.

Dialysis, in its simplest form, involves placing the sol in a container having one end covered with a semi-permeable membrane. The membrane side of the container is placed in water (or solvent) as shown in Figure 2-8. The membrane is permeable to the solvent and the other small molecular weight impurities, but impermeable to the colloidal particles. Diffusion of the impurities through the membrane leads to the eventual depletion of the impurities within the prepared sols (Overbeek, 1952).

Ultrafiltration is a pressure-driven membrane separation process. The solvent and low molecular weight materials pass through the membrane but the membrane rejects particulate matter. Ultrafiltration is similar to the common filtration process except that the membrane pores are very small. The applied pressure is usually in the range of $2 \times 10^2 - 10^4$ kPa. Ultrafiltration is not a method of purification but rather of concentration. Upon the rejection of the solvent, together with the associated impurities, fresh solvent is usually added to the sol and ultrafiltration is once again applied to the sol. The addition of the fresh solvent acts as a washing medium and makes it possible to obtain a sol with little impurities.

Electrodialysis is a membrane process in which dissolved ions are removed from an aqueous solution through membranes under the driving force of a dc electric field. Electrodialysis membranes are ion exchange membranes (Probstein, 1989).

An electrodialysis cell has alternating anion and cation exchange membranes. The sol to be purified is made to flow between the membranes. An anion exchange membrane allows the passage of an anion but not a cation. Conversely, a cation exchange membrane allows the passage of a cation but not an anion. In this manner, it is possible to concentrate the undesirable electrolyte and to deplete the sol from the electrolyte (*e.g.*, NaCl). This is shown in Figure 2-9. The chamber containing the electrolyte-free sol is called the dialysate channel and the chamber containing electrolyte-rich sol is called the concentrate channel.

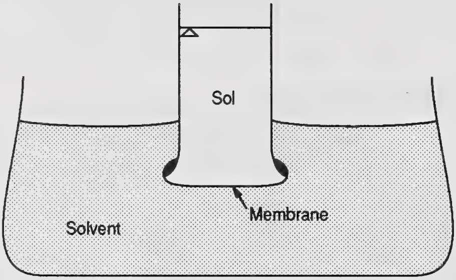

Figure 2-8. A simple dialysis cell.

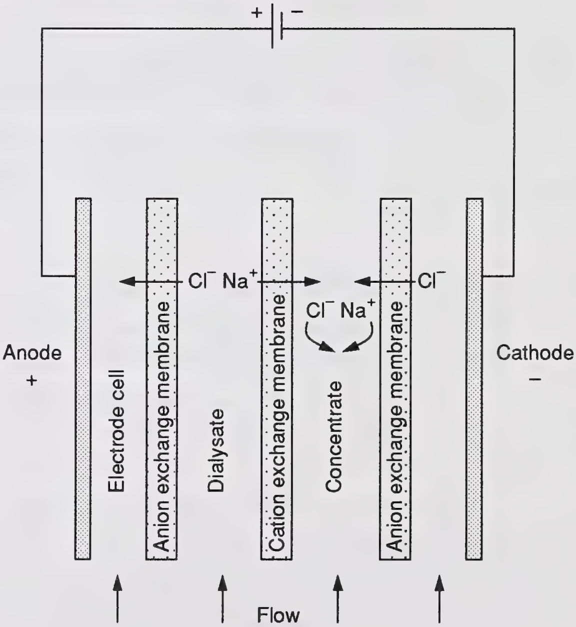

Figure 2-9. Electrodialysis cell pair. Sol purification from Na^+ and Cl^- ions (Adapted from Probstein, 1989).

2.5 NOMENCLATURE

a	particle radius, m
Bo	Bond number, dimensionless
D	immersed depth in water, m
f	frequency of sound, s^{-1}
g	acceleration due to gravity, m/s^2
ΔG	free energy, J
k	Boltzmann constant, 1.382×10^{-23} J/K
L	cube side length, m
N_s	total number of surface molecules
N_t	total number of inner molecules
S	molecule side length, m
T	absolute temperature, K
U	particle velocity, m/s
v	velocity of sound, m/s
γ	interfacial tension, N/m
ε	dielectric constant of a medium, dimensionless
ε_o	permittivity of vacuum, 8.85×10^{-12} C/Vm
θ	angle related to contact angle = π – contact angle
λ	sound wave length, m
μ	fluid viscosity, kg/ms or Pa s
ρ	density, kg/m^3
ϕ	total interaction potential energy, J
ψ_s	surface potential, V

Subscript

a	air
p	particle
w	water

2.6 REFERENCES

Everett, D.H. (1988), *Basic Principles of Colloid*, Royal Soc. of Chemistry, London.

Jirgensons, B. and Straumanis, M.E. (1962), *A Short Textbook of Colloid Chemistry*, MacMillan Co., London.

Matijevic, E. (1976), *Preparation and Characterization of Monodisperse Metal Hydrous Oxide Sols*, Prog. Colloid Polymer Sci. **61**, 24–25.

Nyffenegger, R., Quellet, C., and Ricka, J. (1993), *Synthesis of Fluorescent, Monodisperse, Colloidal Silica Particles*, J. Colloid Interface Sci., **159**, 150–57.

Overbeek, J. Th. G. (1952), *Phenomenology of Lyophobic Systems*, Chapter II in Colloid Science (ed. Kruyt, H.R.), Elsevier, Amsterdam.

Probstein, R.F. (1989), *Physiochemical Hydrodynamics*, Butterworths, Boston.

Russel, W.B., Saville, D.A., and Schowalter, W.R. (1989), *Colloidal Dispersions*, Cambridge University Press, Cambridge.

Stöber, W., Fink, A., and Bohm, E. (1968), *Controlled Growth of Monodisperse Silica Spheres in Micron Size Range*, J. Colloid Interface Sci., **26**, 62–69.

van Blaaderen, A. and Vrij, A. (1993), *Synthesis and Characterization of Monodisperse Colloidal Organo-Silica Spheres*, J. Colloid Interface Sci., **156**, 1–18.

Walbridge, D.J. (1987), *Preparations of Solid/Liquid Dispersions*, Chapter 2 in Solid/Liquid Dispersions (ed. Tadros, Th. F.), Academic Press, London.

ELECTROSTATICS 3

3.1 BASIC ELECTROSTATICS IN VACUUM

It was pointed out earlier that most surfaces attain a surface charge when immersed in an electrolyte solution. Electrostatic forces are essential for stabilizing colloidal suspensions and they play a central role in biological systems. In order to analyse and study the influence of a surface charge, it is necessary to know the governing equations for electrostatics (Feynman *et al.*, 1964; Slater and Frank, 1969; Eyges, 1980).

Maxwell's equations for the special case of electrostatics in a vacuum can be written as

$$\varepsilon_o \vec{\nabla} \cdot \vec{E} = \overset{(e)}{\rho} \tag{3-1}$$

and

$$\vec{\nabla} \times \vec{E} = 0 \tag{3-2}$$

where $\vec{E}$ is the electric field strength or force per unit charge, V/m, N/C

$\overset{(e)}{\rho}$ is the total electric charge density, C/m^3

ε_o is the permittivity of vacuum = 8.854×10^{-12} C^2/Nm^2 or C/Vm.

The electric field strength on a closed surface, S, is related to the total charge, Q, by

$$\int_V \overset{(e)}{\rho}\, dV = Q \tag{3-3a}$$

where V is the volume enclosing a charge Q.

Combining Eqs. (3-1) and (3-3a) leads to

$$\int_V \varepsilon_o \vec{\nabla} \cdot \vec{E} dV = Q \tag{3-3b}$$

The divergence theorem states that

$$\int_V \vec{\nabla} \cdot \vec{E} dV = \int_S \vec{E} \cdot \vec{n} dS$$

Consequently, Eq. (3-3b) becomes

$$\varepsilon_o \int_S \vec{E} \cdot \vec{n} dS = Q \tag{3-4a}$$

where $\vec{n}$ is an outer unit vector as shown in Figure 3-1. Eq. (3-4a) can be written as

$$\int_S \vec{E} \cdot \vec{n} dS = \frac{Q}{\varepsilon_o} \tag{3-4b}$$

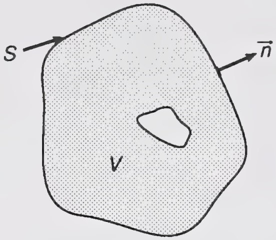

Figure 3-1. Surface S enclosing a total charge Q.

For a spherical surface of radius r centered on a point charge in vacuum, one can write

$$\int_S \vec{E} \cdot \vec{n} dS = \int_S E_r dS = 4\pi r^2 E_r = Q/\varepsilon_o \tag{3-4c}$$

where $\vec{n} \equiv \vec{i}_r$ and $\vec{E} = \vec{i}_r E_r + \vec{i}_\theta E_\theta + \vec{i}_\phi E_\phi$

E_r, E_θ, and E_ϕ are the components of the field strength vector in r, θ, and ϕ directions, respectively. $\vec{i}_r$, $\vec{i}_\theta$, and $\vec{i}_\phi$ are the unit vectors in r, θ, and ϕ directions, respectively. For a point charge in vacuum, one can write

$$E_r = \frac{Q}{4\pi\varepsilon_o r^2} \tag{3-5}$$

or, in a vector notation

$$\vec{E} = \frac{Q}{4\pi\varepsilon_o r^2} \vec{i}_r \tag{3-6}$$

Eq. (3-6) gives the variation of the field strength with distance r for a point charge.

Since the electric field is defined as the force per unit charge, it follows that the force in vacuum exerted by one point charge on another at a relative position of $\vec{r}_{12}$ is given by

$$\vec{F}_{12} = \vec{E}_1 Q_2 = \frac{Q_1 Q_2}{4\pi\varepsilon_o r_{12}^3} \vec{r}_{12} \tag{3-7}$$

The two point charges, Q_1 and Q_2, are shown in Figure 3-2.

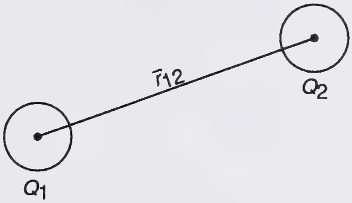

Figure 3-2. Two point charges.

The force vector $\vec{F}_{12}$ is due to the point charges Q_1 and Q_2. Eq. (3-7), known as Coulomb's law, was established by 1795.

The absolute value of the interaction force is then given by

$$F_{12} = \frac{Q_1 Q_2}{4\pi\varepsilon_o r^2} \tag{3-8}$$

F_{12} is the force acting between the two point charges along the line joining their centres.

From the definition of the field strength, one can write $\vec{F} = \vec{E}Q$ for the force. The units are

$$N = \frac{V}{m} C = J/m \tag{3-9}$$

According to Eq. (3-2), the electric field strength is conservative. In other words, the line integral

$$\oint \vec{E} \cdot \vec{t} dl = 0 \tag{3-10}$$

where t is the tangent to a closed curve as shown in Figure 3-3.

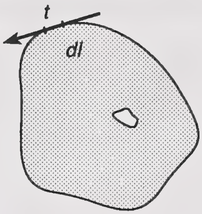

Figure 3-3. Line integral along a closed curve.

To illustrate Eq. (3-10), consider a field strength given as $\vec{E} = \vec{i}_x E_x + \vec{i}_y E_y$; *i.e.*, a field strength parallel to the x-axis as shown in Figure 3-4.

Consider the closed curve ABCD,

where $\vec{t} = -i_x$ along BC
$\vec{t} = i_x$ along DA
$\vec{t} = i_y$ along AB and
$\vec{t} = -i_y$ along CD

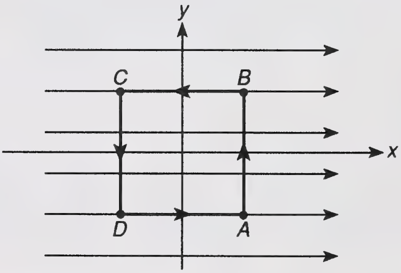

Figure 3-4. Field parallel to x-axis and a line integral.

Applying Eq. (3-10) leads to

$$\int_A^B \left(\vec{i}_x E_x + \vec{i}_y E_y\right) \cdot \vec{i}_y dy + \int_B^C \left(\vec{i}_x E_x + \vec{i}_y E_y\right) \cdot \left(-\vec{i}_x\right)(-dx)$$

$$+ \int_C^D \left(\vec{i}_x E_x + \vec{i}_y E_y\right) \cdot \left(-\vec{i}_y\right)(-dy) + \int_D^A \left(\vec{i}_x E_x + \vec{i}_y E_y\right) \cdot \vec{i}_x dx = 0$$

Simplifying the above expression, one obtains

$$\int_A^B E_y\,dy + \int_B^C E_x\,dx + \int_C^D E_y\,dy + \int_D^A E_x\,dx = 0$$

The values of E_x and E_y for any arbitrary charge distribution must be such that the above equation is satisfied. For the simple case of E_x being a constant and $E_y = 0$, the above equation is satisfied.

A similarity between Eq. (3-2) and irrotational fluid flow exists where for the latter case, we write

$$\vec{\nabla} \times \vec{v} = 0$$

Here, $\vec{v}$ is the fluid flow velocity vector.

Inasmuch as the curl ($\vec{\nabla} \times \cdot$) of a gradient of any scalar function is zero, one can write[◆]

$$\vec{E} = -\vec{\nabla}\psi \tag{3-11}$$

which satisfies $\vec{\nabla} \times \vec{E} = 0$ identically. ψ is the electric field potential, expressed in volts.

Combining Eqs. (3-1) and (3-11) leads to

$$\varepsilon_o \nabla^2 \psi = -\overset{(e)}{\rho} \tag{3-12}$$

For zero charge density, $\overset{(e)}{\rho} = 0$, Eq. (3-12) becomes

$$\nabla^2 \psi = 0 \tag{3-13}$$

[◆] By definition the cross product ($\vec{\nabla} \times \vec{\nabla}\psi$) in Cartesian coordinates is given as

$$\vec{\nabla} \times \vec{\nabla}\psi = \begin{vmatrix} i_x & i_y & i_z \\ \frac{\partial}{\partial x} & \frac{\partial}{\partial y} & \frac{\partial}{\partial z} \\ \frac{\partial \psi}{\partial x} & \frac{\partial \psi}{\partial y} & \frac{\partial \psi}{\partial z} \end{vmatrix}$$

For example, for an isolated point charge (Q) in vacuum, Figure 3-5 shows the isopotential lines ψ_1, ψ_2 with a field strength E_r in the r-direction. For this case,

$$\vec{E} = \vec{i}_r \mathrm{E}_r + \vec{i}_\theta E_\theta + \vec{i}_\phi E_\phi$$

with $E_\theta = E_\phi = 0$ due to symmetry.

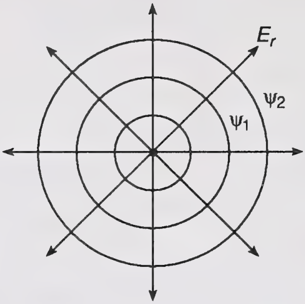

Figure 3-5. Isopotential for a point charge.

For an isolated point charge, there is no θ- and ϕ-dependence, and Eq. (3-13) becomes

$$\frac{1}{r^2}\frac{d}{dr}\left(r^2 \frac{d\psi}{dr}\right) = 0 \tag{3-14}$$

The solution of Eq. (3-14) is given by

$$\frac{d\psi}{dr} = \frac{A_1}{r^2} \quad \text{and} \quad \psi = \frac{-A_1}{r} + A_2 \tag{3-15}$$

where A_1 and A_2 are integration constants.

At large distances, $r \to \infty$, the effect of the point charge is negligible and consequently at $r \to \infty$, $\psi \to 0$. This boundary condition leads to $A_2 = 0$. We have from Eq. (3-4a)

$$\varepsilon_o \int_S \vec{E} \cdot \vec{i}_r dS = Q$$

Recognizing that $\vec{E} \cdot \vec{r} = (\vec{i}_r E_r + \vec{i}_\theta E_\theta + \vec{i}_\phi E_\phi) \cdot \vec{i}_r = E_r$ and $E_r = -d\psi/dr$, the above equation becomes

$$-\int_S \frac{d\psi}{dr} dS = -\int_S \left(\frac{A_1}{r^2}\right) dS = \frac{Q}{\varepsilon_o} \tag{3-16}$$

The above expression gives the constant A_1 as

$$A_1 = -\frac{Q}{4\pi\varepsilon_o} \tag{3-17}$$

The potential of Eq. (3-15) becomes

$$\psi = \frac{Q}{4\pi\varepsilon_o r} \tag{3-18}$$

In vector notation, the electric field strength is then given by

$$\vec{E} = \frac{Q}{4\pi\varepsilon_o r^3}\vec{r} \tag{3-19a}$$

or

$$\vec{E} = \frac{Q}{4\pi\varepsilon_o r^2}\vec{i}_r \tag{3-19b}$$

For a spherical conductor of radius a, we put

$\psi = \psi_s$ at $r = a$

where ψ_s is the surface potential. Eq. (3-18) becomes

$$Q = 4\pi\varepsilon_o a\psi_s \tag{3-20}$$

Eq. (3-20) relates the charge to the potential of a spherical particle in vacuum. The potential of the sphere ψ_s and the sphere's charge Q are related to each other (Russel *et al.*, 1989). Eq. (3-20) is also the expression given for a capacitor, where $4\pi\varepsilon_o a$ is the capacity of the sphere.

The electrostatic equations derived so far are applicable to charges in a vacuum. When the vacuum is replaced by a real medium, the electrostatic equation given by (3-1) needs to be modified. First, we shall discuss briefly the electrical classification of materials and then show how to modify the electrostatic equations in the presence of a medium.

3.2 ELECTRICAL CLASSIFICATION OF MATERIALS

In a very broad sense, materials can be classified as:

1. Conductors (*e.g.*, metals). For our purposes, we can state the following properties for conductors (Neale, 1974):
   - Permit transfer of electric charge, *i.e.*, passage of electric current.
   - Electrical conductivity (reciprocal of resistivity) decreases with increasing temperature.
   - Any free charge associated with a conductor reposes exclusively on its surface. A consequence of this is that there can be no electric field inside a conductor due to electrostatic charges.
   - Surfaces of conductors are equipotential surfaces, *i.e.*, $\psi = \psi_s$ = constant in the absence of power sources or sinks (*i.e.*, batteries)
2. Dielectrics (*e.g.*, plastics, organic liquids, water, gases). For our purposes, dielectric materials have the following properties:
   - Do not permit free passage of electric charge, *i.e.*, free passage of electrons.
   - Local microscopic displacements of charge are permissible (*e.g.*, molecule polarization).
   - Molecules of many dielectrics are permanently polarized due to their asymmetrical molecular structure, *e.g.*, HCl.
   - Dielectrics containing symmetrical molecules or atoms, *e.g.*, *He*, become polarized when exposed to an electric field, as a result of the relative displacement of orbital electrons.
   - Molecules of all dielectrics constitute dipoles in the presence of an electric field.
   - Dielectrics with high values of dielectric constant (to be defined at a later stage) are generally good ionizing media, *e.g.*, water.

Polarization in a dielectric is illustrated in Figure 3-6.

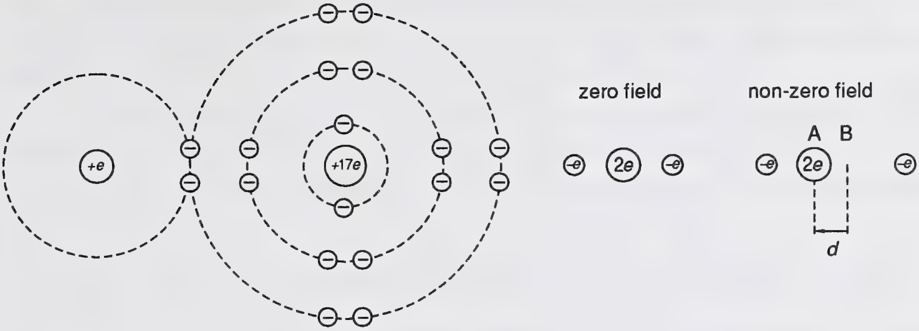

HCl molecule
(permanent dipole)

He atom
(induced dipole)

Figure 3-6. Polarization in a dielectric.

3.3 MAXWELL'S EQUATIONS IN A DIELECTRIC

An excellent review of Maxwell's equations in a dielectric is given by Russel *et al.* (1989). A brief summary is given here.

The molecules of all dielectrics constitute dipoles in the presence of an electric field. A dipole comprises two equal and opposite charges, $+Q$ and $-Q$, separated by a distance d. A dipole moment is defined as $Q\vec{d}$ which is a vector quantity. $\vec{d}$ is the vector orientation between the two charges as shown below in Figure 3-7.

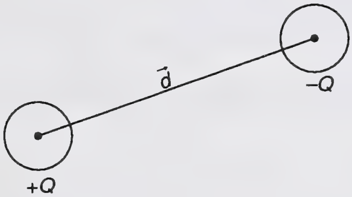

Figure 3-7. Two charges separated by a distance d.

The polarization dipole moment $\vec{P}$ of the individual dipoles is given by

$$\vec{P} = NQ\vec{d} \tag{3-21}$$

where $\vec{P}$ is the polarization dipole moment
Q is the magnitude of the charge separated to produce the dipole
N is the number of dipoles per unit volume
$\vec{d}$ is the vector describing the average orientation of the dipole and the charge separation distance.

For linear material, the dipole polarization moment is proportional to the applied electric field strength, where

(3-22) $$\vec{P} = \chi\varepsilon_o\vec{E}$$

where χ is the susceptibility of the dielectric material. One can think of $\chi\varepsilon_o$ being the proportionality constant for P and E. In view of Eq. (3-1), one can define

(3-23) $$\vec{\nabla} \cdot \vec{P} = -\overset{(p)}{\rho}$$

where $\overset{(p)}{\rho}$ is the volumetric polarization charge density.

Combining Eqs. (3-1) and (3-23) leads to

(3-24) $$\varepsilon_o\nabla \cdot \left[\vec{E} + \frac{\vec{P}}{\varepsilon_o}\right] = \overset{(e)}{\rho} - \overset{(p)}{\rho}$$

Substituting for $\vec{P}$ from Eq. (3-22), one obtains

(3-25) $$\varepsilon_o\nabla \cdot \left[\vec{E}\,(1 + \chi)\right] = \overset{(f)}{\rho}$$

where $\overset{(f)}{\rho}$ is the free charge density C/m^3, which is the difference between the total and polarization charge densities. Let

(3-26) $$1 + \chi = \varepsilon$$

where ε is defined as the dielectric constant of a material. Eq. (3-25) then becomes

(3-27) $$\varepsilon_o\nabla \cdot \left[\varepsilon\vec{E}\right] = \overset{(f)}{\rho}$$

Eq. (3-27) is Maxwell's equation for a dielectric with a free charge density.

When the dielectric constant ε is not a function of position, then we can write

(3-28) $$\varepsilon\varepsilon_o\vec{\nabla} \cdot \vec{E} = \overset{(f)}{\rho}$$

Making use of the potential relationship given by Eq. (3-11), Eq. (3-28) becomes

(3-29) $$\varepsilon\varepsilon_o\nabla^2\psi = -\overset{(f)}{\rho}$$

The above equation is referred to as Poisson's equation which describes the electric potential in a dielectric. It is one of the fundamental equations to be used for the evaluation of the potential ψ in an electrolyte solution (*e.g.*, NaCl in water).

In situations where there is no free charge (*e.g.*, organic material), one can set $\overset{(f)}{\rho}$ to zero and Eq. (3-29) becomes

$$\nabla^2\psi = 0 \tag{3-30}$$

Eq. (3-30) is referred to as Laplace's equation, which describes the electric potential in a material having no free charge.

The force exerted by two point charges in a dielectric becomes

$$F_{12} = \frac{Q_1 Q_2}{4\pi\varepsilon\varepsilon_o r^2} \tag{3-31}$$

which is similar to Eq. (3-8), which was derived for a vacuum. As $\varepsilon>1$, the force between the two charges is reduced by a factor ε due to the presence of the dielectric.

Similarly, the charge and the surface potential for a point charge in a dielectric having $\overset{(f)}{\rho} = 0$ are given by

$$Q = 4\pi\varepsilon\varepsilon_o a\psi_s \tag{3-32}$$

Here, the term $4\pi\varepsilon\varepsilon_o a$ is the capacity of the sphere. Consequently, the capacity is increased by a factor of ε as compared to that in a vacuum; see Eq. (3-20) for comparison.

From the above, one can think of the dielectric constant in terms of a ratio which is given by

$$\begin{aligned}\varepsilon &= \text{dielectric constant of a medium} \\ &= \frac{\text{force between two charges in vacuum}}{\text{force between same charges (at the same separation) in a medium}}\end{aligned}$$

ε is a dimensionless quantity with $\varepsilon>1$.

Typical values for the dielectric constant are given in Table 3-1a (Russel *et al.*, 1989). For gases at atmospheric pressure, $\varepsilon\sim1$ and ε increases with pressure. For example, air at 100 atm has an ε value of about 1.05, whereas at 1 atm, $\varepsilon = 1.0006$. The dielectric constant is a function of temperature. For water, the variation of ε is tabulated in Table 3-1b.

Table 3-1a. Dielectric constants of some common liquids and solids at 25°C

Compound		Dielectric constant	Compound		Dielectric constant
Hydrogen-bonding			Non-hydrogen bonding		
methylformamide	$HCONHCH_3$	182.4	Acetone	$(CH_3)_2CO$	20.7
Formamide	$HCONH_2$	109.5	Chloroform	$CHCl_3$	5.0
Hydrogen fluoride	HF	84[a]	Benzene	C_6H_6	2.3
Water	H_2O	78.5	Carbon tetrachloride	CCl_4	2.2
Formic acid	HCOOH	58.5[b]	Cyclohexane	C_6H_{12}	2.0
Ethylene glycol	$C_2H_4(OH)_2$	40.7	Dodecane	$C_{12}H_{26}$	2.0
Methanol	CH_3OH	32.6	Hexane	C_6H_{14}	1.9
Ethanol	C_2H_5OH	24.3	Crystals		
n-Propanol	C_3H_7OH	20.2	Sodium chloride	NaCl	6.0
Ammonia	NH_3	16.9	Diamond	C	5.7
Acetic acid	CH_3COOH	6.2	Quartz	SiO_2	4.5

[a] Value at 0°C

[b] Value at 16°C

Israelachvili, J.N. (1985), "Intermolecular and Surface Forces," Acad. Press

Table 3-1b. Variation of water dielectric constant with temperature

Temperature, °C	ε
0	87.8
5	85.8
10	83.8
15	81.95
18	80.8
20	80.1
25	78.5
30	76.6
40	73.15
50	69.9
60	66.8
70	63.9
80	61.0
90	58.3
100	55.7

A curve fit equation for the dielectric constant of water is given as $\varepsilon = 87.7 - 0.391T + 0.000741\ T^2$, T in °C

3.4 BOLTZMANN'S PROBABILITY LAW

Here, we shall introduce Boltzmann's probability law using simple concepts. However, at a later stage, a more formalized derivation will be made. Whenever thermal equilibrium exists, the probability that a state with an energy W will be occupied has been shown by Boltzmann (1844–1906) to have the following dependence upon the potential:

$$\text{Probability} \propto \exp\left[-W/kT\right] \tag{3-33}$$

where T is the absolute temperature (K),
k is the Boltzmann constant (J/K) given by R/N_a, where N_a is Avogadro's number and R is the universal gas contant.

The above expression was derived from statistical considerations. As a consequence of expression (3-33), the ionic concentration (number of ions per unit volume) distribution near a charged surface immersed in a $(z{:}z)$ symmetric electrolyte solution is given by

$$n_+ = n_\infty \exp\left(-\frac{ze\psi}{kT}\right) \tag{3-34a}$$

and

$$n_- = n_\infty \exp\left(\frac{ze\psi}{kT}\right) \tag{3-34b}$$

Here ψ is the electric field potential, expressed in volts, at location x, and z is the absolute value of the valency. Here, e is the fundamental charge of an electron, n_∞ is the ionic number concentration (m^{-3}) in the bulk solution, and n_+ and n_- are the ionic number concentrations for the cations and anions at location x, respectively.

Another simple application can be made for the concentration of, say, helium in the atmosphere as a function of distance (height) from the earth's surface. The potential energy is given by mgx, where m is the mass of a helium atom, g is the acceleration due to gravity, and x is the distance from the earth's surface.

The probabilities at height x and zero height to locate a helium atom are: probability (x) = (constant) exp $(-mgx/kT)$; probability (0) = (constant) exp $(0/kT)$. The ratio of these probabilities is equal to the ratio of their concentrations; hence

$$\frac{\text{probability (x)}}{\text{probability (0)}} = \frac{n(x)}{n(0)} \tag{3-35}$$

and we obtain for isothermal conditions

$$n(x) = n(0) \exp\left(-\frac{mgx}{kT}\right) \tag{3-36}$$

where n is the number of *He* atoms per unit volume. n can also be expressed in the units of mol/m^3.

3.5 ORIGIN OF INTERFACIAL CHARGE

Most substances acquire a surface electric charge when brought into contact with an aqueous medium (Probstein, 1989). The stability of colloidal dispersions is very sensitive to the addition of electrolytes and to the surface charge of the colloidal particles. Direct evidence for the existence of charge on particles comes from the phenomenon of particle movement under an applied electric field (electrophoresis) which will be dealt with at a later stage. Although, in the course of electrokinetic studies, we accept the presence of surface charges and may pay less attention to their origin, it is still important to recognize the origin of charge. Surfaces may become electrically charged by a variety of mechanisms. Some of the important mechanisms are (Everett, 1988).

(i) Ionization of surface groups. If a surface contains acidic groups, their dissociation gives rise to a negatively charged surface as shown in Figure 3-8a. Conversely, a basic surface takes on a positive charge, Figure 3-8b. In both cases, the magnitude of the surface charge depends on the acidic or basic strengths of the surface groups and on the pH of the solution. The surface charge can be reduced to zero (at the point of zero charge, PZC) by suppressing the surface ionization. This can be achieved by decreasing pH for the case of a surface containing acidic groups or by increasing pH for the case of a basic surface. Most metal oxides can have either a positive or a negative surface charge depending on the bulk pH.

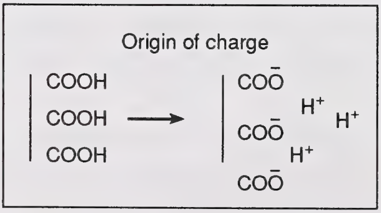

Figure 3-8a. Ionization of acid groups to give a negatively charged surface.

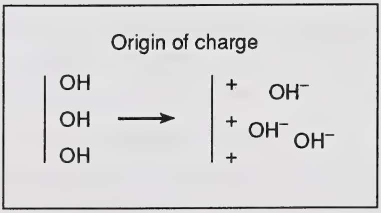

Figure 3-8b. Ionization of basic groups to give a positively charged surface.

(ii) Differential solution of ions from surfaces of sparingly soluble crystals. For example, when a silver iodide crystal (AgI) is placed in water, dissolution occurs until the product of ionic concentration equals the solubility product $[Ag^+][I^-] = 10^{-16}$ $(mol/L)^2$. If equal amounts of Ag^+ and I^- ions were to dissolve, then $[Ag^+] = [I^-] = 10^{-8}$ and the surface would be uncharged. However, silver ions dissolve preferentially, leaving a negatively charged surface. If Ag^+ ions now are added in the form of, say, a silver nitrate ($AgNO_3$) solution, the preferential solution of silver ions is suppressed and the charge falls to zero at a particular concentration. Further addition of $AgNO_3$ leads to a positively charged surface since it is now iodide ions that are preferentially dissolved.

(iii) Isomorphous substitution. Clays may exchange an adsorbed intercalated or structural ion with one of lower valency, thus producing a negatively charged surface. For example, Al^{3+} may replace Si^{+4} in the surface of the clay, producing a negative surface charge. In this case, a point of zero surface charge can be reached by reducing the pH. Here, the added H^+ ions combine with the negative charges on the surface to form OH groups.

(iv) Charged crystal surfaces. It may happen that when a crystal is broken, surfaces with different properties are exposed. Thus, in some clays (*e.g.*, kaolinite), when a platelet is broken, the exposed edges contain AlOH groups which take up H^+ ions to give a positively charged edge. This edge surface charge (positive) may coexist with negatively charged basal surfaces, leading to special properties. In this case, there will be no single PZC, but each type of surface has its own value. For kaolinite, the flat surface is negatively charged and the edges are positively charged. This difference is particularly pronounced at low pH. At high pH, the positive charge on the edges decreases.

(v) Specific ion adsorption. Surfactant ions may be specifically adsorbed, leading in the case of cationic surfactants to a positively charged surface (Figure 3-9a) and in the case of anionic surfactants to a negatively charged surface (Figure 3-9b).

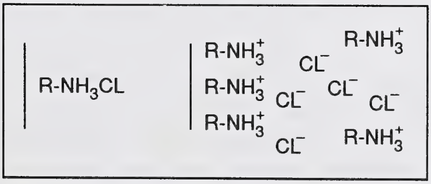

Figure 3-9a. Adsorption of a cationic surfactant.

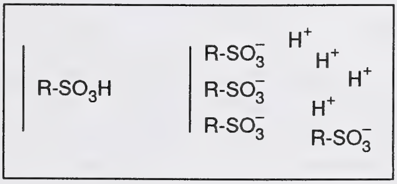

Figure 3-9b. Adsorption of an anionic surfactant.

3.6 POTENTIAL DISTRIBUTION NEAR AN INTERFACE

The effect of any charged surface in an electrolyte solution will be to influence the distribution of nearby ions in the electrolyte solution. Ions of opposite charge to that of the surface (counterions) are attracted towards the surface, while ions of like charge (coions) are repelled from the surface. It is usual to call this ionic atmosphere an electric double layer. The term "double layer" stems from the fact that ideally, two regions of opposite charge are present, as shown in Figure 3-10a.

The concept of double layer was introduced by Helmholtz, who envisaged an arrangement of charges in two parallel planes as shown in Figure 3-10a, forming, in effect, a "molecular condenser." However, thermal motion causes the counterions to be spread out in space, forming a diffuse double layer, as is shown in Figure 3-10b. The theory for such a diffuse double layer was developed independently by Gouy and Chapman in the early 1900s (Hunter, 1981).

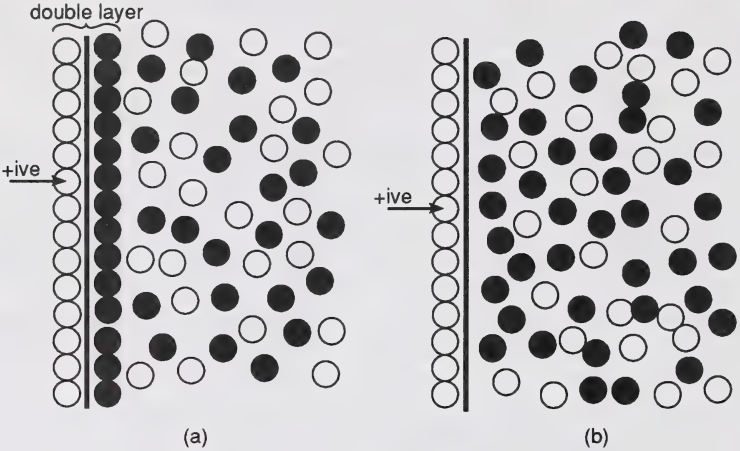

Figure 3-10. The electric double layer. (a) according to the Helmholtz model, (b) the diffuse double layer resulting from thermal motion. ○ positive charge, ● negative charge.

Gouy–Chapman diffuse double layer model. In this model, the charged surface has a potential ψ_s where within the surface, there is one layer of charge. The compensating ions are regarded as point charges immersed in a continuous dielectric medium. The repulsion/attraction coupled with random thermal Brownian motion of the ions within the dielectric medium gives rise to an electric diffuse layer. Within this diffuse layer, there is no charge neutrality. Equilibrium is thus established due to the forces attributed to attraction/repulsion and diffusion due to concentration gradients.

The Gouy–Chapman model provides good quantitative predictions provided that the surface potential is low (~ 0.025 V) and that the electrolyte concentration is not too high. The major defect of the model is that it neglects the finite size of the ions (it assumes that the ions are point charges which can approach the surface without limit). Moreover, the dielectric value of the medium is taken to be constant. A modification to the Gouy–Chapman model is offered by Stern (1924).

The term counterions is used for the ions which have the opposite sign to the surface charge. The term coions is used for the ions which have the same sign as the surface charge. In the analysis, the symbols ψ and ϕ are used interchangeably for the potential unless otherwise specifically stated.

3.6.1 Mathematical Analysis of Double Layer for a Flat Surface: Gouy–Chapman Model

In order to facilitate the analysis, the case of a flat surface will be considered. The objective is to obtain analytical expressions for the distribution of potential and ion concentration due to the presence of the charged surface in a dielectric medium having free charge.

The potential distribution within the diffuse electric double layer is given by the Poisson equation as

$$\varepsilon\varepsilon_o \nabla^2 \psi = -\overset{(f)}{\rho} \tag{3-37}$$

For a one-dimensional problem for the case shown in Figure 3-11, we can write

$$\varepsilon\varepsilon_o \frac{d^2\psi}{dx^2} = -\overset{(f)}{\rho} \tag{3-38}$$

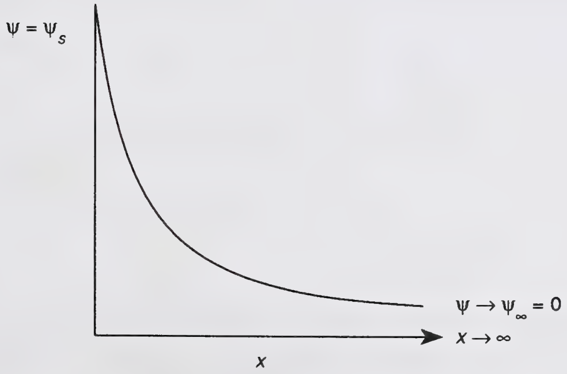

Figure 3-11. Potential distribution near a flat surface.

The charge density is given by

$$\overset{(f)}{\rho} = \sum_{i=1}^{N} n_i z_i e \tag{3-39}$$

where n_i is the ionic number concentration of the ith species, m^{-3}
z_i is the valence of the ith ion species
e is the magnitude of charge on an electron (fundamental charge), 1.602×10^{-19} C
N is the number of ionic species in the electrolyte solution.

Combining Eqs. (3-38) and (3-39) leads to

$$\varepsilon\varepsilon_o \frac{d^2\psi}{dx^2} = -\sum_{i=1}^{N} n_i z_i e \tag{3-40}$$

Recall Boltzmann's relationship (3-33)

$$\text{Probability} = P \propto e^{-W/kT} \tag{3-41}$$

The work W, required to bring one ion of valency z_i (*i.e.*, a charge $z_i e$ from infinity, where $\psi = 0$) to a given location x, having a potential ψ, is given by $W = z_i e\psi$. Hence, the probability of finding the ion at location x is

$$P = \text{constant} \exp\left[-\frac{z_i e\psi}{kT}\right] \tag{3-42}$$

The probability of finding the same ion at the neutral state ($\psi = 0$) is given by the definition as

$$P_o = \text{constant} (\exp (0)) \tag{3-43}$$

The ratio of P to P_o is equal to the ratio of the concentrations of species i at the respective states; hence

$$n_i = n_{i\infty} \exp\left[-\frac{z_i e\psi}{kT}\right] \tag{3-44}$$

$n_{i\infty}$ is the ionic number concentration at the neutral state where $\psi = 0$.

Eq. (3-44) is the Boltzmann distribution equation. Combining Eqs. (3-40) and (3-44) leads to

$$\varepsilon\varepsilon_o \frac{d^2\psi}{dx^2} = -\sum_{i=1}^{N} n_{i\infty} z_i e \exp\left(-\frac{z_i e\psi}{kT}\right) \tag{3-45}$$

Eq. (3-45) is normally referred to as the Poisson–Boltzmann equation defining the charge distribution subject to the appropriate boundary conditions. In order to facilitate the solution of Eq. (3-45), the special case of a single salt will be considered with the added simplification of a symmetric (z:z) electrolyte solution (*e.g.*, NaCl, $CuSO_4$, or AgI).

Special case of a symmetric (z:z) electrolyte: Gouy–Chapman analysis. For the case of a symmetric electrolyte solution (z:z), one can write

$$z_+ = -z_- = z \tag{3-46}$$

where z is the cationic valence. Eq. (3-45) can then be written as

$$\varepsilon\varepsilon_o \frac{d^2\psi}{dx^2} = -n_\infty ez\left[\exp\left(-\frac{ze\psi}{kT}\right) - \exp\left(\frac{ze\psi}{kT}\right)\right] \tag{3-47a}$$

or

$$\varepsilon\varepsilon_o \frac{d^2\psi}{dx^2} = 2n_\infty ez \sinh\left(\frac{ze\psi}{kT}\right) \tag{3-47b}$$

where $n_{+\infty} = n_{-\infty} = n_\infty$ and n_∞ is the ionic number concentration in the bulk solution. The appropriate boundary conditions for Eq. (3-47) are

$x = 0 \qquad \psi = \psi_s$ (surface potential)
$x = \infty \qquad \psi = 0$

The surface potential ψ_s is normally equated to the zeta potential at the shear plane close to the surface.

The solution to Eq. (3-47b) is given by

$$\Psi = 2\ ln\left[\frac{1 + \exp(-\kappa x)\tanh\left(\frac{1}{4}\Psi_s\right)}{1 - \exp(-\kappa x)\tanh\left(\frac{1}{4}\Psi_s\right)}\right] \tag{3-48}$$

where

$$\Psi = \frac{ze\psi}{kT} \tag{3-49}$$

and

$$\Psi_s = \frac{ze\psi_s}{kT} \tag{3-50}$$

Ψ is the dimensionless potential and κ is the inverse Debye length defined as

$$\kappa^{-1} \doteq \left[\frac{\varepsilon\varepsilon_o kT}{2e^2z^2n_\infty}\right]^{1/2} \tag{3-51}$$

κ^{-1} is a measure of the thickness of the electric double layer and it is referred to as the Debye length.

Debye–Hückel Approximation. When the surface potential is small, say $\psi_s \ll 0.025\ V$, the term $ze\psi/kT$ is smaller than unity and one can approximate the hyperbolic function as follows:

$$\sinh\left(\frac{ze\psi}{kT}\right) \cong \frac{ze\psi}{kT} \quad \text{for} \quad \frac{ze\psi}{kT} \ll 1 \tag{3-52}$$

and Eq. (3-47b) can be written as

$$\frac{d^2\psi}{dx^2} = \frac{2e^2z^2n_\infty}{\varepsilon\varepsilon_o kT}\psi = \kappa^2\psi \tag{3-53}$$

With $\psi = \psi_s$ at $x = 0$ and $\psi = 0$ at $x = \infty$, the solution of Eq. (3-53) is given by

$$\psi = \psi_s \exp(-\kappa x) \tag{3-54}$$

or in dimensionless form as

$$\Psi = \Psi_s \exp(-\kappa x) \tag{3-55}$$

Figure 3-12a shows the variation of (ψ/ψ_s) with distance at different electrolyte concentrations using the Debye–Hückel approximation. Increasing the electrolyte concentration leads to fast decay in (ψ/ψ_s) and a smaller double-layer thickness.

Figure 3-12b shows the effect of the valence at fixed electrolyte concentration. The double-layer thickness is smaller for the 3:3 electrolyte as compared to the 1:1 electrolyte. Consequently, (ψ/ψ_s) decays faster for the 3:3 electrolyte.

Figures 3-13 and 3-14 show the decay of the dimensionless potential using various approximate expressions for the solution of the Poisson–Boltzmann equation (Russel *et al.*, 1989). The surface potential ψ_s is taken as –0.134 V, T = 298 K, $\varepsilon = 80$, $\kappa^{-1} = 3.08 \times 10^{-9}$ m and the molarity is 0.01 M.

Values of the Debye length (κ and κ^{-1}) for different electrolyte concentrations and types are given in Table 3-2. κ^{-1} varies from 9.61×10^{-9} m for a molarity of 0.001 for a 1:1 electrolyte to 3.2×10^{-10} m for a 3:3 electrolyte at a molarity of 0.1. Increasing the molarity of the electrolyte tends to decrease the value of the Debye inverse length (κ^{-1}).

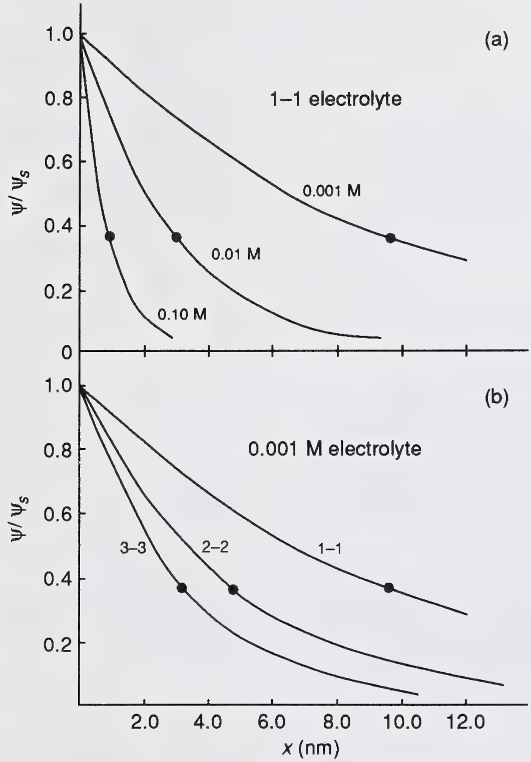

Figure 3-12. Normalized double-layer potential *versus* distance from a surface according to the Debye–Hückel approximation: (a) curves drawn for a 1:1 electrolyte at three concentrations and (b) curves drawn for 0.001 M symmetrical electrolytes of three different valence types. • signifies the corresponding value of κ^{-1} (Hiemenz, 1986).

It is of interest to sketch the variation of the ions concentration ratio along the coordinate normal to the surface.

Boltzmann distribution, Eq. (3-44), gives

$$n_i = n_{i\infty} \exp\left[-\frac{z_i e\psi}{kT}\right] \tag{3-44}$$

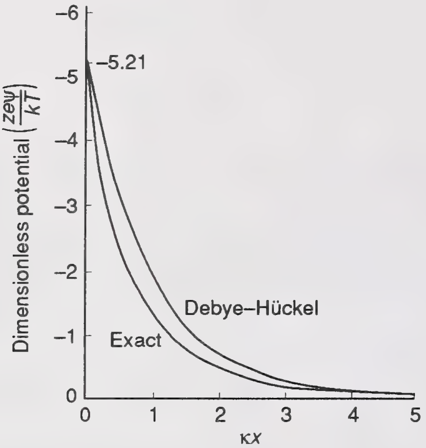

Figure 3-13. The decay of the electrostatic potential near a flat surface in an ionic solution as predicted using the exact solution of the Poisson–Boltzmann equation and the Debye–Hückel approximation (Russel *et al.*, 1989).

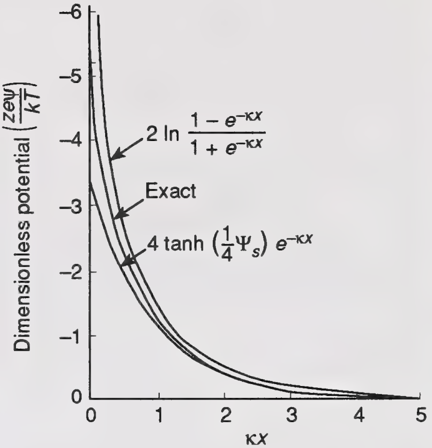

Figure 3-14. The decay of the electrostatic potential near a flat surface according to the exact solution of the Poisson–Boltzmann equation and two approximate solutions (Russel *et al.*, 1989).

For a symmetric (z:z) electrolyte and using Debye–Hückel approximation for the potential, we can write Eq. (3-44) as

$$\frac{n_+}{n_\infty} = \exp\left[-\Psi_s \exp(-\kappa x)\right] \tag{3-56}$$

$$\frac{n_-}{n_\infty} = \exp\left[\Psi_s \exp(-\kappa x)\right] \tag{3-57}$$

The dimensionless potential is given by Eq. (3-50) and the Debye–Hückel relationship for Ψ is given by Eq. (3-55). Plots of Eqs. (3-56) and (3-57) are shown in Figures 3-15a,b. The maximum deviation from the bulk conditions occurs at the surface.

The condition of neutrality is usually assumed to occur far away from the surface. It is given as

$$\sum z_i n_i = 0 \tag{3-58}$$

Table 3-2. Values of κ and κ^{-1} for several different electrolyte concentrations and valences with numerical formulas for these quantities also given for aqueous solutions at 25°C

		Symmetrical electrolyte			Asymmetrical electrolyte	
General formulas		$\kappa\left(m^{-1}\right) = 3.29\times10^{9}\,\lvert z\rvert\,M^{1/2}$	$\kappa^{-1}\,(m) = 3.04\times10^{-10}\,\lvert z\rvert^{-1}\,M^{-1/2}$		$\kappa\left(m^{-1}\right) = 2.32\times10^{9}\left(\sum_i z_i^2M_i\right)^{1/2}$	$\kappa^{-1}\,(m) = 4.30\times10^{-10}\left(\sum_i z_i^2M_i\right)^{-1/2}$
Molarity	$z_+:z_-$			$z_+:z_-$		
0.001	1:1	1.04×10^{8}	9.61×10^{-9}	1:2, 2:1	1.80×10^{8}	5.56×10^{-9}
	2:2	2.08×10^{8}	4.81×10^{-9}	3:1, 1:3	2.54×10^{8}	3.93×10^{-9}
	3:3	3.12×10^{8}	3.20×10^{-9}	2:3, 3:2	4.02×10^{8}	2.49×10^{-9}
0.01	1:1	3.29×10^{8}	3.04×10^{-9}	1:2, 2:1	5.68×10^{8}	1.76×10^{-9}
	2:2	6.58×10^{8}	1.52×10^{-9}	1:3, 3:1	8.04×10^{8}	1.24×10^{-9}
	3:3	9.87×10^{8}	1.01×10^{-9}	2:3, 3:2	1.27×10^{8}	7.87×10^{-10}
0.1	1:1	1.04×10^{9}	9.61×10^{-10}	1:2, 2:1	1.80×10^{9}	5.56×10^{-10}
	2:2	2.08×10^{9}	4.81×10^{-10}	1:3, 3:1	2.54×10^{9}	3.93×10^{-10}
	3:3	3.12×10^{9}	3.20×10^{-10}	2:3, 3:2	4.02×10^{9}	2.49×10^{-10}

(Hiemenz, 1986)

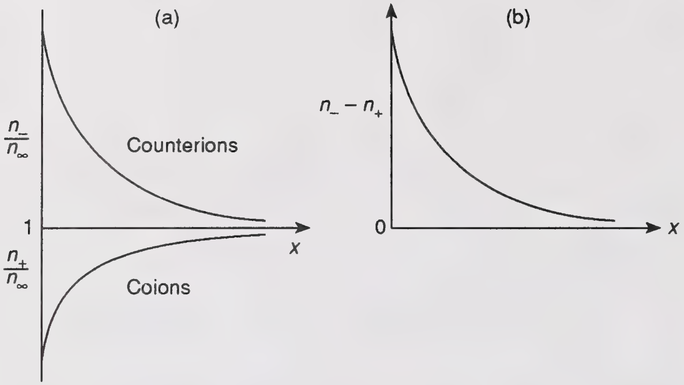

Figure 3-15. (a) Variation of n_+/n_∞ and n_-/n_∞ with distance away from surface, (b) variation of the excess of ions with distance away from the surface.

For a binary electrolyte,

(3-59) $$z_-n_- + z_+n_+ = 0$$

For a symmetric (z:z) electrolyte, Eq. (3-59) leads to

(3-60) $$n_- = n_+$$

The thickness of the Debye double layer κ^{-1} can be evaluated for a symmetric electrolyte as follows. κ^{-1} is given by

$$\kappa^{-1} = \left[\frac{\varepsilon\varepsilon_o kT}{2e^2z^2n_\infty}\right]^{1/2}$$

where ε = 78.5 water at 298 K (Table 3-1b)
ε_o = 8.85×10^{-12} C^2/Nm^2
T = 298 K
e = 1.602×10^{-19} C
N_a = 6.022×10^{23} mol^{-1}

Now n_∞ is the ionic number concentration and is given by

$$n_\infty = \left(\mathrm{M}\ \frac{\mathrm{mol}}{\mathrm{L}}\right) \times \left(1000\ \frac{\mathrm{L}}{\mathrm{m}^3}\right)\left(\mathrm{N}_a\ \frac{1}{\mathrm{mol}}\right)$$

$$n_\infty = 1000\ \mathrm{N}_a\mathrm{M}$$

The Debye length expression becomes

$$\kappa^{-1} = \frac{3.04}{z\sqrt{M}} \times 10^{-10}\ m \tag{3-61}$$

where M is the molarity of a $(z{:}z)$ electrolyte. For $z = 1$, κ^{-1} is given by

M	κ^{-1} μm
10^{-6}	0.304
10^{-4}	0.0304
10^{-2}	0.00304

Table 3-2 gives an extensive tabulation for κ^{-1} for different electrolyte concentrations. It is clear from the above tabulation that κ^{-1} decreases as the electrolyte concentration increases. At high molarity, the electric double-layer thickness becomes very small. On the other hand, in a non-electrolyte system, the double-layer thickness can be thought of extending to infinity (*i.e.*, a large distance from the surface).

3.6.2 Diffuse Electric Double Layer Around a Sphere

When a spherical particle is considered, the corresponding Poisson–Boltzmann equation is given below for a $(z{:}z)$ electrolyte solution.

$$\frac{1}{r^2}\frac{d}{dr}\left(r^2\frac{d\psi}{dr}\right) = \frac{2ezn_\infty}{\varepsilon\varepsilon_o}\sinh\left(\frac{ze\psi}{kT}\right) \tag{3-62}$$

subject to

$$\psi = \psi_s \text{ at } r = a \text{ (sphere surface or shear plane)} \tag{3-63}$$

$$\psi \rightarrow 0 \text{ as } r \rightarrow \infty$$

Eq. (3-62) assumes no angular variation of the potential ψ. No analytical solution exists for Eq. (3-62) with the associated boundary conditions of Eq. (3-63).

For a thin double layer, *i.e.*, $\kappa a \gg 1$, we can rescale Eq. (3-62) with

$$r = a\left(1 + \frac{y}{\kappa a}\right) \tag{3-64a}$$

and

$$\Psi = \frac{ze\psi}{kT} \tag{3-64b}$$

Eq. (3-62) becomes

$$\frac{d^2\Psi}{dy^2} + \frac{2}{\kappa a\left[1 + \frac{y}{\kappa a}\right]} \frac{d\Psi}{dy} = \sinh \Psi \tag{3-65}$$

with

$$\Psi = \Psi_s \text{ at } y = 0 \tag{3-66a}$$

and

$$\Psi \rightarrow 0 \text{ as } y \rightarrow \infty \tag{3-66b}$$

For $\kappa a \rightarrow \infty$, we recover the flat plate solution.

Making use of Debye–Hückel approximation for $\Psi_s << 1$, we obtain

$$\Psi = \Psi_s \exp\left[-\kappa a\left(\left(\frac{r}{a}\right) - 1\right)\right] \tag{3-67}$$

The decay in Ψ is exponential.

Loeb *et al.* (1961) give a comprehensive numerical treatment for the Ψ variation for a sphere for both symmetric and asymmetric electrolytes.

3.6.3 Surface Charge Density and Potential

The solution of the Poisson–Boltzmann equation allows the surface potential Ψ_s to be related to the surface-charge density q_s. Because of electroneutrality, the excess charge in a solution must balance the charge on the particle surface. It follows then for a flat surface

$$q_s = -\int_0^\infty \overset{(f)}{\rho}\, dx \tag{3-68}$$

where x is the coordinate normal to the surface and q_s is the surface charge density, C/m^2. From Eq. (3-38), the above equation gives

$$q_s = \int_0^\infty \varepsilon\varepsilon_o \frac{d^2\psi}{dx^2}\, dx = \varepsilon\varepsilon_o \int_0^\infty \frac{d}{dx}\left(\frac{d\psi}{dx}\right) dx$$

and

$$q_s = \varepsilon\varepsilon_o \left[\frac{d\psi}{dx}\right]_0^\infty = \varepsilon\varepsilon_o \left[\left.\frac{d\psi}{dx}\right|_\infty - \left.\frac{d\psi}{dx}\right|_0\right]$$

As $\left.\frac{d\psi}{dx}\right|_\infty \to 0$, we can write

(3-69) $$q_s = -\,\varepsilon\varepsilon_o \left.\frac{d\psi}{dx}\right|_0$$

Differentiating Eq. (3-48) and substituting the potential gradient at the surface into Eq. (3-69) lead to

(3-70) $$q_s = 2\left[2\varepsilon\varepsilon_o kTn_\infty\right]^{1/2} \sinh\left(\frac{1}{2}\Psi_s\right)$$

For $\Psi_s \ll 1$, one obtains

(3-71) $$q_s = \Psi_s \left[2\varepsilon\varepsilon_o kTn_\infty\right]^{1/2}$$

By setting

$$\kappa^{-1} = \left(\frac{\varepsilon\varepsilon_o kT}{2e^2z^2n_\infty}\right)^{1/2}$$

Eq. (3-70) becomes

(3-72) $$q_s = \left(\frac{2\varepsilon\varepsilon_o kT\kappa}{ez}\right) \sinh\left(\frac{1}{2}\Psi_s\right)$$

and for $\Psi_s \ll 1$, Eq. (3-72) becomes for an isolated flat surface

(3-73) $$q_s = \varepsilon\varepsilon_o\kappa\psi_s$$

Eqs. (3-70) to (3-73) relate the surface charge to the surface potential for a flat surface.

For the case of a sphere, Loeb *et al.* (1961) give an approximate formula for the surface charge as

(3-74) $$q_s = \frac{Q_s}{4\pi a^2} = \frac{\varepsilon\varepsilon_o kT}{ez}\kappa\left[2\sinh\left(\frac{1}{2}\Psi_s\right) + \frac{4}{\kappa a}\tanh\left(\frac{1}{4}\Psi_s\right)\right], \ \frac{\mathrm{C}}{\mathrm{m}^2}$$

For $\Psi_s \ll 1$, one obtains

(3-75) $$q_s = \frac{\varepsilon\varepsilon_o kT\kappa}{ez}\left(1+\frac{1}{\kappa a}\right)\left(\frac{ze\psi_s}{kT}\right) \quad \text{or} \quad q_s = \varepsilon\varepsilon_o\left(\frac{1+\kappa a}{a}\right)\psi_s$$

For $\kappa a \gg 1$, Eq. (3-75) becomes identical to the case of a flat surface. This is because for $\kappa a \gg 1$, the double layer becomes so thin that the surface curvature effect becomes unimportant.

3.7 SURFACE POTENTIAL MODELS

The surface charge, or the surface potential, is very much dependent on the surface chemistry and hence, on the origin of charge and on the bulk solution ionic concentration (Russel *et al.*, 1989). Various investigators proposed different models to predict surface potentials (*e.g.*, Haydon, 1964; Sparnaay, 1972; Chan *et al.*, 1975, 1976; Hunter, 1981, 1991; Takamura and Wallace, 1988). Two models will be discussed here to illustrate the connection between ionic bulk concentration and the surface potential. These models clearly illustrate that by changing the ionic strength, one not only changes the Debye length, but also the surface potential.

3.7.1 Model I

Consider silver iodide particles (AgI) suspended in an aqueous solution containing AgI as the major electrolyte. The difference between the electrochemical potentials of the *k*th ion in the solid phase and in solution is given by

(3-76) $$\Delta\mu^k = \Delta\mu_o^k + ez_k\Delta\psi$$

where z_k is the valence of the *k*th ionic species
$\Delta\psi$ is the electrical potential difference between the surface and the bulk solution

$\Delta\mu^k_o$ is the chemical potential for the kth species between the surface and the bulk solution

e is the elementary charge (1.602×10^{-19} C)

At equilibrium, $\Delta\mu^k = 0$ and we obtain

$$\Delta\psi = -\frac{\Delta\mu^k_o}{ez_k} \tag{3-77}$$

For an ideal solution,

$$d\mu^k_o = -\frac{kT}{n_k}\,dn_k = -kTd\left(ln\ n_\kappa\right) \tag{3-78}$$

where n_k is the ionic number concentration of the kth ionic species, m^{-3}.

Assume that for AgI systems, changes in composition of the solution affect the chemical potentials of Ag^+ and I^- in the solid phase very little; therefore we can write

$$d\Delta\mu^k_o \cong d\mu^k_o \tag{3-79}$$

leading to

$$d\,(\Delta\psi) = \frac{kT}{ez_k}\,d\left[ln\ n_k\right] \tag{3-80}$$

Eq. (3-80) indicates that a ten-fold increase in n_k leads to a relatively small change in the surface potential.

The ions responsible for the change in the surface potential are called the potential-determining ions (p.d.i.). For the system chosen, they are Ag^+ and I^- for AgI solutions. According to Eq. (3-80), the Nernst equation, the interphase potential difference (between the solid and the bulk of the liquid) changes by about 0.06 volts when the concentration of potential determining ions changes by a factor of 10 (Russel *et al.*, 1989).

3.7.2 Model II

A second example illustrates the effect of the bulk solution ionic concentration (Russel *et al.*, 1989). Suppose we have a surface that contains certain molecules that ionize as follows:

$$AH \rightleftharpoons A^- + H^+ \tag{3-81}$$

The dissociation constant is given by

$$K = \frac{[A^-]_s\,[H^+]_o}{[AH]_s} \tag{3-82}$$

$[A^-]_s$ and $[AH]_s$ denote concentration at the surface within the solid phase and $[H^+]_o$ denotes the hydronium ions concentration at the surface within the electrolyte solution liquid phase. Let the total ionizable groups surface concentration be

$$[n]_s = [A^-]_s + [AH]_s \tag{3-83}$$

One can write

$$[A^-]_s = \frac{K\,[n]_s}{K + [H^+]_o} \tag{3-84}$$

As the ionic concentration follows the Boltzmann distribution, we can write for a (1:1) electrolyte

$$[H^+] = [H^+]_b \exp\left[-\frac{e\psi}{kT}\right] \tag{3-85}$$

In the bulk solution we have $\psi = 0$ and $[H^+] = [H^+]_b$. Here $[H^+]_b$ is the concentration of H^+ in the bulk solution. Eq. (3-85) gives

$$[H^+]_o = [H^+]_b \exp\left[-\frac{e\psi_s}{kT}\right] \tag{3-86}$$

The above equation relates the ionic concentration in the solution at the surface to that in the bulk solution. The various concentrations are shown in Figure 3-16.

The surface charge density for a symmetric (1:1) electrolyte is given by Eq. (3-70) as

$$q_s = 2\left[2\varepsilon\varepsilon_o kT [H^+]_b\right]^{1/2} \sinh\left(\frac{e\psi_s}{2kT}\right)$$

For $e\psi_s/2kT \ll 1$, one can write

$$q_s = \left[2\varepsilon\varepsilon_o kT [H^+]_b\right]^{1/2} \left(\frac{e\psi_s}{kT}\right) \tag{3-87}$$

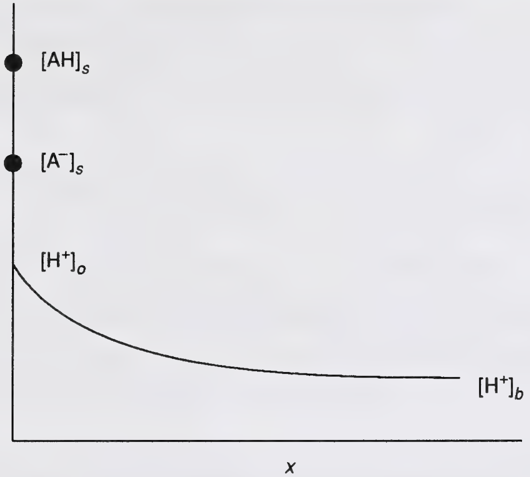

Figure 3-16. Variation of ionic concentration.

The surface charge density is precisely $-e[A^-]_s$; hence $q_s = -e[A^-]_s$ and it leads to

$$-e\left[A^-\right]_s = \left[\frac{2\varepsilon\varepsilon_o e^2 \left[H^+\right]_b}{kT}\right]^{1/2} \psi_s \tag{3-88}$$

Combining Eqs. (3-84) to (3-88) leads to

$$\psi_s = -\left[\frac{kT}{2\varepsilon\varepsilon_o e^2 \left[H^+\right]_b}\right]^{1/2} \left[\frac{e\,[n]_s\,K}{K + \left[H^+\right]_o}\right]$$

where $[H^+]_o$ is given by Eq. (3-86).

Assuming K = 10^{-5} M and $[n]_s = 10^{18}$ sites/m^2 at 20°C, one obtains

$[H^+]_b$	ψ_s, mV
10^{-5} M	−129
10^{-4}	−61
10^{-3}	−13
10^{-2}	−0.7

A change of $[H^+]_b$ of ten-fold affects ψ_s by a factor of 2–20.

Models based on more than one dissociation are given by Hunter (1981). Depending on the origin of charge, other models can be formulated to account for the variation in the surface charge and the ionic strength of the bulk solution. For example, such models can be used to estimate bitumen and solids surface potentials at various levels of pH (Takamura and Wallace, 1988).

3.8 FORCE BETWEEN TWO CHARGED BODIES

When two charged surfaces (or two colloidal particles), each surrounded by an electrical diffuse double layer, approach one another, their respective double layers begin to overlap. As a result, the ionic and potential distributions around a given particle or flat surface in the neighborhood of a second particle are no longer symmetrical. This causes asymmetrical stresses of electrical origin on the particle surface and as a result, the particle experiences a force.

The evaluation of the force can be made from the solution of the Poisson–Boltzmann equation for the potential coupled with the momentum equation. For the sake of simplicity, the force between two charged flat plates in a dielectric will be considered.

Consider two flat plates at constant surface potentials of ψ_a and ψ_b as shown in Figure 3-17. These surface potentials are held constant irrespective of the separation between the plates.

Poisson equation for the case of parallel plates is given by

$$\varepsilon\varepsilon_o \frac{d^2\psi}{dx^2} = -\rho^{(f)} \tag{3-89a}$$

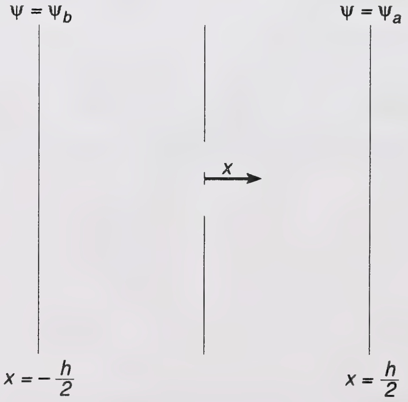

Figure 3-17. Parallel plates geometry.

Making use of Debye–Hückel approximation, Eq. (3-89a) becomes

$$\frac{d^2\psi}{dx^2} = \kappa^2\psi \tag{3-89b}$$

The momentum equation with the appropriate electric force is given by

$$\mu\nabla^2\vec{u} + \rho\vec{g} + \overset{(f)}{\rho}\vec{E} = \vec{\nabla}p \tag{3-90}$$

As there is no fluid flow we have $\vec{u} = \vec{0}$. Neglecting the effect of gravity, we can write Eq. (3-90) as

$$\vec{\nabla}p = \overset{(f)}{\rho}\vec{E} \tag{3-91}$$

For a one-dimensional variation, we have

$$\frac{dp}{dx} = \overset{(f)}{\rho}E_x \tag{3-92}$$

where

$$E_x = -\frac{d\psi}{dx} \tag{3-93}$$

One can combine Eqs. (3-92) and (3-93), leading to

$$\frac{dp}{dx} + \overset{(f)}{\rho}\frac{d\psi}{dx} = 0 \tag{3-94}$$

Combining Eqs. (3-89a) and (3-94) leads to

$$\frac{dp}{dx} - \varepsilon\varepsilon_o\frac{d^2\psi}{dx^2}\cdot\frac{d\psi}{dx} = 0 \tag{3-95}$$

The above equation relates the pressure (in this case, the osmotic pressure) with the potential ψ. The osmotic pressure arises due to variation in the ionic concentration between the plates and the surrounding electrolyte solution.

Integration of Eq. (3-95) gives

$$p - \left(\frac{\varepsilon\varepsilon_o}{2}\right)\left(\frac{d\psi}{dx}\right)^2 = C_1 \tag{3-96a}$$

where C_1 is the integration constant.

C_1 is the required force per unit area to keep the two plates from moving. For this particular case, it turns out that the difference between the osmotic pressure p and the electric force per unit area is constant everywhere within the two plates.

Replacing C_1 by F/A_p, Eq. (3-96a) becomes

$$\frac{F}{A_p} = p - \left(\frac{\varepsilon\varepsilon_o}{2}\right)\left(\frac{d\psi}{dx}\right)^2 \tag{3-96b}$$

We need to determine p and ψ in order to evaluate the force per unit area, F/A_p. The solution of Eq. (3-89b) gives

$$\psi = A_1 \cosh \kappa x + B_1 \sinh \kappa x \tag{3-97}$$

Making use of the boundary conditions of ψ at $x = \pm h/2$, the constants of integration are given by

$$A_1 = \frac{\psi_a + \psi_b}{2 \cosh \frac{\kappa h}{2}} \quad \text{and} \quad B_1 = \frac{\psi_a - \psi_b}{2 \sinh \frac{\kappa h}{2}}$$

For the special case of $\psi_a = \psi_b$, $B_1 = 0$.

The osmotic pressure, p, is given for a dilute system by van't Hoff's law

$$p = \sum \left(n_k - n_\infty\right) kT \tag{3-98}$$

where $\Sigma\,(n_k - n_\infty)$ is the excess ions concentration.

Making use of Boltzmann's distribution, Eq. (3-98) can be written for a $(z{:}z)$ electrolyte as

$$p = kT\left[\left\{n_\infty \exp\left(-\frac{ze\psi}{kT}\right) - n_\infty\right\} + \left\{n_\infty \exp\left(\frac{ze\psi}{kT}\right) - n_\infty\right\}\right]$$

leading to

$$p = \frac{n_\infty kTz^2e^2\psi^2}{k^2T^2} \tag{3-99}$$

where $\frac{ze\psi}{kT}$ is assumed to be much less than unity.

Making use of the expression for p given by Eq. (3-99), the expression for the force per unit area, Eq. (3-96b), becomes

$$\text{(3-100)} \quad \frac{F}{A_p} = n_\infty kT \left(\frac{ze\psi}{kT}\right)^2 - \frac{\varepsilon\varepsilon_o}{2}\left(\frac{d\psi}{dx}\right)^2$$

Making use of the solution for ψ, one obtains

$$\text{(3-101)} \quad \frac{F}{A_p} = \left(\frac{e^2 z^2 n_\infty}{kT}\right)\left[A_1^2 - B_1^2\right]$$

Using the expressions for A_1 and B_1, Eq. (3-101) becomes

$$\text{(3-102)} \quad \frac{F}{A_p} = \frac{e^2 z^2 n_\infty}{kT}\left[\frac{2\psi_a\psi_b \cosh \kappa h - \psi_a^2 - \psi_b^2}{\sinh^2 \kappa h}\right]$$

For the special case of $\psi_a = \psi_b = \psi_s$, the above expression reduces to

$$\text{(3-103)} \quad \frac{F}{A_p} = \left(\frac{2e^2 z^2 n_\infty \psi_s^2}{kT}\right)\left[\frac{\cosh \kappa h - 1}{\sinh^2 \kappa h}\right]$$

For small κh, one can write $\cosh \kappa h \cong 1 + (\kappa h)^2/2$ and $\sinh \kappa h \cong \kappa h$.

Eq. (3-103) becomes for $\kappa h \ll 1$

$$\text{(3-104)} \quad \frac{F}{A_p} = \left(\frac{e^2 z^2 n_\infty}{kT}\right)\psi_s^2 = \frac{1}{2}\,\varepsilon\varepsilon_o\kappa^2\psi_s^2$$

Eq. (3-104) indicates that for small κ, the force per unit area is proportional to ψ_s^2 and it is independent of the separation gap.

For $\kappa h \gg 1$, we can write $\cosh \kappa h \approx \sinh \kappa h \approx (1/2)\, e^{\kappa h}$. Eq. (3-103) becomes for $\kappa h \gg 1$,

$$\text{(3-105)} \quad \frac{F}{A_p} = \left(\frac{4e^2 z^2 n_\infty}{kT}\right)\psi_s^2 e^{-\kappa h}$$

or

$$(3\text{-}106) \qquad \frac{F}{A_p} = 2\varepsilon\varepsilon_o\kappa^2\psi_s^2 e^{-\kappa h}$$

For more details, see Russel *et al.* (1989), Probstein (1989), van de Ven (1989), Ross and Morrison (1988), and Chan *et al.* (1975, 1976).

For $\psi_a \neq \psi_b$, the force per unit area, Eq. (3-102) predicts repulsive interactions at large separations. However, at small separations, the interaction becomes attraction. This is, of course, assuming that the surface potentials are held constant. Figure 3-18 shows a plot for Eq. (3-102) with different dimensionless values of surface potentials. The behaviour at close separations results from a change in the sign of the charge on one of the plates due to the overlapping double layers.

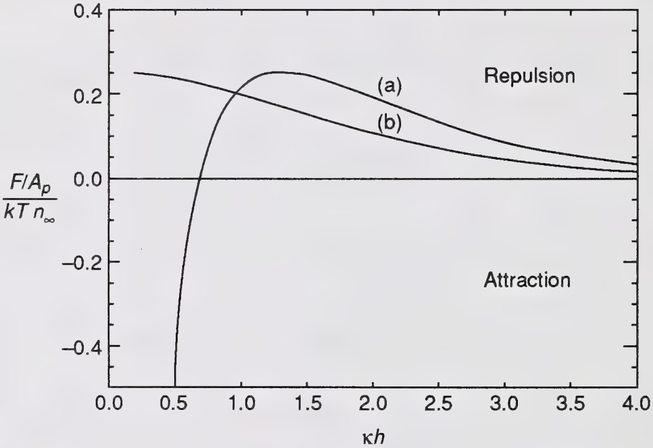

Figure 3-18. Electrostatic force between two flat plates having constant surface potentials.
(a) $\Psi_a = 0.5, \Psi_b = 1.0$
(b) $\Psi_a = \Psi_b = 0.5$

For the case where the surface charges are held constant, one has

$$A_1 = \frac{1}{2} \cdot \frac{\left(q_a + q_b\right)/\varepsilon\varepsilon_o\kappa}{\sinh \frac{1}{2}\kappa h} \qquad B_1 = \frac{1}{2} \cdot \frac{\left(q_a - q_b\right)/\varepsilon\varepsilon_o\kappa}{\cosh \frac{1}{2}\kappa h}$$

where q_a and q_b are the surface charge densities on surfaces *a* and *b* of Figure 3-17.

Depending on the relative magnitude of the surface charges, the force can change from attraction to repulsion as the plates are brought together. Interaction between particles with dissimilar charges are at the heart of heterocoagulation processes (see Hogg *et al.*, 1966; Gregory, 1975; Ohshima *et al.*, 1982; Russel *et al.*, 1989; McCartney and Levine, 1969; Sparnaay, 1972; Overbeek, 1990; Kihira *et al.*, 1992).

For the case of two spheres, the Derjaguin approximation gives (Russel *et al.*, 1989):

Constant potential

$$F \approx 2\pi\varepsilon\varepsilon_o \left(\frac{kT}{ze}\right)^2 \kappa a \Psi_s^2 \frac{\exp(-\kappa h)}{1 + \exp(-\kappa h)} \tag{3-107}$$

Constant charge

$$F \approx 2\pi\varepsilon\varepsilon_o \left(\frac{kT}{ze}\right)^2 \kappa a q_s^{*2} \frac{\exp(-\kappa h)}{1 - \exp(-\kappa h)} \tag{3-108}$$

where $q_s^* = \dfrac{q_s}{\varepsilon\varepsilon_o\kappa\,(kT/ze)}$

For details, see McCartney and Levine (1969).

It should be recognized that for the case of holding the charge constant, the boundary conditions at the plate surface for the case of nearly equal surface potentials become

$$q_s = -\varepsilon\varepsilon_o \left.\frac{d\psi}{dw}\right|_{\text{surface}}$$

as was given by Eq. (3-69). In other words $d\psi/dw$ is held constant rather than ψ on the plate surface. Here, w is the *outward normal* to the surface.

3.9 DERJAGUIN APPROXIMATION

It was indicated earlier that the potential distribution near surfaces other than a flat plate is difficult to obtain analytically. It follows, therefore, that the force experienced due to the approach of two spheres, two cylinders, a sphere and a flat plate, or a cylinder and a flat plate is difficult to evaluate analytically.

A useful approximation is to replace particles with curved boundaries by a series of flat strips, since for each of these, the force per unit area can be found from Eqs. (3-102), (3-105), or (3-106). This is known as the Derjaguin approximation (Derjaguin, 1934; van de Ven, 1989). For the case of interaction between two spheres, the details of the method are outlined by Ross and Morrison (1988). Each surface of the sphere is considered to have a stepped surface and the electrostatic "repulsion" between two charged spheres is approximated as the sum of a series of separate repulsions between parallel rings of graded diameters facing each other in matched pairs. The interaction between the spheres is thus reduced to the sum of interactions between parallel walls at different distances of separation.

Figure 3-19 shows the interaction between two spheres. Let F_{sp} be the total force on the sphere and F_p be the force per unit area on the plate. Then, the total force on the sphere is given by

$$(3\text{-}109)\quad F_{sp} = \int_0^{\infty} F_p \; 2rsds$$

Now, from geometrical considerations, we have

$$(3\text{-}110)\quad \frac{H - H_o}{2} = a - \sqrt{a^2 - s^2}$$

Differentiation of Eq. (3-110) leads to

$$(3\text{-}111)\quad dH = \frac{2sds}{\sqrt{a^2 - s^2}}$$

In the region of interest (*i.e.*, facing areas), $a^2 \gg s^2$ and Eq. (3-111) reduces to

$$(3\text{-}112)\quad dH \approx \frac{2s}{a} ds$$

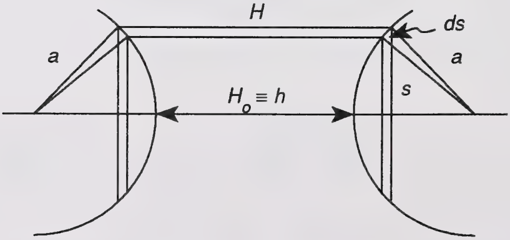

Figure 3-19. Derjaguin geometrical approximation.

The force on a sphere becomes

$$(3\text{-}113) \quad F_{sp} = \int F_p \left[\frac{a\,dH}{2s}\right] 2\pi s$$

leading to

$$(3\text{-}114) \quad F_{sp} = \pi a \int_{H_o}^{\infty} F_p \, dH$$

The expression for $F_p \equiv F/A_p$ is given by Eq. (3-102) or its derivatives. The inherent approximation in Eq. (3-114) is that one has a thin double layer as compared to the particle size.

Making use of expression (3-106) for flat plates having $\kappa h \gg 1$, Eq. (3-114) becomes

$$(3\text{-}115) \quad F_{sp} = \pi a \int_{H_o}^{\infty} 2\varepsilon\varepsilon_o \kappa^2 \psi_s^2 e^{-\kappa H} \, dH$$

The above equation gives the force on the sphere while setting $H_o \equiv h$

$$(3\text{-}116) \quad F_{sp} = 2\pi\varepsilon\varepsilon_o \kappa a \psi_s^2 e^{-\kappa h}$$

where the separation distance (surface-to-surface) is given by h and centre-to-centre separation is given by r, where

$$(3\text{-}117) \quad r = 2a + h$$

Implicitly Eq. (3-116) has the following assumptions:

(a) Gouy–Chapman double layer model,

(b) Debye–Hückel low ψ approximation,

(c) $\kappa a \gg 1$ (*i.e.*, thin double layers).

It should be noted that the expression given by Eq. (3-107), which was derived from Eq. (3-103), reduces to that of Eq. (3-116) for $\kappa h \gg 1$. A brief discussion of other geometries is given by van de Ven (1989).

3.10 ELECTROSTATIC POTENTIAL ENERGY

The repulsion between particles due to electrostatic forces are most conveniently characterized in terms of the electrostatic potential energy, ϕ. Recognizing that work or energy is related to force by

$$\text{Force} = -\frac{\mathrm{d}\,(\text{work})}{\mathrm{d}\,(\text{distance})} = -\frac{\mathrm{d}\,(\text{energy})}{\mathrm{d}\,(\text{distance})} \tag{3-118}$$

one can write

$$\phi = -\int_{\infty}^{h} [\text{force}]\; dh \tag{3-119}$$

where by convention, the potential is given by bringing a particle from infinity to a separation distance h.

For the case of a sphere being brought from infinity to a separation distance h from another identical sphere, we can write using Eq. (3-116)

$$\phi = -\int_{\infty}^{h} 2\pi\varepsilon\varepsilon_o\kappa a\psi_s^2 e^{-\kappa h}\, dh \tag{3-120}$$

Hence

$$\phi = 2\pi a\varepsilon\varepsilon_o\psi_s^2 e^{-\kappa h} \tag{3-121}$$

or

$$\phi = 2\pi a\varepsilon\varepsilon_o\psi^2 e^{-(r-2a)\kappa} \tag{3-122}$$

Hogg *et al.* (1966) made use of the Derjaguin approximation for unequal-sized spheres of radii a_1 and a_2 with surface potential ψ_s to give

$$\phi = \left[\frac{4\pi\varepsilon\varepsilon_o a_1 a_2\psi_s^2}{(a_1 + a_2)}\right] ln\left[1 + \exp(-\kappa h)\right] \tag{3-123}$$

The general expression for the potential of unequal spheres having potential ψ_1 and ψ_2 is given by Hogg *et al.* (1966). It is usually referred to as the HHF expression:

$$\phi = \frac{\pi\varepsilon\varepsilon_o a_1 a_2}{a_1 + a_2}\left\{2\psi_1\psi_2 \; ln\left[\frac{1 + \exp(-\kappa h)}{1 - \exp(-\kappa h)}\right] + \left(\psi_1^2 + \psi_2^2\right) ln\left[1 - \exp(-2\kappa h)\right]\right\} \tag{3-124}$$

Although the HHF equation is widely used, its applicability should be considered very carefully. The Stern potential must be small enough, *i.e.*, $ze\psi/kT < 1$, and the radii of the spheres must be large enough as compared to the thickness of the double layer, $\kappa a > 10$. More recently, Overbeek (1990) developed non-linear formulations for the evaluation of the double-layer interaction energy for dissimilar particles (Kihira *et al.*, 1992; Kihira and Matijevic, 1992).

The reader is referred to previous studies dealing with double-layer interaction for various geometries: Bell *et al.*, 1970; Chan and Chan, 1983; Hogg *et al.*, 1966; McCartney and Levine, 1969; Ohshima *et al.*, 1982; and White, 1977.

3.11 ZETA POTENTIAL

In our previous discussion of the diffuse electric double-layer we have assumed that the ions are point charges and that the inner boundary of the electric double layer is located at the surface of the particle or material under consideration. The location of the outer boundary is characterized by the inverse Debye length. To this end, the surface potential of a particle in a dielectric medium becomes that "seen" by the fluid surrounding the particle. For a stationary surface, the no-slip velocity occurs at the charged particle surface itself.

In real systems, ions are of finite size and they can approach a surface to a distance not less than their radii. Stern (1924) proposed a model in which the electric double layer inner boundary is given by approximately one hydrated ion radius. This inner boundary is referred to as the Stern plane. The gap between the Stern plane and the surface is denoted as the Stern layer. The electric potential changes from the surface potential ψ_s to a Stern plane potential ψ_d within the Stern layer and it decays to zero far away from the Stern plane as shown in Figure 3-20. The centres of any ions "attached" to the surface are located within the Stern layer and they are considered to be immobile. Ions whose centres are located beyond the Stern plane form the diffuse mobile part of the electric double layer. Consequently, the mobile inner part of the electric double layer is located between one to two radii away from the surface. This boundary is referred to as the shear plane as shown in Figure 3-20a. It is on this plane where the no-slip fluid flow boundary condition is assumed to apply. The potential at the shear plane is referred to as the electrokinetic potential, more commonly known as zeta (ζ) potential. It is marginally different in magnitude from the Stern potential ψ_d as shown in Figure 3-20b. Shaw (1980) stated that it is customary to identify ψ_d with ζ and that experimental evidence suggests that the introduced errors are small. Electrophoretic potential measurements give the zeta potential of a surface. Although one at

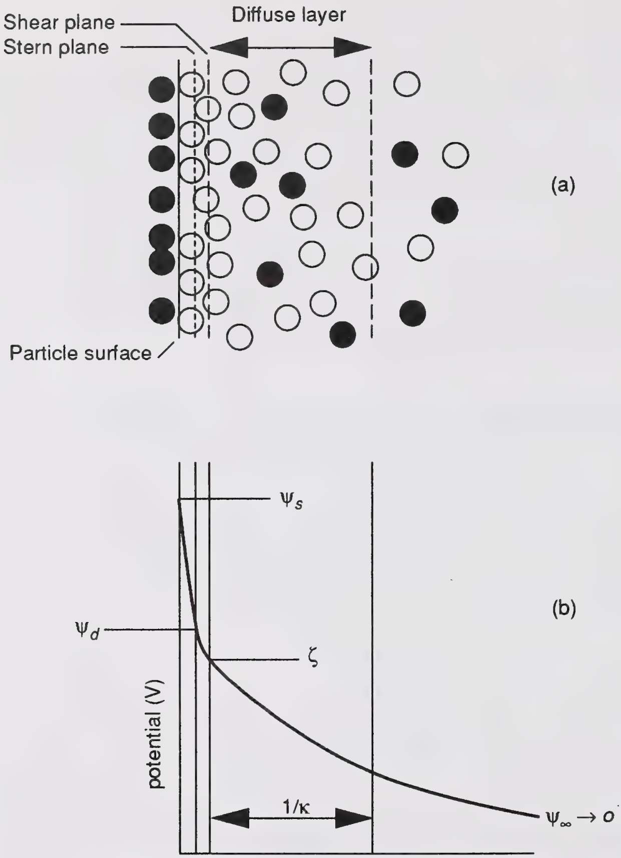

Figure 3-20. Schematic representation of the electric double layer according to Stern's model. ●, coions; ○, counterions (adapted from Shaw, 1980).

times refers to a "surface potential," strictly speaking, it is the zeta potential that needs to be specified. Gouy–Chapman treatment of Section 3.6 deals with the diffuse electric layer whose inner boundary is the shear plane.

It should be noted that adsorbed ions can have marked effects on the zeta potential when compared with the surface potential. Adsorbed polyvalent or surface active counterions can cause reversal of charge to occur within the Stern layer as is shown in Figure 3-21a, where ψ_s and ζ have different signs. On the other hand, adsorption of surface active coions can create a situation in which ψ_d has the same sign as ψ_s and is greater in magnitude than ψ_s. From the above discussion, it is clear that zeta potential measurements do not give direct information about the surface potential itself when adsorbed ions are present (Shaw, 1980).

The mobile portion of the diffuse electric layer interaction with an external or induced electric field gives rise to an electrokinetic transport phenomenon. For example, when an electric field is applied tangentially along a charged surface, the electric field will exert a force on the ions within the mobile diffuse electric layer close to the charged surface, resulting in their motion. In turn, the moving ions will drag the surrounding liquid along, thus resulting in the liquid's flow. The various types of electrokinetic phenomena will be outlined in Chapter 5.

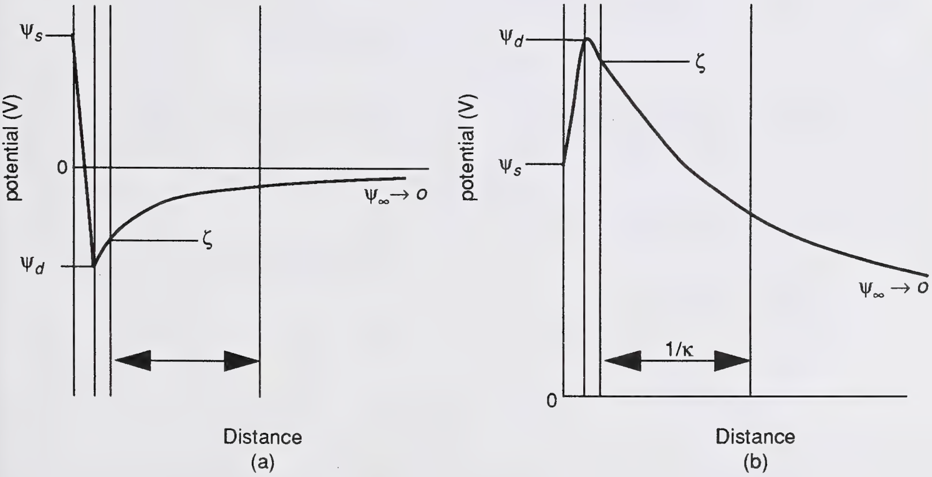

Figure 3-21. Potential variation with distance for a charged surface: (a) potential reversal due to adsorption of surface active or polyvalent counterions, (b) adsorption of surface active coions (adapted from Shaw, 1980).

3.12 SUMMARY OF GOUY–CHAPMAN MODEL

Arbitrary electrolyte	**Symmetrical (*z*:*z*) electrolyte**
Charge density $\overset{(f)}{\rho} = \sum_i z_i e n_i = e \sum z_i n_{i\infty} \exp\left(-\frac{z_i e\psi}{kT}\right)$	Charge density $\overset{(f)}{\rho} = ze\,(n_+ - n_-)$ $= -\,2zen_\infty \sinh\left(\frac{ze\psi}{kT}\right)$
Condition for Neutrality $\sum_i z_i n_i = 0$	Condition for Neutrality $n_+ - n_- = 0$
Poisson–Boltzmann Equation $\nabla^2\psi = -\frac{e}{\varepsilon\varepsilon_o} \sum z_i n_{i\infty} \exp\left(-\frac{z_i e\psi}{kT}\right)$	Poisson–Boltzmann Equation $\nabla^2\psi = \frac{2zen_\infty}{\varepsilon\varepsilon_o} \sinh\left(\frac{ze\psi}{kT}\right)$
Linearized Poisson–Boltzmann Equation $(z_i e\psi/kT) < 1$; Debye–Hückel Approximation $\nabla^2\psi = -\frac{e}{\varepsilon\varepsilon_o} \sum_i \left[z_i n_{i\infty} - \frac{z_i^2 n_{i\infty} e\psi}{kT}\right]$ $= \frac{e^2}{\varepsilon\varepsilon_o kT} \sum_i z_i^2 n_{i\infty}\psi$ or $\nabla^2\psi = \kappa^2\psi$	Linearized Poisson–Boltzmann Equation $(z_i e\psi/kT) < 1$; Debye–Hückel Approximation $\nabla^2\psi = \frac{2zen_\infty}{\varepsilon\varepsilon_o} \cdot \frac{ze\psi}{kT} = \frac{2z^2e^2n_\infty}{\varepsilon\varepsilon_o kT}\psi$ or $\nabla^2\psi = \kappa^2\psi$
where $\kappa^2 = \frac{2e^2}{\varepsilon\varepsilon_o kT} \sum \frac{1}{2} z_i^2 n_{i\infty}$	where $\kappa^2 = \frac{2z^2e^2n_\infty}{\varepsilon\varepsilon_o kT}$
(Adapted from Neale, 1974)	

3.13 FORMS OF VARIOUS NOTATIONS

Various notations are used in the electrostatics literature. The forms of the equations are different depending whether number or molar concentrations are used. For example, Eq. (3-47b) can be written as

$$\frac{d^2\psi}{dx^2} = \frac{2zFc_\infty}{\varepsilon\varepsilon_o} \sinh\left(\frac{zF\psi}{RT}\right) \tag{3-125}$$

with

$$\kappa^{-1} = \left(\frac{\varepsilon\varepsilon_o RT}{2z^2F^2c_\infty}\right)^{1/2}$$

c is the molar concentrations (mol/m^3) and c_∞ is the value of c in the bulk electrolyte solution. This type of notation can be easily converted to the notation used in this chapter by recognizing the following relationships:

(3-126a) $F = eN_a$, Faraday constant

(3-126b) $R = kN_a$, Universal gas constant

(3-126c) $n = cN_a$

and

(3-126d) $Fc = ne$

In this respect, we have

$$\frac{zF}{RT} \equiv \frac{ze}{kT}, \ i.e., \ \frac{e}{kT} \equiv \frac{F}{RT} \tag{3-127}$$

and

$$\frac{2ezn_\infty}{\varepsilon\varepsilon_o} \equiv \frac{2zFc_\infty}{\varepsilon\varepsilon_o} \quad i.e., \ ne \equiv Fc \tag{3-128}$$

and

$$\kappa^{-1} = \left(\frac{\varepsilon\varepsilon_o RT}{2z^2F^2c_\infty}\right)^{1/2} \equiv \left(\frac{\varepsilon\varepsilon_o kT}{2e^2z^2n_\infty}\right)^{1/2} \tag{3-129}$$

where F is Faraday number, C/mol
N_a is Avogadro number, mol^{-1}
c is the ionic molar concentration, mol/m^3
n is the ionic number concentration, m^{-3}
e is the fundamental charge, C
R is the Universal gas constant, J/K mol
k is the Boltzmann constant, J/K

3.14 NOMENCLATURE

a	spherical particle radius, m
A_p	parallel plates area, m^2
c	molar concentration, mol/m^3
c_∞	bulk molar concentration, mol/m^3
$\vec{d}$	vector describing average orientation of the dipole and charge separation distance
e	elementary charge, C
E_x	field strength in x-direction, V/m
E_y	field strength in y-direction, V/m
E_z	field strength in z-direction, V/m
E_r	field strength in r-direction, V/m
E_θ	field strength in θ-direction, V/m
E_ϕ	field strength in ϕ-direction, V/m
$\vec{E}$	electric field strength vector, V/m
F	Faraday number, C/mol
$\vec{F}$	force vector, N
F_p	interaction force between parallel plates, N
F_{sp}	interaction force between spheres, N
g	acceleration due to gravity, m/s^2
H, H_o, h	separation distance, m
$\vec{i}$	unit vector
k	Boltzmann constant, J/K
K	dissociation constant, m^{-3}
l	length, m

m	mass of a helium atom
$\vec{n}$	outwards normal vector
n_∞	ionic number concentration in the bulk solution, m^{-3}
$n_{i\infty}$	ionic number concentration of the ith species in the bulk solution, m^{-3}
n_+	ionic number concentration of the positive ions, m^{-3}
n_-	ionic number concentration of the negative ions, m^{-3}
N	dipole density, m^{-3}
N	number of ionic species
N_a	Avogadro number, mol^{-1}
p	fluid pressure, N/m^2 or Pa
$\vec{P}$	polarization dipole moment, m^2
q_a, q_b, q_s	surface charge density, C/m^2
q_s	surface charge density, C/m^2
Q	total charge, C
r	centre-to-centre separation, m
r	distance between two particles, m
$\vec{r}$	position vector, m
R	Universal gas constant, J/K mol
S	surface area, m^2
$\vec{t}$	tangent vector
T	absolute temperature, K
$\vec{u}$	fluid velocity vector, m/s
V	volume, m^3
W	Energy, J
x	height, coordinate or a distance, m
z	absolute value of valency for a $(z{:}z)$ electrolyte solution
z_i, z_k	valency of the ith ionic species
(x, y, z)	Cartesian coordinates
(r, θ, ϕ)	spherical coordinates

$[\ ]_b$	number bulk concentration, m^{-3}
$[\ ]_o$	number concentration at surface within the electrolyte solution, m^{-3}
$[\ ]_s$	number concentration at surface within the solid phase, m^{-2}

ε_o	permittivity of vacuum, $C^2/N\,m^2$ or C/Vm
ε	dielectric constant, dimensionless
ζ	zeta potential, V
κ	inverse Debye length, m^{-1}
κ^{-1}	Debye length, m
$\overset{(e)}{\rho}$	total electric charge density, C/m^3
$\overset{(f)}{\rho}$	free charge density, C/m^3
$\overset{(p)}{\rho}$	polarization charge density, C/m^3
ϕ	electrostatic potential energy, J
χ	susceptibility of the dielectric material
ψ	potential, V
ψ_a, ψ_b, ψ_c	surface potential, V
ψ_s	surface potential, V
ψ_d	Stern plane potential, V
Ψ	dimensionless potential, $ze\psi/kT$
Ψ_s	dimensionless surface potential, $ze\psi_s/kT$
$\vec{\nabla}$	del operator, m^{-1}
∇^2	Laplacian operator, m^{-2}

3.15 REFERENCES

Bell, G.M., Levine, S., and McCartney, L.N. (1970), *Approximate Methods of Determining the Double-Layer Free Energy of Interaction Between Two-Charged Colloidal Spheres*, J. Colloid Interface Sci., **33**, 355–59.

Chan, B.K. and Chan, D.Y.C. (1983), *Electrical Double-Layer Interaction Between Spherical Colloid Particles: An Exact Solution*, J. Colloid Interface Sci., **92**, 281–83.

Chan, D.Y.C., Healy, T.W., and White, L.R. (1976), *Electrical Double-Layer Interaction Under Regulation by Surface Ionization Equilibria Dissimilar Amphoteric Surfaces*, J. Chem. Soc. Faraday Trans., *I*, **72**, 2844–65.

Chan, D.Y.C., Perram, J.W., White, L.R., and Healy, T.W. (1975), *Regulation of Surface Potential at Amphoteric Surfaces During Particle–Particle Interaction*, J. Chem. Soc. Faraday Trans., *I*, **71**, 1046–57.

Derjaguin, B.V. (1934), Kolloid, Z., **69**, 155.

Everett, D.H. (1988), *Basic Principles of Colloid Science*, Royal Society of Chemistry, London.

Eyges, L. (1980), *The Classical Electromagnetic Field*, Dover Books, New York.

Feynman, R.P., Leighton, R.B., and Sands, M. (1964), *The Feynman Lectures on Physics, vol. II*, Addison–Wesley, Reading, MA.

Gregory, J. (1975), *Interaction of Unequal Double Layers at Constant Charge*, J. Colloid Interface Sci., **51**, 44–51.

Haydon, D.A. (1964), *The Electrical Double-Layer and Electrokinetic Phenomena, in Progress in Surface Science, vol. I* (ed. Danelli, J.F., *et al.*), pp. 94–158, Academic Press, London.

Hiemenz, P.C. (1986), *Principles of Colloid and Surface Chemistry*, 2nd ed., Marcell Dekker, Inc., New York.

Hogg, R., Healy, T.W., and Fuerstenau, D.W. (1966), *Mutual Coagulation of Colloidal Dispersions*, Trans. Faraday Soc., **62**, 1638–51.

Hunter, R.J. (1981), *Zeta Potential in Colloid Science*, Academic Press, London.

Hunter, R.J. (1991), *Foundations of Colloid Science, vol. I.*, Oxford University Press, Oxford.

Israelachvili, J.N. (1985), *Intermolecular and Surface Forces*, Academic Press, London.

Kihira, H. and Matijevic, E. (1992), *An Assessment of Heterocoagulation Theories*, Advances in Colloid and Interface Science, **42**, 1–31.

Kihira, H., Ryde, N., and Matijevic, E. (1992), *Kinetics of Heterocoagulation, I. A Comparison of Theory and Experiment*, Colloids and Surfaces, **64**, 317–24.

Loeb, A.L., Overbeek, J.Th.G., and Wiersema, P.H. (1961), *The Electric Double-Layer Around a Spherical Colloid Particle*, MIT Press, Boston.

McCartney, L.N. and Levine, S. (1969), *An Improvement on Derjaguin's Expression at Small Potentials for the Double-Layer Interaction Energy of Two Spherical Colloidal Particles,* J. Colloid Interface Sci., **30**, 345–54.

Neale, G. (1974), *Lecture Notes in Electrokinetics*, Dept. of Chemical Engineering, University of Alberta, Edmonton, Alberta, Canada.

Ohshima, H., Healy, T.W., and White, L.R. (1982), *Improvement on the Hogg–Healey–Fuerstenau Formulas for the Interaction of Dissimilar Double Layers*, J. Colloid Interface Sci., **89**, 484–93.

Overbeek, J.T.G. (1990), *The Role of Energy and Entropy in the Electrical Double Layer*, Colloids and Surfaces, **51**, 61–75.

Probstein, R.F. (1989), *Physicochemical Hydrodynamics*, Butterworths, Boston.

Ross, S. and Morrison, I.D. (1988), *Colloidal Systems and Interfaces*, John Wiley and Sons, New York.

Russel, W.B., Saville, D.A., and Schowalter, W.R. (1989), *Colloidal Dispersions*, Cambridge University Press, Cambridge.

Shaw, D.J. (1980), *Introduction to Colloid and Surface Chemistry,* 3rd ed., Butterworths, London.

Slater, J.C. and Frank, N.H. (1969), *Electromagnetism*, Dover Books, New York.

Sparnaay, M.J. (1972), *The Electrical Double Layer*, Pergamon Press, New York.

Stern, O. (1924), *Z. Elecktrochem.*, **30**, 508.

Takamura, K. and Wallace, D. (1988), *The Physical Chemistry of the Hot Water Process*, J. Can. Pet. Tech., **27**, 98–106.

van de Ven, T.G.M. (1989), *Colloidal Hydrodynamics*, Academic Press, London.

White, L.R. (1977), *Approximate Analytic Solution of the Poisson–Boltzmann Equation for a Spherical Colloid Particle*, J. Chem. Soc. Faraday Trans., *II*, **73**, 377–96.

TRANSPORT EQUATIONS IN ELECTROLYTIC SOLUTIONS

4

4.1 SINGLE-COMPONENT SYSTEM: NO ELECTRIC FORCE

Fluid flow of a single-component system under laminar flow conditions with constant density and viscosity is governed by the Navier–Stokes equation (Bird *et al.*, 1960). It is given by

$$\text{(4-1)} \qquad \underset{\text{I}}{\rho\frac{\partial\vec{u}}{\partial t}} + \underset{\text{II}}{\rho\vec{u}\cdot\vec{\nabla}\vec{u}} = \underset{\text{III}}{-\vec{\nabla}p} + \underset{\text{IV}}{\mu\nabla^2\vec{u}} + \underset{\text{V}}{\rho\vec{g}}$$

where $\vec{u}$ is the fluid velocity vector as would be measured by a pitot tube or a laser Doppler velocity meter (m/s)
p is the fluid pressure (Pa or N/m^2)
$\vec{g}$ is the acceleration due to gravity (m/s^2)
t is time (s)
ρ is the fluid density (kg/m^3)
μ is the fluid viscosity (Pa s)
$\vec{\nabla}$ is the del operator (m^{-1})
∇^2 is the Laplacian operator (m^{-2})

Each term of Eq. (4-1) represents a force per unit volume of the fluid. Term I relates to the rate of change of the fluid velocity with time at a given location within the flow field. For steady state conditions, the first term drops out. The second term is due to the fluid inertia. It is negligible for low velocity (low Reynolds number) flows. The third term is due to the pressure, the fourth term is due to fluid viscosity (shear stresses), and the last term is due to gravity.

Eq. (4-1) represents the momentum balance on a fluid element and it can be written for any orthogonal coordinate system (Bird *et al.*, 1960).

Conservation of mass leads to

$$\text{(4-2)} \qquad \frac{\partial\rho}{\partial t} = -\vec{\nabla}\cdot\rho\vec{u}$$

For constant density, the left side of Eq. (4-2) becomes zero leading to $\vec{\nabla}\cdot\vec{u} = 0$.

The energy equation (convection-diffusion) is given for constant physical properties (Bird *et al.*, 1960) as

$$\rho C_p \left[\frac{\partial T}{\partial t} + \vec{u} \cdot \vec{\nabla} T \right] = k_f \nabla^2 T \tag{4-3}$$

where C_p is the fluid specific heat (J/kg°C)
T is the fluid temperature (°C or K)
k_f is the fluid thermal conductivity (W/m°C)

For steady two-dimensional flows with negligible inertia, the governing equations become

x-direction momentum equation

$$\frac{\partial p}{\partial x} = \mu \left[\frac{\partial^2 u_x}{\partial x^2} + \frac{\partial^2 u_x}{\partial y^2} \right] + \rho g_x \tag{4-4a}$$

y-direction momentum equation

$$\frac{\partial p}{\partial y} = \mu \left[\frac{\partial^2 u_y}{\partial x^2} + \frac{\partial^2 u_y}{\partial y^2} \right] + \rho g_y \tag{4-4b}$$

Mass conservation

$$\frac{\partial u_x}{\partial x} + \frac{\partial u_y}{\partial y} = 0 \tag{4-5}$$

Energy equation

$$\rho C_p \left[u_x \frac{\partial T}{\partial x} + u_y \frac{\partial T}{\partial y} \right] = k_f \left[\frac{\partial^2 T}{\partial x^2} + \frac{\partial^2 T}{\partial y^2} \right] \tag{4-6}$$

Eqs. (4-4) to (4-6) are solved subject to the appropriate boundary conditions as applicable to the problem at hand.

From the above analysis, it can be observed that for a single-component fluid, one is only interested in the fluid velocity, pressure, and fluid temperature. Moreover, the above equations do not take into account forces other than inertial, viscous, gravitational, and pressure.

4.2 MULTICOMPONENT SYSTEM: ELECTROLYTIC SOLUTIONS

When a fluid contains an electrolyte, we are interested in the movement of the anions and the cations as well as the bulk fluid. To this end, mass transfer in an electrolytic solution requires a description of the movement of mobile ionic species, material balances, current flow, electroneutrality, and fluid mechanics.

4.2.1 Momentum Equations

As was discussed earlier, the momentum equation given by (4-1) does not include the force due to an electric field. The electric force is considered to be a body force as is gravity. The electric force per unit volume of the fluid is given by

$$(4\text{-}7) \qquad \overset{(f)}{\rho}\vec{E} - \frac{1}{2}\varepsilon_o\vec{E}\cdot\vec{E}\vec{\nabla}\varepsilon + \frac{1}{2}\varepsilon_o\vec{\nabla}\left[\left(\frac{\rho\partial\varepsilon}{\partial\rho}\right)_T\vec{E}\cdot\vec{E}\right], \ \frac{\mathrm{N}}{\mathrm{m}^3}$$

ρ is the solution density and $\overset{(f)}{\rho}$ is the free charge density (Russel *et al.*, 1989; Verbrugge and Pintauro, 1989). The force term given by (4-7) is for a variable dielectric constant.

For the special case of ε = constant, the force per unit fluid volume due to the electric field becomes

$$(4\text{-}8) \qquad \overset{(f)}{\rho}\vec{E}, \ \frac{\mathrm{N}}{\mathrm{m}^3}$$

Recognizing that the electric field strength $\vec{E}$ is related to the electric potential ψ by

$$\vec{E} = -\vec{\nabla}\psi$$

one can write for the force term

$$(4\text{-}9) \qquad -\overset{(f)}{\rho}\vec{\nabla}\psi$$

where the units of $\overset{(f)}{\rho}$ are C/m^3 and the units of $\vec{\nabla}\psi$ are V/m.

Introducing the electric force term to Eq. (4-1), we obtain

$$(4\text{-}10) \qquad \rho\frac{\partial\vec{u}}{\partial t} + \rho\vec{u}\cdot\vec{\nabla}\vec{u} = -\vec{\nabla}p + \mu\nabla^2\vec{u} + \rho\vec{g} - \overset{(f)}{\rho}\vec{\nabla}\psi$$

For steady-state creeping flow, the momentum equation becomes

$$\vec{\nabla} p = \mu \nabla^2 \vec{u} + \rho \vec{g} - \overset{(f)}{\rho} \vec{\nabla} \psi \tag{4-11}$$

It should be stressed here that ψ in Eq. (4-11) represents the total electric potential.

The free charge density is given by

$$\overset{(f)}{\rho} = \sum z_i e n_i = F \sum z_i c_i$$

where
e is the fundamental charge
z_i is valency of the ith species
n_i is the ionic concentration
F is the Faraday constant, and
c_i is the molar concentration.

The mass conservation is still given by Eq. (4-2). For steady-state, one obtains

$$\vec{\nabla} \cdot \vec{u} = 0 \tag{4-12}$$

Eqs. (4-11) and (4-12) are the "fluid mechanics" governing equations for the flow and transport of an electrolytic solution under steady-state creeping flow conditions. The velocity vector $\vec{u}$ is that of the solution as defined by Eq. (4-13) in the next section.

4.2.2 Convection-Diffusion-Migration Equation

The movement of an ionic species in an electrolytic solution occurs due to bulk fluid motion, diffusion due to concentration difference and due to migration under the influence of an electric potential. We shall deal first with some basic definitions, then derive the usual convection-diffusion transport equation and finally include the migration term (Bird *et al.*, 1960; Newman, 1991).

The local mass average velocity of the fluid is given by

$$\vec{u} = \frac{\sum_{i=1}^{n} \rho_i \vec{u}_i}{\sum_{i=1}^{n} \rho_i} = \frac{\sum_{i=1}^{n} \rho_i \vec{u}_i}{\rho} \tag{4-13}$$

where $\vec{u}_i$ is the velocity vector of the ith species with respect to a stationary observer (m/s)

$\vec{u}$ is the velocity vector of the bulk fluid with respect to a stationary observer as measured by a pitot tube (m/s)

ρ_i is the mass density of the ith species (kg/m^3)

$$= \frac{\text{mass of species } i}{\text{volume of solution}}$$

The solution density ρ is given by

$$\rho = \sum_{i=1}^{n} \rho_i \tag{4-14}$$

The term $\rho\vec{u}$ represents the local rate at which mass passes through a unit area that is normal to the velocity vector $\vec{u}$.

Similarly, a molar average velocity $\overrightarrow{u^*}$ may be correspondingly defined as

$$\overrightarrow{u^*} = \frac{\sum_{i=1}^{n} c_i\vec{u}_i}{\sum_{i=1}^{n} c_i} = \frac{\sum_{i=1}^{n} c_i\vec{u}_i}{c} \tag{4-15}$$

where c_i is the molar concentration of the ith species (mol/m^3)

$$= \frac{\text{number of moles of species } i}{\text{volume of solution}}$$

The total molar concentration, c, is given by

$$\sum_{i=1}^{n} c_i = c \tag{4-16}$$

The molar concentration (mol/m^3) and mass density (kg/m^3) are related by

$$c_i = 1000 \frac{\rho_i}{M_i} \tag{4-17}$$

where M_i is the molar mass (kg/kmol) of the ith species.

The mass fraction of the ith species is given by

(4-18) $$w_i = \frac{\rho_i}{\rho}$$

The molar (mole) fraction is given by

(4-19) $$x_i\left(= \text{or } y_i\right) = \frac{c_i}{c}$$

The mean or average molar mass of a mixture is given by

$$\overline{M} = 1000\,\frac{\rho}{c}$$

It should be recalled that the mass of a mole of a substance is called the molar mass, $\overline{M}$, and its units are kg/kmol. It has the same magnitude as the formerly used molecular weight (Probstein, 1989). The factor 1000 appears in order to reconcile the fact that c is given by mol/m^3, not as kmol/m^3 or mol/L.

For a dilute system, the mass flux of the ith species with respect to the mass average velocity, $\vec{u}$, is given by Fick's law as

(4-20) $$-D_i\vec{\nabla}\rho_i,\ \text{kg/m}^2\text{s}$$

Similarily, the molar flux of the ith species with respect to the molar average velocity, $\overrightarrow{u^*}$, is given by

(4-21) $$-D_i\vec{\nabla}c_i,\ \text{mol/m}^2\text{s}$$

The flux given by Fick's law is purely due to diffusion as a result of the molecular motion.

The mass flux of the ith species with respect to a fixed observer is given by

(4-22) $$\vec{j}_i = \rho_i\vec{u}_i\ ,\ \text{kg/m}^2\text{s}$$

The corresponding molar flux is given by

(4-23) $$\overrightarrow{j_i^*} = c_i\vec{u}_i\ ,\ \text{mol/m}^2\text{s}$$

where $\vec{j}_i$ and $\vec{j}_i^*$ are the mass and molar fluxes of the *i*th species with respect to a fixed observer

D_i is the diffusion coefficient of the *i*th species

$\vec{u}_i$ is the velocity of the *i*th species with respect to a stationary observer

The flux of the *i*th species with respect to a stationary observer is a combination of the convective flux due to bulk movement and the diffusional flux. Consequently, one can write for the flux of the *i*th species

Mass basis

$$\vec{j}_i = \rho_i\vec{u}_i = \rho_i\vec{u} - D_i\vec{\nabla}\rho_i \tag{4-24}$$

Molar basis

$$\overrightarrow{j_i^*} = c_i\vec{u}_i = c_i\overrightarrow{u^*} - D_i\vec{\nabla}c_i \tag{4-25}$$

For a dilute system, $\vec{u} \approx \vec{u^*}$ and we can write Eq. (4-25) as

$$\overrightarrow{j_i^*} = c_i\vec{u}_i = c_i\vec{u} - D_i\vec{\nabla}c_i \tag{4-26}$$

The first term on the right of Eq. (4-26) is the flux due to bulk motion. The second term on the right hand side is the flux of the *i*th species due to diffusion resulting from the concentration gradient, $\vec{\nabla}c_i$.

When an electrolyte solution is subjected to an electric field, migration of the ions will occur. Therefore, it is necessary to include an additional term to account for the ionic migration in Eqs. (4-24) or (4-26) (Probstein, 1989).

The flux due to migration in an electric field is proportional to the force acting on the particle multiplied by the ions concentration. The force per mole on the *i*th species is given by the product of $-\nabla\psi$ and z_iF:

$$-z_iF\vec{\nabla}\psi, \ \frac{\mathrm{N}}{\mathrm{mol}} \tag{4-27}$$

where z_iF is the charge per mole and F is the Faraday number.

The force per unit volume acting on the ions is then given by

(4-28) $$-z_iFc_i\vec{\nabla}\psi,\ \frac{\mathrm{N}}{\mathrm{m}^3}$$

The flux of the ith species due to migration is then given by

(4-29) $$-\upsilon_iz_iFc_i\vec{\nabla}\psi,\ \frac{\mathrm{mol}}{\mathrm{m}^2\mathrm{s}}$$

where υ_i is the mobility of the ith species and it is the proportionality constant between the flux and the force. The units for υ are $\mathrm{m^2mol/Js}$ or mol m/Ns.

The flux of the ith species is then given by

(4-30) $$\overrightarrow{j_i^*} = c_i\vec{u} - D_i\vec{\nabla}c_i - \upsilon_iz_iFc_i\vec{\nabla}\psi$$

Eq. (4-30) gives the molar flux of the ith species in $\mathrm{mol/m^2s}$. The first term of the right side of Eq. (4-30) is the flux due to bulk convection; the second term on the right side is due to the concentration difference (*i.e.*, diffusional process), and the last term is due to migration.

The counterpart of Eq. (4-30) in terms of mass flux is given by

(4-31) $$\vec{j_i} = \rho_i\vec{u} - D_i\vec{\nabla}\rho_i - \upsilon_iz_iF\rho_i\vec{\nabla}\psi$$

where $\vec{j_i}$ is in units of $\mathrm{kg/m^2s}$. In electrokinetic studies, it is preferable to work with a molar flux.

Making use of a relationship relating the ith species diffusion coefficient to its mobility, one can write

(4-32) $$D_i = RT\upsilon_i \quad \text{(Nernst–Einstein equation)}$$

the molar flux equation (4-30) becomes

(4-33) $$\overrightarrow{j_i^*} = c_i\vec{u} - D_i\vec{\nabla}c_i - \frac{z_iFc_iD_i}{RT}\vec{\nabla}\psi$$

It is also possible to define a flux based on number concentration in terms of number of ions per unit time per area. Recognizing

(4-34a) $$F = eN_a$$

(4-34b) $$kN_a = R$$

and

(4-34c) $$n_i = N_a c_i$$

Eqs. (4-34a) and (4-34b) give

(4-34d) $$\frac{F}{RT} = \frac{e}{kT}$$

Making use of Eqs. (4-34c) and (4-34d), Eq. (4-33) becomes

(4-35) $$\overrightarrow{j_i^*} = \frac{1}{N_a}\left[n_i\vec{u} - D_i\vec{\nabla}n_i - \frac{z_i e n_i D_i}{kT}\vec{\nabla}\psi\right]$$

In terms of a flux based on number concentration, one obtains

(4-36) $$\overrightarrow{j_i^{**}} = N_a \overrightarrow{j_i^*}, \quad \frac{1}{\text{m}^2\text{s}}$$

and we can write

(4-37) $$\overrightarrow{j_i^{**}} = n_i\vec{u} - D_i\vec{\nabla}n_i - \frac{z_i e n_i D_i}{kT}\vec{\nabla}\psi$$

Defining a mobility as (Russel *et al.*, 1989)

(4-38) $$\omega_i = \frac{D_i}{kT}$$

we can write Eq. (4-37) as

(4-39) $$\overrightarrow{j_i^{**}} = n_i\vec{u} - kT\omega_i\vec{\nabla}n_i - z_i e n_i \omega_i\vec{\nabla}\psi$$

Clearly, one can write the ionic flux in various forms. All the forms are interrelated and usually either $\overrightarrow{j_i^*}$ or $\overrightarrow{j_i^{**}}$ is used. The flux relationships, Eqs. (4-31), (4-33), and (4-39) are called Nernst–Planck equations.

4.2.3 Boltzmann Distribution

The Boltzmann distribution was previously derived using heuristic arguments. One can make use of the Nernst–Planck relationship to derive the Boltzmann distribution for the ionic number concentration near a charged surface.

Consider a flat surface whose normal is in the x-direction. Eq. (4-37) gives

$$j_{ix}^{**} = n_i u_x - D_i \frac{dn_i}{dx} - \frac{z_i e n_i D_i}{kT} \frac{d\psi}{dx} \tag{4-40}$$

where the subscript x denotes the x-direction. Assuming equilibrium with a zero fluid velocity and a zero flux, j_{ix}^{**}, Eq. (4-40) becomes

$$\frac{dn_i}{dx} + \left(\frac{z_i e n_i}{kT} \right) \frac{d\psi}{dx} = 0 \tag{4-41a}$$

or

$$\frac{d\left(ln\ n_i\right)}{dx} + \frac{z_i e}{kT} \frac{d\psi}{dx} = 0 \tag{4-41b}$$

Let

$$n_i = n_{i\infty} \quad \text{at} \quad \psi = \psi_\infty \tag{4-42}$$

The solution of Eq. (4-41b) subject to boundary condition (4-42) is given by

$$n_i = n_{i\infty} \exp\left[-\frac{z_i e\,(\psi - \psi_\infty)}{kT} \right] \tag{4-43}$$

For $\psi_\infty = 0$, we obtain

$$n_i = n_{i\infty} \exp\left[-\frac{z_i e \psi}{kT} \right] \tag{4-44}$$

Here we recover the Boltzmann distribution.

It should be noted that the Nernst–Planck relationship gave the Boltzmann distribution with the explicit assumptions of $j_{ix}^{**} = 0$ and $u_x = 0$. In a flow system the above assumptions may not be true. However, at a non-conducting stationary surface, one can still make use of Eq. (4-41b). Here, Eq. (4-41b) becomes the necessary boundary condition for the particular electrokinetic problem.

4.2.4 Conservation of Ionic Mass

If one is to carry out a material balance over a stationary volume element within an electrolyte solution, one can show quite easily that

$$\frac{\partial c_i}{\partial t} = -\vec{\nabla} \cdot \overrightarrow{j_i^*} + R_i \tag{4-45}$$

where the left side of Eq. (4-45) is the accumulation rate within the volume element. The first right side term is the net input and the last term is the production rate due to chemical reactions given as mol/m^{3}s (Newman, 1991).

For steady state with no chemical reaction, Eq. (4-45) becomes

$$\vec{\nabla} \cdot \overrightarrow{j_i^*} = 0 \tag{4-46}$$

Eq. (4-46) constitutes the continuity or material balance for the ith species.

4.2.5 Current Density

The flow of current is a result of the individual flux of all the ionic species present in the electrolyte solution. The current density A/m^2 is given by

$$\vec{i} = F \sum z_i \overrightarrow{j_i^*} \tag{4-47a}$$

or

$$\vec{i} = e \sum z_i \overrightarrow{j_i^{**}} \tag{4-47b}$$

Making use of Eqs. (4-37) and (4-47b), one can write

$$\vec{i} = e\vec{u} \sum z_i n_i - e \sum D_i z_i \vec{\nabla} n_i - \frac{e^2 \vec{\nabla} \psi}{kT} \sum z_i^2 D_i n_i \tag{4-48a}$$

or

$$\vec{i} = F\vec{u} \sum z_i c_i - F \sum D_i z_i \vec{\nabla} c_i - F^2 \vec{\nabla} \psi \sum z_i^2 \upsilon_i c_i \tag{4-48b}$$

For the special case of an electrically neutral electrolyte solution, the first term on the right-hand side of Eq. (4-48) drops out where

$$\sum z_i n_i = \sum z_i c_i = 0 \tag{4-49}$$

This is equivalent to saying that the bulk motion of a fluid with a zero volume charge density can contribute nothing to the current density.

When there is no concentration gradient and the electrolyte solution is electrically neutral, we consider the last term on the right side of the Eq. (4-48b) to obtain

$$\vec{i} = -\left[F^2 \sum z_i^2 \upsilon_i c_i\right] \vec{\nabla}\psi \tag{4-50}$$

Setting σ to be the conductivity of the solution, one can write

$$\vec{i} = -\sigma\vec{\nabla}\psi \tag{4-51}$$

where

$$\sigma = F^2 \sum z_i^2 \upsilon_i c_i = \frac{e^2}{kT} \sum z_i^2 D_i n_i \text{, S/m} \tag{4-52}$$

where S has the units of siemens = ampere/volt.

Eq. (4-51) is an expression of Ohm's law valid for electrically neutral electrolyte in the absence of concentration gradients (Newman, 1991).

In order to compare electrolyte conductivities, it becomes necessary to normalize with concentration. We can define a molar conductivity for an ionic species as

$$\lambda_i = \frac{\sigma_i}{c_i} = F^2 z_i^2 \upsilon_i \text{, } \frac{\text{S m}^2}{\text{mol}} \tag{4-53}$$

This is the conductivity a solution would have if there were one mole of the substance in one cubic metre of the solution. λ_i is the molar conductivity.

In some literature equivalent conductivity is defined as λ_i/z_i. One should be careful in reading tables for the conductivity. Moreover, the symbols used are also differently defined.

The conductivity of a solution is given by

$$\sigma = \sum \lambda_i c_i \tag{4-54}$$

For a single salt electrolyte, we have

$$\sigma = \lambda_+ c_+ + \lambda_- c_- \text{, S/m} \tag{4-55}$$

For example, the molar conductivity of Na_2SO_4 (*i.e.*, σ value per one mole of Na_2SO_4/m^3) is given by Table 4-5 at 298 K

$$\begin{aligned} 2\lambda_+ + 1\lambda_- &= (2 \times 5.01 + 16)\, 10^{-3} \\ &= 260.2 \times 10^{-4}\ \text{S m}^2/\text{mol} \end{aligned}$$

The conductivity values are sensitive to the solution temperature. They are provided in Tables 4-1 to 4-5.

Table 4-1. Standard solutions for calibrating conductivity cells

Grams of KCl per kg H_2O	σ, S/m			
	0°C	18°C	25°C	25°C (Ref. 2)
76.5829	6.514	9.781	11.131	
7.47458	0.7134	1.1163	1.2852	1.2854
0.745819	0.07733	0.12201	0.14083	0.14086
7.45510 (0.1 M)				1.28217
0.745510 (0.01 M)				0.14079

Data are from Reference 1 except last column.

1. Marsh, K.N., ed., *Recommended Reference Materials for the Realization of Physicochemical Properties*, Blackwell, Oxford, 1987.
2. Wu, Y.C., Pratt, K.W., and Koch, W.F., *J. Solution Chem.*, 18, 515, 1989.

Table 4-2. Equivalent conductivity of electrolytes in aqueous solution

		Concentration, mol/L						
Compound	Infinite dilution	0.0005	0.001	0.005	0.01	0.02	0.05	0.1
$AgNO_3$	133.29	131.29	130.45	127.14	124.70	131.35	115.18	109.09
$1/2BaCl_2$	139.91	135.89	134.27	127.96	123.88	119.03	111.42	105.14
$1/2CaCl_2$	135.77	131.86	130.30	124.19	120.30	115.59	108.42	102.41
$1/2Ca(OH)_2$	258	–	–	233	226	214	–	–
$1/2CuSO_4$	133.6	121.6	115.20	94.02	83.08	72.16	59.02	50.55
HCl	425.95	422.53	421.15	415.59	411.80	407.04	398.89	391.13
KBr	151.9	–	–	146.02	143.36	140.41	135.61	131.32
KCl	149.79	147.74	146.88	143.48	141.20	138.27	133.30	128.90
$KClO_4$	139.97	138.69	137.80	134.09	131.39	127.86	121.56	115.14
$1/3K_3Fe(CN)_6$	174.5	166.4	163.1	150.7	–	–	–	–
$1/4K_4Fe(CN)_6$	184		167.16	146.02	134.76	122.76	107.65	97.82
$KHCO_3$	117.94	116.04	115.28	112.18	110.03	107.17	–	–
KI	150.31	–	–	144.30	142.11	139.38	134.90	131.05
KIO_4	127.86	125.74	124.88	131.18	118.45	114.08	106.67	98.2
KNO_3	144.89	142.70	141.77	138.41	132.75	132.34	126.25	120.34
$KMnO_4$	134.8	–	133.3	–	126.5	–	–	113
KOH	271.5	–	234	230	228	–	219	213
$KReO_4$	128.20	126.03	125.12	121.31	118.49	114.49	106.40	97.40
$1/3LaCl_3$	145.9	139.6	137.0	127.5	121.8	115.3	106.2	99.1
LiCl	114.97	113.09	112.34	109.35	107.27	104.60	100.06	95.81
$LiClO_4$	105.93	104.13	103.39	100.52	98.56	96.13	92.15	88.52
$1/2MgCl_2$	129.34	125.55	124.15	118.25	114.49	109.99	103.03	97.05
NH_4Cl	149.6	–	146.7	134.4	141.21	138.25	133.22	128.69
NaCl	126.39	124.44	123.68	120.59	118.45	115.70	111.01	106.69
$NaClO_4$	117.42	115.58	114.82	111.70	109.54	106.91	102.35	98.38
NaI	126.88	125.30	124.19	121.19	119.18	116.64	112.73	108.73
$NaOOCCH_3$	91.0	89.2	88.5	85.68	83.72	81.20	76.88	72.76
$NaOOC_2H_5$	85.88	84.20	83.50	80.86	79.01	76.59	–	–
$NaOOC_3H_7$	82.66	81.00	80.27	77.54	75.72	73.35	69.29	65.24
NaOH	247.7	245.5	244.6	240.7	237.9	–	–	–
Na picrate	80.45	–	78.6	757	73.7	–	66.3	61.8
$1/2Na_2SO_4$	129.8	125.68	124.09	117.09	112.38	106.73	97.70	89.94
$1/2SrCl_2$	135.73	131.84	130.27	124.18	120.23	115.48	108.20	102.14
$1/2ZnSO_4$	132.7	121.3	114.47	95.44	84.87	74.20	61.17	52.61

The values of the equivalent conductivities, λ_i/z_i are given in 10^{-4} S m^2 mol^{-1} at a temperature of 25°C. (CRC Handbook of Chemistry and Physics, 71st edition, ed. Lide, D.R., CRC Press (1991). Reprinted with permission.)

Table 4-3. Equivalent ionic conductivity at infinite dilution (values are for aqueous solution at 25°C)

Ion	λ_i/z_i (10^{-4} S m^2 mol^{-1})	Ion	λ_i/z_i (10^{-4} S m^2 mol^{-1})	Ion	λ_i/z_i (10^{-4} S m^2 mol^{-1})
Inorganic cations		Inorganic cations		Inorganic cations	
Ag^+	61.9	$1/3Dy^{3+}$	65.6	NH_4^+	73.5
$1/3Al^{3+}$	61	$1/3Er^{3+}$	65.9	$N_2H_5^+$	59
$1/2Ba^{2+}$	63.6	$1/3Eu^{3+}$	67.8	Na^+	50.08
$1/2Be^{2+}$	45	$1/2Fe^{2+}$	54	$1/3Nd^{3+}$	69.4
$1/2Ca^{2+}$	59.47	$1/3Fe^{3+}$	68	$1/2Ni^{2+}$	50
$1/2Cd^{2+}$	54	$1/3Gd^{3+}$	67.3	$1/4[Ni_2(trien)_3]^{4+}$	52
$1/3Ce^{3+}$	69.8	H^+	349.65	$1/2Pb^{2+}$	71
$1/2Co^{2+}$	55	$1/2Hg_2^{2+}$	68.6	$1/3Pr^{3+}$	69.5
$1/3[Co(NH_3)_6]^{3+}$	101.9	$1/2Hg^{2+}$	63.6	$1/2Ra^{2+}$	66.8
$1/3[Co(en)_3]^{3+}$	74.7	$1/3Ho^{3+}$	66.3	Rb^+	77.8
$1/6[CO2(trien)^3]^{6+}$	69	K^+	73.48	$1/3Sc^{3+}$	64.7
$1/3Cr^{3+}$	67	$1/3La^{3+}$	69.7	$1/3Sm^{3+}$	68.5
Cs^+	77.2	Li^+	38.66	$1/2Sr^{2+}$	59.4
$1/2Cu^{2+}$	53.6	$1/2Mg^{2+}$	53.0	TI^+	74.7
D^+ (deuterium)	213.7 (18°)	$1/2Mn^{2+}$	53.5	$1/3Tm^{3+}$	65.4
Inorganic cations		Inorganic cations		Inorganic cations	
$1/2UO_2^{2+}$	32	$1/3[Fe(CN)_6]^{3-}$	100.9	OCN^-	64.6
$1/3Y^{3+}$	62	$H^2AsO_4^-$	34	OH^-	198
$1/3Yb^{3+}$	65.6	HCO_3^-	44.5	PF_6^-	56.9
$1/2Zn^{2+}$	52.8	HF_2^-	75	$1/2PO_3F^{2-}$	63.3
Inorganic anions		$1/2HPO_4^{2-}$	33	$1/2PO_4^{3-}$	69.0
$Au(CN)_2^-$	50	$H^2PO_4^-$	33	$1/4P_2O_7^{4-}$	96
$Au(CN)_4^-$	36	$H^2PO_2^-$	46	$1/3P_3O_9^{3-}$	83.6
$B(C_6H_5)_4^-$	21	HS^-	65	$1/5P_3O_{10}^{5-}$	109
Br^-	78.1	HSO_3^-	50	$1/3P_4O_{13}^{2-}$	94
Br_3^-	43	HSO_4^-	50	ReO_4^-	54.9
BrO_3^-	55.7	$H^2SbO_4^-$	31	SCN^-	66
CN^-	78	I^-	76.8	$1/2SO_3^{2-}$	79.9
CNO^-	64.6	IO_3^-	40.5	$1/2SO_4^{2-}$	80.0
$1/2CO_3^{2-}$	69.3	IO_4^-	54.5	$1/2S_2O_3^{2-}$	85.0
Cl^-	76.31	MnO_4^-	61.3	$1/2S_2O_4^{2-}$	66.5
ClO_2^-	52	MoO_4^-	74.5	$1/2S_2O_6^{2-}$	93
ClO_3^-	64.6	$N(CN)_2^-$	54.5	$1/2S_2O_8^{2-}$	86
ClO_4^-	67.3	NO_2^-	71.8	$Sb(OH)_6^-$	31.9
$1/3[Co(CN)_6]^{3-}$	98.9	NO_3^-	71.42	$SeCN^-$	64.7
$1/2CrO_4^{2-}$	85	$NH_2SO_3^-$	48.6	$1/2SeO_4^{2-}$	75.7
F^-	55.4	N_3^-	69	$1/2WO_4^{2-}$	69
$1/4[Fe(CN)_6]^{4-}$	110.4				

(CRC Handbook of Chemistry and Physics, 71st edition, ed. Lide, D.R., CRC Press (1991). Reprinted with permission.)

Table 4-3. continued.

Organic cations		Organic cations	
Benzyltrimethylammonium	34.6	Octadecyltriethylammonium	17.9
i-Butylammonium	38	Octadecyltrimethylammonium	19.9
Butyltrimethylammonium	33.6	Octadecyltripropylammonium	17.2
n-Decylpyridinium	29.5	Octyltrimethylammonium	26.5
Decyltrimethylammonium	24.4	Pentylammonium	37
Diethylammonium	42.0	Piperidinium	37.2
Dimethylammonium	51.8	Propylammonium	40.8
Dipropylammonium	30.1	Pyrilammonium	24.3
n-Dodecylammonium	23.8	Tetra-*n*-butylammonium	19.5
Dodecyltrimethyammonium	22.6	Tetradecyltrimethylammonium	21.5
Ethanolammonium	42.2	Tetraethylammonium	32.6
Ethylammonium	47.2	Tetramethylammonium	44.9
Ethyltrimethylammonium	40.5	Tetra-*i*-pentylammonium	17.9
Hexadecyltrimethylammonium	20.9	Tetra-*n*-pentylammonium	17.5
Hexyltrimethylammonium	29.6	Tetra-*n*-propylammonium	23.4
Histidyl	23.0	Triethylammonium	34.3
Hydroxyethyltrimethylarsonium	39.4	Triethylsulfonium	36.1
Methylammonium	58.7	Trimethylammonium	47.23
Octadecylpyridinium	20	Trimethylhexylammonium	34.6
Octadecyltributylammonium	16.6	Trimethylsulfonium	51.4
		Tripopylammonium	26.1

Organic cations		Organic cations	
Acetate	40.9	1/2Diethylbarbiturate^{2-}	26.3
p-Anistate	29.0	Dihydrogencitrate	30
1/2Azelate^{2-}	40.6	1/2Dimethylmalonate^{2-}	49.4
Benzoate	32.4	3,5-Dinitrobenzoate	28.3
Bromoacetate	39.2	Dodecylsulfate	24
Bromobenzoate	30	Ethylmalonate	49.3
n-Butyrate	32.6	Ethylsulfate	39.6
Chloroacetate	42.2	Fluoroacetate	44.4
m-Chlorobenzoate	31	Fluorobenzoate	33
o-Chlorobenzoate	30.2	Formate	54.6
1/3Citrate^{3-}	70.2	1/2Fumarate^{2-}	61.8
Crotonate	33.2	1/2Glutarate^{2-}	52.6
Cyanoacetate	43.4	Hydrogenoxalate	40.2
Cyclohexane carboxylate	28.7	Isovalerate	32.7
1/2 1,1-Cyclopropane-dicarboxylate^{2-}	53.4	Iodoacetate	40.6
Decysulphate	26	Lactate	38.8
Dichloroacetate	38.3	1/2Malate^{2-}	58.8

Table 4-4. Values of equivalent conductances and diffusion coefficients of selected ions at infinite dilution in water at 25°C (Newman, 1991)

Ion	z_i	$\frac{\lambda_i}{z_i} \times 10^4 \, \frac{S \cdot m^2}{equiv}$	$D_i \times 10^9 \, \frac{m^2}{s}$	Ion	z_i	$\frac{\lambda_i}{z_i} \times 10^4 \, \frac{S \cdot m^2}{equiv}$	$D_i \times 10^9 \, \frac{m^2}{s}$
H^+	1	349.8	9.312	OH^-	–1	197.6	5.260
Li^+	1	38.69	1.030	Cl^-	–1	76.34	2.032
Na^+	1	50.11	1.334	Br^-	–1	78.3	2.084
K^+	1	73.52	1.957	I^-	–1	76.8	2.044
NH_4^+	1	73.4	1.954	NO_3^-	–1	71.44	1.902
Ag^+	1	61.92	1.648	HCO_3^-	–1	41.5	1.105
Tl^+	1	74.7	1.989	HCO_2^-	–1	54.6	1.454
Mg^{2+}	2	53.06	0.7063	$CH_3CO_2^-$	–1	40.9	1.089
Ca^{2+}	2	59.50	0.7920	SO_4^{2-}	–2	80	1.065
Sr^{2+}	2	59.46	0.7914	$Fe(CN)_6^{3-}$	–3	101	0.896
Ba^{2+}	2	63.64	0.8471	$Fe(CN)_6^{4-}$	–4	111	0.739
Cu^{2+}	2	54	0.72	IO_4^-	–1	54.38	1.448
Zn^{2+}	2	53	0.71	ClO_4^-	–1	67.32	1.792
La^{3+}	3	69.5	0.617	BrO_3^-	–1	55.78	1.485
$Co(NH_3)_6^{3+}$	3	102.3	0.908	HSO_4^-	–1	50	1.33

Table 4-5. Molar conductivity of some ions at infinite dilution in water (Atkinson, 1972)

Ion	Temperature, T		Molar conductivity	Ion	Temperature, T		Molar conductivity
	K	°C	$\lambda \times 10^3$ S m^2 mol^{-1}		K	°C	$\lambda \times 10^3$ S m^2 mol^{-1}
H^+	288	15	30.1	OH^-	298	25	19.8
	298	25	35.0	Cl^-	288	15	6.14
	308	35	39.7		298	25	7.63
Li^+	298	25	3.87		308	35	9.22
Na^+	288	15	3.98	Br^-	288	15	6.33
	298	25	5.01		298	25	7.83
	308	35	6.15		308	35	9.42
Ca^{2+}	298	25	11.9	NO_3^-	298	25	7.14
Cu^{2+}	298	25	10.8	HCO_3^-	298	25	4.45
La^{3+}	298	25	20.0	SO_4^{2-}	298	25	16.0

4.2.6 Conservation of Charge

It is a physical law of nature that electric charge is conserved. This is implicitly built into the basic transport relationships.

Multiplying Eq. (4-45) by $z_i F$ yields

$$F\frac{\partial}{\partial t} z_i c_i = -F\vec{\nabla} \cdot z_i \overrightarrow{j_i^*} + F z_i R_i \tag{4-56}$$

Summation over all species yields

$$F\frac{\partial}{\partial t} \sum z_i c_i = -F\vec{\nabla} \cdot \sum z_i \overrightarrow{j_i^*} + F \sum z_i R_i \tag{4-57}$$

The last term of Eq. (4-57) is zero as long as all homogeneous reactions that give rise to the R_i term are electrically balanced. The left side is zero for an electrically neutral system or at steady-state conditions. Recognizing that the first term on the right side is related to the current (see Eq. (4-47a)), one can write for the steady-state conditions or for the electroneutrality condition

$$\vec{\nabla} \cdot \vec{i} = 0 \tag{4-58}$$

The above equation is the mathematical expression of the conservation of charge.

It should be noted that the flux equations were derived on the assumption that the solution is dilute and that the concentrations are used to establish the driving forces. However, for a non-dilute solution the gradient of the electrochemical potential is used as the driving force for diffusion and migration. The equivalent of the Nernst–Planck equation becomes

$$\overrightarrow{j_i^*} = c_i \vec{u} - \upsilon_i c_i \vec{\nabla} \mu_i \tag{4-59}$$

where μ is the electrochemical potential, comprising of the chemical potential and the electrical potential as was discussed in section 3.7. Here the driving force per mole is $-\nabla \mu_i$ The electrochemical potential μ_i depends on the local electrical state and composition. For more details the reader is referred to Newman (1991).

4.2.7 Example: Evaluation of Current Density

Evaluate the current density for a 0.01 molar NaCl solution at 298 K for a field strength E_x of 1000 V/m. Assume electrical neutrality and uniform ionic concentration. The current density equation is given by

$$i_x = -\sigma \frac{d\psi}{dx}$$

where x is the current flow direction. From Table 4-2 the molar conductance is given by 118.45×10^{-4} m^2 S/mol.

$$i_x = -\left(118.45 \times 10^{-4} \frac{\text{m}^2\text{S}}{\text{mol}}\right)\left(0.01 \frac{\text{kmol}}{\text{m}^3} \times \frac{1000 \text{ mol}}{\text{kmol}}\right) \times \left(-1000 \frac{\text{V}}{\text{m}}\right)$$

$$i_x = 118.45 \frac{\text{A}}{\text{m}^2}$$

4.3 SUMMARY OF GOVERNING EQUATIONS

In Chapters 3 and 4, the necessary equations needed to solve electrokinetic problems were derived and discussed. A summary of the governing equations is given below. Steady state, absence of a chemical reaction, and constant physical properties (density, viscosity, and dielectric constant) are assumed.

Conservation of mass for the electrolyte solution

$$\vec{\nabla} \cdot \vec{u} = 0$$

Conservation of ionic species

$$\vec{\nabla} \cdot \overrightarrow{j_i^*} = 0 \quad \text{or} \quad \vec{\nabla} \cdot \overrightarrow{j_i^{**}} = 0$$

Conservation of current

$$\vec{\nabla} \cdot \vec{i} = 0$$

Momentum equation (equation of motion)

$$\text{(4-10)} \quad \rho\vec{u} \cdot \vec{\nabla}\vec{u} = -\vec{\nabla}p + \mu\nabla^2\vec{u} + \rho\vec{g} - \overset{(f)}{\rho}\vec{\nabla}\psi$$

The creeping flow form is

$$\vec{\nabla}p = \mu\nabla^2\vec{u} + \rho\vec{g} - \overset{(f)}{\rho}\vec{\nabla}\psi$$

where

$$\vec{E} = -\vec{\nabla}\psi$$

and

$$\overset{(f)}{\rho} = \sum n_i z_i e = \sum c_i z_i F$$

Poisson equation

$$\varepsilon\varepsilon_o \nabla^2 \psi = -\overset{(f)}{\rho}$$

Ionic flux, Nernst–Planck equation

$$\begin{aligned} \overrightarrow{j_i^*} &= c_i \vec{u} - D_i \vec{\nabla} c_i - \left(\frac{z_i e}{kT}\right) D_i c_i \vec{\nabla}\psi \\ &= c_i \vec{u} - D_i \vec{\nabla} c_i - \left(\upsilon_i z_i F\right) c_i \vec{\nabla}\psi \\ &= c_i \vec{u} - D_i \vec{\nabla} c_i - \left(\frac{z_i F}{RT}\right) D_i c_i \vec{\nabla}\psi \end{aligned}$$

and

$$\overrightarrow{j_i^{**}} = n_i \vec{u} - D_i \vec{\nabla} n_i - \left(\frac{z_i e}{kT}\right) D_i n_i \vec{\nabla}\psi$$

Nernst–Einstein relationship

$$D_i = RT\,\upsilon_i$$

Stokes–Einstein relationship

$$D_i = \frac{kT}{f_i}$$

where f_i is the friction coefficient of an ion and it is given by $6\pi a\mu$ for a spherical particle.

Current density

$$\vec{i} = F\vec{u}\sum z_i c_i - F\sum z_i D_i \vec{\nabla} c_i - \left[F^2 \sum z_i^2 \upsilon_i c_i\right]\vec{\nabla}\psi$$

$$= e\vec{u}\sum z_i n_i - e\sum z_i D_i \vec{\nabla} n_i - \left[\frac{e^2}{kT} \sum z_i^2 D_i n_i\right]\vec{\nabla}\psi$$

Solution electrical conductivity σ is given by

$$\sigma = F^2 \sum z_i^2 \upsilon_i c_i = \frac{e^2}{kT}\sum z_i^2 D_i n_i$$

Some useful relationships

$$F = eN_a$$

$$R = kN_a$$

$$n_i = N_a c_i$$

$$\frac{z_i e}{kT} = \frac{z_i F}{RT}$$

Table 4-6. Continuity (conservation) equation in several coordinate systems for constant fluid density: $\vec{\nabla} \cdot \vec{u} = 0$

Rectangular coordinates (x, y, z):

(A) $$\frac{\partial}{\partial x}(u_x) + \frac{\partial}{\partial y}(u_y) + \frac{\partial}{\partial z}(u_z) = 0$$

Cylindrical coordinates (r, θ, z):

(B) $$\frac{1}{r}\frac{\partial}{\partial r}(ru_r) + \frac{1}{r}\frac{\partial}{\partial \theta}(u_\theta) + \frac{\partial}{\partial z}(u_z) = 0$$

Spherical coordinates (r, θ, ϕ):

(C) $$\frac{1}{r^2}\frac{\partial}{\partial r}\left(r^2 u_r\right) + \frac{1}{r\sin\theta}\frac{\partial}{\partial \theta}(u_\theta \sin\theta) + \frac{1}{r\sin\theta}\frac{\partial}{\partial \phi}\left(u_\phi\right) = 0$$

The corresponding conservation equations for the ionic species ($\vec{\nabla} \cdot \vec{j}^*$) and current density ($\vec{\nabla} \cdot \vec{i}$) can be written in analogous steady-state manner to those shown in Table 4-6.

Table 4-7. Steady-state equation of motion in Cartesian coordinates (x, y, z)

In terms of velocity gradients for a Newtonian electrolyte solution with constant ρ, μ, and ε:

x-component

(A)
$$\rho\left(u_x \frac{\partial u_x}{\partial x} + u_y \frac{\partial u_x}{\partial y} + u_z \frac{\partial u_x}{\partial z}\right) = -\frac{\partial p}{\partial x} + \mu\left(\frac{\partial^2 u_x}{\partial x^2} + \frac{\partial^2 u_x}{\partial y^2} + \frac{\partial^2 u_x}{\partial z^2}\right) + \rho g_x - \frac{(f)}{\rho}\frac{\partial \psi}{\partial x}$$

y-component

(B)
$$\rho\left(u_x \frac{\partial u_y}{\partial x} + u_y \frac{\partial u_y}{\partial y} + u_z \frac{\partial u_y}{\partial z}\right) = -\frac{\partial p}{\partial y} + \mu\left(\frac{\partial^2 u_y}{\partial x^2} + \frac{\partial^2 u_y}{\partial y^2} + \frac{\partial^2 u_y}{\partial z^2}\right) + \rho g_y - \frac{(f)}{\rho}\frac{\partial \psi}{\partial y}$$

z-component

(C)
$$\rho\left(u_x \frac{\partial u_z}{\partial x} + u_y \frac{\partial u_z}{\partial y} + u_z \frac{\partial u_z}{\partial z}\right) = -\frac{\partial p}{\partial z} + \mu\left(\frac{\partial^2 u_z}{\partial x^2} + \frac{\partial^2 u_z}{\partial y^2} + \frac{\partial^2 u_z}{\partial z^2}\right) + \rho g_z - \frac{(f)}{\rho}\frac{\partial \psi}{\partial z}$$

Table 4-8. Steady-state equation of motion in cylindrical coordinates (r, θ, z)

In terms of velocity gradients for a Newtonian electrolyte solution with constant ρ, μ, and ε:

r-component

$$\text{(A)}\quad \rho\left(u_r \frac{\partial u_r}{\partial r} + \frac{u_\theta}{r}\frac{\partial u_r}{\partial \theta} - \frac{u_\theta^2}{r} + u_z \frac{\partial u_r}{\partial z}\right) = -\frac{\partial p}{\partial r}$$

$$+ \mu\left[\frac{\partial}{\partial r}\left(\frac{1}{r}\frac{\partial}{\partial r}(r u_r)\right) + \frac{1}{r^2}\frac{\partial^2 u_r}{\partial \theta^2} - \frac{2}{r^2}\frac{\partial u_\theta}{\partial \theta} + \frac{\partial^2 u_r}{\partial z^2}\right] + \rho g_r - \rho^{(f)}\frac{\partial \psi}{\partial r}$$

θ-component

$$\text{(B)}\quad \rho\left(u_r \frac{\partial u_\theta}{\partial r} + \frac{u_\theta}{r}\frac{\partial u_\theta}{\partial \theta} + \frac{u_r u_\theta}{r} + u_z \frac{\partial u_\theta}{\partial z}\right) = -\frac{1}{r}\frac{\partial p}{\partial \theta}$$

$$+ \mu\left[\frac{\partial}{\partial r}\left(\frac{1}{r}\frac{\partial}{\partial r}(r u_\theta)\right) + \frac{1}{r^2}\frac{\partial^2 u_\theta}{\partial \theta^2} + \frac{2}{r^2}\frac{\partial u_r}{\partial \theta} + \frac{\partial^2 u_\theta}{\partial z^2}\right] + \rho g_\theta - \rho^{(f)}\frac{1}{r}\frac{\partial \psi}{\partial \theta}$$

z-component

$$\text{(C)}\quad \rho\left(u_r \frac{\partial u_z}{\partial r} + \frac{u_\theta}{r}\frac{\partial u_z}{\partial \theta} + u_z \frac{\partial u_z}{\partial z}\right) = -\frac{\partial p}{\partial z}$$

$$+ \mu\left[\frac{1}{r}\frac{\partial}{\partial r}\left(r\frac{\partial}{\partial r}u_z\right) + \frac{1}{r^2}\frac{\partial^2 u_z}{\partial \theta^2} + \frac{\partial^2 u_z}{\partial z^2}\right] + \rho g_z - \rho^{(f)}\frac{\partial \psi}{\partial z}$$

Table 4-9. Steady-state equation of motion in spherical coordinates (r, θ, ϕ)◆

In terms of velocity gradients for a Newtonian electrolyte solution with constant ρ, μ, and ε:

r-component

(A)
$$\rho\left(u_r\frac{\partial u_r}{\partial r} + \frac{u_\theta}{r}\frac{\partial u_r}{\partial \theta} + \frac{u_\phi}{r\sin\theta}\frac{\partial u_r}{\partial \phi} - \frac{u_\theta^2 + u_\phi^2}{r}\right)$$
$$= -\frac{\partial p}{\partial r} + \mu\left(\nabla^2 u_r - \frac{2}{r^2}u_r - \frac{2}{r^2}\frac{\partial u_\theta}{\partial \theta} - \frac{2}{r^2}u_\theta\cot\theta - \frac{2}{r^2\sin\theta}\frac{\partial u_\phi}{\partial \phi}\right)$$
$$+ \rho g_r - \overset{(f)}{\rho}\frac{\partial \psi}{\partial r}$$

θ-component

(B)
$$\rho\left(u_r\frac{\partial u_\theta}{\partial r} + \frac{u_\theta}{r}\frac{\partial u_\theta}{\partial \theta} + \frac{u_\phi}{r\sin\theta}\frac{\partial u_\theta}{\partial \phi} + \frac{u_r u_\theta}{r} - \frac{u_\phi^2\cot\theta}{r}\right)$$
$$= -\frac{1}{r}\frac{\partial p}{\partial \theta} + \mu\left(\nabla^2 u_\theta + \frac{2}{r^2}\frac{\partial u_r}{\partial \theta} - \frac{u_\theta}{r^2\sin^2\theta} - \frac{2\cos\theta}{r^2\sin^2\theta}\frac{\partial u_\phi}{\partial \phi}\right)$$
$$+ \rho g_\theta - \overset{(f)}{\rho}\frac{1}{r}\frac{\partial \psi}{\partial \theta}$$

ϕ–component

(C)
$$\rho\left(u_r\frac{\partial u_\phi}{\partial r} + \frac{u_\theta}{r}\frac{\partial u_\phi}{\partial \theta} + \frac{u_\phi}{r\sin\theta}\frac{\partial u_\phi}{\partial \phi} + \frac{u_\phi u_r}{r} + \frac{u_\theta u_\phi}{r}\cot\theta\right)$$
$$= -\frac{1}{r\sin\theta}\frac{\partial p}{\partial \phi} + \mu\left(\nabla^2 u_\phi - \frac{u_\phi}{r^2\sin^2\theta} + \frac{2}{r^2\sin\theta}\frac{\partial u_r}{\partial \phi} + \frac{2\cos\theta}{r^2\sin^2\theta}\frac{\partial u_\theta}{\partial \phi}\right)$$
$$+ \rho g_\phi - \overset{(f)}{\rho}\frac{1}{r\sin\theta}\frac{\partial \psi}{\partial \phi}$$

◆ In these equations,

$$\nabla^2 = \frac{1}{r^2}\frac{\partial}{\partial r}\left(r^2\frac{\partial}{\partial r}\right) + \frac{1}{r^2\sin\theta}\frac{\partial}{\partial \theta}\left(\sin\theta\frac{\partial}{\partial \theta}\right) + \frac{1}{r^2\sin^2\theta}\left(\frac{\partial^2}{\partial \phi^2}\right)$$

4.4 NOMENCLATURE

c	total molar concentration, mol/m^3
c_i	molar concentration of the ith species, mol/m^3
C_p	fluid specific heat, J/kg K
D	diffusion coefficient, m^2/s
D_i	diffusion coefficient of the ith species, m^2/s
e	elementary charge, C
$\vec{E}$	electric field strength vector, V/m
F	Faraday number, C/mol
$\vec{g}$	gravitational vector, m/s^2
$\vec{i}$	current density vector, A/m^2
i_x	current density in x-direction
$\vec{j}_i$	mass flux vector of the ith species w.r.t. a stationary observer, kg/m^{2}s
$\vec{j}_i^*$	molar flux vector of the ith species w.r.t. a stationary observer, mol/m^{2}s
$\vec{j}_i^{**}$	ionic flux vector of the ith species w.r.t. a stationary observer, 1/m^{2}s
k	Boltzmann constant, J/K
k_f	fluid thermal conductivity, W/mK
M	solution molarity, mol/dm^3 $\cong$ mol/L
$\bar{M}$	average molar mass, kg/kmol
M_i	molar mass of the ith species, kg/kmol
n_i	ith ionic number concentration, m^{-3}
$n_{i\infty}$	ith ionic number concentration in the bulk solution, m^{-3}
N_a	Avogadro number, mol^{-1}
p	fluid pressure, Pa or N/m^2
R	gas constant, J/K mol
t	time, s
T	temperature, K
$\vec{u}$	fluid velocity vector, m/s
$\vec{u}_i$	velocity vector of the ith species with respect to a stationary observer, m/s

w_i	mass fraction, dimensionless
(x, y, z)	Cartesian coordinates, m
x_i, y_i	mole fraction, dimensionless
z	absolute value of the valency for a $(z{:}z)$ electrolyte
z_i	valency of the ith ionic species
ε	dielectric constant of a material, dimensionless
ε_o	permittivity of vacuum, C/mV
λ_i	molar conductivity of the ith ionic species, S m^2/mol
μ	fluid viscosity, kg/ms or Pa s
μ_i	electrochemical potential of the ith species, J/mol
υ	mobility, m^2 mol/Js or mol m/Ns
ρ	fluid density, kg/m^3
ρ_i	mass density of the ith species, kg/m^3
$\overset{(f)}{\rho}$	free charge density, C/m^3
σ	electrolyte solution electrical conductivity, S/m or A/Vm
ψ	electric potential, V
ψ_∞	potential in the bulk electrolyte solution, V
ω	mobility, m^2/Js or m/Ns
$\vec{\nabla}$	del operator, m^{-1}
∇^2	Laplacian operator, m^{-2}

4.5 REFERENCES

Atkinson, G. (1972), *Electrochemical Information*, in American Institute of Physics Handbook, 3rd ed. (ed. Gray, D.E.), McGraw–Hill, New York.

Bird, R.B., Stewart, W.E., and Lightfoot, E.N. (1960), *Transport Phenomena*, John Wiley and Sons, New York.

Newman, J.S. (1991), *Electrochemical Systems*, 2nd ed., Prentice Hall, Englewood Cliffs, N.J.

Probstein, R.F. (1989), *Physicochemical Hydrodynamics*, Butterworths, Boston.

Russel, W.B., Saville, D.A., and Schowalter, W.R. (1989), *Colloidal Dispersions*, Cambridge University Press, Cambridge.

Verbrugge, M.W. and Pintauro, P.N. (1989), *Transport Models for Ion-Exchange Membranes, Modern Aspects of Electrochemistry*, No. 19.

ELECTROKINETIC PHENOMENA

5

Electrokinetics is the general term associated with the bulk relative motion between two charged phases. The electrokinetic phenomenon arises when attempts are made to shear off the mobile part of the electric double-layer from a charged surface.

If an electric field is applied tangentially along a charged surface, a force is exerted on the surface and on the ions in the double-layer. The charged surface (plus attached material) tends to move in the appropriate direction, while the ions in the mobile part of the double-layer show a net migration in the opposite direction, carrying solvent along with them, and thus causing the solvent's flow. Similarly, an electric field is created if the charged surface and the diffuse part of the double layer are made to move relative to each other (Shaw, 1980).

The four traditional electrokinetic phenomena are

5.1 ELECTROOSMOSIS

This is the movement of an electrolyte solution relative to a stationary charged surface (*i.e.*, a capillary tube, porous media) due to an applied electric field. The pressure necessary to counter-balance electroosmotic flow is termed the electroosmotic pressure.

A typical electroosmotic fluid flow in a capillary is shown in Figure 5-1. When the capillary tube is negatively charged, the applied electric field exerts a force along the cathode direction on the excess positively charged ions near the surface. The positively charged ions drag the electrolyte solution and flow occurs towards the cathode.

The electroosmosis phenomenon can be employed for the drainage of porous media and in the evaluation of the surface charge.

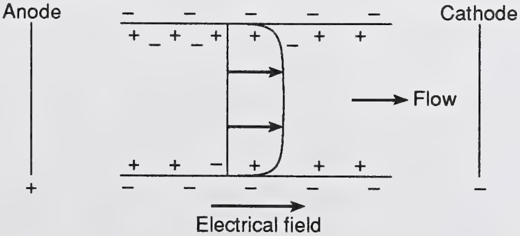

Figure 5-1. Electroosmotic flow in a capillary.

5.2 ELECTROPHORESIS

It is the movement of a charged surface plus attached material relative to a stationary liquid by an applied field. A typical particle electrophoresis is shown in Figure 5-2. Due to the presence of the anode and cathode terminals, an electric field, *E*, becomes established from left to right. The negatively charged colloidal particle migrates towards the anode.

Electrophoresis phenomenon is usually employed in measuring the surface potential of a charged particle.

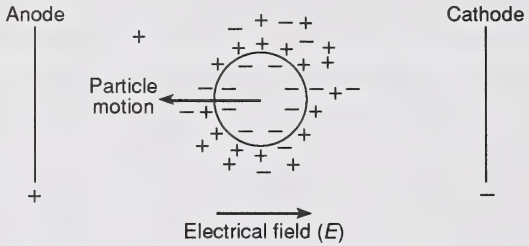

Figure 5-2. Electrophoresis of a particle.

5.3 STREAMING POTENTIAL

An electric field is created when an electrolyte solution or a liquid is made to flow along a stationary charged surface. This electric field is called streaming potential with zero current flow. For example, a streaming potential is set up when an electrolyte solution is pumped through a positively charged capillary as shown in Figure 5-3. The electric field due to the flow is from left to right.

The principle of streaming potential is used in sea water desalination. The streaming potential phenomenon is opposite to electroosmosis.

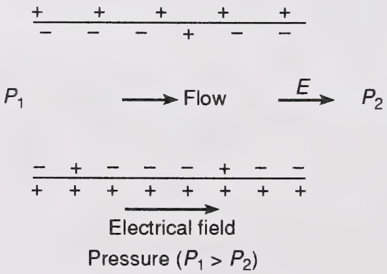

Figure 5-3. Streaming potential within a capillary tube.

5.4 SEDIMENTATION POTENTIAL

An electric field is created when charged particles move relative to a stationary liquid. The movement of the particles could be under gravitational or centrifugal fields. This phenomenon is sometimes called the Dorn effect or the migration potential. It is the least studied among the electrokinetic phenomena.

A sedimentation potential in a cylinder is illustrated in Figure 5-4.

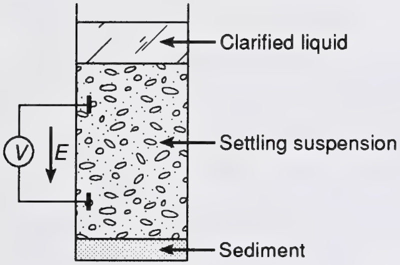

Figure 5-4. Setting up of a sedimentation potential for a gravity settling suspension.

5.5 REFERENCES

Shaw, D.J. (1980), *Introduction to Colloid and Surface Chemistry*, 3rd ed., Butterworths, London.

ELECTROOSMOSIS AND STREAMING POTENTIAL PHENOMENA

6

6.1 ELECTROOSMOSIS IN A CIRCULAR CHARGED CAPILLARY

It was pointed out earlier that electroosmosis is the phenomenon associated with the movement of the bulk electrolyte solution or a liquid carrying a free charge relative to a stationary charged surface under the influence of an imposed electric field. For example, an electrolyte solution in a porous medium can be made to move when an electric field is applied. In order to understand electroosmotic flow in a porous medium or in capillary tubes of varying cross-section, it is first necessary to be able to analyse the simple situation of electroosmotic flow in a straight circular capillary tube.

In this analysis, we shall present electroosmotic flow in a straight tube having a low surface potential. The flow to be considered is fully developed; *i.e.*, no end effects are present. By and large, the analysis is that given by Rice and Whitehead (1965). Improvements to include a high surface potential are given by Levine *et al.* (1975).

Consider a capillary tube having a negatively charged surface with a surface potential of ψ_s. Figures 6-1 and 6-2 depict the flow geometry.

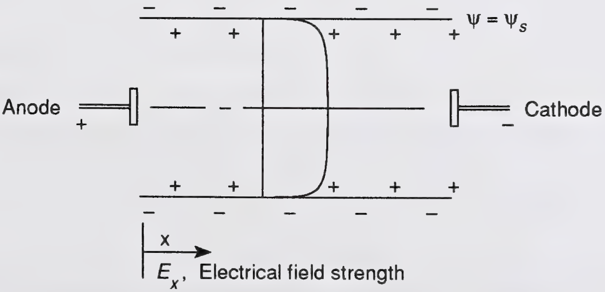

Figure 6-1. Electroosmotic flow in a circular capillary.

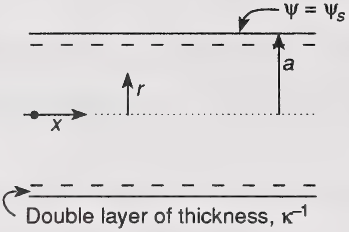

Figure 6-2. Flow geometry for electroosmosis.

The capillary ends are subjected to an electrical potential. The established field strength E and the local potential ϕ are related by

$$E_x = -\frac{\partial \phi}{\partial x}$$

The field strength E is in the x-direction as shown in Figure 6-1.

For our capillary tube, the concentration of cations (positive ions) predominates in the Debye sheath next to the charged capillary walls. The application of an external electric field results in a net migration towards the cathode of the ions in the surface water layer. Due to viscous drag, the water in the channel is drawn by the migrating ions and it flows through the channel. Consequently, there is an electric current as well.

Consider a symmetric (1:1) electrolyte flowing in a capillary tube having a surface potential ψ_s ($=\zeta$). Let the total potential at a point (r, x) be

$$\text{(6-1)} \qquad \phi = \phi(r,x) = \psi(r) + \left[\phi_o - xE_x\right]$$

where $\psi(r)$ is the potential due to the double layer at the equilibrium state corresponding to no fluid motion and no applied external field

ϕ_o is the value of the imposed potential at $x = 0$

$\phi_o - xE_x$ is the potential due to the field E_x in the absence of the double layer

E_x is the electric field, constant (fully developed flow field)

Eq. (6-1) assumes that one can use the principle of superposition for the potential. In other words, one can sum the potential due to the double layer and the potential due to the imposed electrical field.

The Poisson equation defining the potential in cylindrical coordinates is given by

$$\text{(6-2)} \qquad \frac{1}{r}\frac{\partial}{\partial r}\left(r\frac{\partial \phi}{\partial r}\right) + \frac{\partial^2 \phi}{\partial x^2} = -\frac{\overset{(f)}{\rho}}{\varepsilon\varepsilon_o}$$

Making use of Eq. (6-1), Eq. (6-2) becomes

$$\frac{1}{r}\frac{d}{dr}\left[r\frac{d\psi}{dr}\right] = -\frac{\overset{(f)}{\rho}}{\varepsilon\varepsilon_o} \tag{6-3}$$

The free charge density $\overset{(f)}{\rho}$ is given by

$$\overset{(f)}{\rho} = \sum e z_k n_k \tag{6-4}$$

Now assume that n_k, the ionic number concentration, is given by the Boltzmann distribution,

$$n_k = n_\infty \exp\left[-\frac{z_k e\psi}{kT}\right] \tag{6-5}$$

For simplicity, assume $z = -z_- = z_+ = 1$. Here, n_∞ is the cation or anion number concentration in the neutral electrolyte.

Eq. (6-5) leads to

$$n_+ = n_\infty \exp\left[-\frac{e\psi}{kT}\right] \tag{6-6a}$$

and

$$n_- = n_\infty \exp\left[\frac{e\psi}{kT}\right] \tag{6-6b}$$

The free charge density, Eq. (6-4), becomes

$$\overset{(f)}{\rho} = e\left(n_+ - n_-\right) = en_\infty\left[\exp\left(-\frac{e\psi}{kT}\right) - \exp\left(\frac{e\psi}{kT}\right)\right] \tag{6-7}$$

or

$$\overset{(f)}{\rho} = -2en_\infty \sinh\left(\frac{e\psi}{kT}\right)$$

If $e\psi/kT$ is small (*i.e.*, $\psi \leq 25$ mV), we can write $\sinh e\psi/kT \approx e\psi/kT$, whereby the Debye-Hückel approximation is invoked and one obtains

$$\overset{(f)}{\rho} = -2n_\infty e\left(\frac{e\psi}{kT}\right) \tag{6-8}$$

Note that the $(e\psi/kT)$ term can be used to obtain a dimensionless quantity for ψ by putting $\Psi = e\psi/kT$.

The Poisson–Boltzmann equation emerges by combining Eqs. (6-3) and (6-8) for a (1:1) electrolyte solution:

$$\frac{1}{r}\frac{d}{dr}\left(r\frac{d\psi}{dr}\right) = \frac{2n_\infty e^2\psi}{\varepsilon\varepsilon_o kT} \tag{6-9}$$

Let the reciprocal double-layer thickness (Debye length) be defined for a (1:1) electrolyte as

$$\kappa = \left(\frac{2n_\infty e^2}{\varepsilon\varepsilon_o kT}\right)^{1/2} \qquad \text{(1:1 electrolyte solution)} \tag{6-10}$$

Eq. (6-9) becomes

$$\frac{1}{r}\frac{d}{dr}\left(r\frac{d\psi}{dr}\right) = \kappa^2\psi \tag{6-11}$$

The boundary conditions are

(6-12a) at $r = 0$, the solution of Eq. (6-11) is finite, or $d\psi/dr = 0$

and

(6-12b) at $r = a$, $\psi = \psi_s$

The solution to Eq. (6-11) satisfying condition (6-12b) is

$$\psi = BI_o(\kappa r) \tag{6-13}$$

where I_o is the zero-order modified Bessel function of the first kind and B is a constant of integration.

At $r = a$, $\psi = \psi_s$ and hence the solution becomes

$$\psi = \psi_s\,\frac{I_o(\kappa r)}{I_o(\kappa a)} \tag{6-14}$$

where a is the capillary tube radius.

The free charge density distribution is then given by

$$\overset{(f)}{\rho}(r) = -\varepsilon\varepsilon_o\kappa^2\psi = -\varepsilon\varepsilon_o\kappa^2\psi_s \frac{I_o(\kappa r)}{I_o(\kappa a)} \tag{6-15}$$

To this point we have solved for the electric parameters using a Boltzmann distribution. This was done on the assumption that the radial flux $j_r = 0$ in the Nernst–Planck equation and that $u_r = 0$. In other words, the Nernst–Planck equation was implicitly used to provide the Boltzmann equation.

The modified Navier–Stokes equation in the axial flow direction is given by

$$\mu\frac{1}{r}\frac{d}{dr}\left[r\frac{du_x}{dr}\right] = \frac{dp}{dx} + \overset{(f)}{\rho}\frac{\partial\phi}{\partial x} \tag{6-16}$$

with

$$E_x = -\frac{\partial\phi}{\partial x} \tag{6-17}$$

As the flow is assumed to be fully developed, we have

$$E_x = E \tag{6-18}$$

with E being a constant.

From (6-15), the momentum equation becomes (setting $P_x = -dp/dx$)

$$\mu\frac{1}{r}\frac{d}{dr}\left[r\frac{du_x}{dr}\right] = -P_x + \varepsilon\varepsilon_o\psi_s\kappa^2E_x\frac{I_o(\kappa r)}{I_o(\kappa a)} \tag{6-19}$$

The boundary conditions are

$$u_x = 0 \qquad \text{at } r = a \tag{6-20a}$$

and

$$\frac{d\,u_x}{dr} = 0 \qquad \text{at } r = 0 \tag{6-20b}$$

The solution of Eq. (6-19) subject to (6-20a,b) is given by

$$(6\text{-}21) \qquad u_x(r) = \frac{a^2 P_x}{4\mu}\left[1 - \left(\frac{r}{a}\right)^2\right] - \frac{\varepsilon\varepsilon_o \psi_s}{\mu}\left[1 - \frac{I_o(\kappa r)}{I_o(\kappa a)}\right] E_x$$

The velocity of the electrolyte is the sum of the Poiseuille flow term and the electrokinetic term. Eqs. (6-14) and (6-21) define the solution to the electroosmotic flow in the circular capillary.

We can make use of the general solution given by Eq. (6-21) and derive interesting limiting cases.

Let $P_x = 0$; *i.e.*, there is no imposed pressure gradient as is the case for a capillary connecting two large reservoirs as shown in Figure 6-3.

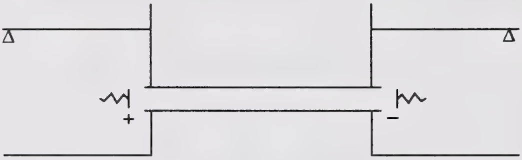

Figure 6-3. Open reservoirs with $P_x = 0$.

Eq. (6-21) gives

$$(6\text{-}22) \qquad u_x(r) = -\frac{\varepsilon\varepsilon_o \psi_s}{\mu}\left[1 - \frac{I_o(\kappa r)}{I_o(\kappa a)}\right] E_x$$

For given κa and $\varepsilon\varepsilon_o$, $u_x(r)$ increases linearly with the surface potential ψ_s and the electric field strength E_x. Also, $u_x(r)$ is inversely proportional to the fluid viscosity (other parameters being constant).

Let

$$(6\text{-}23) \qquad I_o(\kappa r)/I_o(\kappa a) = A$$

The properties of A and $(1 - A)$ are shown in Figure 6-4. The term in the square brackets of Eq. (6-22) is always positive. For a negative surface potential the axial velocity $u_x(r)$ becomes positive.

For $\kappa a >> 1$, *i.e.*, a thin double layer, $I_o(\kappa r)/I_o(\kappa a) \approx 0$ and Eq. (6-22) becomes

$$(6\text{-}24) \qquad u_x(r) \approx -\frac{\varepsilon\varepsilon_o \psi_s E_x}{\mu} = \text{constant} \neq f(r)$$

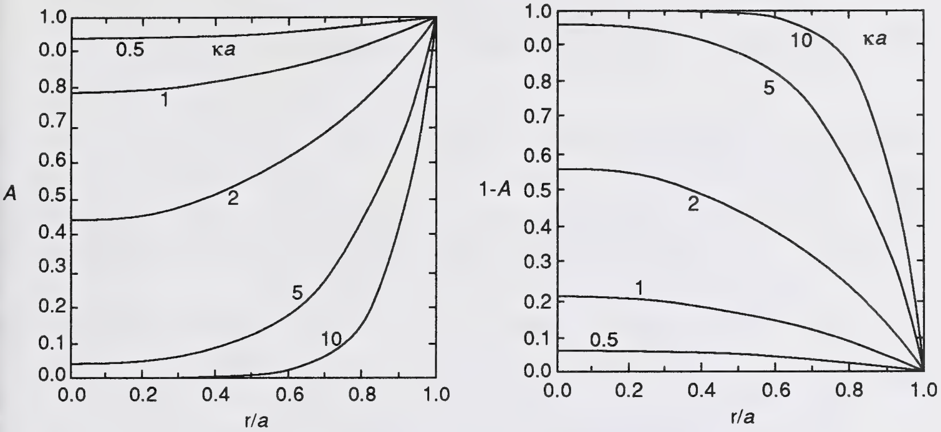

Figure 6-4. Properties of $I_o(\kappa r)/I_o(\kappa a)$.

This is called the Helmholtz–Smoluchowski equation. It is the classical equation for the flow of an electrolyte past a charged surface under the influence of an electric field along the surface. Here the fluid moves as a plug as if the fluid slips at the wall. A plot of Eq. (6-22) is shown in Figure 6-5 for various values of κ*a*.

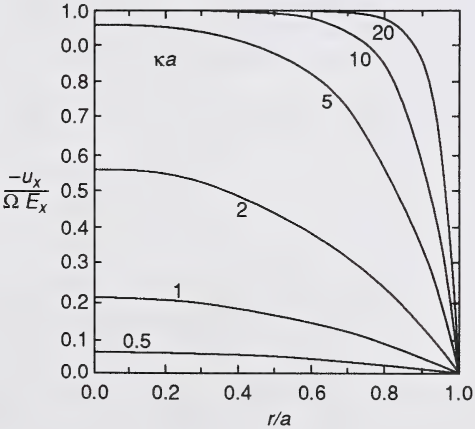

Figure 6-5. Electroosmotic dimensionless velocity profiles for the special case of $P_x = 0$ where $\Omega = \varepsilon\varepsilon_o\psi_s/\mu$.

For the special case of $\kappa a << 1$, *i.e.*, overlapping electric double layers, one can write a series expansion for I_o in terms of κa and κr to obtain

$$(6\text{-}25) \qquad u_x(r) = -\frac{\varepsilon\varepsilon_o\psi_s}{4\mu} E_x (\kappa a)^2 \left(1 - \left(\frac{r}{a}\right)^2\right)$$

Note that if $\kappa a \rightarrow 0$ then $u_x(r) \rightarrow 0$ and we have no electroosmotic flow for very overlapping double layers. Eq. (6-25) gives a parabolic velocity profile. The term $-\varepsilon\varepsilon_o\psi_s E_x (\kappa a)^2/4\mu$ is equivalent to $(a^2 P_x/4\mu)$ which is the pressure-driven Poiseuille flow.

The Poiseuille-type flow characteristics at low values of κa are due to the large overlap of the double layer with a virtually constant net free charge density across the capillary. This state gives rise to a fluid body force similar to that of a pressure gradient.

Again for the special case of $P_x = 0$, the volumetric flow rate is given by

$$(6\text{-}26) \qquad V = \int_0^a u_x(r)\, 2\pi r dr$$

and

$$(6\text{-}27) \qquad V_{el} = -\left[\frac{\varepsilon\varepsilon_o\psi_s}{\mu}\right] A_c E_x \left[1 - \frac{2\, I_1(\kappa a)}{(\kappa a)\, I_o(\kappa a)}\right]$$

where I_1 is first-order modified Bessel function of the first kind
A_c is the cross-sectional area of the capillary tube and it is equal to πa^2
V_{el} is the volumetric flow rate due to the electroosmotic flow

A dimensionless form of V_{el} is shown in Figure 6-6. As can be observed from Figure 6-6, the greatest advantage in having electroosmotic flow is for the case of large κa (*i.e.*, a thin double layer).

For the general case ($P_x \neq 0$), the total volumetric flow rate V is given by

$$(6\text{-}28) \qquad V = \frac{P_x a^2}{8\mu} A_c - \frac{\varepsilon\varepsilon_o\psi_s}{\mu} A_c E_x \left[1 - \frac{2\, I_1(\kappa a)}{(\kappa a)\, I_o(\kappa a)}\right]$$

When $V = 0$, *i.e.*, there is no net flow, the ratio of the developed pressure gradient to the electric field is then given by

$$(6\text{-}29) \qquad \frac{P_x}{E_x} = \left(\frac{8\,\varepsilon\varepsilon_o\psi_s}{a^2}\right)\left[1 - \frac{2\, I_1(\kappa a)}{\kappa a\, I_o(\kappa a)}\right]$$

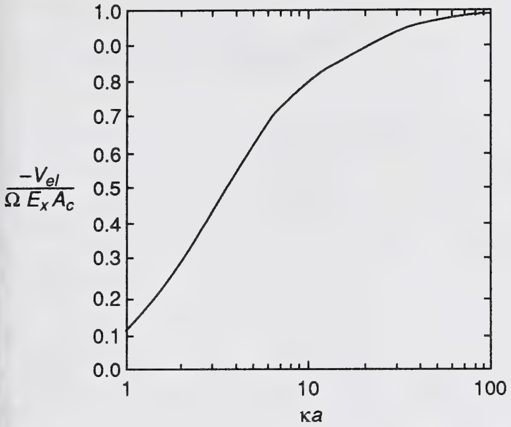

Figure 6-6. Variation of the dimensionless electroosmotic volumetric flow rate with κa with $P_x = 0$, where $\Omega = \varepsilon\varepsilon_o\psi_s/\mu$.

P_x becomes the electroosmotic pressure. For $\kappa a \gg 1$ (*i.e.*, a thin double layer), Eq. (6-29) becomes

$$\frac{P_x}{E_x} = \frac{8\,\varepsilon\varepsilon_o\psi_s}{a^2} \tag{6-30}$$

For the special case of $V = 0$, one can make use of Eq. (6-29) to evaluate the local axial velocity profile as given by Eq. (6-21) to obtain

$$\frac{u_x(r)}{E_x} = \left(\frac{\varepsilon\varepsilon_o\psi_s}{\mu}\right)\left\{2\left(1 - \left(\frac{r}{a}\right)^2\right)\left[1 - \frac{2\,I_1\,(\kappa a)}{\kappa a\,I_o\,(\kappa a)}\right] - \left[1 - \frac{I_o\,(\kappa r)}{I_o\,(\kappa a)}\right]\right\} \tag{6-31}$$

For the special case of a thin double layer, $\kappa a \gg 1$, Eq. (6-31) gives

$$\frac{u_x(r)}{E_x} = \left(\frac{\varepsilon\varepsilon_o\psi_s}{\mu}\right)\left[1 - \frac{2r^2}{a^2}\right] \tag{6-32}$$

Eq. (6-32) is valid for $(r/a) < 1$.

The dimensionless velocity profiles,

$$-\frac{u_x\,(r)}{\left(\frac{\varepsilon\varepsilon_o\,\psi_s}{\mu}\right)E_x}$$

given by Eq. (6-31) are shown in Figure 6-7. As the volumetric flow rate V is zero, the axial velocity u_x has to change direction in order to conserve mass balance.

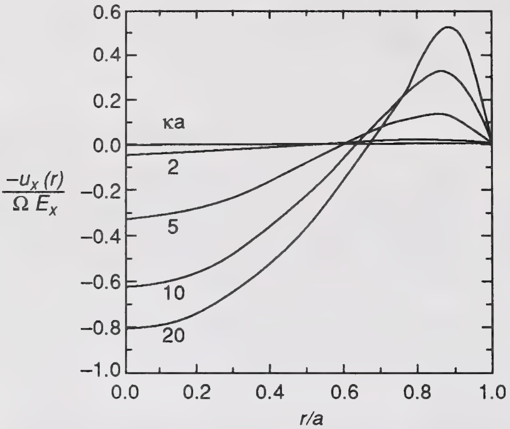

Figure 6-7. Variation of the dimensionless axial velocity with radial position for the special case of $V = 0$ at various values of κa.

For a negative surface potential, *i.e.*, $\psi_s < 0$, the flow near the capillary wall, $r/a \approx 1$, is in the positive direction. The flow near the wall is due to the migration of the positive ions close to the wall under the applied field E_x. In this region, the contribution of P_x to the flow is not significant. On the other hand, in the regions near the centre of the capillary tube, the flow is in the opposite direction where the ions migration is negligible and the contribution of P_x to the flow dominates.

An important feature of Figure 6-7 is the presence of a cylindrical shell within the capillary tube where the electrolyte solution velocity is zero. The radial position of this shell is usually referred to as the stationary surface, or stationary plane for the case of a parallel plates duct. If one is to place a charged particle at the stationary surface, then the electrophoretic velocity of the particle is *not* influenced by the velocity of the electrolyte solution. Consequently, electrophoresis devices are designed to observe particle movements along such a surface for the measurement of electrophoretic particle velocity and the subsequent evaluation of the particle surface charge (Shaw, 1980).

Table 6-1 gives the values of the stationary radial position (made dimensionless with a). In the limit of $\kappa a \rightarrow \infty$, the dimensionless radial position becomes $\sqrt{1/2}$.

Table 6-1. Dimensionless radial position R_{st} of the stationary surface for a low surface charge capillary.

κa	R_{st}
1	0.57867
2	0.58241
5	0.602165
10	0.63500
20	0.66851
50	0.69238
100	0.69989
200	0.703536
500	0.705687
∞	0.707107

Plot for Table 6-1.

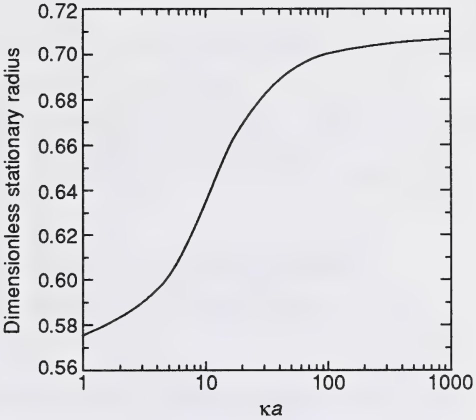

For a capillary radius of about 1 mm, κa can be considered to be very large for most electrolyte solutions and $R_{st} = 0.7071$.

For the general case of electroosmotic flow, the effectiveness of the electric field can be estimated using the volumetric flow ratio, VFR, defined as

$$\text{VFR} = \frac{\text{flow rate due to electroosmosis}}{\text{flow rate due to pressure}} \tag{6-33}$$

From Eq. (6-28) we can write

$$\text{VFR} = -\frac{8\,\varepsilon\varepsilon_o\psi_s\,E_x\left[1-\dfrac{2\,I_1\,(\kappa a)}{\kappa a\,I_o\,(\kappa a)}\right]}{a^2P_x} \tag{6-34}$$

For given values of ψ_s, $\varepsilon\varepsilon_o$, E_x, and P_x, we obtain

$$\text{VFR} \propto \frac{\left[1-\dfrac{2\,I_1\,(\kappa a)}{\kappa a\,I_o\,(\kappa a)}\right]}{a^2} \tag{6-35}$$

For the case of $\kappa a \gg 1$, *i.e.*, thin double layers, the numerator on the right side of Eq. (6-35) becomes unity and

$$\text{VFR} \propto \frac{1}{a^2} \tag{6-36}$$

Here the electric field becomes very effective in driving the flow.

For the case of $\kappa a \ll 1$ where the capillary tube is characterized by overlapping double layers, the term [•] of Eq. (6-35) becomes zero. The electric field becomes ineffective in driving the flow in the capillary tube. The variation of the term in the square brackets of Eq. (6-34) is also given by Figure 6-6.

6.2 CURRENT FLOW IN ELECTROOSMOSIS

The total current I is given by Eq. (4-48a) as

$$I = 2\pi \int_0^a u_x(r) \sum e z_i n_i r dr - 2\pi e \int_0^a \sum D_i z_i \frac{\partial n_i}{\partial x} r dr - \frac{e^2}{kT} 2\pi \int_0^a \sum \frac{\partial \phi}{\partial x} z_i^2 D_i n_i r dr \tag{6-37}$$

For a fully developed flow there is no axial variation in the ionic concentration and hence, the second term of Eq. (6-37) becomes zero. For a (1:1) electrolyte solution, we obtain

$$I = 2\pi \int_0^a u_x(r) r \rho^{(f)} dr + \frac{2\pi e^2}{kT} E_x \int_0^a \left(\sum r D_i n_i\right) dr \tag{6-38}$$

Let $D_i = D$, *i.e.*, $D_+ = D_- = D$ and $z = 1$; then the ionic number concentrations are given by

$$n_+ = n_\infty \exp\left(-\frac{e\psi}{kT}\right) \tag{6-39a}$$

and

$$n_- = n_\infty \exp\left(\frac{e\psi}{kT}\right) \tag{6-39b}$$

leading to

$$\sum n_i = 2n_\infty \cosh\left(\frac{e\psi}{kT}\right)$$

For $e\psi/kT \ll 1$, we can write

$$\sum n_i \cong 2n_\infty$$

and Eq. (6-38) becomes

$$I = 2\pi \int_0^a u_x(r)\, r \overset{(f)}{\rho}\, dr + \frac{2\pi e^2 E_x}{kT} D\,(2n_\infty) \int_0^a r dr$$

or

$$(6\text{-}40) \qquad I = 2\pi \int_0^a u_x(r)\, r \overset{(f)}{\rho}\, dr + \frac{2\pi a^2 n_\infty e^2 E_x D}{kT}$$

Recall that the electrolyte solution conductivity σ is defined by Eq. (4-52) as

$$\sigma = \frac{e^2}{kT} \sum z_i^2 D_i n_i \cong 2n_\infty e^2 \frac{D}{kT}$$

Here σ is taken to be constant across the radial position by making use of the assumption that $e\psi/kT \ll 1$. This is also true for all $e\psi/kT$ when $\kappa a \gg 1$. However, σ is not constant for $e\psi/kT \gtrsim 1$ and when κa is not so large (Levine *et al.*, 1975). The total current becomes

$$(6\text{-}41) \qquad I = 2\pi \int_0^a u_x(r)\, r \overset{(f)}{\rho}\, dr + \sigma E_x A_c$$

with $A_c = \pi a^2$ and $\overset{(f)}{\rho}$ is given by combining Eqs. (6-8) and (6-14).

The contribution to the total current given by the first term on the right side of Eq. (6-41) is due to the fluid bulk flow that is influenced by the pressure gradient and the imposed electrical field. The contribution of the second term on the right side of Eq. (6-41) to the total current is due to the electric conductivity of the electrolyte solution within the capillary tube.

Let $\Omega = \varepsilon\varepsilon_o \psi_s/\mu$ and $A_1 = I_1(\kappa a)/I_o(\kappa a)$; then Eq. (6-41) becomes

$$(6\text{-}42) \qquad I = E_x A_c \sigma \left\{ 1 - \frac{\Omega^2 \mu^2 \kappa^2}{\sigma} \left[1 - \frac{2A_1}{\kappa a} - A_1^2 \right] \right\} - \Omega P_x A_c \left[1 - \frac{2A_1}{\kappa a} \right]$$

The first term in Eq. (6-42) is due to the applied electric field. The second term is due to the applied pressure.

For the case of $P_x = 0$, *i.e.*, the current and the volumetric flow rate are due to the applied electric field only, Eqs. (6-27) and (6-42) can be combined to give

$$\left(\frac{V}{I}\right)_{P_x=0} = -\frac{\Omega}{\sigma} f(\kappa a, \beta) \tag{6-43}$$

where

$$f(\kappa a, \beta) = \frac{1 - \dfrac{2A_1}{\kappa a}}{1 - \beta\left[1 - \dfrac{2A_1}{\kappa a} - A_1^2\right]} \tag{6-44}$$

and

$$\beta = \frac{\Omega^2 \mu \kappa^2}{\sigma} \tag{6-45}$$

Eq. (6-43) represents the ratio of the volumetric flow rate to the applied current at zero pressure gradient. This ratio is directly related to the function $f(\kappa a, \beta)$ which is given by Figure 6-8.

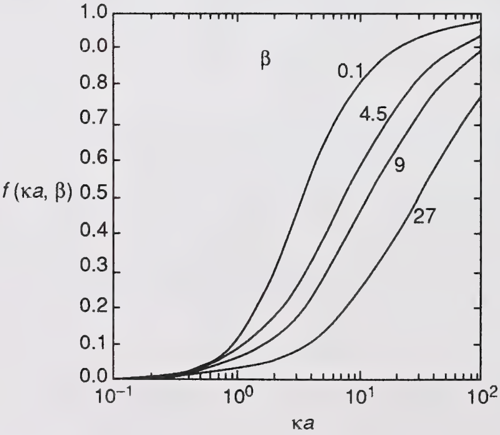

Figure 6-8. Variation of $f(\kappa a, \beta)$ with κa for various β values.

For the special case of thin double layers, $\kappa a \gg 1$, $f(\kappa a,\beta) \rightarrow 1$, and Eq. (6-43) becomes

$$\left(\frac{V}{I}\right)_{P_x=0} = -\frac{\Omega}{\sigma} \tag{6-46}$$

The ratio of (V/I) at zero pressure gradient is inversely proportional to the conductivity of the electrolyte solution.

6.3 STREAMING POTENTIAL ANALYSIS

The streaming potential is the steady potential which builds up across a capillary in the presence of an applied pressure gradient and is just sufficient to prevent any net current flow. Here, of course, we do not have an *applied* electric field, but we have an *induced* electric field. The streaming potential occurs when flow takes place in a capillary under an applied pressure gradient (Rice and Whitehead, 1965).

Setting $I = 0$ in Eq. (6-42) and rearranging, one obtains

$$\left(\frac{E_x}{P_x}\right)_{I=0} = \frac{\Omega}{\sigma} f(\kappa a,\beta) \tag{6-47}$$

Eq. (6-47) gives the ratio of (E_x/P_x) at zero electric current. Comparison between (6-43) and (6-47) leads to

$$-\left(\frac{V}{I}\right)_{P_x=0} = \left(\frac{E_x}{P_x}\right)_{I=0} = \frac{\Omega}{\sigma} f(\kappa a,\beta) \tag{6-48}$$

$$= \frac{\Omega}{\sigma} = \left(\frac{\varepsilon\varepsilon_o\psi_s}{\mu\sigma}\right) \text{ for } \kappa a \gg 1$$

Eq. (6-48) relates electroosmosis with streaming potential flows. Eq. (6-48) is in accordance with the Onsager principle of reciprocity for irreversible phenomena.

6.4 ELECTROVISCOUS EFFECT

When a liquid is forced through a narrow capillary under an applied pressure gradient (in the absence of an externally applied electric field), an induced streaming potential gradient E_x is established and the volumetric flow rate is given by Eq. (6-28). Note that the term E_x is now given by Eq. (6-48) as E_x is no longer an independent variable imposed by the experimentalist.

The volumetric flow rate under a zero-current condition is given by combining Eq. (6-28) with Eq. (6-47):

$$V = \frac{P_x a^2 A_c}{8\mu} - \frac{P_x A_c \Omega^2}{\sigma}\left[1 - \frac{2A_1}{\kappa a}\right] f(\kappa a, \beta)$$

The first term on the right side of the above expression is due to the imposed pressure gradient. It is positive in value. The second term on the right side of the above expression is due to the induced potential (streaming potential). This term is positive irrespective of the sign of the surface potential ψ_s. Consequently, the induced potential gives rise to a reduced volumetric flow rate for a given applied pressure. The reduction in the volumetric flow rate gives the appearance of an increased viscosity, hence the term "electroviscous effect."

The reduced rate of flow results in an apparent viscosity μ_a defined by

$$V = \frac{P_x a^2 A_c}{8\,\mu_a} \tag{6-49}$$

Substituting Eq. (6-49) into (6-28) leads to

$$\frac{P_x a^2}{8\,\mu_a} A_c = \frac{P_x a^2}{8\,\mu} A_c - \frac{\varepsilon\varepsilon_o \psi_s}{\mu} E_x A_c\left[1 - \frac{2A_1}{\kappa a}\right] \tag{6-50}$$

Now $(E_x/P_x)_{I=0}$ for the case of streaming potential is given by Eq. (6-47); hence $I = 0$ and

$$\mu_a = \frac{\mu}{1 - \dfrac{8\,\beta\left[1 - \dfrac{2A_2}{\kappa a}\right]^2}{(\kappa a)^2\left\{1 - \beta\left[1 - \dfrac{2A_1}{\kappa a} - A_1^2\right]\right\}}} \tag{6-51}$$

A plot of Eq. (6-51) is given in Figure 6-9. It clearly shows that for large β and small κa values, μ_a/μ can be substantially larger than unity. A maximum value of μ_a/μ occurs at $\kappa a \approx 2.2$. Figure 6-9 clearly shows that packed beds having large β with κa close to 2 would not be very permeable to the electrolyte flow.

For the case of $\kappa a \gg 1$, we obtain

$$\mu_a = \frac{\mu}{1 - \dfrac{8\beta}{(\kappa a)^2}} \tag{6-52}$$

where

$$\frac{\beta}{(\kappa a)^2} = \left(\frac{\varepsilon\varepsilon_o\psi_s}{\mu}\right)^2 \frac{\mu\kappa^2}{\sigma}\,\frac{1}{(\kappa a)^2} = \frac{\varepsilon^2\varepsilon_o^2\psi_s^2}{\mu\sigma a^2}$$

Hence

$$\text{(6-53)} \qquad \mu_a = \frac{\mu}{1 - \dfrac{8\,\varepsilon^2\varepsilon_o^2\psi_s^2}{\mu a^2\sigma}} \cong \mu\left[1 + \frac{8\,\varepsilon^2\varepsilon_o^2\psi_s^2}{\mu a^2\sigma}\right]$$

This is Elton's (1948) result. The fluid acts as if it has a higher viscosity because of the additional force opposing the flow.

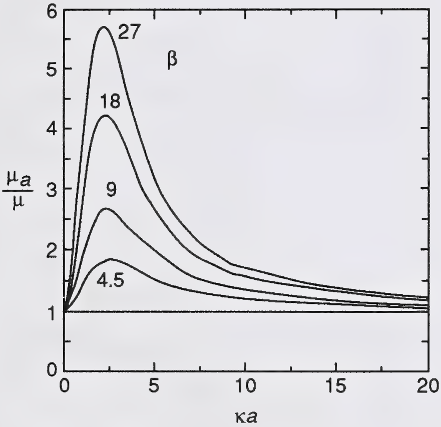

Figure 6-9. Variation of normalized apparent viscosity with κ*a*.

6.5 HIGH SURFACE POTENTIAL

The study of Levine *et al.* (1975) extended the analysis presented here which was given by Rice and Whitehead (1965) for $e\psi/kT = \Psi \ll 1$. This was possible through the use of the approximation given by Philip and Wooding (1970), where

$\sinh\Psi \cong \Psi$ for $\Psi < 1$.

and

$\sinh\Psi \cong 1/2\exp(\Psi)$ for $\Psi > 1$.

The equivalent equation for the axial velocity as given by (6-21) becomes

$$u_x(r) = \frac{a^2 P_x}{4\mu}\left(1 - \left(\frac{r}{a}\right)^2\right) - \frac{\varepsilon\varepsilon_o}{\mu}\left(\psi_s - \psi(r)\right) E_x \qquad (6\text{-}54)$$

The total volumetric flow rate as given by Levine *et al.* is

$$V = \frac{P_x a^2 A_c}{8\mu} - \frac{\varepsilon\varepsilon_o \psi_s A_c}{\mu}\,(1 - G)\, E_x \qquad (6\text{-}55)$$

$$G = \frac{2}{a^2\psi_s}\int_0^a r\psi(r)\, dr \qquad (6\text{-}56)$$

The function (1 – *G*) is shown in Figure 6-10. The curve shown in Figure 6-6 is identical to that for $\Psi_s \rightarrow 0$ of Figure 6-10. At κ*a* = 1 with $\Psi_s \rightarrow 0$, Figure 6-10 indicates that (1 – G) ≅ 0.11. This is in agreement with Figure 6-6 which shows that the term in the square brackets of Eq. (6-28) is also ~ 0.11. However, for $\Psi_s = 10$, (1 – G) is ≈ 0.55. Consequently, a large deviation occurs when a high value of Ψ_s is used in Rice and Whitehead's (1965) analysis which was derived for $\Psi_s < 1$. Levine *et al.* (1975) also showed that large differences in (μ_a/μ) are involved for $\Psi_s > 1$ when their results are compared with Rice and Whitehead's (1965) study.

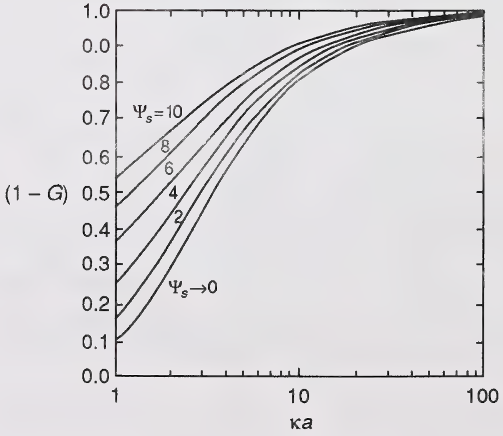

Figure 6-10. Plot of (1 – *G*) *versus* κ*a* for various values of the dimensionless surface potential = $\Psi_s = \psi e/kT$ (Levine *et al.*, 1975).

The electrokinetic parameters describing electroosmosis and streaming potential for long capillaries having different cross-sectional areas, *e.g.*, circle, ellipse, and infinite slit were treated by Anderson and Koh (1977). Based on principles similar to those outlined for the electroosmosis phenomenon, Sasidhar and Ruckenstein (1981,1982) studied electrolyte osmosis through capillaries, and Jacazio *et al.* (1972) analysed the process of electrokinetic salt rejection in hyperfiltration through porous materials. Using a similar type of analysis, salt rejection in sinusoidal capillary tubes was studied by Masliyah (1994).

The studies reported above make use of the Poisson–Boltzmann equation in describing the electrokinetic transport phenomena. However, the Poisson–Boltzmann equation assumes ideal solution behaviour of both the solute and the solvent. Electrokinetic models have been developed to account for finite ion size, ion hydration effects, and electric-field dependent solvent dielectric constant (Gur *et al.*, 1978a,b; Babchin and Masliyah, 1993). The resulting modified Poisson–Boltzmann (MPB) equation was used to show that ions of identical charge and different ionic size can yield different concentrations, dielectric constant profiles and electric potentials within a capillary tube. The MPB equation was also used by Gur *et al.* (1978a) and Ravina and Gur (1985) to study electroviscous effects in capillaries and by Pintauro and Verbrugge (1989) and Guzman-Garcia *et al.* (1990) to study electrolyte transport in ion-exchange membranes. The difference in the results obtained by the use of the Poisson–Boltzmann equation and its modified form is significant when the surface potential is high and the electrolyte concentration is large.

6.6 NOMENCLATURE

a	capillary tube radius, m
A_c	capillary tube cross-sectional area, m^2
e	elementary charge, C
E_x	electric field in axial direction, V/m
I_0	zero-order modified Bessel function
I_1	first-order modified Bessel function
I	total current
k	Boltzmann constant, J/K
n_+	ionic number concentration of the cations, m^{-3}
n_-	ionic number concentration of the anions, m^{-3}
n_∞	ionic number concentration in the bulk solution, m^{-3}
p	fluid pressure, Pa
P_x	negative pressure gradient, $-dp/dx$, Pa/m
r	radial coordinates, m

T	absolute temperature, K
u_x	local axial fluid velocity, m/s
V	total volumetric flow rate, m^3/s
V_{el}	volumetric flow rate due to electrical field, m^3/s
x	axial coordinates, m
z	absolute value of a (z:z) electrolyte solution valency
z_k	valency of kth species

β	$\Omega^2 \mu \kappa^2/\sigma$
ε	dielectric constant, dimensionless
ε_o	permittivity of vacuum, C/mV
κ	inverse Debye length, m^{-1}
μ	electrolyte solution viscosity, Pa s
μ_a	apparent electrolyte solution viscosity, Pa s
$\rho^{(f)}$	free charge density, C/m^3
σ	electrolyte solution conductivity, S/m or A/Vm
ϕ	total potential, V
ϕ_o	total potential at $x = 0$, V
ψ	potential due to electric double layer, V
ψ_s	surface potential, V
Ψ	dimensionless surface potential
Ω	$\varepsilon\varepsilon_o \psi_s/\mu$

6.7 REFERENCES

Anderson, J.L. and Koh, W.H. (1977), *Electrokinetic Parameters for Capillaries of Different Geometries*, J. Colloid Interface Sci., **59**, 149–58.

Babchin, A.J. and Masliyah, J. (1993), *Modified Nernst–Planck Equation for Hydration Effects*, J. Colloid Interface Sci., **160**, 258–59.

Elton, G.A.H. (1948), *Electroviscosity I. The Flow of Liquids Between Surfaces in Close Proximity*, Proc. Roy. Soc. Lond. **194A**, 259–74.

Gur, Y., Ravina, I., and Babchin, A.J. (1978a), *On the Electrical Double Layer Theory. I. Numerical Method for Solving a Generalized Poisson–Boltzmann Equation*, J. Colloid Interface Sci., **64**, 326–32.

Gur, Y., Ravina, I., and Babchin, A.J. (1978b), *On the Electrical Double Layer Theory. II. The Poisson–Boltzmann Equation Including Hydration Forces*, J. Colloid Interface Sci., **64**, 333–41.

Guzman-Garcia, A.G., Pintauro, P.N., Verbrugge, M.W., and Hill, R.F. (1990), *Development of a Space-Charge Transport Model for Ion-Exchange Membranes*, AIChEJ., **36**, 1061–74.

Jacazio, A., Probstein, R.F., Sonin, A.A., and Yung, E. (1972), *Electrokinetic Salt Rejection in Hyperfiltration Through Porous Materials. Theory and Experiment*, J. Phys. Chem., **76**, 4015–23.

Levine, S., Marriott, J.R., Neale, G., and Epstein, N. (1975), *Theory of Electrokinetic Flow in Fine Cylindrical Capillaries at High Zeta-Potentials*, J. Colloid Interface Sci., **52**, 136–49.

Masliyah, J. (1994), *Salt Rejection in a Sinusoidal Capillary Tube,* J. Colloid Interface Sci., accepted for publication.

Philip, J.R. and Wooding, R.A. (1970), *Solution of the Poisson–Boltzmann Equation About a Cylindrical Particle*, J. Chem. Phys., **52**, 953–59.

Pintauro, P.N. and Verbrugge, M.W. (1989), *The Electric-Potential Profile in Ion-Exchange Membranes*, J. Membrane Sci., **44**, 197–212.

Ravina, I. and Gur, Y. (1985), *Rheological Model of Pore Water*, J. Rheology, **29**, 131–45.

Rice, C.L. and Whitehead, R. (1965), *Electrokinetic Flow in a Narrow Cylindrical Capillary*, J. Phys. Chem., **69**, 4017–24.

Sasidhar, V. and Ruckenstein, E. (1981), *Electrolyte Osmosis Through Capillaries*, J. Colloid Interface Sci., **82**, 439–57.

Sasidhar, V. and Ruckenstein, E. (1982), *Anomalous Effects During Electrolyte Osmosis Across Charged Porous Membranes*, J. Colloid Interface Sci., **85**, 332–62.

Shaw, D.J. (1980), *Introduction to Colloid and Surface Chemistry*, 3rd ed., Butterworths, London.

ELECTROPHORESIS 7

7.1 ELECTROPHORESIS

When an electric field is applied to a suspension of particles (or a single particle), the particles migrate along the field owing to the presence of the surface charge. This phenomenon is called electrophoresis.

The analysis to be presented is aimed at evaluating the electrophoretic velocity of a charged particle when it is placed in an electric field. Let us first consider the problem at its limiting cases of large and small Debye lengths. Let us also assume that the particle is rigid and non-conducting with a uniformly distributed surface charge. In general the assumption of a non-conducting particle is appropriate as most conducting particles become polarized by the applied electric field and hence prevent the passage of the electric current through the particle. In this manner, the particle behaves as a non-conductor (Probstein, 1989).

7.2 LARGE DEBYE LENGTH, $\kappa a \ll 1$

Consider a spherical non-conducting particle (Figure 7-1) placed in an electrolyte solution subjected to an electric field.

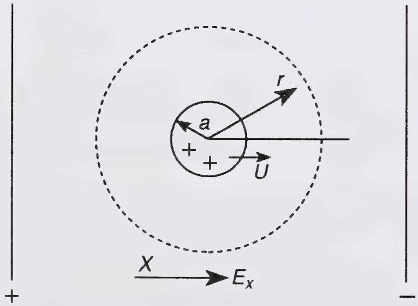

Figure 7-1. Electrophoresis of a particle for $\kappa a \ll 1$.

Assuming no angular variation in the potential, the Poisson Eq. (3-37) becomes

$$\varepsilon\varepsilon_o \frac{1}{r^2}\frac{d}{dr}\left(r^2 \frac{d\psi}{dr}\right) = -\overset{(f)}{\rho} \tag{7-1}$$

where

$$\overset{(f)}{\rho} = \sum n_i z_i e \tag{7-2}$$

Assuming that the particle Peclet number $Pe \approx 0$, then the Nernst–Planck equation gives the Boltzmann distribution as

$$n_i = n_\infty \exp\left(-\frac{z_i e\psi}{kT}\right) \tag{7-3}$$

where n_∞ is the ionic number concentration in the bulk electrolyte (outside the electric double layer).

Combining Eqs. (7-1) to (7-3) and making use of the Debye–Hückel approximation of $ze\psi/kT \ll 1$, one obtains for a $(z{:}z)$ electrolyte

$$\frac{1}{r^2}\frac{d}{dr}\left(r^2 \frac{d\psi}{dr}\right) = \frac{2e^2z^2n_\infty}{\varepsilon\varepsilon_o kT}\psi \tag{7-4}$$

Let

$$\kappa = \left(\frac{2e^2z^2n_\infty}{\varepsilon\varepsilon_o kT}\right)^{1/2}$$

where κ is the inverse Debye length. Eq. (7-4) then becomes

$$\frac{1}{r^2}\frac{d}{dr}\left(r^2 \frac{d\psi}{dr}\right) = \kappa^2\psi \tag{7-5}$$

Let

$$\xi = r\psi \tag{7-6}$$

and Eq. (7-5) becomes

(7-7) $$\frac{d^2\xi}{dr^2} = \kappa^2\xi$$

The solution of the above equation is given by

$$\xi = Ae^{-\kappa r} + Be^{\kappa r} = r\psi$$

The boundary conditions are

(a) $\psi \rightarrow \psi_\infty = 0$ as $r \rightarrow \infty$

and

(b) $\psi \rightarrow \psi_s = \zeta$ (zeta potential) at $r = a$

The surface potential ψ_s of the particle is assumed to be that of its zeta potential.

BC (a) indicates that $B = 0$. The solution becomes

(7-8) $$\psi = \frac{a\zeta}{r} \exp\left(\kappa(a - r)\right)$$

where a is the particle radius.

Eq. (7-8) gives

(7-9) $$\left(\frac{d\psi}{dr}\right)_{r=a} = -\zeta\left[\frac{1 + \kappa a}{a}\right]$$

The above expression will be needed at a later stage.

It should be recalled that the assumption of a zero Peclet number was used to obtain the Boltzmann distribution and hence Eq. (7-9). This assumption implies that the electrolyte velocity does not affect the ionic equilibrium at zero flow.

Consider a stationary diffuse double layer arising from a spherical non-conducting charged particle of radius a. The total amount of charge in the electrolyte is given by

(7-10) $$\overset{(f)}{Q} = \int_a^\infty \left(4\pi r^2\right) \overset{(f)}{\rho}\, dr$$

From Eq. (7-1), Eq. (7-10) becomes

$$\overset{(f)}{Q} = -4\pi\varepsilon\varepsilon_o \int_a^{\infty} r^2 \left[\frac{1}{r^2}\frac{d}{dr}\left(r^2\frac{d\psi}{dr}\right)\right] dr$$

and

$$\overset{(f)}{Q} = -4\pi\varepsilon\varepsilon_o \left[r^2\frac{d\psi}{dr}\right]_a^{\infty} \tag{7-11}$$

Now at $r \rightarrow \infty$, $(d\psi/dr) \rightarrow 0$, and Eq. (7-11) gives

$$\overset{(f)}{Q} = 4\pi a^2\varepsilon\varepsilon_o \left(\frac{d\psi}{dr}\right)_{r=a} \tag{7-12}$$

The surface charge density of the particle is given by

$$q_s = -\frac{\overset{(f)}{Q}}{4\pi a^2} = -\varepsilon\varepsilon_o\left(\frac{d\psi}{dr}\right)_{r=a} \tag{7-13}$$

The total surface charge is given by

$$Q_s = -4\pi a^2\varepsilon\varepsilon_o\left(\frac{d\psi}{dr}\right)_{r=a} \tag{7-14}$$

Combining Eqs. (7-13) and (7-9) leads to

$$q_s = \varepsilon\varepsilon_o\zeta\left(\frac{1+\kappa a}{a}\right) \tag{7-15}$$

or

$$\zeta = \frac{Q_s}{4\pi a\varepsilon\varepsilon_o\,(1+\kappa a)} \tag{7-16}$$

Eq. (7-16) can be rearranged to give

(7-17) $$\zeta = \frac{Q_s}{4\pi a \varepsilon \varepsilon_o} - \frac{Q_s}{4\pi \varepsilon \varepsilon_o \left(a + \frac{1}{\kappa}\right)}$$

The above expression relates the surface charge and potential for a sphere at low potentials. The surface potential is the sum of two superposed potentials. One arises from charge Q_s on the surface of radius a and a second arises from a charge $-Q_s$ on a sphere of radius $a + 1/\kappa$.

For large Debye length, *i.e.*, $\kappa a \ll 1$, Eq. (7-17) becomes

(7-18) $$\zeta = \frac{Q_s}{4\pi a \varepsilon \varepsilon_o}$$

This equation is the relationship between the total charge and the zeta potential for $\kappa a \ll 1$. The particle can be treated as a point charge in an unperturbed electric field strength of E_x ($= E_\infty$). At equilibrium the particle moves with a constant velocity U and the hydrodynamic force is equal to the electric drag; hence,

(7-19) $$Q_s E_\infty = 6\pi\mu U a$$

From Eq. (7-18), one obtains

(7-20) $$U = \frac{2}{3}\,\frac{\varepsilon\varepsilon_o \zeta E_\infty}{\mu} \qquad \text{for } \kappa a \ll 1.$$

This is Hückel equation for the electrophoretic velocity. Eq. (7-20) can be written as

(7-21) $$\frac{U}{E_\infty} = \frac{2}{3}\,\frac{\varepsilon\varepsilon_o \zeta}{\mu}$$

where U/E_∞ is the velocity per unit field strength or the electrophoretic mobility, in Cs/kg or (m/s)/(V/m).

As would be expected, increasing the surface potential ζ or decreasing the electrolyte viscosity μ would increase the electrophoretic mobility. The Hückel equation is valid for large Debye lengths and, in particular, for non-electrolyte systems, *e.g.*, organic liquids.

7.3 SMALL DEBYE LENGTH, $\kappa a \gg 1$

When the Debye length is small compared with the particle characteristic length, say its radius, we can neglect the particle curvature effects and treat the particle surface as being locally plane as shown in Figure 7-2. The electric field may therefore be considered to be applied parallel to the surface.

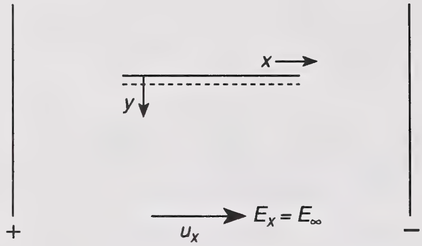

Figure 7-2. Electrophoresis for large $\kappa a \gg 1$.

Previous analysis of electroosmosis, Eq. (6-27), gave for $\kappa a \to \infty$

$$\frac{(\text{volumetric flow rate})}{\left[\dfrac{\varepsilon\varepsilon_o\zeta}{\mu} \cdot A_c E_\infty\right]} \to 1$$

Hence

$$U = \frac{\varepsilon\varepsilon_o\zeta E_\infty}{\mu} \quad \text{for } \kappa a \gg 1. \tag{7-22}$$

This is the Helmholtz–Smoluchowski equation valid for a small Debye length ($\kappa a \to \infty$) which usually occurs when the electrolyte molarity is high. Eq. (7-22) was derived with the assumption that $ze\zeta/kT \ll 1$.

One can also derive Eq. (7-22) in an alternative way with no borrowing from electrophoresis as is shown by Figures 7-2 and 7-3. The Navier–Stokes equation for flow over a flat surface (recall curvature is not important here) becomes

$$\mu \frac{d^2 u_x}{dy^2} = -\overset{(f)}{\rho} E_x = -\overset{(f)}{\rho} E_\infty \tag{7-23}$$

The Poisson equation is given by

$$\varepsilon\varepsilon_o \frac{d^2\psi}{dy^2} = -\overset{(f)}{\rho} \tag{7-24}$$

Combining Eqs. (7-23) and (7-24) gives

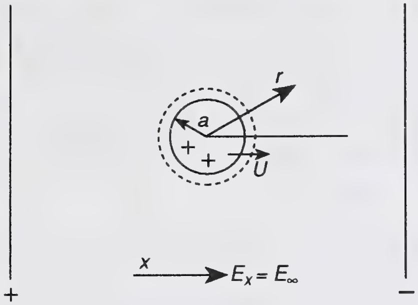

Figure 7-3. Electrophoresis of a particle with $\kappa a \gg 1$.

$$\mu \frac{d^2 u_x}{dy^2} = \varepsilon\varepsilon_o E_\infty \frac{d^2\psi}{dy^2}$$

Integrating the above equation leads to

$$\mu \frac{du_x}{dy} = \varepsilon\varepsilon_o E_\infty \frac{d\psi}{dy} + A_1 \tag{7-25}$$

$$\frac{du_x}{dy} \to 0 \quad \text{and} \quad \frac{d\psi}{dy} \to 0, \text{ as } y \to \infty$$

Hence, $A_1 \to 0$.

Integrating once again, Eq. (7-25) gives

$$u = \frac{\varepsilon\varepsilon_o E_\infty \psi}{\mu} + A_2$$

Since $u \to 0$ and $\psi \to 0$ as $y \to \infty$, it leads to $A_2 \to 0$. Hence, we obtain the Helmholtz–Smoluchowski equation:

$$U = \frac{\varepsilon\varepsilon_o \zeta E_\infty}{\mu} \quad \text{for } \kappa a \gg 1$$

where at $y = 0$, $u = U$ and $\psi = \zeta$.

Eq. (7-22) is valid for $\kappa a \geq 100$ and $ze\zeta/kT < 1$. In some literature Eq. (7-22) is simply referred to as Smoluchowski's equation. Note that both the Hückel and Helmholtz–Smoluchowski (H–S) equations are independent of particle size. Moreover, since the H–S equation (for large κa) was derived by assuming a flat surface, *i.e.*, no curvature effect, we can conclude that it should also be valid for any shape provided that the electric double layer is very thin everywhere and that the particle is non-conducting.

7.4 IMPROVED SOLUTIONS: ARBITRARY DEBYE LENGTH

The electrophoretic velocities derived so far are for either $\kappa a \gg 1$ or $\kappa a \ll 1$. In particular, the H–S equation was derived with the particle being treated as locally flat and the ionic convection (relaxation effect) was neglected.

Henry (1931) derived an analytical expression for the electrophoresis of a single spherical particle that is valid for a small zeta potential (the Debye–Hückel approximation) and for an arbitrary double-layer thickness. However, the ionic convection was neglected.

Overbeek (1943) and Booth (1950) were the first researchers to correctly account for the ionic convection about a spherical particle but their results are only valid for small zeta potentials ($ze\zeta/kT$).

Wiersema *et al.* (1966) relaxed the constraint of a small zeta potential and numerically solved the governing equations for the electrophoresis of a non-conducting sphere. Ionic convection was considered. Numerical difficulties at high ζ were encountered. O'Brien and White (1978) numerically solved the governing equations for arbitrary ζ and κa. Their work represents a proper solution of the electrophoresis for a sphere (Kozak and Davis, 1989a). For a finite-thickness double layer, three effects need to be considered (Shaw, 1980). These are given below.

Electrophoretic retardation: The ions in the electrolyte solution are affected by the field strength and cations tend to move towards the cathode (negative) and the anions tend to move towards the anode (positive). The movement of the ions tends to drag the neutral electrolyte molecules along. The motion of the whole electrolyte tends to retard the movement of the particle, hence the term electrophoretic retardation. Solving the Navier–Stokes equation together with the electric force term would account for this effect.

Relaxation: Due to the movement of the particle under consideration relative to the mobile ions in the double layer, the distribution of the ions around the particle is not symmetric. A finite time (relaxation time) is required for the original symmetry to be restored by diffusion and conduction. This asymmetry gives rise to a retardation force called the relaxation effect. If one takes into account the Nernst–Planck equation in the analysis, *i.e.*, $Pe \neq 0$, the relaxation effects would be included. When $\kappa a < 0.1$ or $\kappa a > 300$, the relaxation effects are not important. For large $ze\zeta/kT$, the relaxation effect is important. The shape of the electric double layer with the relaxation effect being considered is shown in Figure 7-4.

Surface conductance: Due to the presence of a charged surface, the distribution of the ions in the mobile region of the electric double layer gives rise to a higher conductivity close to the

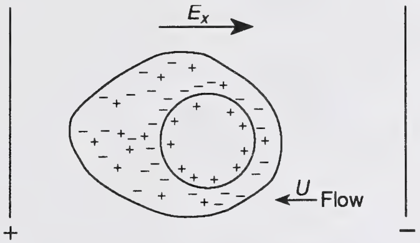

Figure 7-4. Double layer distortion due to relaxation effect for a stationary particle.

surface than that in the bulk electrolyte. When ζ and κa are small, the conductivity in the double layer is close to that of the bulk electrolyte. When κa or ζ is not small, the electrophoretic mobility of a particle is affected by the different conductivity in the double layer. This effect is called the surface conductance. If the surface conductance is important (large κa and/or ζ), the calculated zeta potentials may be quite low (Shaw, 1980).

7.4.1 Henry's Solution

Two main assumptions were made with Henry's approach.

1. The electric double layers are not distorted by the flow. The total potential within the double layer is a linear combination of the electric double layer potential and the potential due to the externally imposed electric field.
2. The Debye–Hückel approximation for low surface potential is assumed.

Due to Henry's assumptions, effects arising from relaxation and surface conductance are not accounted for in the analysis.

Henry assumed that the problem can be decomposed into two parts. One part is to solve for a stationary charged particle within the electrolyte. The second part is to solve for a charged particle in a dielectric having no free charge but with an external electric field being applied. Figure 7-5 depicts Henry's approach.

The potential due to the double layer is given by

$$\varepsilon\varepsilon_o \nabla^2 \psi = -\overset{(f)}{\rho} \tag{7-26}$$

Neglecting θ-variation, making use of the fact that $ze\zeta/kT << 1$ and assuming that the Boltzmann distribution is valid, Eq. (7-26) becomes

$$\frac{1}{r^2}\frac{d}{dr}\left(r^2\frac{d\psi}{dr}\right) = \kappa^2\psi \tag{7-27}$$

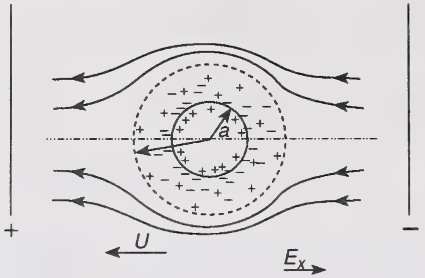

Figure 7-5. Electrophoresis with no retardation effects; stationary particle; Henry's solution.

where

$$\kappa = \left(\frac{2\, e^2 z^2 n_\infty}{\varepsilon \varepsilon_o k T} \right)^{1/2}$$

The boundary conditions are

$r \to \infty \qquad \psi \to 0$
$r \to a \qquad \psi \to \zeta$

The solution (see previous section) is given by

$$\psi = \zeta \left(\frac{a}{r} \right) e^{-(r-a)\kappa} \tag{7-28}$$

The potential given by Eq. (7-28) is solely due to the double layer. No applied electric field is present. The potential decay is shown in Figure 7-6.

Now consider a particle in a charge-free dielectric. The potential due to the external field is ϕ. The governing equation becomes

$$\nabla^2 \phi = 0 \tag{7-29}$$

with

$$\vec{E} = -\vec{\nabla}\phi \tag{7-30}$$

Eq. (7-29) can be written as

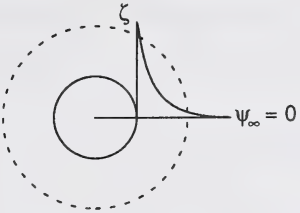

Figure 7-6. Potential decay due to a charged sphere in a dielectric medium.

$$\frac{1}{r^2 \sin\theta}\frac{\partial}{\partial\theta}\left(\sin\theta\,\frac{\partial\phi}{\partial\theta}\right) + \frac{1}{r^2}\frac{\partial}{\partial r}\left(r^2\frac{\partial\phi}{\partial r}\right) = 0 \tag{7-31}$$

The boundary conditions (this is simply an electrostatic problem) are

$$\text{BC1}^{\blacklozenge} \qquad \phi = -E_\infty r\cos\theta \quad \text{for } r \to \infty \tag{7-32a}$$

and

$$\text{BC2} \qquad \frac{\partial\phi}{\partial r} = 0 \quad \text{at } r = a \tag{7-32b}$$

BC2 is obtained by recognizing that at the surface $j_{ir}^{**} = 0$, $u_r = 0$, and $n_i = 0$. E_∞ is the undisturbed electric field strength.

The solution of Eq. (7-31) subject to the boundary conditions of Eq. (7-32) is given by

$$\phi = -E_\infty\left[r + \frac{a^3}{2r^2}\right]\cos\theta \tag{7-33}$$

It is now necessary to evaluate the hydrodynamic and electric forces exerted on the charged particle. The hydrodynamic forces can be evaluated from the solution of the Navier–Stokes equation modified for the electric force.

◆ The boundary condition given by Eq. (7-32a) signifies a uniform electric field strength at large distances from the particle. The use of Eq. (7-32a) can be demonstrated below.

$$i_r E_r + i_\theta E_\theta = -\left[i_r\frac{\partial\phi}{\partial r} + i_\theta\frac{1}{r}\frac{\partial\phi}{\partial\theta}\right]$$

The momentum equation for creeping flow is given by

$$\mu\nabla^2\vec{u} - \vec{\nabla}p = \overset{(f)}{\rho}\,\nabla\,(\phi + \psi) \tag{7-34}$$

The continuity equation is given as

$$\vec{\nabla}\cdot\vec{u} = 0 \tag{7-35}$$

Continuation of footnote from page 135

where

$$E_r = -\frac{\partial\phi}{\partial r} \quad \text{and} \quad E_\theta = -\frac{1}{r}\frac{\partial\phi}{\partial\theta}$$

Setting $\phi = -E_\infty\, r\cos\theta$, we obtain

$$\frac{\partial\phi}{\partial r} = -E_\infty\,\cos\theta \quad \text{and} \quad \frac{\partial\phi}{\partial\theta} = r\,E_\infty\sin\theta$$

leading to $E_r = E_\infty\cos\theta$ and $E_\theta = -E_\infty\sin\theta$

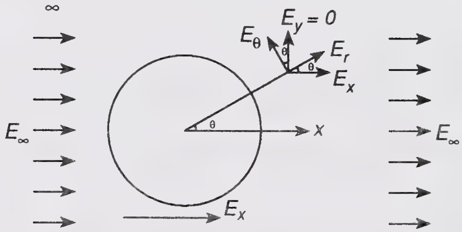

Figure 7-7. Electric field strength boundary condition at large distances.

From Figure 7-7, we can write
$E_x = E_r\cos\theta - E_\theta\sin\theta$

Substituting for E_r and E_θ, we obtain
$E_x = (E_\infty\cos\theta)\cdot\cos\theta - (-E_\infty\sin\theta)\sin\theta = E_\infty$

The electric field strength in y-direction is given by
$E_y = E_r\sin\theta + E_\theta\cos\theta$ and
$E_y = (E_\infty\cos\theta)\sin\theta - (E_\infty\sin\theta)\cos\theta = 0$

The above analysis shows that Eq. (7-32a) leads to $E_x = E_\infty$ and $E_y = 0$ which is the condition of uniform field strength.

The boundary conditions are given by

(7-36a) $$u_r = -U\cos\theta \quad \text{at } r \to \infty$$

(7-36b) $$u_\theta = U\sin\theta \quad \text{at } r \to \infty$$

and

(7-36c) $$u_r = u_\theta = 0 \quad \text{at } r = a$$

Here the spherical particle is held stationary with the fluid flowing at a velocity of U as is shown in Figures 7-5 and 7-8. The potential ψ is given by Eq. (7-28) and the potential ϕ is given by Eq. (7-33). The solution to Eqs. (7-34) and (7-35) subject to the boundary conditions of Eq. (7-36) is given by Henry (1931). The mathematical manipulations are quite involved. The solution provides expressions for P, u_r, and u_θ as a function of r and θ.

The hydrodynamic force F_H exerted by the fluid on the particle is given by

(7-37) $$F_H = 2\pi a^2 \int_o^\pi \left[-P_{rr}\cos\theta + \tau_{r\theta}\sin\theta\right]_{r=a} \sin\theta \; d\theta$$

where

(7-38a) $$P_{rr} = -P + 2\mu\frac{\partial u_r}{\partial r}$$

and

(7-38b) $$\tau_{r\theta} = \mu\left[r\frac{\partial\left(\frac{u_\theta}{r}\right)}{\partial r} + \frac{1}{r}\frac{\partial u_r}{\partial\theta}\right]$$

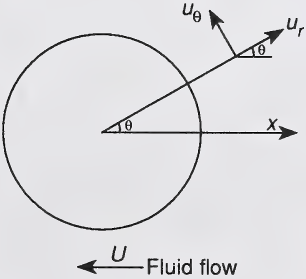

Figure 7-8. Stationary particle in a uniform velocity field.

P_{rr} and $\tau_{r\theta}$ represent the normal and tangential stresses exerted by the fluid on the particle. Figure 7-9 shows the hydrodynamic surface forces. Note that F_H is taken as positive when measured along the velocity U (in opposite direction to x).

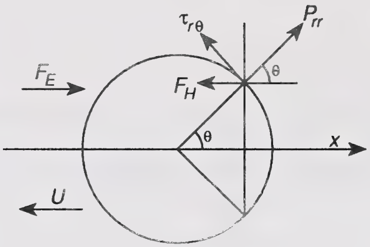

Figure 7-9. Hydrodynamic and electric surface forces on a particle.

The electric force due to the electric field is given by the product of the particle surface charge and the electric field strength E_∞. The surface charge is given by Eq. (7-14). The electric force in x-direction F_E is given by

$$F_E = \left[-4\pi a^2 \varepsilon\varepsilon_o \left.\frac{\partial\psi}{\partial r}\right|_{r=a} \right] E_\infty \tag{7-39}$$

where the term in brackets is the total surface charge. Note that ϕ does not contribute to the force F_E, as it acts in a charge free dielectric. A detailed derivation of Eq. (7-39) will be given later in section 7-6.

At steady state, the sum of the hydrodynamic and electric forces is zero as the particle does not have any acceleration. This leads to

$$F_H = F_E \tag{7-40}$$

and

$$U = \left[\frac{\frac{2}{3}\,\zeta\varepsilon\varepsilon_o E_\infty}{\mu} \right] f(\kappa a) \tag{7-41}$$

where

$$f(\kappa a) = 1 + \frac{1}{16}(\kappa a)^2 - \frac{5}{48}(\kappa a)^3 - \frac{1}{96}(\kappa a)^4 + \frac{1}{96}(\kappa a)^5 - \frac{1}{8}(\kappa a)^4 e^{\kappa a}\left(1 - \frac{(\kappa a)^2}{12}\right)\int_{\infty}^{\kappa a}\left(\frac{e^{-t}}{t}\right) dt \tag{7-42}$$

plot of the function f, usually called Henry's function, is given in Figure 7-10.

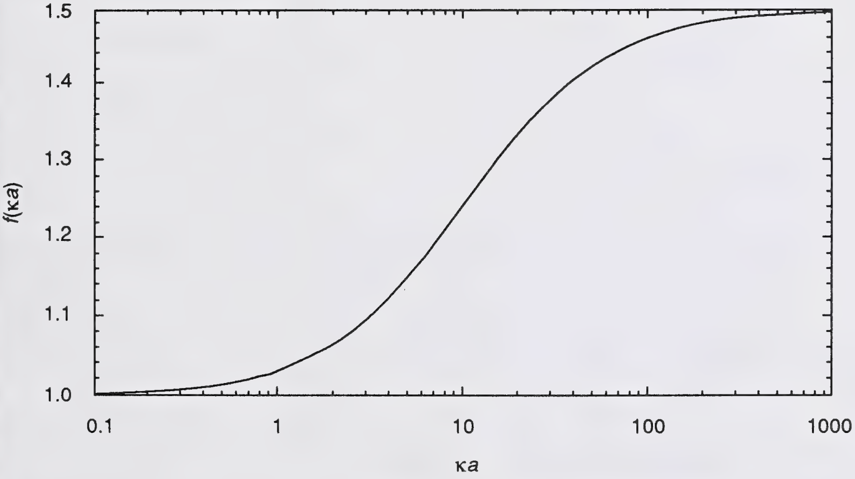

Figure 7-10. Variation of Henry's function with κ*a*.

From Figure 7-10 it can be seen that for $\kappa a \ll 1$, $f(\kappa a) \rightarrow 1$, and the electrohoretic velocity given by Eq. (7-41) reduces to Hückel's expression, Eq. (7-20). For the ase of $\kappa a \gg 1$, *i.e.*, a thin electric double layer $f(\kappa a) \rightarrow 3/2$ and Eq. (7-41) gives the lectrophoretic velocity as given by Eq. (7-22) for the Helmholtz–Smoluchowski expression.

Strictly speaking, Henry's equation is valid for small values of surface potential; *e.*, $ze\zeta/kT \ll 1$ for all κ*a* values. It should also be noted that in Henry's derivation, it was ssumed that the fluid moves with a velocity U while the particle is held stationary in the lectric field. This is equivalent to a moving particle having a velocity U in a stagnant fluid, ith the electric field strength being the same. Table 7-1 gives values of Henry's function as alculated using Eq. (7-42).

Table 7-1. Values of Henry's correction factor evaluated using MATLAB

κa	$f(\kappa a)$
0	1.000
0.5	1.009
1.0	1.027
2	1.065
3	1.101
4	1.133
5	1.160
10	1.24
25	1.37
50	1.43
100	1.46
∞	1.50

A curve fit equation for $f(\kappa a)$ is given by

$$f(\kappa a) = 1.5 - \frac{0.5}{1 + a_1(\kappa a)^{a_2}}$$

where $a_1 = 0.07234$
$a_2 = 1.129$

7.4.2 Effect of Particle Conductivity and Shape

The results of Henry (1931) discussed so far dealt with a non-conducting sphere. The conductivity of a particle affects (distorts) the applied electric field. Dukhin and Derjaguin (1974) give a full discussion on the effect of the particle conductivity. Henry, in his original work, considered the case of a non-conducting sphere. The general expression for the case of a spherical particle is given by

$$U = \frac{2\zeta\varepsilon\varepsilon_o E_\infty}{3\mu} F(\kappa a, K') \tag{7-43}$$

where

$$K' = \frac{\sigma_p}{\sigma_o} \tag{7-44a}$$

and

$$F(\kappa a, K') = 1 + 2\sigma\,[f(\kappa a) - 1] \tag{7-44b}$$

and

$$(7\text{-}44c) \qquad \sigma = \frac{(1 - K')}{(2 + K')}$$

Here σ_p and σ_o are the electric conductivities of the particle and bulk electrolyte medium, respectively. $f(\kappa a)$ is Henry's function.

For a non-conducting spherical particle $\sigma_p = 0$ and $K' = 0$. This leads to $\sigma = 1/2$ and

$$F(\kappa a, K') \equiv f(\kappa a)$$

Eq. (7-43) then becomes

$$U = \left(\frac{2}{3}\ \frac{\zeta\varepsilon\varepsilon_o E_\infty}{\mu}\right) f(\kappa a)$$

which is Eq. (7-41).

For a perfectly conducting sphere, $\sigma_p \rightarrow \infty$ leading to

$K' \rightarrow \infty$ and $\sigma \rightarrow -1$

Hence

$$U = \frac{2}{3}\ \frac{\zeta\varepsilon\varepsilon_o E_\infty}{\mu}\left[3 - 2f(\kappa a)\right]$$

As $f(\kappa a) = 1$ for $\kappa a \rightarrow 0$ (large Debye length) the above equation indicates that $[3 - 2f(\kappa a)] \rightarrow 1$. Consequently, for $\kappa a \rightarrow 0$, both the conducting and non-conducting spheres behave in a similar manner. This is quite reasonable as, for a large Debye length, the electric field is undisturbed by the presence of a particle. However, for $\kappa a \rightarrow \infty$ the situation is different for the conducting sphere. Here $f(\kappa a) \rightarrow 3/2$ as $\kappa a \rightarrow \infty$ and $[3 - 2f(\kappa a)] \rightarrow 0$. Hence $U \rightarrow 0$ for $\kappa a \rightarrow \infty$ (small Debye length).

For the case of an arbitrary particle shape having $K' = 1$ (*i.e.*, $\sigma_p = \sigma_o$) σ becomes 0 leading to $F(\kappa a, 1) = 1$. This is Hückel's model where the electric field is distorted by the double layer but not by the presence of the particle.

For the case of non-conducting cylinders aligned parallel to the electric field, the electric field E_∞ is always parallel to the particle surface for all κa values. Here Smoluchowski's model is valid; *i.e.*, $F = 3/2$ for all κa values.

Gorin (1939) extended Henry's solution for the case of non-conducting cylinders oriented normal to the electric field. The F values are given in Figure 7-11. The above analysis includes *all* Henry's assumptions cited earlier. It should be remembered, however,

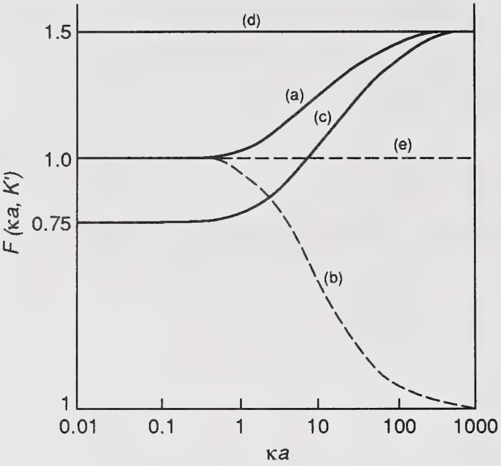

Figure 7-11. Value of Henry's (1931) function for particles of various shapes: (a) non-conducting sphere ($K' = 0$); (b) conducting sphere ($K' = \infty$); (c) and (d) non-conducting cylinder ($K' = 0$) with axis perpendicular and parallel to field, respectively; and (e) particle of any shape with $K' = 1$. K' is the relative conductivity of the particle compared to that of the medium ($K' = \sigma_p/\sigma_o$) (Hunter, 1981).

that due to polarization *all* particles act as non-conductors and hence having $K' \neq 0$ is an academic curiosity (Hunter, 1981).

For a randomly oriented cylinders, Keizer *et al.* (1975) showed that

$$U_{\text{effective}} = \frac{1}{3}\left(U_{\parallel} + 2\,U_{\perp}\right) \tag{7-45}$$

where $U_{\parallel}$ and $U_{\perp}$ are the electrophoretic mobilities of cylinders parallel and normal to the electric field, respectively.

For more details on electrophoresis of cylinders and arbitrary shape particles, the reader can refer to Hunter (1981), Morrison (1970), and Van der Drift *et al.* (1979).

7.4.3 Alternate Forms of the Electrophoretic Velocities

The solutions given so far are expressed in terms of a constant potential at the particle surface. We shall now discuss the case of electrophoretic velocity of spherical particles expressed in terms of a constant surface charge.

For the limiting case of thick electric double layer, $\kappa a \ll 1$, one can combine Eqs. (7-18) with (7-20) to give

$$U = \frac{Q_s E_\infty}{6\pi a \mu} \qquad \text{for } \kappa a \ll 1 \tag{7-46}$$

Similarly, for the case of a thin electric double layer, $\kappa a \gg 1$, combining Eq. (7-16) with (7-22) leads to

$$U = \frac{Q_s E_\infty}{4\pi a^2 \mu \kappa} \qquad \text{for } \kappa a \gg 1 \tag{7-47}$$

Eqs. (7-46) and (7-47) are the Hückel and Helmholtz–Smoluchowski expressions for constant surface charge, respectively.

Making use of the dimensionalization given by Russel *et al.* (1989), we can write

$$\beta^* = \frac{aeE_\infty}{kT} \qquad \text{, electric field strength} \tag{7-48a}$$

$$q_s^* = \frac{eQ_s}{4\pi a \varepsilon \varepsilon_o kT} \qquad \text{, surface charge density, and} \tag{7-48b}$$

$$U^* = \frac{U}{\left[\dfrac{\varepsilon\varepsilon_o \left(\dfrac{kT}{e}\right)^2}{\mu a}\right]} \qquad \text{, electrophoretic velocity} \tag{7-48c}$$

Making use of Eq. (7-48), the dimensionless electrophoretic velocity U^* can be given for the two boundary conditions as

Constant surface charge

$$U^* = \frac{2}{3}\beta^* q_s^* \qquad \text{for } \kappa a \ll 1 \tag{7-49a}$$

and

$$U^* = \beta^* \frac{q_s^*}{\kappa a} \qquad \text{for } \kappa a \gg 1 \tag{7-50a}$$

Putting $\zeta^* = e\zeta/kT$, the electrophoretic velocities corresponding to Eqs. (7-20) and (7-22) are given in dimensionless form as

Constant surface potential

(7-49b) $$U^* = \frac{2}{3}\beta^* \zeta^* \qquad \text{for } \kappa a \ll 1$$

and

(7-50b) $$U^* = \beta^* \zeta^* \qquad \text{for } \kappa a \gg 1$$

It is possible to generalize the limiting cases given above for both constant surface potential and surface charge in terms of Henry's solution.

The dimensionless form of Eq. (7-16) is

(7-51) $$\zeta^* = \frac{q_s^*}{(1 + \kappa a)}$$

Making use of the above expression, Henry's solution becomes (Russel *et al.*, 1989),

Constant surface charge

(7-52) $$U^* = \left(\frac{2}{3}\right)\left(\frac{\beta^* q_s^*}{1 + \kappa a}\right) f(\kappa a)$$

Constant surface potential

(7-53) $$U^* = \frac{2}{3}\beta^* \zeta^* f(\kappa a)$$

Figure 7-12 shows the electrophoretic mobility ($3U^*/2\beta^* q_s^*$) for the case of a constant surface charge and ($3\,U^*/2\beta^*\zeta^*$) for the case of a constant surface potential. Figure 7-12 shows that changes in κa affect the mobility when either the charge or the potential is held constant. In the latter case, the mobility stays non-zero because as the double-layer thickness diminishes, the particle charge increases.

It should be remembered that although we treated the case of holding the surface charge or the potential constant, the particle charge or its potential and the diffuse-layer thickness are closely related to each other in an experimental situation. For a given particle, changes in ionic strength alter the particle charge as well as the diffuse-layer thickness (Russel *et al.*, 1989).

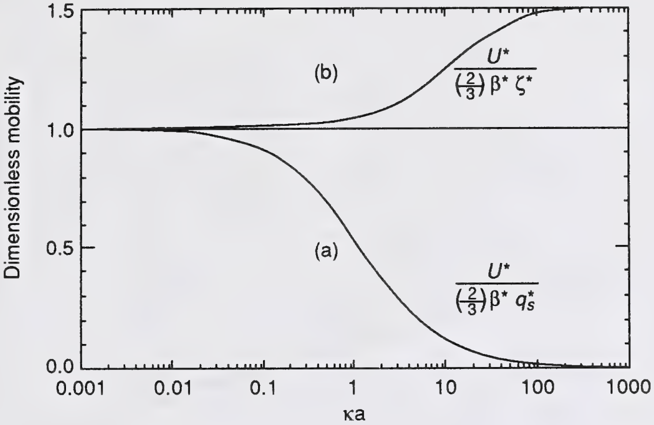

Figure 7-12. Electrophoretic mobility for a spherical particle as a function of the dimensionless diffuse layer thickness. (a) Henry's solution for constant surface charge. (b) Henry's solution for constant surface potential.

7.5 NUMERICAL SOLUTIONS: HIGH SURFACE POTENTIAL

For the general case of arbitrary Debye length and surface potential, O'Brien and White (1978) developed a computational scheme to solve the governing electrophoretic equations for a constant surface potential. Figures 7-13 to 7-15 summarize the solutions given by O'Brien and White. Figures 7-13 and 7-14 show the variation of normalized electrophoretic mobility with the dimensionless zeta potential for small and large κa, respectively.

Figure 7-13 shows that for $\zeta^* \leq 2$, for $\kappa a \rightarrow 0$, the slope of $3U^*/2\beta^*$ *versus* ζ^* is unity as would be expected from Eq. (7-49b). For $\kappa a \rightarrow \infty$, the slope given by Figure 7-14 is 3/2 in accordance with Eq. (7-50b). Deviation from Henry's solution occurs for $\zeta^* \gtrsim 2$ where $3U^*/2\beta^*$ *versus* ζ^* curves are no longer linear. For $0.01 < \kappa a < 2.75$, the increase in $3U^*/2\beta^*$ with ζ^* becomes more gradual and for $\kappa a \approx 2$, $3U^*/2\beta^*$ becomes independent of ζ^*. In other words, the particle mobility becomes unaffected by its surface potential. For $\kappa a \gtrsim 3$, the normalized mobility function $3U^*/2\beta^*$ has a maximum value which becomes particularly pronounced at high κa values. This maximum value occurs at $\zeta^* \cong 5-7$ which corresponds to $\zeta \cong 0.125-0.175$ V for a (1:1) electrolyte solution.

Figure 7-15 shows effects due to the valence character of the electrolyte. The electrolyte solutions correspond to (1:1), KCl; (2:1), $Ba(NO_3)_2$; and (3:1), $LaCl_3$. The maximum in the mobility moves from $\zeta^* \cong -5$ for the (1:1) electrolyte to $\zeta^* \cong -2.5$ for the (2:1) electrolyte and to $\zeta^* \cong -1.7$ for the (3:1) electrolyte. These values are in the ratios of 1:1/2:1/3 which are inversely proportional to the valencies.

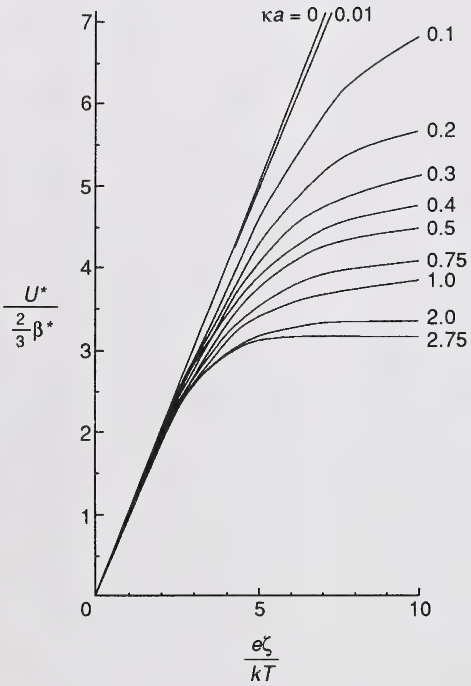

Figure 7-13. Electrophoretic mobility of a spherical particle in KCl (κ*a* < 3) (O'Brien and White, 1978).

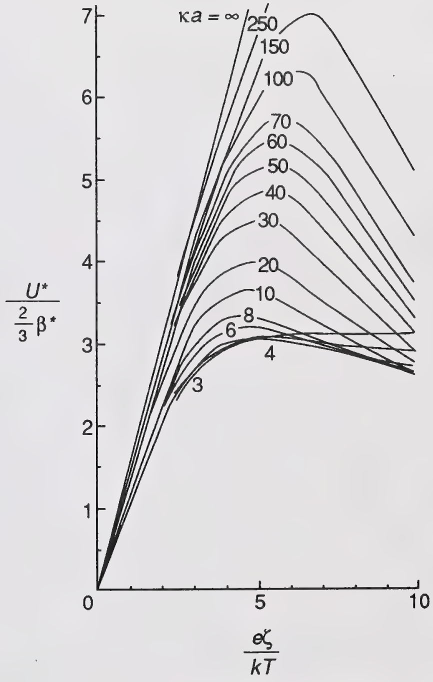

Figure 7-14. Electrophoretic mobility of a spherical particle in KCl (κ*a* > 3) (O'Brien and White, 1978).

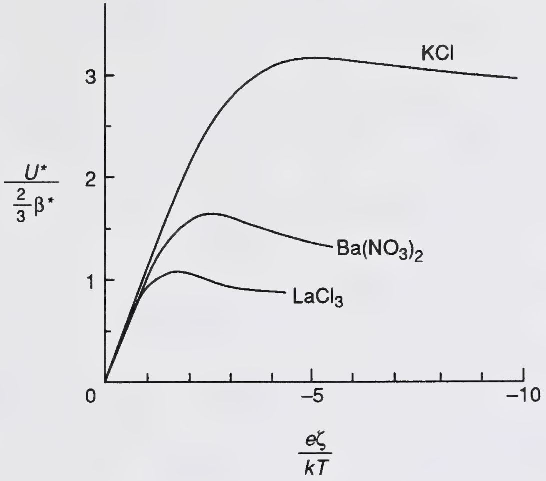

Figure 7-15. Effect of counterion valence on the electrophoretic mobility of a spherical particle at $\kappa a = 5$ (O'Brien and White, 1978).

Note that the maxima exhibited by the mobility $3U^*/2\beta^*$ above $(e\zeta/kT) \sim 3$ introduces difficulty in the estimation of U^* as shown in Figure 7-16 where two possible values for ζ^* exist.

The solution given by O'Brien and White (1978) takes into consideration the relaxation, the electrophoretic retardation, and high surface potential effects.

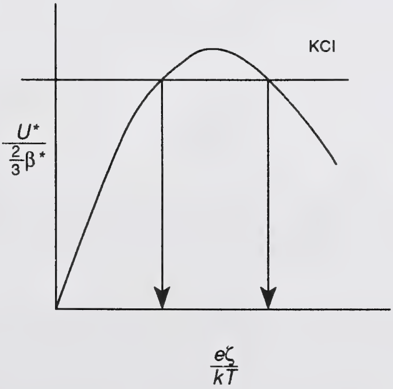

Figure 7-16. Evaluation of electrophoric mobility at large ζ^* values.

7.6 ELECTRIC FORCE ON A CHARGED PARTICLE IN AN ELECTRIC FIELD

The force on a spherical particle as stated by Eq. (7-39) is simply the product of the surface charge and the uniform field strength E_∞. Here, a more formal derivation is made for the electric force on the spherical particle as given by Henry's solution.

Consider a charged spherical particle located in a dielectric containing free charge; the electric force in x-direction F_E exerted on the particle is given by

$$F_E = \int_S \left[q_s E_x\right]_a dS \tag{7-54}$$

where the subscript x denotes x-direction and subscript a is for $r = a$.

For the special case of no angular variation in ψ, the charge density q_s is given by Eq. (7-13) as

$$q_s = -\varepsilon\varepsilon_o \left.\frac{d\psi}{dr}\right|_{r=a} \tag{7-55}$$

The electric field strength E_r is given by

$$E_r = -\frac{\partial}{\partial r}(\psi + \phi) \tag{7-56}$$

As $\partial\phi/\partial r = 0$ (Eq. 7-32b) then at $r = a$, we have

$$E_r = -\frac{d\psi}{dr} \quad \text{(independent of } \theta) \tag{7-57}$$

Now

$$E_\theta = -\frac{1}{r}\frac{\partial}{\partial\theta}(\psi + \phi) = -\frac{1}{r}\frac{\partial\phi}{\partial\theta} \tag{7-58}$$

The term $\partial\psi/\partial\theta = 0$ because of the imposed assumption that there is no θ-dependence for ψ.

The electric field strength in x-direction is given by

$$E_x = -E_\theta \sin\theta + E_r \cos\theta \tag{7-59}$$

The electric field strength components are shown in Figure 7-17.

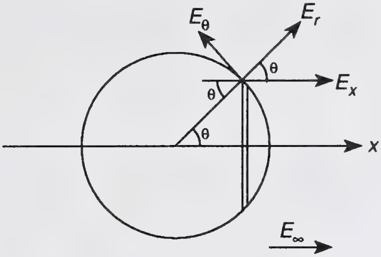

Figure 7-17. Electric field strength variation at the surface.

Making use of Eqs. (7-57) and (7-58), we obtain

$$E_x = \frac{1}{r}\frac{\partial\phi}{\partial\theta}\sin\theta - \frac{d\psi}{dr}\cos\theta \tag{7-60}$$

The solution for ϕ is given by Eq. (7-33) as

$$\phi = -E_\infty\left[r + \frac{1}{2}\frac{a^3}{r^2}\right]\cos\theta$$

The electric force in x-direction is then given by

$$F_E = \int_0^\pi -\left[\varepsilon\varepsilon_o\frac{d\psi}{dr}\right]_a \cdot \left[\frac{1}{a}\frac{\partial\phi}{\partial\theta}\sin\theta - \frac{d\psi}{dr}\cos\theta\right]_a [2\pi a\sin\theta]\, a d\theta \tag{7-61}$$

As the integral

$$\int_0^\pi \cos\theta\sin\theta\, d\theta = 0$$

the term $d\psi/dr\cos\theta$ of Eq. (7-61) does not contribute to the force term and Eq. (7-61) reduces to

$$F_E = -2\pi a\varepsilon\varepsilon_o\left.\frac{d\psi}{dr}\right|_a \int_0^\pi \left.\frac{\partial\phi}{\partial\theta}\right|_a \sin^2\theta\, d\theta \tag{7-62}$$

From Eq. (7-33), we obtain

$$\left.\frac{\partial\phi}{\partial\theta}\right|_a = \frac{3a}{2} E_\infty \sin\theta$$

and Eq. (7-62) becomes

$$F_E = -3\pi a^2 \varepsilon\varepsilon_o E_\infty \left.\frac{d\psi}{dr}\right|_a \int_0^\pi \sin^3\theta \, d\theta \tag{7-63}$$

The electric force on the particle in x-direction is then given by

$$F_E = \left[-4\pi a^2 \varepsilon\varepsilon_o \left.\frac{d\psi}{dr}\right|_a \right] E_\infty \tag{7-64}$$

The above expression was used in Eq. (7-39) to evaluate the electric force in Henry's solution.

7.7 EFFECT OF PARTICLE CONCENTRATION ON THE ELECTROPHORETIC MOBILITIES: SPHERICAL PARTICLES

In most cases, when measurements of an electrophoretic nature are made, several particles, *i.e.*, a suspension of particles (swarm of particles), are considered. It is important to know how the particle concentrations affect the electrophoretic mobilities U/E_∞. Conversely, electrophoretic mobility can be used to deduce electrolyte flow in a packed bed of particles or a porous bed where electrophoresis and electroosmosis are simply opposite expressions of the same relative motion of particles and liquid.

It is reasonable to state that in a regime where double-layer thickness is very small, *i.e.*, $\kappa a \gg 1$, one would expect that the electrophoretic velocity of a given particle is not affected by the presence of other particles, especially at low particle concentrations. Here, the particle electrophoretic mobility U/E_∞ would not be a concentration dependent. For the case of $\kappa a \gg 1$, one would expect Smoluchowski's equation to hold (Reed and Morrison, 1976; Hunter, 1981).

For the case of either very high particle concentrations or small κa, the double layers of adjacent particles overlap and one would not expect Henry's equation for a single particle to hold. Moreover, for $\kappa a \ll 1$, one would also expect Hückel's equation to be inappropriate even for fairly dilute suspensions.

In order to study the effect of particle concentration, it is necessary to model the particles suspension itself. Among the early models is that of Möller *et al.* (1961). They developed a model which led to an expression for the variation of electrophoretic mobility of monodisperse spheres of uniform and constant surface charge as the double layers overlap. In this model each particle is enclosed by a spherical shell of the electrolyte medium which contains just enough excess ions to neutralize the total charge on the surface of the particle.

The particles and their surrounding shells are considered to be of uniform size. The ratio of the particle radius to the outer shell radius is related to the suspension volume fraction α_p; *i.e.*,

$$\frac{a}{b} = \alpha_p^{1/3} \tag{7-65}$$

where a is the particle radius and b is the outer shell radius as shown in Figure 7-18.

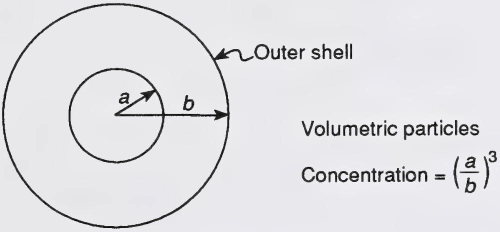

Figure 7-18. Cell model simulating a suspension of a spherical particles.

Möller *et al.* (1961) gave an expression for the electrophoretic mobility of a particle in a suspension. It is given by

$$U = \frac{\varepsilon\varepsilon_o\zeta E_\infty}{\mu} \cdot g_1\left(\kappa a, \alpha_p\right)$$

where $g_1(\kappa a, \alpha_p)$ is a function of κa and α_p and U/E_∞ is the electrophoretic mobility of the particle.

The limits of the applicability of the Möller *et al.* (1961) expression is given by Levine and Neale (1974b):

α_p	0.0001	0.001	0.01	0.05	0.2	0.4	0.6
κa	0.5	0.7	1.2	2.3	5	8	15

Figure 7-19 shows as dashed curves the values of $g_1(\kappa a, \alpha_p)$. It is clear that for very small κa the particle concentration has a marked effect on the particle mobility.

Levine and Neale (1974a) extended Henry's solution and the model given by Möller *et al.* (1961) for the case of suspension of spherical particles. Similarly, each particle was envisaged as being surrounded by a hypothetical concentric shell of electrolyte. Henry's theory (1931) for the electrophoresis of a single isolated sphere is used whereby the hydrodynamic and electrical boundary conditions as $r \rightarrow \infty$ are applied at the outer shell of $r = b$. The cell model is given by Figure 7-18.

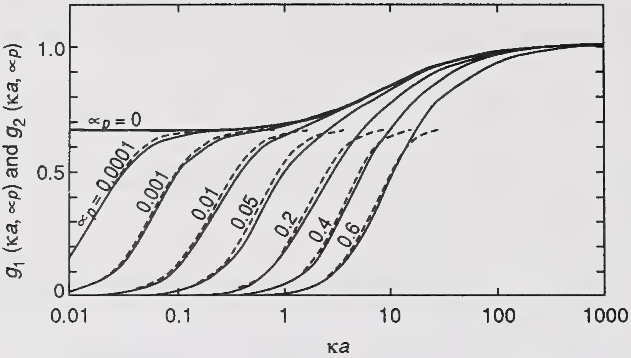

Figure 7-19. Plot of g_1 $(\kappa a,\alpha_p)$ and g_2 $(\kappa a,\alpha_p)$ *versus* κa for various values of α_p; solid lines, theory of Levine and Neale (1974a,b); dashed lines, theory of Möller *et al.* (1961) (Levine and Neale, 1974b).

A brief outline of the cell model is given below. The total potential is assumed to be $(\phi + \psi)$ where ψ arises from the double layer and ϕ from the applied field. The following equations are solved:

$$\varepsilon\varepsilon_o \nabla^2 \psi = -\overset{(f)}{\rho} \tag{7-66}$$

where $\psi = \psi(r)$, *i.e.*, ψ depends on radial distance only

$\overset{(f)}{\rho}$ is the free charge density.

The boundary conditions are

$$\frac{d\psi}{dr} = -\frac{q_s}{\varepsilon\varepsilon_o} \text{ at } r = a \tag{7-67a}$$

and

$$\frac{d\psi}{dr} = 0 \text{ at } r = b \tag{7-67b}$$

where q_s is the surface charge density.

Boundary condition (7-67a) relates the ψ gradient to the surface charge q_s. As an equivalent to this boundary condition one can equally use $\psi = \zeta$ at $r = a$. The boundary condition (7-67b) indicates that there is no current entering the particle; *i.e.*, the surface is non-conducting.

The potential due to the external field $\phi(r,\theta)$ is governed by

$$\nabla^2\phi = 0 \tag{7-68}$$

with the boundary conditions

$$\frac{\partial\phi}{\partial r} = 0 \qquad \text{at } r = a \tag{7-69a}$$

and

$$\frac{\partial\phi}{\partial r} = -E_\infty \cos\theta \qquad \text{at } r = b \tag{7-69b}$$

Figure (7-7) shows the coordinate system.

Making use of the Debye–Hückel approximation, the solutions of the potentials are given by

$$\psi(r) = \left(\frac{q_s a}{\varepsilon\varepsilon_o}\right)\left(\frac{a}{r}\right)\left[\frac{\sinh(\kappa b - \kappa r) - \kappa b \cosh(\kappa b - \kappa r)}{(1 - \kappa^2 ab)\sinh(\kappa b - \kappa a) - (\kappa b - \kappa a)\cosh(\kappa b - \kappa a)}\right] \tag{7-70}$$

and

$$\phi(r,\theta) = \frac{-E_\infty}{(1 - \alpha_p)}\left[r + \frac{a^3}{2r^2}\right]\cos\theta \tag{7-71}$$

The fluid flow around a typical particle is governed by the Navier–Stokes equation. For creeping flow, the equation of motion is given by

$$\mu\nabla^2\vec{u} = \vec{\nabla}p + \overset{(f)}{\rho}\vec{\nabla}(\phi + \psi) \tag{7-72}$$

with the continuity equation

$$\vec{\nabla}\cdot\vec{u} = 0 \tag{7-73}$$

The boundary conditions are

$$u_r(r,\theta) = u_\theta(r,\theta) = 0 \qquad \text{at } r = a \tag{7-74a}$$

$$u_r(r,\theta) = -U\cos\theta \qquad \text{at } r = b \tag{7-74b}$$

and

$$\text{(7-74c)} \quad \frac{1}{r}\frac{\partial(ru_\theta)}{\partial r} - \frac{1}{r}\frac{\partial u_r}{\partial \theta} = \text{flow vorticity} = 0 \text{ at } r = b$$

Here it is assumed that the particle is held stationary with the electrolyte flowing past it. This situation is given by the boundary conditions of Eq. (7-74a). At $r = b$ it is assumed that the electrolyte flow is uniform (Eq. 7-74b). At the outer shell, the vorticity is set to zero. This boundary condition is referred to as the Kuwabara's model simulating flow over a packed bed of spheres (Kuwabara, 1959). One could have used the boundary condition of setting $\tau_{r\theta} = 0$ at $r = b$. This is referred to as Happel's model (1958). U represents the streaming flow velocity at $r = b$. Kozak and Davis (1989a) gave the reasons for the preference of using Kuwabara's model. However, the solutions from the two models are essentially the same.

The solution of Eqs. (7-72) and (7-73) subject to the boundary conditions of Eq. (7-74) is given by Levine and Neale (1974a). Making use of a force balance similar to Henry's approach, the function $g_2(\kappa a,\alpha_p)$ that accounts for the presence of neighboring particles is evaluated and it is shown in Figure 7-19. The correction factor g_2 is defined as

$$U = \left(\frac{\varepsilon\varepsilon_o\zeta E_\infty}{\mu}\right) g_2(\kappa a,\alpha_p)$$

Here U refers to the electrophoretic particle velocity. The function g_2 was derived assuming $ze\zeta/kT < 1$.

For $\alpha_p = 0$, g_2 function becomes $(2/3)\,f(\kappa a)$, where $f(\kappa a)$ is Henry's function. The plot for $g_2(\kappa a,\alpha_p)$ against κa for various particle concentrations α_p clearly shows that at $\kappa a > 10^3$, the concentration has little effect on the electrophoretic mobility, *i.e.*, $g_2(\kappa a,\alpha_p) \cong 1.0$, and the Smoluchowski equation can be used. For $\kappa a \ll 1$, $g_2(\kappa a,\alpha_p)$ becomes 2/3 only when $\alpha_p = 0$. In this limit of κa, the particle concentration has a marked effect on $g_2(\kappa a,\alpha_p)$.

For the case of high surface potential, Kozak and Davis (1989a) used Kuwabara's model to include the relaxation effect as well. Some of their results are shown in Figures 7-20 to 7-22 for large values of κa. Deviation from Smoluchowski's equation is shown on these plots. Their dimensionless mobility is defined such that the dimensionless mobility for the Smoluchowski equation is equal to $2(ze\zeta/kT)$ where $(ze\zeta/kT)$ is the dimensionless surface potential. In other words, the dimensionless mobility is defined by Kozak and Davis (1989a) as

$$M^* = \frac{2\mu U z e}{\varepsilon\varepsilon_o E_\infty kT} = \frac{2U^*}{\beta^*}$$

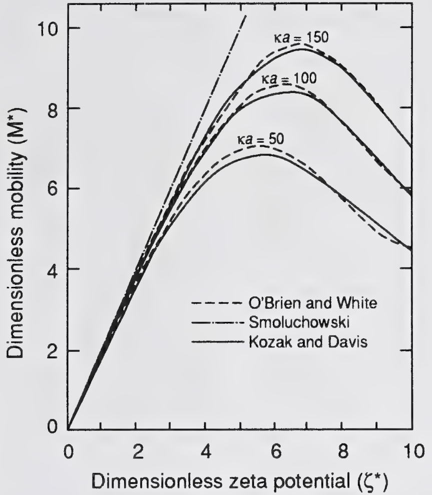

Figure 7-20. A comparison among the analyses of O'Brien and White (1978) for a (*z–z*) electrolyte; Smoluchowski, Kozak, and Davis (1989a) for single spheres (Kozak and Davis, 1989a).

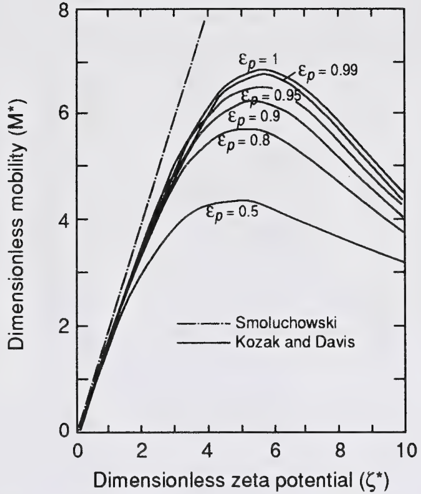

Figure 7-21. The effects of porosity and zeta potential on the dimensionless mobility for κ*a* = 50 (Kozak and Davis, 1989a).

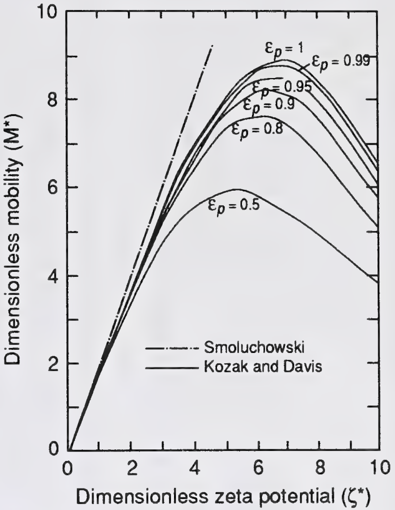

Figure 7-22. The effects of porosity and zeta potential on the dimensionless mobility for κ*a* = 150 (Kozak and Davis, 1989a).

The Smoluchowski equation in dimensionless form is then given by

$$M^* = 2\zeta^*$$

Figure 7-20 shows Kozak and Davis work for $\alpha_p = 0$ ($\varepsilon_p = 1$, porosity). For a single sphere, it compares well with O'Brien and White (1978) where high potential and relaxation effects are taken into account in the analysis. Figures 7-21 and 7-22 are given for $\varepsilon_p = (1 - \alpha_p)$ in the range of 0.5 to 1.0. The deviation from the Smoluchowski analysis becomes even greater at a higher surface potential. Various asymptotic expansion expressions are given by Kozak and Davis (1989b).

It should be noted, however, that although the analysis was made using a higher potential, polarization usually occurs at a high potential leading to a variable dielectric constant ε. Moreover, the above models neglect the effect of a finite ion size. The above simplifications would lead to a greater deviation from Henry's curve. For models dealing with a variable dielectric constant and finite size of ions, the reader is referred to Gur *et al.* (1978a,b), Pintauro and Verbrugge (1989), Verbrugge and Pintauro (1989), and Datta and Kotamarthi (1990).

An experimental study on electrophoresis of porous aggregates was conducted by Miller and Berg (1993). They obtained reasonable agreement between the experimentally measured electrophoretic mobility of porous aggregates and the aforementioned theoretical analyis of Levine and Neale (1974a,b) and with the theoretical study of Miller *et al.* (1992). The theoretical analysis tends to underestimate the effect of the porosity of the aggregates.

7.8 EFFECT OF PARTICLE CONCENTRATION ON THE ELECTROPHORETIC MOBILITIES: CIRCULAR CYLINDERS NORMAL TO THE ELECTRICAL FIELD

Electrophoresis of a swarm of fibres (circular cylinders) is important for the study of the electrokinetic transfer phenomenon of colloidal particles in fibrous media. For the case of the electric field normal to a circular cylinder, Henry (1931) analysed the case of the electrophoretic mobility of an isolated cylinder. Abramson *et al.* (1942) further developed Henry's analysis of an isolated cylinder to obtain results for intermediate values of κa where "a" represents the circular cylinder radius. Van der Drift *et al.* (1979) applied Henry's approach, relaxing the constraint of linearization of the Boltzmann equation that describes the charge density.

The extension of the analysis for the electrophoretic mobility for the case of a mat of cylindrical fibres was conducted by Guzy *et al.* (1983), and Kozak and Davis (1986). The latter combined Henry's approach with Kuwabara's cell model to analyse the electrophoretic mobility of a mat of cylinders normal to the electric field strength. The governing equations are similar to those of Levine and Neale (1974a), except that they are cast in cylindrical coordinates. The Debye Hückel approximations are employed.

For the case of the cell model, the fibrous mat concentration is given by

$$\alpha_p = \left(\frac{a}{b}\right)^2 = 1 - \varepsilon_p \tag{7-75}$$

where a is the cylinder radius
b is the outer shell radius
α_p and ε_p are the mat concentration and porosity, respectively.

Strictly speaking, the cell model is applicable to an ordered array of fibres as shown in Figure 7-23. The effect of the mat porosity is given in Figure 7-24. As is for the case of a suspension of spheres, the effect of particle concentrations is important when the electric double layers overlap, $\kappa a \ll 1$ (Kozak and Davis, 1986). The correction factor is shown in Figure 7-24 and is given by

$$U = \frac{\varepsilon\varepsilon_o\zeta E_\infty}{\mu}\, g_3\left(\kappa a, \varepsilon_p\right) \tag{7-76}$$

where U is the electrophoretic velocity of a cylinder within the mat.

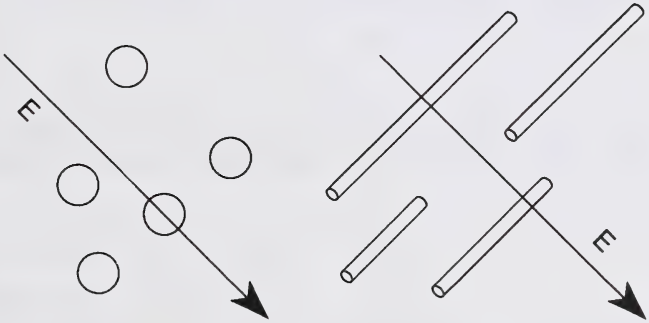

Figure 7-23. Electrophoretic mobility of a mat of cylinders.

For large values of κa [$\kappa a > 20$ and for $(\kappa b - \kappa a) > 4$] the solution for the electrophoretic mobility is given by

$$U = \frac{\varepsilon\varepsilon_o\zeta E_\infty}{\mu}\left[1 - \frac{\left(2 + \varepsilon_p\right)}{\varepsilon_p \kappa a} + \frac{6.9984 + 11.4984\varepsilon_p}{\varepsilon_p(\kappa a)^2} + O(\kappa a)^{-3}\right] \tag{7-77}$$

For an isolated cylinder $\varepsilon_p = 1$ and Eq. (7-77) which is valid for $\kappa a > 20$ becomes

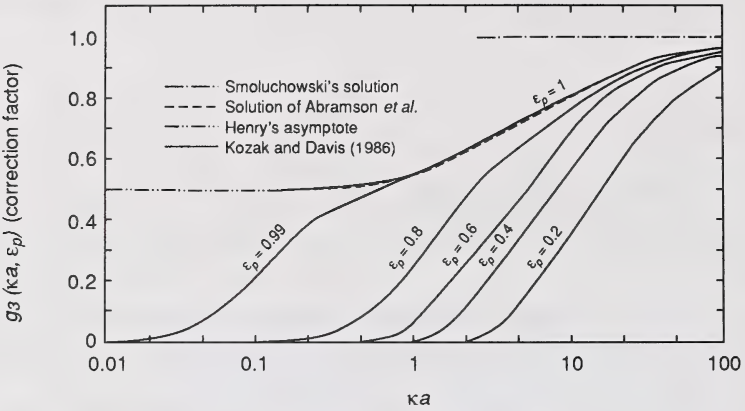

Figure 7-24. A comparison among the results of Smoluchowski's equation, Henry's solution (1931), the solution of Abramson *et al.* (1942), and Kozak and Davis (1986) for the case of cylinders (Kozak and Davis, 1986).

$$U = \frac{\varepsilon\varepsilon_o \zeta E_\infty}{\mu}\left[1 - \frac{3}{\kappa a} + \frac{18.5}{(\kappa a)^2} + \ldots\right] \tag{7-78a}$$

The above expression for an isolated cylinder is very similar to the corresponding expression due to Henry (1931) for the case of an isolated sphere which is given as (Hunter, 1981)

$$U = \frac{\varepsilon\varepsilon_o \zeta E_\infty}{\mu}\left[1 - \frac{3}{\kappa a} + \frac{25}{(\kappa a)^2} - \frac{220}{(\kappa a)^3} + \ldots\right] \quad \text{for } \kappa a \gtrsim 20 \tag{7-78b}$$

For the limit of small κa ($\kappa a < 0.01$), the asymptotic solution for all ε_p for the case of cylinders is given by

$$U \cong \frac{\varepsilon\varepsilon_o \zeta E_\infty}{2\mu}\left[1 - \frac{2\left(1-\varepsilon_p\right)}{2\left(1-\varepsilon_p\right) - \kappa a \; ln \; \kappa a}\right] \tag{7-79}$$

In the limit of $\varepsilon_p \rightarrow 1$ and $\kappa a \ll 1$, Eq. (7-79) reduces to Hückel's expression for the case of an isolated cylinder with the electric field normal to the axis of the cylinder. Eq. (7-79) together with Figure 7-24 clearly show that when the double layer is thick, the presence of the surrounding fibres (cylinders) has a significant effect on the electrophoretic mobility of the cylinders. For $\kappa a \le 0.1$, the overlapped electric layers would reduce the electroosmotic velocity even in a very dilute mat of cylinders.

An important observation is that the expressions derived for the electrophoretic velocity for a swarm of spheres or a mat of cylindrical fibres are equally valid for electro-osmotic flow within a rigid bed of spheres or a mat of fibres. This is because both processes involve the relative motion of solid particles and electrolyte under the influence of an externally applied electric field, in the absence of an applied pressure gradient (Levine and Neale, 1974a).

Settling of particles under a gravitational field is very much influenced by the swarm concentration. In general, for monodispersed spherical particles, suspension settling velocity in a tube is given by

$$\frac{U_s}{U_\infty} = \left(1 - \alpha_p\right)^{4.6} \tag{7-80}$$

where U_s is the settling velocity of a suspension having a solids concentration α_p
U_∞ is the settling velocity of a single sphere in an infinite medium.

The above hindered settling expression shows a very strong dependence of (U_s/U_∞) on α_p. In contrast, when κa is large, *i.e.*, for thin electric double layer, the effect of the particle concentration is not important. This would suggest that for a flow in a packed bed or a porous medium, electroosmosis becomes an effective means for inducing fluid flow when κa is large.

7.9 NOMENCLATURE

a	radius of a sphere or a cylinder, m
A_c	cross-sectional flow area, m^2
b	outer radius of the cell model
D	particle diffusion coefficient
E_r	electric field in the radial direction, V/m
E_x	electric field in x-direction, V/m
E_y	electric field in the y-direction, V/m
E_θ	electric field strength in the angular direction, V/m
E_∞	electric field strength far from a particle, V/m
$f(\kappa a)$	Henry's function, dimensionless
F_E	force on a particle due to electric drag, N
F_H	force on a particle due to hydrodynamic drag, N

$F(\kappa a,K')$	generalized Henry's function defined by Eq. (7-44b)
$g_1(\kappa a,\alpha_p)$	Möller *et al.* (1961) function to account for κa and spherical particles concentration, dimensionless
$g_2(\kappa a,\alpha_p)$	Levine and Neale (1974a,b) function to account for κa and spherical particles concentration, dimensionless
$g_3(\kappa a,\varepsilon_p)$	Kozak and Davis (1986) function to account for κa and cylindrical fibres concentration, dimensionless
k	Boltzmann constant, J/K
K'	ratio of a particle to medium electric conductivity defined by Eq. (7-44a)
M^*	dimensionless mobility = $2U^*/\beta^*$
n_∞	ionic number concentration in the bulk solution, m^{-3}
Pe	particle Peclet number, Ua/D
q_s	surface charge density, C/m^2
q_s^*	dimensionless surface charge density defined by Eq. (7-48b)
$\overset{(f)}{Q}$	total free charge, C
Q_s	total surface charge, C
r	radial coordinate, m
t	dummy variable
T	absolute temperature, K
u_r	local radial fluid velocity, m/s
u_x	local fluid velocity in x-direction, m/s
u_θ	local angular fluid velocity, m/s
$\vec{u}$	local fluid velocity vector, m/s
U	electrophoretic particle velocity, m/s; fluid velocity far from the particle or fluid velocity at the outer shell of a cell
U^*	dimensionless electrophoretic velocity defined by Eq. (7-44c)
U_s	settling velocity of a suspension of particles, m/s
U_∞	settling velocity of a spherical particle in infinite dilution, m/s
(x,y)	Cartesian coordinates
z	absolute value of the valency for a $(z{:}z)$ electrolyte

α_p	concentration of spherical particles in a suspension contraction of cylinders in a mat, dimensionless
β^*	dimensionless electric field strength defined by Eq. (7-48a)
ε	dielectric constant of a material, dimensionless
ε_o	permittivity of vacuum, C/mV
ε_p	porosity of a suspension = $1 - \alpha_p$
ζ	zeta potential, V
ζ^*	dimensionless zeta potential = $ze\zeta/kT$
θ	angular coordinate
κ	inverse Debye length, m^{-1}
μ	fluid viscosity, Pa s
ξ	transformation variable
$\rho^{(f)}$	free charge density, C/m^3
σ	conductivity function, dimensionless
ϕ	potential due to electric field, V
ψ	potential due to double layer, V
$\vec{\nabla}$	del operator, m^{-1}
∇^2	Laplace operator, m^{-2}

7.10 REFERENCES

Abramson, H.A., Moyer, L.S., and Gorin, M.H. (1942), *Electrophoresis of Proteins*, 125–33, Reinhold, New York.

Booth, F. (1950), *The Cataphoresis of Spherical, Solid Non-Conducting Particles in a Symmetrical Electrolyte*, Proc. Roy. Soc. Lond., **203A**, 514.

Datta, R. and Kotamarthi, V.R. (1990), *Electrokinetic Dispersion in Capillary Electrophoresis*, AIChEJ, **36**, 916–25.

Dukhin, S.S. and Derjaguin, B.V. (1974), *Electrokinetic Phenomena, Surface and Colloid Science* (ed. Matijevic, E.), **7**, John Wiley, New York.

Gorin, M.H. (1939), *in* Abramson *et al.*, Chem. Revs., **24**, 364.

Gur, Y., Ravina, I., and Babchin, A.J. (1978a), *On the Electrical Double Layer Theory. I. A Numerical Method for Solving a Generally Set Poisson, Boltzmann Equation*, J. Colloid Interface Sci., **64**, 326–32.

Gur, Y., Ravina, I., and Babchin, A.J. (1978b), *On the Electrical Double Layer Theory. II. The Poisson–Boltzmann Equation Including Hydration Forces*, J. Colloid Interface Sci., **64**, 333–41.

Guzy, C.J., Bonano, E.J., and Davis, E.J. (1983), *The Analysis of Flow and Colloidal Particle Retention in Fibrous Porous Media*, J. Colloid Interface Sci., **95**, 523–43.

Happel, J. (1958), *Viscous Flow in Multiparticle Systems*, AIChEJ, **4**, 197–201.

Henry, D.C. (1931), *The Cataphoresis of Suspended Particles, Part I. The Equation of Cataphoresis*, Proc. Roy. Soc. Lond., **133A**, 106–29.

Hunter, R.J. (1981), *Zeta Potential in Colloid Science*, Academic Press, London.

Keizer, A., van der Drift, W.P.J.T., and Overbeek, J.Th.G. (1975), Biophys. Chem., **3**, 107.

Kozak, M.W. and Davis, E.J. (1986), *Electrokinetic Phenomena in Fibrous Porous Media*, J. Colloid Interface Sci., **112**, 403–11.

Kozak, M.W. and Davis, E.J. (1989a), *Electrokinetics of Concentrated Suspensions and Porous Media. I. Thin Electrical Double Layers*, J. Colloid Interface Sci., **127**, 497–510.

Kozak, M.W. and Davis, E.J. (1989b), *Electrokinetics of Concentrated Suspensions and Porous Media. 2. Moderately Thick Electrical Double Layers*, J. Colloid Interface Sci., **129**, 166–74.

Kuwabara, S. (1959), *The Forces Experienced by Randomly Distributed Parallel Circular Cylinders or Spheres in a Viscous Flow at Small Reynolds Numbers*, J. Phys. Soc. Japan, **14**, 527–32.

Levine, S. and Neale, G.H. (1974a), *The Prediction of Electrokinetic Phenomena Within Multiparticle Systems. I. Electrophoresis and Electroosmosis*, J. Colloid Interface Sci., **47**, 520–29.

Levine, S. and Neale, G.H. (1974b), *Electrophoretic Mobility of Multiparticle Systems*, J. Colloid Interface Sci., **49**, 330–32.

Miller, N.P. and Berg, J.C. (1993), *Experiments on the Electrophoresis of Porous Aggregates*, J. Colloid Interface Sci., **159**, 253–54.

Miller, N.P., Berg, J.C., and O'Brien, R.W. (1992), *The Electrophoretic Mobility of a Porous Aggregate*, J. Colloid Interface Sci., **153**, 237–43.

Möller, J.H.M., Van Os, G.A.J., and Overbeek, J.Th.G. (1961), *Interpretations of the Conductance and Transference of Boviar Serum Albumin Solutions*, Trans. Faraday Soc., **57**, 325–37.

Morrison, F.A. (1970), *Electrophoresis of a Particle of Arbitrary Shape*, J. Colloid Interface Sci., **34**, 210–14.

Overbeek, J.Th.G., (1943), Kollidchem. Beih, **54**, 287.

O'Brien, R.W. and White, L.R. (1978), *Electrophoretic Mobility of a Spherical Colloidal Particle*, J. Chem. Soc. Faraday Trans., *II*, **74**, 1607–26.

Probstein, R.F. (1989), *Physicochemical Hydrodynamics*, Butterworths, Boston.

Pintauro, P.N. and Verbrugge, M.W. (1989), *The Electric-Potential Profile in Ion-Exchange Membrane Pores*, J. Membrane Sci., **44**, 197–212.

Reed, L.D. and Morrison, F.A. (1976), *Hydrodynamic Interaction in Electrophoresis*, J. Colloid Interface Sci., **54**, 117–33.

Russel, W.B., Saville, D.A., and Schowalter, W.R. (1989), *Colloidal Dispersions*, Cambridge University Press, Cambridge.

Shaw, D.J. (1980), *Introduction to Colloid and Surface Chemistry*, 3rd ed., Butterworths, London.

Van der Drift, W.P.J.T., Keizer, A.D.E., and Overbeek, J.Th.G. (1979), *Electrophoretic Mobility of a Cylinder with High Surface Charge Density*, J. Colloid Interface Sci., **71**, 67–78.

Verbrugge, M.W. and Pintauro, P.N. (1989), *Transport Models for Ion-Exchange Membranes, Modern Aspects of Electrochemistry, #19.*

Wiersema, P.H., Loeb, A.L., and Overbeek, J.Th.G. (1966), *Calculation of the Electrophoretic Mobility of a Spherical Colloid Particle*, J. Colloid Interface Sci., **22**, 78–99.

SEDIMENTATION POTENTIAL 8

8.1 SEDIMENTATION POTENTIAL

An electrical potential gradient is set up when colloidal particles suspended in an electrolyte solution are forced to move under the influence of a gravitational, centrifugal, ultrasonic, or other field. This electrical potential is also referred to as the migration potential or the Dorn effect (Dorn, 1878). It is the least investigated electrokinetic phenomenon discussed so far.

As a charged particle moves downward, some of the ions in the diffuse layer close to the particle are sheared off (*i.e.*, left behind). The liquid behind each particle therefore carries an excess of counterions compared with the liquid ahead of the particle. As the total current must be zero, an induced electric field is set up such that the net current becomes zero (Neale, 1974). Consequently, when electrodes are placed near the top and bottom of a settling tube, an induced potential gradient can be measured.

Figure 8-1 shows the electric field for a settling particle. The induced field E will in turn exert a force on the particle and on the ions. This force always acts to retard the particle. For a system having a very fine suspension of particles in plain water ($\kappa a \ll 1$), *i.e.*, a weak electrolyte, the observed sedimentation velocity can be appreciably smaller than the expected values from the hydrodynamic calculations.

A simplistic derivation for the induced sedimentation potential can be made as follows:

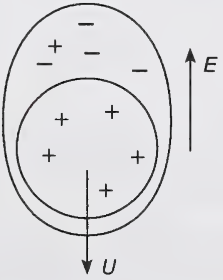

Figure 8-1. Settling of a charged particle in an electrolyte.

The sedimentation potential is the converse of the streaming potential and we can write (see Eq. (6-48))

$$\left(\frac{E_x}{P_x}\right)_{I=0} = \frac{\Omega}{\sigma} \mathrm{f}(\kappa a,\beta) = \frac{\varepsilon\varepsilon_o\psi_s}{\mu\sigma} f(\kappa a,\beta) \tag{8-1}$$

for $\kappa a \to \infty$, *i.e.*, thin double layer, the function $f(\kappa a,\beta) \to 1$ and Eq. (8-1) becomes

$$E_{sed} = \frac{\varepsilon\varepsilon_o\zeta}{\sigma\mu} P_{sed} \tag{8-2}$$

where $\psi_s \equiv \zeta$

For a (1:1) electrolyte solution, the solution electrical conductivity σ is given by Eq. (4-52) as

$$\sigma = \frac{2n_\infty e^2 D}{kT} \tag{8-3}$$

P_{sed} denotes the "driving pressure" gradient causing sedimentation. Although Eq. (8-1) was derived for a straight, circular capillary, it is still valid for an arbitrary cross section provided the double layer is everywhere very thin ($\kappa a \to \infty$) and ζ is small.

The pressure gradient for the case of sedimentation shown in Figure 8-2 can be calculated as follows:

Total driving force $\frac{4}{3}\pi a^3 (\rho_s - \rho_f)\, gN$

Driving pressure $\frac{4}{3}\pi a^3 (\rho_s - \rho_f)\, g\frac{N}{A}$

Driving pressure gradient $\frac{4}{3}\pi a^3 (\rho_s - \rho_f)\, \frac{gN}{AL}$

Now the number of particles per unit volume is given by $n_o = N/AL$. Hence, the particle volume fraction α_p is given by $\alpha_p = (4/3)\pi a^3 n_o$. Here a is the radius of the spherical particle and g is the acceleration due to gravity.

The "pressure gradient" is then given by

$$P_{sed} = (\rho_s - \rho_f)\, \alpha_p g \tag{8-4}$$

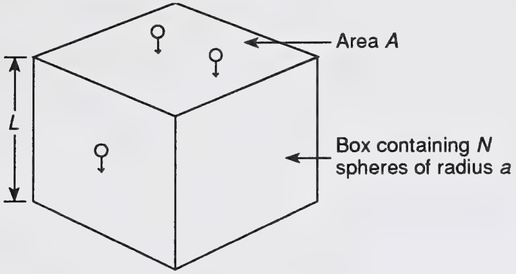

Figure 8-2. A volume element within sedimenting spheres.

Combining Eqs. (8-2) and (8-4) leads to

$$E_{sed} = \frac{\varepsilon\varepsilon_o\zeta\,(\rho_s - \rho_f)\,\alpha_p g}{\mu\sigma} \qquad \text{for } \kappa a \gg 1 \text{ and } \alpha_p \ll 1 \tag{8-5}$$

The sedimentation potential given by Eq. (8-5) is that stated by Smoluchowski (1903, 1921). Here ρ_s and ρ_f are the solids and the fluid densities, respectively. μ is the fluid viscosity. Experimental results show that Eq. (8-5) is obeyed for Pyrex glass powder ($a \sim 50$ μm) settling in a dilute KCl solution (see Booth, 1954). Eq. (8-5) also states that E_{sed} is independent of particle size and that $E_{sed} \rightarrow 0$ as $\alpha_p \rightarrow 0$.

Smoluchowski pointed out the existence of a reduction on the sedimentation rate due to the presence of the induced electric field. Let U_o denote the steady rate of fall when the surface of the particle is uncharged and U is the steady rate when the particle carries a uniform surface charge such that its surface potential is ζ. Smoluchowski's expression for a single spherical particle is given by

$$\frac{U}{U_o} = \left[1 + \frac{\varepsilon^2\varepsilon_o^2\zeta^2}{4\pi a^2\sigma\mu}\right]^{-1} \qquad \text{for } \kappa a \gg 1 \tag{8-6}$$

The effect on the settling velocity is very small.

Example

Consider a sedimenting suspension, having a volume fraction of 0.1, of spherical particles with $a = 10 \times 10^{-6}$ m. The ζ value is 0.05 V. The liquid is water and it contains 0.01 M of KCl at 25°C. Particle density is 2600 kg/m^3. Evaluate the sedimentation potential.

$$\varepsilon_o = 8.85 \times 10^{-12} \frac{C^2}{Nm^2} \text{ or } \left(\frac{C}{Vm}\right)$$

$$\varepsilon = 80$$

$$\sigma = 0.141 \frac{A}{Vm}$$

$$g = 9.81 \frac{m}{s^2}$$

$$\mu = 0.001 \text{ Pa s}$$

$$E_{sed} = \frac{80 \times 8.85 \times 10^{-12} \times 0.05\,(2600 - 1000)(0.1)\,9.81}{0.001 \times 0.141}$$

Using Eq. (8-5), one obtains

$$E_{sed} = 0.0004 \frac{V}{m}$$

This is a very weak electric field; however, a high impedance millivolt meter can be used for the measurement (Hunter, 1981).

From Eq. (8-6), we obtain

$$\frac{U}{U_o} = [1 + 0.00114]^{-1} = 0.9989$$

8.2 SEDIMENTATION POTENTIAL FOR A MULTIPARTICLE SYSTEM (A SEDIMENTING SUSPENSION): EXTENSION

Smoluchowski (1921), as indicated in the previous section, gave the expressions for the sedimentation potential and for the retardation of a settling suspension for $\kappa a >> 1$. Booth (1954) and Sengupta (1968) extended Smoluchowski's analysis to include arbitrary κa values for a single particle.

Smoluchowski's expression as given by Eq. (8-5) is valid only for very dilute systems. The effects of double-layer interaction and hydrodynamic interaction between the particles were not explicitly accounted for. Levine *et al.* (1976) made use of Kuwabara's cell model to predict the sedimentation potential and retardation effect for a swarm of monosized spheres having arbitrary values of α_p and κa.

The basic results given by Levine *et al.* (1976) are

$$E_{sed} = \frac{9\varepsilon\varepsilon_o \zeta U \alpha_p}{2\sigma a^2} \gamma\left(\kappa a, \alpha_p\right) \tag{8-7}$$

and

$$\frac{U}{U_o} = \left[1 + \frac{\varepsilon^2 \varepsilon_o^2 \zeta^2}{4\pi a^2 \sigma \mu} H\left(\kappa a, \alpha_p\right)\right]^{-1} \tag{8-8}$$

γ and H are complicated functions of κa and α_p and they are given graphically in Figures 8-3 and 8-4. Eqs. (8-7) and (8-8) correctly reduce to Smoluchowski's expressions for the case of a single sphere surrounded by a very thin double layer; *i.e.*, $\alpha_p \rightarrow 0$, $\kappa a \rightarrow \infty$ and ζ is small.

Figure 8-3 shows that $\gamma > 1$ and it increases with α_p for a given value of κa. The variation of γ indicates that the sedimentation potential becomes more pronounced with increasing suspension concentration. Similarly, U/U_o decreases with increasing suspension concentration. The sedimentation potential effect would be negligible for small κa for all values of α_p.

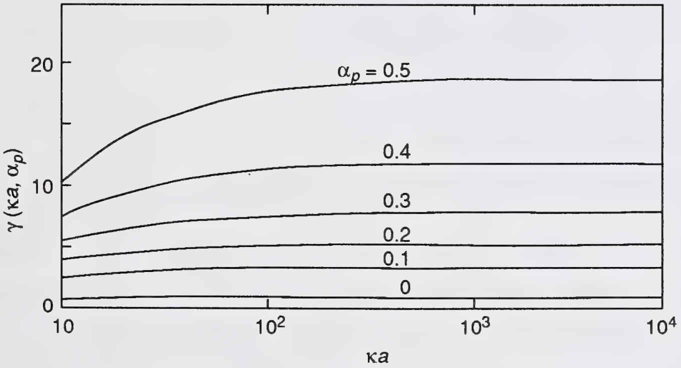

Figure 8-3. Variation of function γ with κa and α_p (Levine *et al.*, 1976).

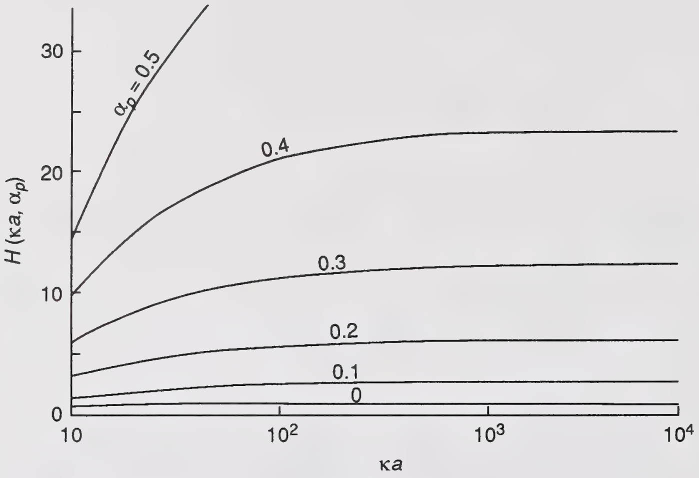

Figure 8-4. Variation of function H with κa and α_p (Levine *et al.*, 1976).

8.3 NOMENCLATURE

a	spherical particle radius, m
A	cross-sectional area of volume element, m^2
E_{sed}	sedimentation potential, V/m
g	acceleration due to gravity, m/s^2
H	function to account for α_p and κa variation, dimensionless
L	length of volume element, m
n_∞	number of particles per unit volume, m^{-3}
N	total number of spherical particles in a volume element
P_{sed}	pressure gradient due to settling, N/m^3
U	settling velocity of the suspension under the influence of the sedimentation potential, m/s
U_o	settling velocity of the suspension without the influence of the sedimentation potential, m/s

α_p	volume fraction of particles in the suspension, dimensionless
γ	function to account for α_p and κa variation, dimensionless
ε	dielectric constant of a material, dimensionless
ε_o	permittivity of vacuum, C/mV
ζ	zeta potential, V
κ	inverse Debye length, m^{-1}
μ	fluid viscosity, Pa s
ρ_f	electrolyte solution density, kg/m^3
ρ_s	spherical particles density, kg/m^3
σ	electrolyte solution electrical conductivity, S/m or A/Vm

8.4 REFERENCES

Booth, F. (1954), *Sedimentation Potential and Velocity of Solid Spherical Particles*, J. Chem. Phys., **22**, 1956–68.

Dorn, E. (1878), Ann. Physik, **3**, 20.

Hunter, R.J. (1981), *Zeta Potential in Colloid Science*, Academic Press, London.

Levine, S., Neale, G., and Epstein, N. (1976), *The Prediction of Electrokinetic Phenomena Within Multiparticle Systems II: Sedimentation Potential*, J. Colloid Interface Sci., **57**, 424–37.

Neale, G. (1974), *Lecture Notes in Electrokinetics*, Dept. of Chemical Engineering, University of Alberta, Edmonton, Alberta, Canada.

Sengupta, M. (1968), *The Sedimentation of Non-Conducting Solid Spherical Particles*, J. Colloid Interface Sci., **26**, 240–43.

Smoluchowski, M. von (1903), Bull. Akad. Sci. Cracovie, Classe Sci. Math. Natur., **1**, 182.

Smoluchowski, M. von (1921) in *Handbuch der Electrizitat und des Magnetismus*, (Graetz), **II**, 366, Barth, Leipzig.

DISPERSION FORCES 9

9.1 DISPERSION FORCES BETWEEN BODIES IN VACUUM

The mutual attraction of particles in a vacuum is a consequence of the dispersion forces, often called the London–van der Waals forces. The dispersion attraction forces are due to the spontaneous fluctuation of the electronic cloud in one material causing a corresponding fluctuation in neighboring material, leading, on the average, to an attractive force (Ross and Morrison, 1988). These forces are strictly quantum mechanical in nature and they are expressed in terms of the same oscillator strengths as appear in the equations for the dispersion of light. The following text is taken from Ross and Morrison (1988).

> "The calculation of magnitudes of dispersion attractions between particles has been attempted by two different approaches. One is based on a molecular model which is attributed to Hamaker and one is based on a molar model of condensed media, attributed to Lifshitz (1956).
>
> In the molecular model, the attraction between particles is calculated by summing the attractive energies between all pairs of molecules in the separate particles, ignoring multibody perturbations. This approximation is equivalent to predicting the spectra of condensed media as the sum of the molecular spectra. Corrections have been introduced to account for such factors as third body perturbations, the effect of intervening material and retardation of the dispersion forces due to the finite speed of light.
>
> In the molar model of particle–particle dispersion attractions, the lowering of the zero-point energy of a particle, due to the coordinator of its instantaneous electric moments with those of a nearby particle, is calculated by quantum electrodynamics. The expressions derived require as data the dielectric susceptibilities of the particles as a function of frequency and are more complex than those from the Hamaker theory. The complexity of Lifshitz formulae and the difficulty of obtaining the necessary material constants have hampered its use. Ninham and Parsegian (1970) have, however, developed a numerical method to approximate the necessary material functions from a few, readily obtained values, and have made the use of this theory practicable for some common materials."

In the Hamaker model the free energy of interaction separates into a material-dependent constant (called the Hamaker constant) and a geometry-dependent integral. The Lifshitz theory, on the other hand, gives such a separation of terms only for the special case of interactions between parallel plates.

A brief description of Hamaker's approach will be given. The reader is referred to Russel *et al.* (1989), Ross and Morrison (1988), and Hunter (1991) for details and for further references.

Hamaker (1937) made use of the potential given by Eq. (9-1) for two molecules and integrated it for all molecules in the two separate particles to obtain the dispersion energy of attraction between two macroscopic particles as shown in Figure 9-1. The work done by the attractive forces in bringing the two particles from infinity to a given separation distance is Gibbs free energy ΔG due to the dispersion interaction. At a constant temperature, we obtain

$$\Delta G = -\int_{V_1}\int_{V_2} \frac{c\rho_1\rho_2}{r^6}\, dV_1V_2 \tag{9-1}$$

where dV_1 and dV_2 are differential volume elements of V_1 and V_2
ρ_1 and ρ_2 are the molecular number densities (molecules per unit volume)
c is a material constant.

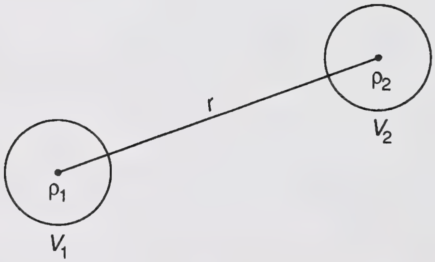

Figure 9-1. Attraction between two bodies.

Ross and Morrison summarize the assumptions made by Hamaker:

(a) The interactions can be considered pair wise; *i.e.*, multibody forces are ignored.
(b) The bodies are assumed to have uniform density up to the interfaces.
(c) The interactions of the molecular clouds are instantaneous.
(d) The intervening medium is a vacuum.
(e) All the dispersion force attractions are due to one dominant frequency.

(f) Effects of free charge and permanent dipoles are negligible.

(g) The bodies (particles) are not distorted by the attractive forces.

As a consequence of these assumptions the $(c\rho_1\rho_2)$ term is a constant. For example, for the case of planar or parallel slabs of thickness δ_1 and δ_2 separated by a distance, h, in vacuum, one has

$$\Delta G = V_A = -\left(\frac{A_{12}}{12\pi}\right)\left[h^{-2} + \left(h + \delta_1 + \delta_2\right)^{-2} - \left(h + \delta_1\right)^{-2} - \left(h + \delta_2\right)^{-2}\right] \tag{9-2}$$

where

$$A_{12} = c\pi^2\rho_1\rho_2 \tag{9-3}$$

A_{12} is known as the Hamaker constant for bodies 1 and 2.

For $h \ll \delta_1, \delta_2$, Eq. (9-2) becomes

$$V_A = -\frac{A_{12}}{12\pi h^2}, \frac{\text{J}}{\text{m}^2} \tag{9-4}$$

where V_A is the attractive potential (energy). The symbol V_A is common in the literature, but one can also use ϕ_A or ϕ_{Attr}. The negative sign signifies an attractive force. The Hamaker constant has values in the range of $10^{-21} - 10^{-19}$ J.

The concept of cohesion work can be utilized to estimate A_{12}. The work of cohesion consists of producing two new interfaces from a given material. It measures the attraction between the molecules of the two portions being produced. The cohesion work due to the dispersion force for material 1 is given by

$$W_{11}^d = 2\gamma^d \tag{9-5}$$

where γ^d is the theoretical surface tension due to dispersion energies. For a given material the attraction potential is

$$V_A = -\frac{A_{11}}{12\pi r_1^2} \tag{9-6}$$

where A_{11} is the Hamaker constant for material 1 that is being separated to produce two parts and r_1 is the intermolecular distance. However, the cohesion work is related to the attraction potential by

$$W_{11}^d = -V_A \tag{9-7}$$

and we obtain

$$A_{11} = 24\pi\, \gamma^d r_1^2 \tag{9-8}$$

Eq. (9-8) was originally derived by Fowkes (1964) and was used to calculate the Hamaker constant using surface tension data (Hiemenz, 1986; Ross and Morrison, 1988). A system for which the Fowkes equation is apt to work best is for a nonpolar material such as alkane. Here, the attractive forces are due to the dispersion forces. For alkane, with $\gamma^d \cong 25$ mJ/m^2 and $r_1 = 0.2$ nm, one obtains $A_{11} = 7.5 \times 10^{-20}$ J.

For the attraction force between two materials 1 and 2, the cohesion work is approximated by

$$W_{12}^d = -V_A = \frac{A_{12}}{12\pi r_{12}^2} = 2\left(\gamma_1^d \gamma_2^d\right)^{1/2} \tag{9-9}$$

where

$$r_{12} = (r_1 r_2)^{1/2} \tag{9-10}$$

r_{12} is the intermolecular distance approximated by the root mean square of the individual intermolecular distances.

Eq. (9-9) leads to

$$A_{12} = 24\pi\, r_{12}^2 \left(\gamma_1^d \gamma_2^d\right)^{1/2} \tag{9-11}$$

From (9-8) and (9-10), the above equation gives

$$A_{12} = (A_{11} A_{22})^{1/2} \tag{9-12}$$

Eqs. (9-8) and (9-12) give the means to evaluate the Hamaker constant for two materials in vacuum using surface tension data. Values for Hamaker constants are given in Tables 9-1 and 9-2.

For the case of two equal spheres with $h \ll a$ shown in Figure 9-2, the dispersion attractive force in vacuum is given by

$$V_A = -\frac{A_{12}a}{12h}, \text{ J} \tag{9-13}$$

where $(2a + h)$ is the distance between the sphere centres.

Table 9-1. Hamaker constants A_{11} for unretarded interaction for some common materials

	Hamaker Constant
Substance	A_{11}(J)($\times 10^{20}$)
Gold	45.3
Silver	39.8
Germanium	29.9
Silicon	25.5
Selenium	16.2
Alumina	15.4
Magnesia	10.5
Water	4.35
Ionic crystals	6.3–15.3
Oxides	10.6–15.5
Metals	16.2–45.5
Polymers	6.15–6.6
Acetone	4.20
Carbon tetrachloride	4.78
Chlorobenzene	5.89
Cyclohexane	4.82
Decane	5.45
Diethyl ether	4.30
1,4-Dioxane	5.26
Dodecane	5.84
Ethyl acetate	4.17
Hexadecane	6.31
Hexane	4.32
Methyl ethyl ketone	4.53
Octane	5.02
Pentane	3.94
Toluene	5.40
Natural rubber	8.58
Polybutadiene	8.20
Polybutene-1	8.03
Polydimethylsiloxane	6.27
Polyethylene oxide	7.51
Polyisobutylene	10.10
Polystyrene	9.80
Polystyrene	6.57
Polyvinyl acetate	8.91
Polyvinyl chloride	10.82
Polypropylene oxide	3.95

(Ross and Morrison, 1988)

Table 9-2. Hamaker constants A_{121} for the non-retarded interaction across a film of water (1 – substance, 2 – water)

	Hamaker Constant
Substance	A_{121}(J)($\times 10^{20}$)
Gold	33.5
Silver	26.6
Germanium	16.0
Silicon	11.9
Selenium	4.77
Alumina	4.12
Magnesia	1.60
Crystalline quartz	1.70
Fused quartz	0.833
Fused silica	0.849
Calcite	2.23
Calcium flouride	1.04
Sapphire	5.32
Ionic crystals	0.31–4.85
Oxides	1.76–4.17
Metals	3–33.4
Polymers	0.35
Polyisoprene	0.743
Polymethyl methacrylate	1.05
Polystyrene, average of 2	0.931
Polystyrene	0.27
Polystyrene	0.35
Polytetrafluoroethylene	0.333
"Teflon FEP"	0.381
Polyvinyl chloride	1.30
Pentane	0.336
Hexane	0.360
Heptane	0.386
Octane	0.410
Nonane	0.435
Decane	0.462
Undecane	0.471
Dodecane	0.502
Tridecane	0.504
Tetradecane	0.514
Pentadecane	0.526
Hexadecane	0.540

(Ross and Morrison, 1988)

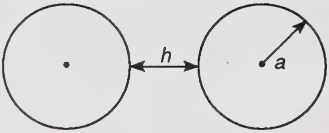

Figure 9-2. Interaction between two spheres.

Table 9-3 gives various expressions for the attraction potentials for the different geometries (Mahanty and Ninham, 1976).

The expressions for the attraction forces were derived with the assumption that the speed of light is infinite. The energy of the interaction is usually decreased at large distances because the time of electric field propagation from one body to another body and back is such that the fluctuating electric moments become slightly out of phase. The correction due to the finite speed of light is called the retardation correction. This correction is unity for $h = 0$ and it decreases monotonically with increasing h.

For the case of two parallel plates, Gregory (1981) gives the retarded potential as

$$V_A = -\frac{A_{12}}{12\pi h^2}\left[\frac{1}{1 + 5.32\frac{h}{\lambda}}\right] \tag{9-14a}$$

where $\lambda = 10^{-7}$ m (London wavelength). Note that the bracketed term of Eq. (9-14a) is unity for $h = 0$ and tends to 0 as $h \rightarrow \infty$. For the case of two equal-sized spheres, the effect of retardation on the interparticle dispersion potential is given by Schenkel and Kitchener (1960) as

$$V_A = \frac{aA_{12}}{12h}\left[\frac{1}{1 + 1.77p}\right] \qquad \begin{matrix} h/a \ll 1 \\ p \leq 0.57 \end{matrix} \tag{9-14b}$$

$$V_A = -\frac{aA_{12}}{h}\left[\frac{2.45}{60p} - \frac{2.17}{180p^2} + \frac{0.59}{420p^3}\right] \qquad \begin{matrix} h/a \ll 1 \\ p \geq 0.57 \end{matrix} \tag{9-14c}$$

where $p = 2\pi h/\lambda$.

Other expressions are given by Schenkel and Kitchener (1960), Gregory (1981), and Hunter (1991).

Table 9-3. Potential energy of attraction between two particles with the indicated geometries

Particles	V_A	Definitions/limitations
Two spheres	$-\frac{A}{6}\left[\frac{2a_1a_2}{h^2+2a_1h+2a_2h}+\frac{2a_1a_2}{h^2+2a_1h+2a_2h+4a_1a_2}+\ln\left(\frac{h^2+2a_1h+2a_2h}{h^2+2a_1h+2a_2h+4a_1a_2}\right)\right]$	a_1, a_2 = radii; h = separation of surfaces along line of centres (dimensional)
Two spheres of equal radius	$-\frac{A}{6}\left[\frac{2a^2}{h^2+4ah}+\frac{2a^2}{h^2+4ah+4a^2}+\ln\left(\frac{h^2+4ah}{h^2+4ah+4a^2}\right)\right]$	$a_1 = a_1 = a$
Two spheres of equal radius	$-\frac{Aa}{12h}$	$a \gg h$
Two spheres of unequal radius	$-\frac{Aa_1a_2}{6h(a_1+a_2)}$	a_1 and $a_2 \gg h$
Two plates of equal thickness	$-\frac{A}{12\pi}\left(\frac{1}{h^2}+\frac{1}{(h+2\delta)^2}-\frac{2}{(h+\delta)^2}\right)$	δ = thickness of plates h = separation of surfaces
Identical blocks	$-\frac{A}{12\pi h^2}$	$\delta \to \infty$

(Mahanty and Ninham, 1976)

9.2 EFFECTS OF INTERVENING MEDIUM

Hamaker's approach for the evaluation of the dispersion force was used when the medium between the two materials was vacuum. A correction to the Hamaker constant is needed when the intervening medium is a dielectric.

A usual approximation is to estimate the effect of an intervening medium 1 between two bodies of composition 2 and 3 by considering a pseudochemical reaction as shown:

(9-15)

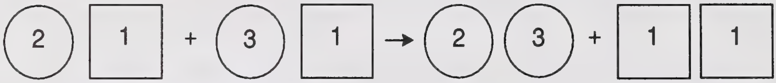

The change in potential energy is

$$\Delta\phi = \phi_{23} + \phi_{11} - \phi_{21} - \phi_{31} \tag{9-16}$$

Each term on the right side of Eq. (9-16) depends in the same way on the size and distance parameters and differs only in molecular parameters which are fully contained in the Hamaker constant (Hiemenz, 1986). One can write

$$A_{312} = A_{23} + A_{11} - A_{12} - A_{13} \tag{9-17}$$

A_{312} is the overall Hamaker interaction parameter for bodies 3 and 2 being intervened by medium 1. As was pointed out earlier, the interaction between dissimilar bodies is given by the geometrical mean of the homogeneous interactions for the bodies; *i.e.*,

$$A_{12} \approx (A_{11}\,A_{22})^{1/2} \tag{9-18}$$

where A_{ii} is the Hamaker constant for two bodies of the same material in vacuum.

Making use of Eq. (9-18), A_{312} of Eq. (9-17) becomes

$$A_{312} = \left(A_{22}A_{33}\right)^{1/2} + \left(A_{11}A_{11}\right)^{1/2} - \left(A_{11}A_{22}\right)^{1/2} - \left(A_{11}A_{33}\right)^{1/2} \tag{9-19}$$

or

$$A_{312} = \left[A_{33}^{1/2} - A_{11}^{1/2}\right]\left[A_{22}^{1/2} - A_{11}^{1/2}\right]$$

For the special case of $A_{22} \equiv A_{33}$, Eq. (9-19) gives

$$A_{212} = \left(A_{11}^{1/2} - A_{22}^{1/2}\right)^2 \tag{9-20}$$

Eq. (9-20) defining A_{212} indicates that for all values of A_{11} and A_{22}, the parameter A_{212} is positive. This means that the potential energy V_A is always negative (*i.e.*, attractive) for two similar bodies with an intervening medium. However, the general expression (9-19) shows that A_{312} parameter can have a negative value. Here, a repulsion potential can occur between two dissimilar bodies with an intervening medium. The dispersion force between a particle and an air bubble (air-water-solid) can therefore be repulsive depending on the particle and the intervening medium.

In the literature, it is sometimes customary to lump the Hamaker parameter with the term due to the retardation effects as one variable denoted as $A_{eff}(h)$, with $A_{eff}(0)$ being the Hamaker constant with no retardation effects. Table 9-4 gives values for $A_{eff}(0)$ for various materials. Figure 9-3 gives plots of A_{eff} variation with distance h for polystyrene parallel plates in pure water and salt water. $A_{eff}(h)$ accounts for the retardation effects.

Table 9-4.

	$A_{eff}(0)\ 10^{20}$, J		
	Vacuum	Water	
polystyrene	7.9	1.3	
hexadecane	5.4	–	(Parsegian and Weiss, 1981)
gold	40	30	
silver	50	40	
copper	40	30	
water	4.0	–	
pentane	3.8	0.34	
decane	4.8	0.46	
hexadecane	5.2	0.54	
water	3.7	–	(Hough and White, 1980)
quartz			
fused	6.5	0.83	
crystalline	8.8	1.70	
fused silica	6.6	0.85	
calcite	10.1	2.23	
calcite fluoride	7.2	1.04	
sapphire	15.6	5.32	
poly (methyl methacrylate)	7.1	1.05	
poly (vinyl chloride)	7.8	1.30	
polyisoprene	6.0	0.74	
poly (tetrafluoroethylene)	3.8	0.33	

(Russel *et al.*, 1989)

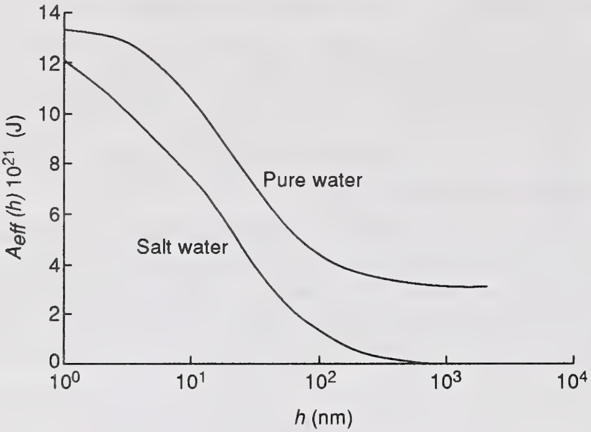

Figure 9-3. Calculated values for the effective Hamaker constant for interaction between polystyrene blocks across pure and salt water (Parsegian, 1975).

9.3 POTENTIAL ENERGY CURVES AND DLVO THEORY

In a colloidal system, whether colloidal particles flocculate or coalesce depends on the net interaction resulting from the combined attractive and repulsive forces to which the colloidal particles are subjected. For a system where electrostatic and dispersion forces are dominant, the stability of the system, *i.e.*, whether coagulation occurs or not, is dependent on the electrostatic repulsion due to the presence of the electric double layer and the dispersion attractive forces (London–van der Waals). This concept was developed independently by Derjaguin and Landau in the USSR, and Verwey and Overbeek in the Netherlands. It is known as the DLVO theory.

In order to appreciate the contribution of potential energy due to the electrostatic and London–van der Waals forces, it is best to consider the sum of the interactive potential energies due to these two types of forces for a case of two flat parallel plates.

The repulsive force between two parallel plates having similar surface potential was derived previously and it is given, with the usual Debye–Hückel approximation of low potential, by

$$F_R = 2\varepsilon\varepsilon_o\kappa^2\psi_s^2 \exp(-\kappa h), \text{ N/m}^2 \tag{9-21}$$

where F_R is the repulsive force due to the surface charge and
ψ_s is the surface potential given by the surface zeta potential ζ.

The potential or energy due to the repulsive force is defined by the energy required to bring two plates from infinity to a separation distance, h. The potential energy is related to the force by

$$\frac{dV_R}{dh} = -F_R \tag{9-22}$$

Integration of Eq. (9-22) leads to

$$\int_{\infty}^{V_R} dV_R = \int_{\infty}^{h} -F_R dh \tag{9-23}$$

Setting $(V_R)_\infty$ as zero, Eqs. (9-21) and (9-23) give

$$V_R = -\int_{\infty}^{h} 2\varepsilon\varepsilon_o \kappa^2 \psi_s^2 \exp(-\kappa h)\, dh \tag{9-24}$$

The repulsive potential for the case of two parallel plates is then given by

$$V_R = 2\varepsilon\varepsilon_o \kappa \psi_s^2 \exp(-\kappa h),\ \mathrm{J/m^2} \tag{9-25}$$

The potential (energy) due to the dispersion force between two similar plates (2) in a medium (1) is given by

$$V_A = -\frac{A_{212}}{12\pi h^2} \tag{9-26}$$

The total free energy per unit area of the interaction between the two flat parallel plates as a function of separation distance h is given by combining Eqs. (9-25) and (9-26):

$$V = 2\varepsilon\varepsilon_o \kappa \psi_s^2 \exp(-\kappa h) - \frac{A_{212}}{12\pi h^2},\ \frac{\mathrm{J}}{\mathrm{m}^2} \tag{9-27}$$

The above expression for the total energy of interaction V determines the stability of the two parallel plates. This stability analysis for a colloidal dispersion is in essence the DLVO theory for colloidal stability. The total energy V given by Eq. (9-27) shows that V is dependent on the system properties such as ε and A_{212} and on the "manipulated" physical characteristics of the system as manifested by κ and ψ_s.

In a similar fashion, we can write the total interaction energy for two equal spheres as

$$V = 2\pi a \varepsilon\varepsilon_o \psi_s^2 \exp(-\kappa h) - \frac{aA_{212}}{12h} \tag{9-28}$$

where $(h + 2a)$ is the distance between the spheres centres
a is the sphere radius and
κ is the inverse Debye length.

Unretarded dispersion potential is assumed.

Figure 9-4 shows three different total interaction energy curves for the case of two parallel plates. The repulsive energy is an exponential function of the interparticle distance h with a range of the order of $1/\kappa$. On the other hand, the London–van der Waals forces decrease as the inverse power of the interparticle distance. Consequently, the London–van der Waals attraction force predominates at small and large interparticle distances, whereas the electric double layer repulsion dominates at intermediate distances (Probstein, 1989).

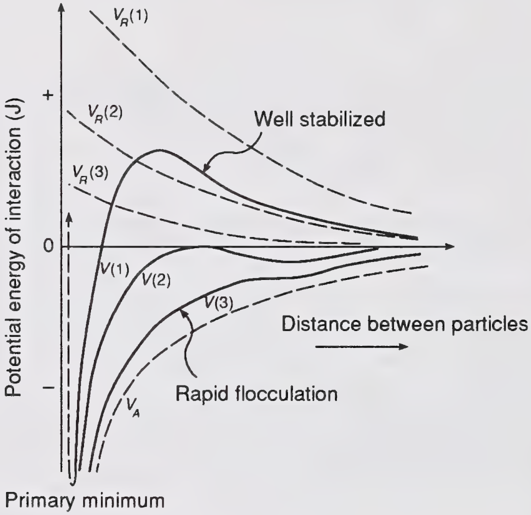

Figure 9-4. Total interaction energy curves obtained by the summation of an attraction curve with different repulsion curves (Shaw 1980).

In Figure 9-4, curve $V(1)$ represents a well-stabilized colloidal system with a repulsive energy maximum. This maximum is called the primary maximum. If the potential energy maximum is large compared with the thermal energy kT of the colloidal particles, the system should be stable at least under no-shear conditions.

Curve $V(3)$ represents a case where the colloidal dispersion is unstable and rapid coagulation will occur. Here, the double-layer repulsion does not dominate at any interparticle distance. Curve $V(2)$ represents the transition between stability and flocculation (coagulation) at the primary minimum.

An interesting additional feature of the potential energy *versus* distance plot is the presence of a secondary minimum at relatively large interparticle distances as given by curve $V(2)$. If this minimum is relatively deep (several kT values), it should give rise to a loose flocculation. However, this type of a flocculated dispersion can be easily redispersed by agitation.

It should be noted that at very small distances, repulsion due to the overlapping of electron clouds (Born repulsion) predominates. Consequently, at such small distances there is a deep minimum (primary minimum) in the potential energy curves. This region of the potential energy curves is shown only for curve $V(1)$ of Figure 9-4.

Figure 9-5 shows the influence of the Debye length $1/\kappa$ on the total energy interaction of two similar spheres. The variation in κ can be thought of in terms of electrolyte concentration. Large values of κ indicate higher electrolyte concentrations. Figure 9-5 clearly shows that for $\kappa = 10^8\ \mathrm{m}^{-1}$ a stable colloidal system is obtained. Increasing κ to $10^9\ \mathrm{m}^{-1}$ gives an unstable system where coagulation will occur. The electrolyte causes the diffuse part of the double layer to compress. When the double layer is reduced in thickness, the colloidal particles flocculate because the particles can get close enough to each other for the London–van der Waals forces to dominate.

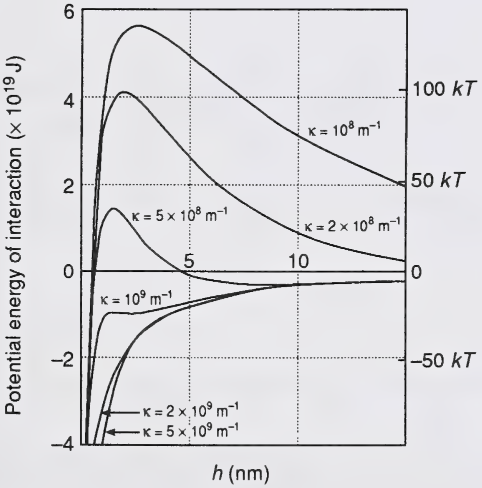

Figure 9-5. Influence of electrolyte concentration on the total potential energy of interaction of two spherical particles: $a = 10^{-7}$ m; $T = 298$ K; $z = 1$; $A_{22} = 2 \times 10^{-19}$ J; $A_{11} = 0.4 \times 10^{-19}$ J; $\varepsilon = 78.5$; $\psi_s = 0.05$ V (Shaw, 1980).

9.4 SCHULZE–HARDY RULE

One of the earliest generalizations regarding the effect of added electrolyte is a result known as the Schulze–Hardy Rule (1900) (Hiemenz, 1986). This rule states that it is the valence of the ions of opposite charge to the colloidal particle (counterions) that have the main effect on the stability of the colloidal particle. The critical flocculation concentration (CFC) value for a particular electrolyte is essentially determined by the valence of the counterion regardless of the nature of the ions having the same charge as the surface (*i.e.*, coions). The CFC is the critical concentration of electrolyte required to flocculate the colloidal particles. In the above rule it is understood that the electrolyte is a non-adsorbing indifferent electrolyte where its addition has no effect on the surface potential ψ_s.

The essentials of the Schulze–Hardy rule can be derived from the DLVO theory. The primary maximum of curve $V(2)$ is the demarcation point between stability and instability. At this point

$$V_R + V_A = 0 \tag{9-29}$$

and

$$\frac{dV_R}{dh} + \frac{dV_A}{dh} = 0 \tag{9-30}$$

Making use of the potential energy between two identical spheres valid for higher surface potential and for a $(z{:}z)$ electrolyte (Overbeek, 1972), one can write

$$V = \frac{32\pi a\varepsilon\varepsilon_o (kT)^2}{z^2 e^2} \tanh^2\left[\frac{ze\psi_s}{4kT}\right] \exp(-\kappa h) - \frac{aA_{212}}{12h} \tag{9-31}$$

with

$$\kappa = \left(\frac{2e^2 z^2 n_\infty}{\varepsilon\varepsilon_o kT}\right)^{1/2}$$

where the first term of Eq. (9-31) is the double-layer repulsive potential V_R and the second term is the attractive dispersion potential V_A.

Application of Eqs. (9-29) and (9-30) to (9-31) leads to having the maximum in V occur at a value equal to κ^{-1} and

$$n_{crit} = \frac{49.63}{z^6 l_b^3}\left[\frac{kT}{A_{212}}\right]^2 \tanh^4\left(\frac{ze\psi_s}{4kT}\right) \tag{9-32}$$

where n_{crit} is the number concentration of ions and *CFC* is given in mol/L (molarity); *i.e.*,

(9-33) $$\frac{1}{1000\,N_a}\,n_{crit} = CFC$$

and

(9-34) $$l_b = \frac{e^2}{4\pi\varepsilon\varepsilon_o kT}$$

For large potential ψ_s, tanh $[ze\psi_s/4kT]$ becomes ≈ 1 and

(9-35) $$CFC \propto \frac{1}{z^6}$$

which explains the Schulze–Hardy rule (Russel *et al.*, 1989). Here, the coagulating effectiveness of the dominating ion increases with its valency in the proportion of 1:64:729 for uni, di, and trivalent ions, respectively. Thus, if the univalent ion requires 729 units of concentration for coagulation, the divalent ion would require 64 units, and the trivalent ion would require 1 unit.

For small potential,

(9-36) $$\tanh \frac{ze\psi_s}{4kT} \approx \frac{ze\psi_s}{4kT}$$

and

(9-37) $$CFC \propto \frac{\psi_s^4}{z^2}$$

which also partially explains the Schulze–Hardy rule. Here the surface potential becomes important as well.

The effect of the surface potential on the critical flocculation concentration (CFC) for $z = 1$, 2, and 3 are given in Figure 9-6 (Shaw, 1980).

The reason that the valency of the counterions is important and not the valency of the coion can be explained by making use of the Boltzman distribution. For a positive surface potential, ψ_s is positive and the counterion distribution is given by

(9-38) $$n_- = n_\infty \exp\left[\frac{e\psi_s\,|z_-|}{kT}\right]$$

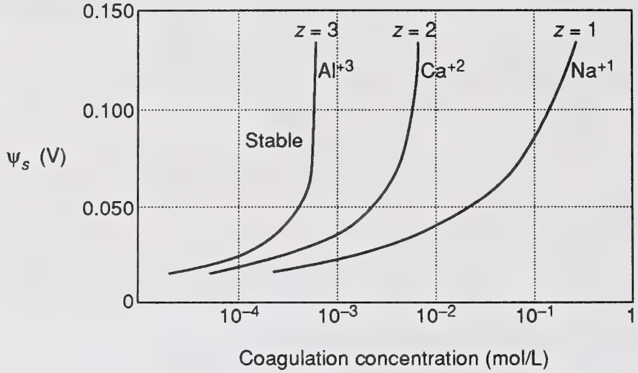

Figure 9-6. Coagulation concentrations calculated by taking $A = 10^{-19}$ J, for counterion charge numbers 1, 2, and 3. The colloidal system is predicted to be stable above and to the left of each curve and coagulated below and to the right (Shaw, 1980).

where z_- is the valency of the counterions. For the case of coions:

$$n_+ = n_\infty \exp\left[-\frac{|z_-|\, e\psi_s}{kT}\right] \tag{9-39}$$

For the case of large ψ_s, Eqs. (9-38) and (9-39) indicate that $n_- \gg n_+$ within the double layer close to the surface. Hence the counterions become the controlling ions.

The DLVO theory predicts that ions having the same valency have the same flocculation capability. However, experimental results indicate that the ion effectiveness is different for different ions having the same valency.

A more complete sequence of the variations in effectiveness is as follows (Hiemenz, 1986):

1. For monovalent cations

   $Cs^+ > Rb^+ > NH_4^+ > K^+ > Na^+ > Li^+$

2. For monovalent anions

   $F^- > Cl^- > Br^- > NO_3^- > I^-$

9.5 VERIFICATION OF THE DLVO THEORY

Many attempts have been made to verify the DLVO theory taking into account both the dispersion and electrostatic forces. The major difficulty was the limitation due to the roughness of the surfaces used. It was Tabor and Winterton (1969) who first recognized that sheared muscovite mica provides a molecularly smooth surface ideal for such measurements. Figure 9-7 shows the comparison between experimental and theoretical results for the evaluation of the Hamaker constant. The experiments were conducted in a vacuum. Allowing for experimental errors, the agreement between the theory and experiment can be brought to within 10%.

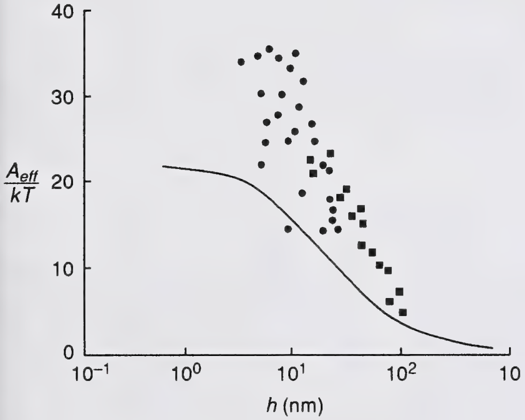

Figure 9-7. Effective Hamaker constant *versus* separation for mica plates interacting across a vacuum (Chan and Richmond, 1977): ● data from Tabor and Winterton (1969); ■, data from Israelachvili and Tabor (1973); ——, calculation (Russel *et al.*, 1989).

For the case of the force between mica plates in aqueous electrolyte solutions, Figure 9-8 shows the force between two mica plates divided by the radius of curvature R of the plates (Israelachvili, 1985). Here, the agreement between the experimental results and the theoretical predictions is excellent. The experimental device used in the measurements is described by Israelachvili and Adams (1978). Such an apparatus is shown in Figure 9-9. The force was measured between the macroscopic surfaces, in a configuration of crossed cylinders at nanometre separations. The surfaces consisted of ~1 μm thick mica sheet silvered on the back and glued to quartz pieces with a radius of curvature of 10 mm. The separation was measured optically using a spectrometer. The results shown in Figure 9-8 are restricted to situations where there are no hydration effects arising from the presence of hydrated metal ions on the mica surface.

The study of Israelachvili and Adams (1978) and the later studies of Pashley (1981a,b) and of Pashley and Israelachvili (1984) indicated that counterion hydration on the mica surface can give rise to an additional short-range repulsive force between mica surfaces in aqueous solutions of K^+ and Na^+ of given molarity. This hydration force is not affected by an increase in temperature (up to 65°C) and it is completely absent in pure water where H_3O^+ is the counterion.

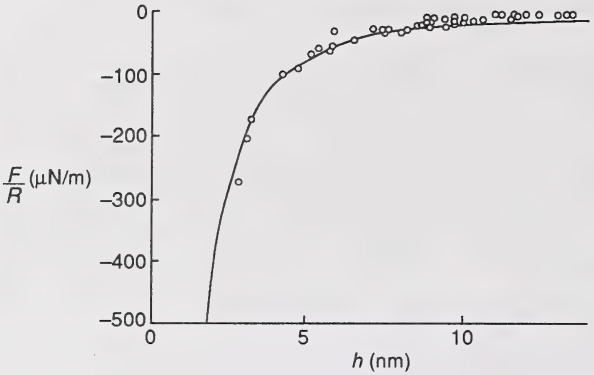

Figure 9-8. Force measured between mica plates in aqueous electrolyte solutions compared with predictions; *R* denotes the radius of curvature of the mica plates (Israelachvili, 1985).

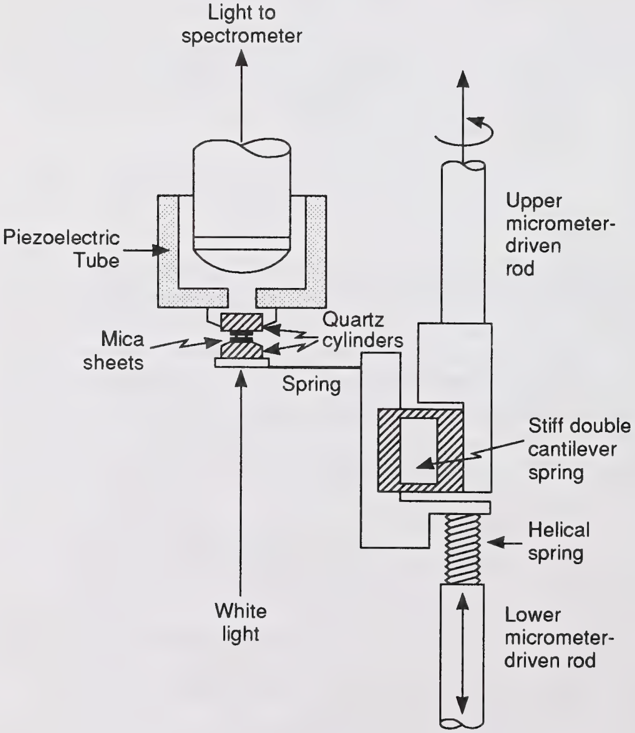

Figure 9-9. Schematic drawing of apparatus to measure long-range forces between two crossed cylindrical sheets of mica (of thickness ~1 μm and radius of curvature ~12 mm) immersed in an electrolyte. By use of white light and multiple beam interferometry, the shapes of and separation between the two mica surfaces may be independently measured. The separation between the two mica surfaces can be controlled by use of two micrometer-driven rods and a piezoelectric crystal tube to better than 0.1 nanometres (Israelachvili and Adams, 1978).

Figure 9-10 shows a case where force measurements were made in a 4×10^{-5} M KCl electrolyte solution. The agreement with the DLVO theory is excellent and the primary maximum occurs at a separation distance of 2 nm. However, at higher KCl concentrations, say 3×10^{-4} and 10^{-3} M, no primary maximum was observed and there appears to be an additional repulsive force which cannot be accounted for by the DLVO theory. If one is to account for the solvent structure, then the total interaction potential energy can be given by

$$V = V_A + V_R + V_s \tag{9-40}$$

where V_s is the potential due to the solvent structure. This term is necessitated in order to reconcile experimental measurements with the classical DLVO theory. At present, the lack of an adequate theory for the structure of water prevents theoretical evaluation of the potential V_s. Its magnitude for mica can be estimated using Israelachvili and Adams type measurements. The difference between the measured total potential and that given by the DLVO theory would then be the V_s term (Hunter, 1991). In general, discrepancy in the region of $0 < h < 5 \times 10^{-9}$ m occurs when the term V_s is non-zero.

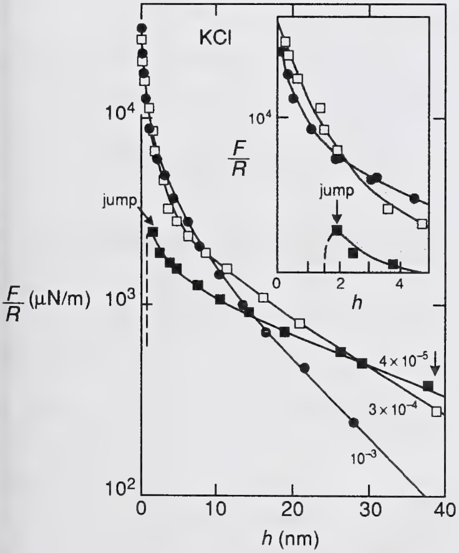

Figure 9-10. Forces measured between mica surfaces in KCl solutions at pH 5.7. ●, 10^{-3} M; □, 3×10^{-4} M; ■, 4×10^{-5} M. In 4×10^{-5} M no hydration forces were present, hence the surfaces jumped into a primary minimum from h ≅ 2 nm. At 10^{-3} and 10^{-4} M strong hydration forces prevented primary minimum adhesion. The inset shows the short-range forces in more detail (Pashley, 1981b).

In aqueous solutions, positive values of V_s are due to the presence of "hydration forces" and negative values are believed to be due to "hydrophobic forces." Both types of interaction decay exponentially with a decay length typically on the order of several nanometres (Hunter, 1991; Xu and Yoon, 1989,1990).

For electrokinetic modelling where the hydration of the ions in the electric double layer occurs, it becomes necessary to modify the Boltzmann distribution and to assume a variable dielectric constant within the electric double layer. The reader can refer to the studies by Gur *et al.* (1978a,b) and Guzman-Garcia *et al.* (1990) for details.

In the above discussions, we only dealt with aqueous systems. A non-aqueous medium is usually characterized with a low dielectric constant and poor dissociation of the electrolytes. By and large the ionic strengths are much lower than 10^{-6} M and the inverse Debye length is fairly large. Electrostatic stabilization in non-aqueous media is reviewed by van der Hoeven and Lyklema (1992).

The reader is referred to Israelachvili (1985) for a comprehensive discussion on dispersion forces.

9.6 NOMENCLATURE

a, a_1, a_2	radius of a spherical body, m
A	Hamaker constant, J
$A_{eff}(h)$	Hamaker "constant" accounting for retardation effects, J
$A_{eff}(o)$	Hamaker "constant" not accounting for retardation effects, J
A_{11}	Hamaker constant for similar bodies (or material) in vacuum, J
A_{12}	Hamaker constant for bodies 1 and 2 in vacuum, J
A_{312}	Hamaker constant for materials 3 and 2 with an intervening medium 1, J
c	material constant
CFC	critical flocculation concentration of electrolyte solution required to flocculate a colloidal system, mol/L
F_R	electrostatic repulsive force, N (N/m^2 for the case of parallel plates)
ΔG	Gibbs free energy, J
h	gap between two bodies (surface to surface distance), m
n_{crit}	critical ion number concentration, m^{-3}
n_+	coions number concentration, m^{-3} (assuming $\psi_s > 0$)
n_-	counterions number concentration, m^{-3} (assuming $\psi_s > 0$)
n_∞	ion number concentration in the bulk solution, m^{-3}
r	distance separating centres of two bodies, m
r_1	intermolecular distance, m
V	total interaction potential, J (J/m^2 for the case of parallel plates)
V_A	attractive potential energy due to London–van der Waals forces, J (or J/m^2 for the case of parallel plates)

V_R	electrostatic repulsive potential, J (J/m^2 for the case of parallel plates)
V_s	potential due to ionic structure, J (J/m^2 for the case of parallel plates)
V_1, V_2	volumes of bodies 1 and 2, respectively, m^3
W_{11}^d	cohesion work for material 1 due to dispersion forces, J
z	absolute value of the valency for a (z:z) electrolyte
z_-	valency of counterions (assuming $\psi_s > 0$)
z_+	valency of coions (assuming $\psi_s > 0$)
$\gamma^d, \gamma_1^d, \gamma_2^d$	surface tension due to dispersion energies, N/m
ε	dielectric constant of a material, dimensionless
ε_o	permittivity of vacuum, C/mV
ζ	zeta potential, V
κ	inverse Debye length, m^{-1}
ρ_1, ρ_2	molecular density of bodies 1 and 2, respectively, mol/m^3
ψ_s	surface potential, V

9.7 REFERENCES

Chan, D. and Richmond, P. (1977), *van der Waals Forces for Mica and Quartz: Calculations from Complete Dielectric Data*, Proc. Roy. Soc. Lond., **353A**, 163–76.

Fowkes, F.M. (1964), *Attractive Forces at Interfaces*, Ind. Eng. Chem., **56**, 40–52.

Gregory, J. (1981), *Approximate Expressions for Retarded van der Waals Interaction,* J. Colloid Interface Sci., **84**, 138–45.

Gur, Y. Ravina, I. and Babchin, A.J. (1978a), *On the Electrical Double Layer Theory. I A Numerical Method for Solving a Generalized Poisson–Boltzmann Equation,* J. Colloid Interface Sci., **64**, 326–32.

Gur, Y., Ravina, I., and Babchin, A.J. (1978b), *On the Electrical Double Layer Theory. II. The Poisson–Boltzmann Equation Including Hydration Forces*, J. Colloid Interface Sci., **64**, 333–41.

Guzman-Garcia, A.G., Verbrugge, M.W., and Hill, R.F. (1990), *Development of a Space-Charge Transport Model for Ion-Exchange Membranes*, AIChEJ, **36**, 1061–74.

Hamaker, H.C. (1937), *London–van der Waals Attraction Between Spherical Particles,* Physica, **4**, 1058–72.

Hiemenz, P.C. (1986), *Principles of Colloid and Surface Chemistry,* 2nd ed., Marcel Dekker, New York.

Hough, D.B. and White, L.R. (1980), *The Calculation of Hamaker Constants from Lifshitz Theory With Applications to Wetting Phenomena*, Advances Colloid Interface Sci. **14**, 3–41.

Hunter, R.J. (1991), *Foundations of Colloid Science, vol. I.,* Oxford University Press, Oxford.

Israelachvili, J.N. (1985), *Intermolecular and Surface Forces,* Academic Press, London.

Israelachvili, J.N. and Adams, G.E. (1978), *Measurement of Forces Between Two Mica Surfaces in Aqueous Electrolyte Solutions in the Range 1–100 nm,* J. Chem. Soc., Faraday Trans., *I*, **74**, 975–1001.

Israelachvili, J.N. and Tabor, D. (1973), *Van der Waals Forces Theory and Experiment,* Prog. Surface Membrane Sci., **7**, 1–55.

Lifshitz, E.M. (1956), *The Theory of Molecular Attractive Forces Between Solids,* Soviet Physics JETP, **2**, 73–83.

Mahanty, J. and Ninham, B.W. (1976), *Dispersion Forces,* Academic Press, London.

Ninham, B.W. and Parsegian, V.A. (1970), *van der Waals Forces. Special Characteristics in Lipid-Water Systems and a General Method of Calculation Based on the Lifshitz Theory*, Bio. Phys. J., **10**, 646–63.

Overbeek, J. Th. (1972), *Colloid and Surface Chemistry. A Self-Study Course. Part 2,* Lyophobic Colloids, Cambridge, Mass., MIT Center for Advanced Eng. Study.

Parsegian, V.A. (1975), *Long Range van der Waals Forces, in Physical Chemistry: Enriching Topics in Colloid and Surface Science* (eds. Van Olphen, H. and Mysels, K.J.).

Parsegian, V.A. and Weiss, G.H. (1981), *Spectroscopic Parameters for Computation of van der Waals Forces,* J. Colloid Interface Sci., **81**, 285–89.

Pashley, R.M. (1981a), *Hydration Forces Between Mica Surfaces in Aqueous Electrolyte Solutions,* J. Colloid Interface Sci., **80**, 153–62.

Pashley, R.M. (1981b), *DLVO and Hydration Forces Between Mica Surfaces in* Li^+, Na^+ *and* Cs^+ *Electrolyte Solutions,* J. Colloid Interface Sci., **83**, 531–46.

Pashley, R.M. and Israelachvili, J.N. (1984), *DLVO and Hydration Forces Between Mica Surfaces in* Mg^{2+}, Ca^{2+}, Sr^{2+} *and* Ba^{2+} *Chloride Solutions,* J. Colloid Interface Sci., **97**, 446–55.

Probstein, R.F. (1989), *Physicochemical Hydrodynamics*, Butterworths, Boston.

Ross, S. and Morrison, I.D. (1988), *Colloidal Systems and Interfaces*, John Wiley, New York.

Russel, W.B., Saville, D.A., and Schowalter, W.R. (1989), *Colloidal Dispersions,* Cambridge University Press, Cambridge.

Schenkel, J.M. and Kitchener, J.A. (1960), *A Test of the Derjaguin–Verwey–Overbeek Theory With a Colloidal Suspension,* Trans. Faraday Soc. **56**, 161–73.

Shaw, D.J. (1980), *Introduction to Colloid and Surface Chemistry*, 3rd ed., Butterworths, London.

Tabor, D. and Winterton, R.M. (1969), *Direct Measurements of Normal and Retarded van der Waals forces,* Proc. Roy. Soc. Lond., **312A**, 435–50.

van der Hoeven, P.H.C. and Lyklema, J. (1992), *Electrostatic Stabilization in Non-Aqueous Media,* Advances Colloid Interface Sci., **42**, 205–77.

Xu, Z. and Yoon, R.-H. (1989), *The Role of Hydrophobic Interactions in Coagulation*, J. Colloid Interface Sci., **132**, 532–41.

Xu, Z. and Yoon, R.-H. (1990), *A Study of Hydrophobic Coagulation,* J. Colloid Interface Sci., **134**, 427–34.

COAGULATION OF PARTICLES 10

10.1 GENERAL

In previous chapters, we dealt with electrostatic and dispersion forces and discussed the DLVO theory. In this context, we were able to discern whether two particles when brought together would flocculate. Our arguments were based solely on physical-chemical reasoning and consequently we only dealt with the equilibrium state of the colloid and ignored the dynamic process in attaining the flocculated state, if such a state is favoured. When suspended colloidal particles in solution are not stabilized, the rate at which they flocculate depends on the frequency with which they encounter each other. This encounter frequency is a function of the fluid and particles velocity, Brownian motion, and forces of other origin, *e.g.*, electrostatic, dispersion, and steric forces.

When particles of comparable size collide with each other, the collision leads to the "fusing" together and the formation of a single larger particle. This process is termed flocculation or coagulation. Here, it is usually necessary to know the velocity field of the interacting particles and the prevailing interaction forces. On the other hand, when a particle collides with a much larger particle, or a surface, such a process is termed deposition. The study of deposition usually involves a knowledge of the prevailing forces and flow field around the larger particle undisturbed by the presence of the much smaller particle. The hydrodynamic forces on the small particle are deduced from the known flow field about the larger particle.

The physics of particle–particle interaction in air as opposed to a liquid are similar. Dissimilarities between aerosol interaction or hydrosol (colloidal solution) interaction arise from the magnitudes of the prevailing forces and the ratio of an aerosol particle diameter to the gas molecule free path. For example, charged aerosols are strongly influenced by electrostatic forces at comparatively large distances from a surface. On the other hand, electrostatic forces in an aqueous medium are restricted to the presence of the electric double layers (Spielman, 1977).

For submicron particles, the primary collision mechanism is due to the Brownian motion. When coagulation is caused solely by the Brownian motion, it is referred to as perikinetic flocculation. On the other hand, when coagulation is caused solely by deterministic forces, *e.g.*, hydrodynamic forces, it is called orthokinetic flocculation.

As was stated earlier, the interparticle potential typically includes an attractive part due to the London–van der Waals forces and a repulsive part due to the electrostatic forces. When the electrostatic repulsive forces are absent, particles undergo flocculation and the flocculation process is termed rapid coagulation. When the electrostatic repulsive forces or any other repulsive forces, *e.g.*, steric forces are present, the flocculation process is termed slow coagulation. The rate of coagulation is a measure of the colloidal system stability.

10.2 PARTICLE–PARTICLE FLOCCULATION

Brownian motion, hydrodynamic, and other interparticle interaction determine the rate of collision between particles. Smoluchowski (1917) was the first to study the rate of coagulation of particles due solely to the Brownian motion with the particles diffusion coefficients taken as constant. His model was essentially that of diffusion of non-interacting spheres to a test sphere. The diffusion dynamics were described by the radial component of the diffusion equation in spherical coordinates with a uniform diffusivity (Feke and Schowalter, 1983). Smoluchowski evaluated the rate of diffusion of the particles to a test sphere and derived an expression for the collision frequency.

Smoluchowski also evaluated the collision frequency of spherical particles in a shear flow in the absence of the Brownian motion. Here, it was assumed that the particles follow undisturbed streamlines and that no interparticle forces are present. Comparison of the collision frequency of the two asymptotic cases clearly demonstrated the coagulation enhancement due to shear flow.

Fuchs (1934) generalized Smoluchowski's analysis for the Brownian motion to include arbitrary interaction potential assuming a constant particle diffusion coefficient. Derjaguin and Landau (1941) and Verwey and Overbeek (1948) incorporated the electrostatic and dispersion attraction forces into the arbitrary interaction potential derived by Fuchs to show the effect of these forces on the collision frequency between colloidal particles. Further improvements on Fuchs' derivation were made by Spielman (1970) and Honig *et al.* (1971) who included the variation of the particle diffusion coefficient due to the presence of another particle. More recently, van de Ven and Mason (1976), Zeichner and Schowalter (1977), and van de Ven (1989) evaluated collision frequency, in the absence of the Brownian motion, by incorporating hydrodynamic and interaction potentials into the flow equations.

In the following sections, we shall explore, in some detail, the historical developments together with the more recent studies.

10.2.1 Brownian Motion

The coefficient of diffusion D is an important transport property of a colloidal particle and it can be expressed in terms of the particle size. Consider one-dimensional diffusion of a swarm of colloidal particles. Assume that such a swarm is released over a narrow slit at $x = 0$ and $t = 0$. The number of released colloidal particles per unit area is N_i. At time $t = 0$, the concentration of the particles for $x \neq 0$ is zero. With increasing time, the colloidal particles diffuse due to the Brownian motion within the medium. Figure 10-1 shows the spread of the particles at time t in one dimension. The governing equation for the spread of the particles is given by the convection-diffusion equation, while dropping out the

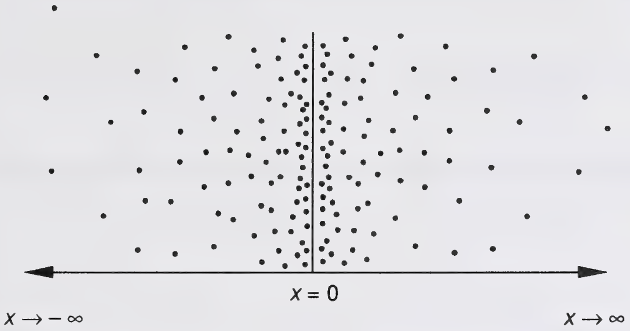

Figure 10-1. Diffusion in a one-dimensional plane.

convection term,

$$\frac{\partial n}{\partial t} = D\frac{\partial^2 n}{\partial x^2} \tag{10-1}$$

where $n(x,t)$ is the number of particles per unit volume at distance x and at time t (Friedlander, 1977). The initial and boundary conditions are

$n(\infty, t) = 0$ for all t

and

$n(-\infty, t) = 0$ for all t

Initially all the particles are located at $x = 0$ and $n(x, 0) = 0$ for $|x| > 0$.

The solution to Eq. (10-1) is given by Gaussian distribution, *viz.*

$$n(x,t) = \frac{N_i}{2(\pi D t)^{1/2}} \exp\left(-\frac{x^2}{4Dt}\right) \tag{10-2}$$

where N_i is the number of particles released at $x = 0$ per unit cross-sectional area. It is given by

$$N_i = \int_{-\infty}^{\infty} n(x,t)\,dx$$

The mean square displacement at time t of the particles from $x = 0$ is given by

$$\overline{x^2} = \frac{1}{N_i} \int_{-\infty}^{\infty} x^2\, n(x,t)\, dx \tag{10-3}$$

Making use of the expression for $n(x,t)$ given by Eq. (10-2), the mean square displacement becomes

$$\overline{x^2} = 2Dt \tag{10-4}$$

Eq. (10-4) states that the mean square displacement of the diffusing particles is proportional to the lapsed time t.

A force balance on a colloidal particle can be given as

$$m \frac{dv}{dt} = -fv + F(t) \tag{10-5}$$

This equation is known as the Langevin equation. The colloidal particle mass is m and its velocity at time t is given by v. The term f is the friction coefficient. At infinite dilution and in the absence of charge, it is given by the Stokes expression as

$$f = 6\pi\mu a \tag{10-6}$$

The units of f are Ns/m. Here a is the colloidal particle radius and μ is the medium (continuous phase) viscosity.

The second term on the right side of Eq. (10-5) represents the fluctuating force resulting from the thermal motion of the medium molecules. The random trajectories of the colloidal particles are due to the random fluctuations in the forces that the colliding fluid molecules collectively exert on them (van de Ven, 1989). The fluctuating force $F(t)$ is assumed to be independent of the particle velocity v and its mean value over a long time t is zero.

Eq. (10-5) can be rewritten as

$$\frac{d(vx)}{dt} + \beta vx = v^2 + xA(t) \tag{10-7}$$

where $\beta = f/m$
$A(t) = F(t)/m$, and
$v = dx/dt$.

Integrating Eq. (10-7) between $t = (0,t)$ and recognizing that at $t = 0$, $vx = 0$, one obtains

$$vx = \exp(-\beta t) \int_0^t v^2 \exp(\beta\tau)\, d\tau + \exp(-\beta t) \int_0^t A(t)x \exp(\beta\tau)\, d\tau \tag{10-8}$$

τ is a variable of integration. Making use of averaging arguments, Friedlander (1977) showed that at large times

$$\frac{\overline{x^2}}{2} = \frac{\overline{v^2}t}{\beta} \tag{10-9}$$

We can now make use of a physical argument made by Einstein that relates the Brownian motion of a colloidal particle to the molecular motion of the medium. As the particles share the molecular-thermal motion of the fluid, the principle of equipartition of energy is assumed to apply to the translational energy of the colloidal particles leading to

$$\frac{m\overline{v^2}}{2} = \frac{kT}{2} \tag{10-10}$$

Combining Eq. (10-9) with (10-10) and making use of the β definition lead to

$$\overline{x^2} = 2t\,\frac{kT}{f} \tag{10-11}$$

Comparing Eq. (10-4) with (10-11) leads to

$$D = \frac{kT}{f} \tag{10-12}$$

This is the Stokes–Einstein expression for the coefficient of diffusion of an inert spherical particle. van de Ven (1989) discusses the various forms of the diffusion coefficient as influenced by the approximity of other particles, the particle surface potential, the Debye length, and the size of the electrolytes. At infinite dilution, the diffusion coefficient of an inert particle in a medium is given by

$$D = D_\infty = \frac{kT}{6\pi\mu a} \tag{10-13}$$

where k is Boltzmann constant and T is the absolute temperature. Here a is the particle radius and the medium viscosity is μ. In the above analysis, the diffusion coefficient D was assumed to be constant and not affected by the presence of surrounding particles.

10.2.2 Collision Frequency

In this section, we shall derive the kinetic equation for coagulation. Here particle collisions lead to coagulation and hence a reduction in the total number of particles and an increase in the particle average size. We shall assume that *every* collision leads to coagulation.

Consider a colloidal system containing an infinite number of species ($i = 1, 2, 3 \ldots \infty$) characterized solely by its volume v_i. Let J_{ij} be the collision frequency per unit volume occurring between two classes of spherical particles characterized by volume v_i and v_j, respectively. When particle i collides with particle j a third particle is formed having a volume of $(v_i + v_j)$. The collision frequency per unit volume J_{ij} can be given as

$$J_{ij} = \beta(v_i, v_j)\; n_i\, n_j \tag{10-14}$$

where n_i is the number concentration of species i. Here $\beta(v_i, v_j)$ is the collision frequency function. This function is dependent on the system properties and on the prevailing interparticle forces.

The rate of formation per unit volume of particles of size k by collision of particles of size i and j is given by

$$\frac{1}{2} \sum_{i+j=k} J_{ij} \tag{10-15}$$

The notation $i + j = k$ means that the summation is taken over those collisions for which a volume v_k can be produced; *i.e.*,

$$v_i + v_j = v_k \tag{10-16}$$

The factor 1/2 in Eq. (10-15) is present because each collision is counted twice in the summation. Eq. (10-15) is due to the generation of the kth species. In turn, particle k collides with other particles leading to particle volumes larger than v_k.

The disappearance term is given by

$$\sum_{i=1}^{\infty} J_{ik} \tag{10-17}$$

The net balance equation for the kth species is given by

$$\frac{dn_k}{dt} = \frac{1}{2} \sum_{\substack{i=1 \\ i+j=k}}^{i=k-1} J_{ij} - \sum_{i=1}^{\infty} J_{ik} \qquad \text{For } k = 1, 2, 3, \ldots \infty \tag{10-18}$$

Making use of Eq. (10-14), the above equation becomes

$$\text{(10-19)}\qquad \frac{dn_k}{dt} = \frac{1}{2}\sum_{\substack{i=1\\ i+j=k}}^{i=k-1} \beta_{ij} n_i n_j - n_k \sum_{i=1}^{\infty} \beta_{ik} n_i \qquad k = 1, 2, 3, \ldots \infty$$

Here $\beta_{ij} = \beta(v_i, v_j)$

Eq. (10-19) is the dynamic equation for the evolution of the population of particle k with time. It is a fairly general equation that accounts for the generation and loss of a population. The solution of Eq. (10-19) depends on the collision frequency function β_{ij} which is determined solely by the mechanism of the particle collisions which is dependent on the prevailing interparticle forces.

10.2.3 Brownian Coagulation: Without a Field Force, the Smoluchowski Solution

First, we shall deal with the diffusion of colloidal particles due to their Brownian motion. To begin with, the particles are assumed to be non-interacting and the only prevailing forces are due to the Brownian motion. In other words, forces due to electrostatic and dispersion are not accounted for. This analysis was put forward by M. von Smoluchowski in the early 1900s.

Consider a diffusional flux of spherical particles of volume v_j diffusing towards a particle of volume v_i. Particle v_i is the reference or test particle fixed at the coordinate system. In the absence of a convective flux, the diffusion equation is given by

$$\text{(10-20)}\qquad \frac{\partial n_j}{\partial t} = \frac{D}{r^2}\frac{\partial}{\partial r}\left(r^2 \frac{\partial n_j}{\partial r}\right)$$

where n_j is the number concentration of particle v_j and r is the radial coordinate of the spherical coordinate system. Angular symmetry is assumed. The initial condition is given as

At $\quad t = 0 \quad n_j = n_{j\infty} \quad$ for $r > a_i + a_j$

The boundary conditions are

At $\quad r = a_i + a_j \quad n_j = 0 \quad$ for $t > 0$

and

At $\quad r \rightarrow \infty \quad n_j = n_{j\infty} \quad$ for $t > 0$

Here a_i is the radius of the particles having volume v_i and $n_{j\infty}$ represents the uniform number concentration of the jth particle. One can solve Eq. (10-20) by making use of the transformation (Friedlander, 1977)

$$(10\text{-}21a) \quad w = \left(\frac{n_{j\infty} - n_j}{n_{j\infty}}\right)\left(\frac{r}{a_i + a_j}\right)$$

and

$$(10\text{-}21b) \quad y = \frac{r - (a_i + a_j)}{a_i + a_j}$$

The transformed form of Eq. (10-20) is

$$(10\text{-}22) \quad \frac{\partial w}{\partial t} = D' \frac{\partial^2 w}{\partial y^2}$$

where $D' = D/(a_i + a_j)^2$

The solution of Eq. (10-22) is given by

$$(10\text{-}23) \quad w = 1 - erf\left(\frac{y}{2\,(D't)^{1/2}}\right)$$

where *erf* is the error function which has the property of *erf* (0) = 0. At $t \to \infty$, Eq. (10-23) gives

$$(10\text{-}24) \quad n_j = n_{j\infty}\left[1 - \frac{a_1 + a_j}{r}\right]$$

This is the steady-state solution which can be obtained by setting $\partial n_j/\partial t = 0$ in Eq. (10-20). It is interesting to note that steady state is reached in relatively short times (Probstein, 1989). For particles of radius a, the characteristic time for Brownian diffusion is

$$(10\text{-}25) \quad \frac{a^2}{D} = \frac{a^2}{\left[\dfrac{kT}{6\pi\mu a}\right]} = \frac{6\pi\mu a^3}{kT}$$

For a colloidal particle with $a = 10^{-7}$ m in water at room temperature, the characteristic time is about 5×10^{-3} s indicating that steady state is reached relatively quickly.

The total rate (particles per unit time) at which particles j arrive at the surface $r = a_i + a_j$ is given by

$$D\left[4\pi r^2 \frac{\partial n_j}{\partial r}\right]_{r=a_i+a_j} = 4\pi\left(a_i + a_j\right) D n_{j\infty}\left[1 + \frac{a_i + a_j}{(\pi D t)^{1/2}}\right] \tag{10-26}$$

The steady-state rate at which particles j arrive at the collision radius of the test particle i is given by

$$4\pi\,(a_i + a_j)\,D\,n_{j\infty}$$

The collision rate frequency per unit volume between particles i and j is then given by

$$J_{ij} = 4\pi\,(a_i + a_j)\,D n_{i\infty}\,n_{j\infty} \tag{10-27}$$

Making use of Eq. (10-14), β_{ij} for the case of the Brownian coagulation is given by

$$\beta_{ij} = 4\pi\,(a_i + a_j)\,D \tag{10-28}$$

It is necessary now to quantify the diffusion coefficient D. When the test particle i is also in Brownian motion, the diffusion coefficient D should be relative to the motion of the two particles given by $(x_i - x_j)$ where x_i and x_j are the displacement of the particles in x-direction. From Eq. (10-4), one can write

$$\overline{\left(x_i - x_j\right)^2} = 2Dt \tag{10-29}$$

Expanding Eq. (10-29) leads to

$$\overline{x_i^2} - 2\,\overline{x_i x_j} + \overline{x_j^2} = 2Dt \tag{10-30}$$

As the motions of the two particles are independent of each other, $\overline{x_i x_j} = 0$. Eqs. (10-4) and (10-30) give

$$D_i + D_j = D \tag{10-31}$$

Making use of Eqs. (10-27) and (10-31), we can write for the collision rate per unit volume

$$J_{ij} = 4\pi\,(a_i + a_j)(D_i + D_j)\, n_{i\infty}\, n_{j\infty} \tag{10-32}$$

Stokes–Einstein Eq. (10-13) when combined with Eq. (10-32) gives

$$J_{ij} = \left[\frac{2kT}{3\mu}\left(a_i + a_j\right)\left(\frac{1}{a_i} + \frac{1}{a_j}\right)\right] n_{i\infty}\, n_{j\infty} \tag{10-33}$$

and

$$\beta_{ij} = \frac{2kT}{3\mu}\left(a_i + a_j\right)\left(\frac{1}{a_i} + \frac{1}{a_j}\right) \tag{10-34}$$

For convenience, the ∞ subscript will be dropped and n_i and n_j become the prevailing concentrations. Substituting for β_{ij} in the population balance, Eq. (10-19) yields the kinetic equation describing the change in the population of the kth particle. Eq. (10-33) represents the collision rate caused solely by the Brownian motion.

In order to obtain an analytical solution to Eq. (10-19), a simplifying assumption is necessary. Smoluchowski assumed that $a_i = a_j$, which leads to

$$\left(a_i + a_j\right)\left(\frac{1}{a_i} + \frac{1}{a_j}\right) = 4 \tag{10-35}$$

For an initially monodisperse colloidal system, the assumption of $a_i = a_j$ is valid. However, at long times it is not true. To a large extent, its justification rests on experimental evidence. Making use of Eq. (10-35), the collision frequency function becomes

$$\beta\left(v_i = v_j\right) = \frac{8kT}{3\mu} = K \tag{10-36}$$

where K is a constant independent of particle size. The population balance Eq. (10-19) becomes

$$\frac{dn_k}{dt} = \frac{K}{2} \sum_{\substack{i=1\\ i+j=k}}^{i=k-1} n_i n_j - K n_k \sum_{i=1}^{\infty} n_i \qquad k = 1, 2, \ldots, \infty \tag{10-37}$$

Let the total number of particles per unit volume in a closed system at time t be $N(t)_{tot}$; then

$$N(t)_{tot} = \sum_{i=1}^{\infty} n_i$$

Summing Eq. (10-37) over all particles $k = 1, 2, \ldots, \infty$, one obtains

$$\frac{dN_{tot}}{dt} = \frac{K}{2} \sum_{k=1}^{\infty} \sum_{\substack{i=1 \\ i+j=k}}^{i=k-1} n_i n_j - KN_{tot}^2$$

The first term on the right side of the above equation is given by $(K/2)\, N_{tot}^2$ leading to

$$\frac{dN_{tot}}{dt} = -\frac{K}{2} N_{tot}^2 \tag{10-38}$$

The above equation for the Brownian coagulation is analogous to second-order reaction kinetics. The initial condition is given by $N_{tot} = N_0$ at $t = 0$. Integration of Eq. (10-38) leads to

$$N_{tot}(t) = \frac{N_0}{1 + KN_0 \frac{t}{2}} \tag{10-39}$$

The above equation shows the decay in the total number of particles with time. Making use of Eq. (10-37), it can be shown (*e.g.*, Friedlander, 1977) that

$$n_k(t) = N_0 \frac{\left(\frac{t}{t_{Br}}\right)^{k-1}}{\left(1 + \frac{t}{t_{Br}}\right)^{k+1}} \tag{10-40}$$

where

$$t_{Br} = \frac{3\mu}{4N_0 kT} = \frac{2}{KN_0} \tag{10-41a}$$

The characteristic time t_{Br} is known as the flocculation time and it is the time for the concentration to halve itself (Probstein, 1989; Zeichner and Schowalter, 1979). Figure 10-2 shows the variation of n_k/N_0 for $k = 1, 2, \ldots, 4$ with dimensionless time, t/t_{Br}. It is interesting to note that (N_{tot}/N_0) and (n_1/N_0) decay monotonically; however, (n_k/N_0) with $k \geq 2$ exhibits a maximum before its final decay.

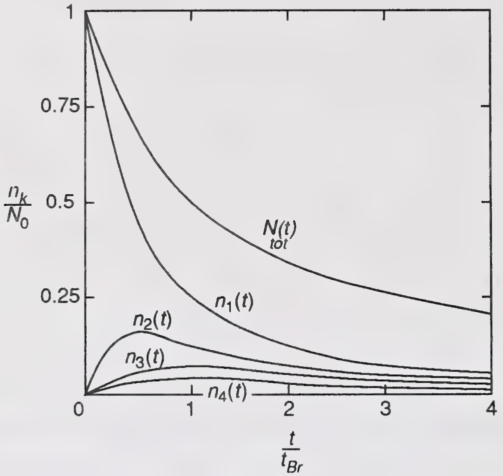

Figure 10-2. The variations in N_{tot}, n_1, n_2, ... with time for an initially monodisperse colloidal system. The total number concentration N_{tot} and the concentration of species n_1 both decrease, monotonically with increasing time. The concentrations of $n_2(t)$ and $n_3(t)$ and $n_4(t)$ pass through a maximum (Friedlander, 1977).

One can rewrite the expression for the characteristic time t_{Br} as

$$t_{Br} = \frac{\pi \mu a^3}{\alpha_p kT} \qquad (10\text{-}41b)$$

where α_p is the colloidal particles volume fraction. Table 10-1 shows the time scale for the formation of a doublet under Brownian motion.

Table 10-1. Characteristic time t_{Br} for Brownian coagulation of spherical particles in water at 293 K for $\alpha_p = 0.1$

a, m	t_{Br}, s
10^{-8}	7.77×10^{-6}
10^{-7}	7.77×10^{-3}
10^{-6}	7.77
10^{-5}	7.77×10^{3}

It is clear from Table 10-1 that Brownian coagulation is not important for particles much larger than 10 μm where the characteristic time becomes fairly large.

10.2.4 Brownian Coagulation: Effect of a Field Force

Fuchs (1934) was the first to introduce an interparticle field force to the Smoluchowski Brownian coagulation analysis. Once again, we consider a test particle of radius a_i to which particles a_j are diffusing. Here particles i and j exert a force on each other. Let this force be $F(r)$ and it is a function of position. The steady-state collision rate per unit area between particles j and the surface of the test particle i is given by

$$-\left(-D\frac{dn_j}{dr}+\frac{F(r)}{f}n_j\right)$$

The diffusion coefficient D is relative to the motion of the two particles and for an infinite medium it is given by Eqs. (10-13) and (10-31).

The total collision rate (particles per unit time) between particles j and the test particle i is given by

$$-\left[-D\,\frac{dn_j}{dr}+\frac{F(r)}{f}\,n_j\right]4\pi r^2 = \text{constant}$$

Defining the force $F(r)$ by its potential $\phi(r)$ leads to

$$\left[D\,\frac{dn_j}{dr}+\frac{1}{f}\,\frac{d\phi}{dr}\,n_j\right]4\pi r^2 = \text{constant}$$

Making use of Eq. (10-12) one obtains for the total collision rate between particles j and the test particle i,

$$4\pi r^2 D\left[\frac{dn_j}{dr}+\frac{n_j}{kT}\,\frac{d\phi}{dr}\right] = \text{constant} \qquad (10\text{-}42)$$

Differentiation of Eq. (10-42) w.r.t. r gives

$$\frac{d}{dr}\left[r^2 D\left(\frac{dn_j}{dr}+\frac{n_j}{kT}\,\frac{d\phi}{dr}\right)\right] = 0 \qquad (10\text{-}43)$$

where $n_j = 0$ at $r = a_i + a_j$

and

$n_j = n_{j\infty}$ at $r = \rightarrow \infty$

Solution of Eq. (10-43) subject to the above boundary conditions gives

$$(10\text{-}44) \quad n_j = n_{j\infty} \frac{\exp\left(-\dfrac{\phi(r)}{kT}\right) \displaystyle\int_{a_1+a_2}^{r} \exp\left(\dfrac{\phi(r)}{kT}\right) \dfrac{dr}{r^2}}{\displaystyle\int_{a_i+a_j}^{\infty} \dfrac{\exp\left(\dfrac{\phi(r)}{kT}\right)}{r^2}\, dr}$$

The total rate at which particles j arrive at surface $r = a_i + a_j$ is given by

$$D \left[4\pi r^2 \frac{dn_i}{dr}\right]_{r=a_i+a_j}$$

Making use of Leibnitz's rule for the differentiation of integrals, the collision rate per unit volume between particles i and j is then given by

$$(10\text{-}45) \quad J_{ij} = \left[\frac{4\pi D\,(a_i + a_j)}{(a_i + a_j) \displaystyle\int_{a_i+a_j}^{\infty} \dfrac{\exp\left(\dfrac{\phi(r)}{kT}\right)}{r^2}\, dr}\right] n_{i\infty} n_{j\infty}$$

The term in the square brackets is β_{ij}. The denominator in the square bracket is the stability ratio W. Making use of Eq. (10-31) and the Stokes–Einstein equation for D_i, setting $n_{i\infty} = n_{j\infty} = n$, $a_i = a_j = a$ for the case of a monodispersion and putting $J = J_{ij}$, one obtains

$$(10\text{-}46) \quad J = \frac{8kT}{3\mu} \cdot \frac{1}{2a \displaystyle\int_{2a}^{\infty} \dfrac{\exp\left(\dfrac{\phi(r)}{kT}\right)}{r^2}\, dr}\, n^2$$

For coagulation solely due to Brownian motion, *i.e.*, in the absence of any external force, Eq. (10-33) can be written for $a_i = a_j = a$ and $n_{i\infty} = n_{j\infty} = n$ as

$$J_{o,Br} = \frac{8kT}{3\mu}\, n^2 \tag{10-47}$$

where $J_{o,Br}$ denotes the Smoluchowski collision rate per unit volume due solely to Brownian motion. Combining Eqs. (10-46) and (10-47) leads to

$$W = \frac{J_{o,Br}}{J} \tag{10-48}$$

where W is the stability ratio. For the case of constant diffusion coefficient it is given as

$$W = 2a \int_{2a}^{\infty} \frac{\exp\left(\dfrac{\phi(r)}{kT}\right)}{r^2}\, dr \tag{10-49}$$

When $\phi(r)$ is a positive function, it signifies repulsion between the particles and it leads to $J < J_{o,Br}$ where $W > 1$. A large value for W means a stable system. In general, the potential $\phi(r)$ can have the form of the London–van der Waals (attractive) potential or an electrostatic (repulsive) potential. W is equal to unity for $\phi = 0$.

Figure 10-3 shows the effect of attractive London–van der Waals forces on the rapid Brownian coagulation J, normalized with the Smoluchowski Brownian coagulation $J_{o,Br}$. When $A/kT = 0$, the stability ratio is unity and it decreases with A/kT indicating rapid coagulation. However, the results as presented in Figure 10-3, which are based on the analysis presented here, are not in agreement with the experimental data. The major simplifying assumption lies in the fact that the diffusion coefficient is taken to be constant and independent of the gap width between the two particles.

Independently, Derjaguin and Muller (1967), Spielman (1970), and Honig *et al.* (1971) modified the analysis of the Brownian motion coagulation with interparticle potential to account for the decrease in the diffusion coefficient which occurs when two particles are very close.

The diffusion coefficient tensor $\underline{\underline{D}}$ for the case of two spheres is given by Brenner (1961) and van de Ven (1989) as

$$\underline{\underline{D}} = \left(D_i + D_j\right)_{\infty} \begin{bmatrix} d_{\|} & 0 \\ 0 & d_{\perp}(h) \end{bmatrix} \tag{10-50}$$

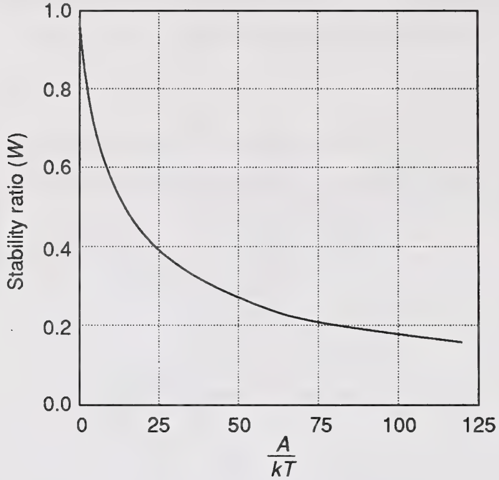

Figure 10-3. Variation of stability ratio W with A/kT. Dispersion potential is defined as

$$\phi = \frac{-Aa}{12\,(r-2a)} = \frac{-A}{12h}$$

The diffusion coefficient is a constant. A is the Hamaker constant.

where $d_{\parallel}(h)$ and $d_{\perp}(h)$ are correction factors for the diffusion coefficient of sphere i relative to sphere j. Symbols $\parallel$ and $\perp$ signify the relative diffusion parallel and normal to the two surfaces, respectively (van de Ven, 1989).

The correction factors, $d_{\parallel}(h)$ and $d_{\perp}(h)$, can be thought of as being due to hydrodynamic interactions between the two spheres. $D_{i\infty}$ and $D_{j\infty}$ are the particle diffusion coefficients at infinite dilution and they are given by Eq. (10-13). For the case of spheres of equal radii, we set $d_{\perp}(h) = 1/G(h)$. Here h is the dimensionless gap width between the spheres, where

$$\frac{r}{a} = 2 + h \quad \text{with } a_i = a_j = a$$

and r is the dimensional distance between the spheres centres. $G(h)$ is a complex function of h. A simplified form for $G(h)$ is given by Honig *et al.* (1971) for the case of equal-sized spheres:

$$G(h) \approx \frac{6h^2 + 13h + 2}{6h^2 + 4h} \tag{10-51}$$

The above expression indicates that

$G(h) \to 1$ as $h \to \infty$

and

$G(h) \to 1/(2h)$ as $h \to 0$

For $h \to 0$, the diffusion coefficient D becomes much smaller than D_∞ indicating a retardation in the Brownian coagulation process.

Following an approach similar to that adopted previously, the coagulation rate per unit volume, for equal-sized spherical particles having a variable diffusion coefficient, becomes

$$J = \frac{8kT}{3\mu} \frac{1}{2 \int_0^\infty \frac{G(h) \exp\left(\frac{\phi(h)}{kT}\right)}{(2+h)^2} dh} n^2 \tag{10-52}$$

with

$$W = \frac{J_{o,Br}}{J} \tag{10-53}$$

where W is modified to

$$W = 2 \int_0^\infty \frac{G(h) \exp\left(\frac{\phi(h)}{kT}\right)}{(2+h)^2} dh \tag{10-54}$$

The characteristic time becomes

$$t_{Br} = \frac{\pi \mu a^3 W}{\alpha_p kT} = \frac{3\mu W}{4N_0 kT} \tag{10-55}$$

where α_p is the volume fraction of the particles and N_0 is their initial number concentration.

If one is to assume that $\phi(h) = 0$, *i.e.*, a complete absence of an external potential and that the diffusion coefficient is affected by the gap width, then $W \rightarrow \infty$ indicating that Brownian motion alone cannot lead to coagulation. In other words, when hydrodynamic interaction that affects D is taken into account, the above analysis predicts that no coagulation should occur at all because the viscous friction becomes infinitely large as the particles approach each other. To this end, one should recognize the importance of the London–van der Waals attraction forces in the coagulation process.

Figure 10-4 shows the variation of the stability ratios in the absence of electrostatic repulsion for the case of a constant and a variable diffusion coefficient. With D being a constant, the stability ratio decreases with (A/kT) and it has a value of unity at $A/kT \rightarrow 0$ as was shown earlier in Figure 10-3. However, when correction for D is considered, the value of the stability ratio is higher than unity for $A/kT \leq 75$ indicating the effects of hydrodynamic interactions in retarding the coagulation process. This is strictly due to the decrease of the particle mobility close to a rigid surface. The expression for $\phi(h)$ used in Figure 10-4 is given by

$$\phi(h) = -\frac{A}{6}\left[\frac{2}{h^2 + 4h} + \frac{2}{(h+2)^2} + ln\,\frac{h^2 + 4h}{(h+2)^2}\right] \tag{10-56}$$

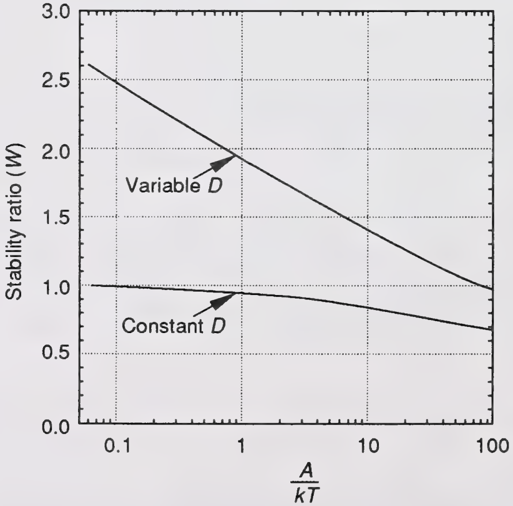

Figure 10-4. Variation of stability ratio W with A/kT for constant and variable D. The dispersion potential is given by Eq. (10-56).

where h is the dimensionless gap width and a is the spherical particles radius. Experimental results for rapid coagulation confirm the analysis summarized by Eq. (10-54). Figure 10-5 and Table 10-2 show the stability ratio for rapid coagulation of polystyrene particles in water as a function of initial radius. The theoretical curve uses a retarded dispersion potential (Russel *et al.*, 1989).

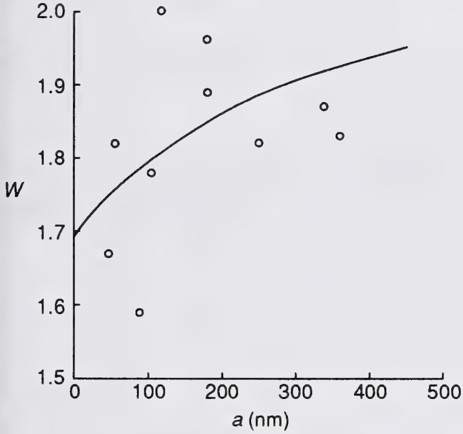

Figure 10-5. Stability ratio for rapid coagulation of polystyrene in water as a function of the sphere radius: ——, prediction from retarded dispersion potential; ○, data from Table 10-2 (Russel *et al.*, 1989).

Table 10-2. Data for rapid coagulation experiments with polystyrene particles (Russel *et al.*, 1989)

	$2a$, μm	W	A/kT
Mathews and Rhodes (1970)	0.714	1.83	1.5
Lips and Willis (1973)	0.207	1.78	1.9
	0.357	1.89	1.2
	0.500	1.82	1.87
Lichtenbelt, Pathmananoharan, and Wiersema (1974)	0.091	1.67	2.7
	0.109	1.82	1.5
	0.176	1.59	4.1
	0.234	2.00	0.7
	0.357	1.96	0.7
Feke and Schowalter (1983)	0.675	1.87	1.1

Higashitani and Matsuno (1979) modified the population balance equation given by Eq. (10-19) to account for the interparticle potential and a variable diffusion coefficient. For the *initial* stage of the coagulation of a monodisperse system where a_i and a_j are not too widely different, the modified population balance equation takes the form

$$\text{(10-57)} \qquad \frac{dn_k}{dt} = \frac{1}{2W} \sum_{\substack{i=1 \\ i+j=k}}^{i=k-1} \beta_{ij} n_i n_j - \frac{1}{W} n_k \sum_{i=1}^{\infty} \beta_{ik} n_i \qquad k = 1, 2, 3 \ldots 10$$

where β_{ij} is defined by Eq. (10-34), W is defined by Eq. (10-54), and $G(h)$ is given by Eq. (10-51).

The experimental results of Higashitani and Matsuno (1979) for (n_k/N_0) variation with time are given in Figure 10-6 for polystyrene particles. The experimental conditions were such that the electrostatic repulsion forces were absent. Excellent agreement with theory is shown. This plot is similar to the case of the Smoluchowski Brownian motion

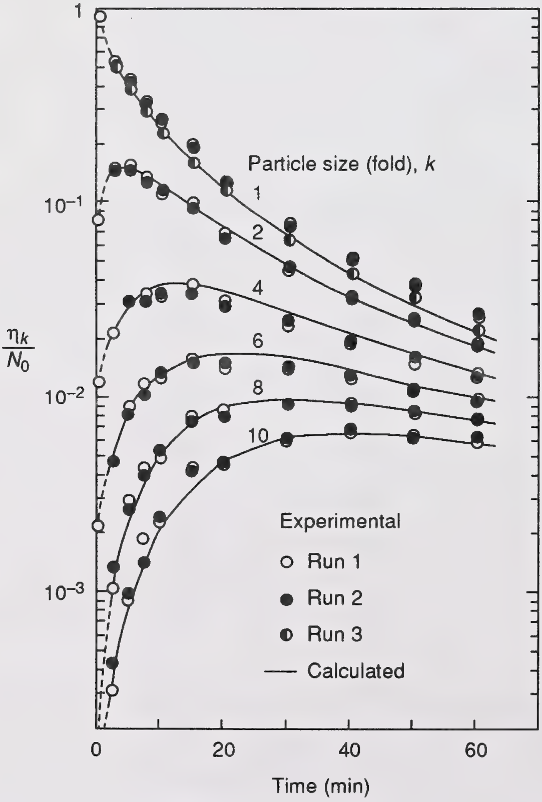

Figure 10-6. Rapid Brownian flocculation for polystyrene spheres with $a = 0.487$ µm and $W = 1.74$. The calculated curves are from Eqs. (10-40) and (10-55) (Higashitani and Matsuno, 1979).

coagulation shown in Figure 10-2 where $W = 1$ and the diffusion coefficient is constant. The dispersion potential was given by Eq. (10-56) with $A = 9 \times 10^{-21}$ J. The excellent agreement with the solution of Eq. (10-57) is a further verification of the theoretical analysis presented for rapid coagulation.

The dimensionless groups that control coagulation due to Brownian motion with added interparticle potential can be arrived at by making use of the dimensionless form of the flux or collision rate equation. The collision rate between the j particles and the i test particle, including transfer by convection (dropping the index j), is given for steady state in Cartesian coordinates by

$$\frac{d}{dx}\left[D\left(-\frac{dn}{dx}-\frac{n}{kT}\frac{d\phi}{dx}\right)+u_x n\right] = 0 \tag{10-58}$$

where u_x is the fluid velocity in x-direction. Strictly speaking, u_x is equal to the particle hydrodynamic velocity v_x.

The non-retarded potential due to dispersion is usually given by

$$\phi_A = Af(X) \tag{10-59}$$

where A is the Hamaker constant.

The potential due to electrostatic force for identical charged spheres is given by

$$\phi_R = 2\pi\varepsilon\varepsilon_o \psi_s^2 a\, g(X,\kappa a) \tag{10-60}$$

The functions f and g are dimensionless functions and

$$X = \frac{x}{a} \tag{10-61a}$$

Let

$$U = \frac{u_x}{a\dot{\gamma}} \tag{10-61b}$$

where $a\dot{\gamma}$ is the characteristic velocity and $\dot{\gamma}$ is the shear rate. U is the dimensionless velocity.

Making use of Eqs. (10-59) to (10-61), Eq. (10-58) becomes

$$\frac{d}{dX}\left[\frac{D}{a}\left(-\frac{dn}{dX}-\frac{n}{kT}A\frac{df(X)}{dX}-\frac{n}{kT}2\pi\varepsilon\varepsilon_o\psi_s^2 a\frac{dg\,(X,\kappa a)}{dX}\right)+a\dot{\gamma}\,Un\right] = 0 \tag{10-62a}$$

Assuming D to be a constant that is equal to $2D_\infty$ and rearranging, Eq. (10-62a) becomes

$$\text{(10-62b)} \quad \frac{d}{dX}\left[-\frac{dn}{dX}-\left(\frac{A}{kT}\right)n\,\frac{df(X)}{dX}-\frac{n}{2}\left(\frac{4\pi\varepsilon\varepsilon_o a\psi_s^2}{kT}\right)\frac{dg\,(X,\kappa a)}{dX}+\frac{1}{2}\left(\frac{a^2\dot{\gamma}}{D_\infty}\right)Un\right]=0$$

Let

$$\text{(10-63a)} \quad N_A = \frac{A}{kT}$$

$$\text{(10-63b)} \quad N_R = \frac{4\pi\varepsilon\varepsilon_o a\psi_s^2}{kT}$$

and

$$\text{(10-63c)} \quad Pe = \frac{a^2\dot{\gamma}}{D_\infty}$$

where Pe is the Peclet number which is a measure of convection to diffusion transport
N_A is a dimensionless parameter that describes the relative importance of the dispersion potential to Brownian motion
N_R is a dimensionless parameter that describes the relative importance of the electrostatic potential to Brownian motion.

Particle coagulation is governed by the dimensionless groups given by Eq. (10-64) in addition to the inverse Debye length κa. The governing equation is

$$\text{(10-64)} \quad \frac{d}{dX}\left[-\frac{dn}{dX}-nN_A\frac{df}{dX}-\frac{n}{2}N_R\frac{dg}{dX}+\frac{Pe}{2}Un\right] = 0$$

It is possible to define other dimensionless groups. They are given by

$$\text{(10-65a)} \quad Pe = \frac{6\pi a^3\dot{\gamma}\mu}{kT}$$

= hydrodynamic potential/Brownian motion

$$(10\text{-}65b)\quad N_r = \frac{N_R}{N_A} = \frac{4\pi\varepsilon\varepsilon_o a\psi_s^2}{A}$$

= electrostatic potential/dispersion potential

and

$$(10\text{-}65c)\quad N_f = \frac{Pe}{N_A} = \frac{6\pi a^3\dot{\gamma}\mu}{A}$$

= hydrodynamic potential/dispersion potential

The dimensionless parameters of Eq. (10-65) are used by the Princeton University research group. The pulp and paper research group at McGill University uses

$$(10\text{-}66a)\quad C_R = \left(\frac{N_r}{N_f}\right) = \frac{2\varepsilon\varepsilon_o\psi_s^2}{3a^2\mu\dot{\gamma}}$$

= electrostatic force/hydrodynamic force

and

$$(10\text{-}66b)\quad C_A = \frac{1}{6N_f} = \frac{A}{36\pi\mu a^3\dot{\gamma}}$$

= dispersion potential/hydrodynamic potential

It should be recognized that additional dimensionless groups would enter into the analysis when retardation dispersion expressions, unequal sphere sizes, ion size, gravitational and inertial forces, surface tension, variable diffusion coefficient, and dielectric constant are considered. It is clear from Eq. (10-64) that by setting $N_A = N_R = Pe = 0$, the coagulation is due solely to Brownian motion. We turn our attention now to coagulation due to a non-zero Peclet number.

10.2.5 Coagulation Due to Shear in the Absence of Brownian Motion: The Smoluchowski Solution

Smoluchowski (1917) was the first to study particle coagulation due to shear. This represents the case of the Peclet number being very large ($Pe \to \infty$). The simplest case is that of a laminar shear flow having a constant shear rate $\dot{\gamma}$. It is assumed that the particles follow straight streamlines. This situation is equivalent to the case of negligible inertia. The geometry of the flow is shown in Figure 10-7.

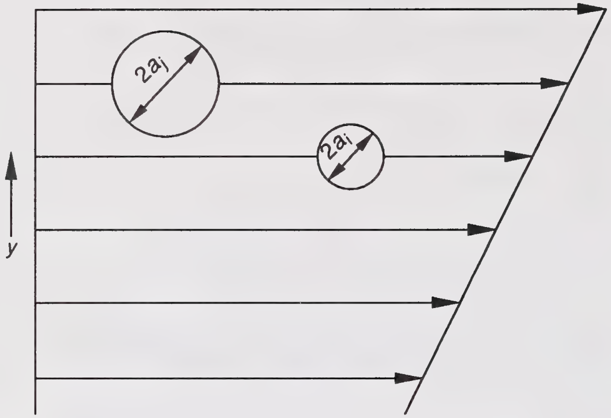

Figure 10-7. Coagulation due to shear for particles of radii a_i and a_j.

For the purpose of the analysis, we consider a stationary test spherical particle of radius a_i located at the origin with particles having a radius of a_j moving towards it along the flow streamlines. When the centres of the two spheres are less or equal to $(a_i + a_j)$, coagulation occurs. Equivalently, contact between the two spheres occurs when $y \leq (a_i + a_j) \sin\theta$ as shown in Figure 10-8. The velocity in x-direction u_x is given by

$$u_x = \dot{\gamma} y \tag{10-67}$$

where $\dot{\gamma}$ is the shear rate and it is taken as a constant.

The number of a_j particles per unit time entering element dy is given by

$$2\left[\left(a_i + a_j\right) \cos\theta\right] [\dot{\gamma} y]\; n_j dy$$

The total number of collisions per unit time between the j particles and the test particle is given by

$$2(2) \int_0^{a_i + a_j} \left[\left(a_i + a_j\right) \cos\theta\right] \dot{\gamma} y\, n_j dy \tag{10-68}$$

where the factor 2(2) in Eq. (10-68) accounts for the four quadrants of the test sphere.

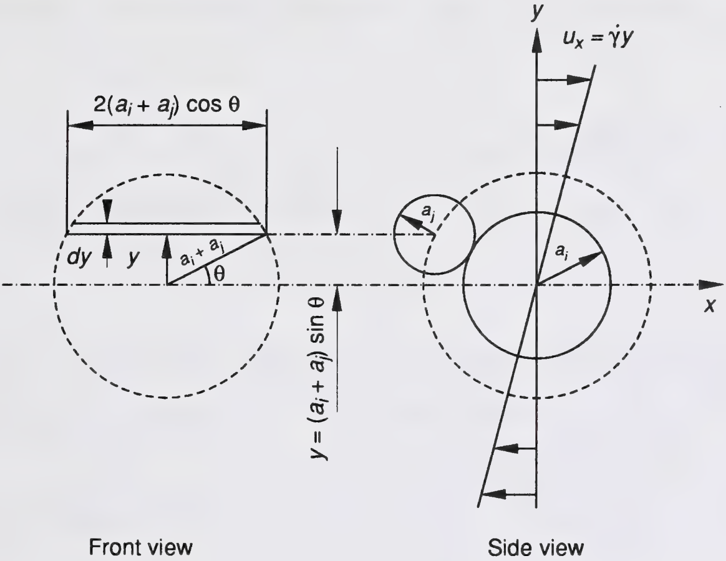

Figure 10-8. Flow geometry for Smoluchowski coagulation under shear flow (adapted from Probstein, 1989).

Substituting for y and including the number concentration of all the test particles, Eq. (10-68) yields

$$J_{ij} = 4 n_i n_j \left(a_i + a_j\right)^3 \dot{\gamma} \int_0^{\pi/2} \cos^2\theta \, \sin\theta \, d\theta$$

Hence

$$(10\text{-}69) \qquad J_{ij} = \frac{4}{3}\left(a_i + a_j\right)^3 \dot{\gamma}\, n_i n_j$$

with

$$(10\text{-}70) \qquad \beta_{ij} = \frac{4}{3}\left(a_i + a_j\right)^3 \dot{\gamma}$$

where J_{ij} is the collision frequency per unit volume.

For a monodisperse system, at the initial stage of coagulation, one can assume that $a_i = a_j = a$, $n_i = n_j = n$, and $J_{ij} = J_{o,sh}$ leading to

$$J_{o,sh} = \left(\frac{32}{3}\right) a^3 \dot{\gamma} n^2 \quad \text{and} \quad \beta = \left(\frac{32}{3}\right) a^3 \dot{\gamma}$$

where $J_{o,sh}$ is Smoluchowski collision frequency per unit volume due solely to shear.

The population balance Eq. (10-19) becomes

$$\frac{dn_k}{dt} = \frac{1}{2} \sum_{i=1}^{i=k-1} \frac{32}{3} a^3 \dot{\gamma} n_i n_j - n_k \sum_{i=1}^{\infty} \frac{32}{3} a^3 \dot{\gamma} n \tag{10-71}$$

Summing over all k, the above equation gives

$$\frac{dN_{tot}}{dt} = -\frac{16}{3} a^3 \dot{\gamma} N_{tot}^2 \tag{10-72}$$

where

$$N_{tot} = \sum_{i=1}^{\infty} n_i$$

The volume fraction of the particles α_p at the *inital stage* of coagulation is given by

$$\alpha_p = \frac{4}{3} \pi a^3 N_{tot} = \text{constant}$$

Making use of α_p definition, Eq. (10-72) becomes

$$\frac{dN_{tot}}{dt} = -\frac{4}{\pi} \dot{\gamma} \alpha_p N_{tot} \tag{10-73}$$

The initial condition is given by

$$N_{tot}(0) = N_0 \quad \text{at } t = 0$$

The solution of Eq. (10-73) is

$$\underset{tot}{N(t)} = N_0 \exp\left(-\frac{t}{t_{sh}}\right) \tag{10-74}$$

where

$$t_{sh} = \frac{\pi}{4\dot{\gamma}\alpha_p} \tag{10-75}$$

t_{sh} is a characteristic coagulation time for flocculation due solely to shear.

Comparing Eqs. (10-38) and (10-72) leads to

$$\frac{\text{rate of coagulation due to shear}}{\text{rate of coagulation due to Brownian motion}} = \frac{4\,a^3\,\dot{\gamma}\,\mu}{kT}$$

One can observe that the above ratio increases with increasing particle radius, shear rate, and fluid viscosity. For $a = 10^{-5}$ m (10 μm), $\dot{\gamma} = 1\ \text{s}^{-1}$, $\mu = 10^{-3}$ Pa s, and $T = 300\ K$, the ratio of shear coagulation to diffusion becomes about 1000. Reducing the particle size to one micron, the ratio becomes about unity.

Coagulation in the absence of the Brownian motion represents the case of a very high Peclet number ($Pe \rightarrow \infty$).

10.2.6 Coagulation Due to Shear in the Absence of Brownian Motion: With Hydrodynamic and Field Forces

In the previous section, we dealt with particle coagulation where the flow field is unaffected by the presence of the particles. Here we shall deal with the case of coagulation due to shear with the full description of the flow field. Simple shear will be assumed where $u_x = \dot{\gamma}y$.

The simplest case of laminar shear flow past a sphere is given by Cox *et al.* (1968). The streamlines of the flow are shown in Figure 10-9. The streamlines can be thought of as the tracing or the trajectory of a neutral particle with a zero radius. Figure 10-9b clearly shows that there exist open and closed streamlines separated by a limiting streamline or surface.

The case of two spheres in a simple shear flow, the creeping flow problem was solved by Lin *et al.* (1970), Batchelor and Green (1972), Kao *et al.* (1977), and Kim and Mifflin (1985). With the origin of the coordinates placed at the centre of sphere 1, the relative position of sphere 2 is given by the spherical coordinates (r, θ, ϕ) as shown in Figure 10-10.

For a simple shear far from the spheres, the flow velocities are given by

$$u_x = \dot{\gamma}y \tag{10-76a}$$

with

$$u_y = u_z = 0 \tag{10-76b}$$

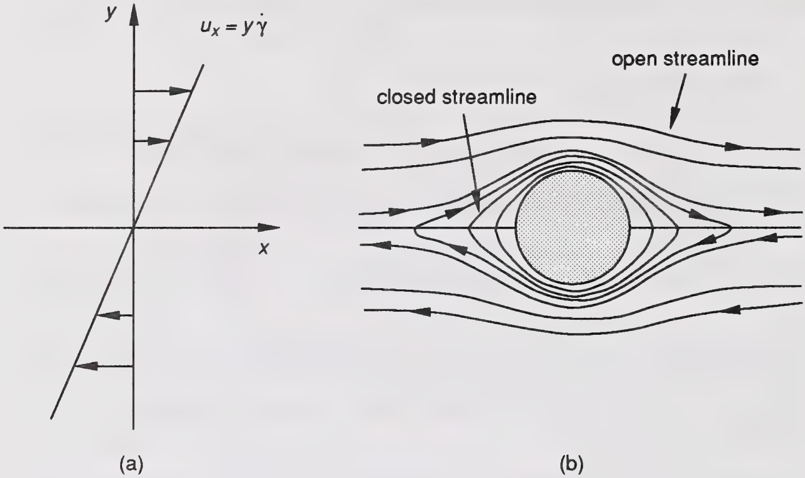

Figure 10-9. Laminar shear flow about a sphere: (a) flow field far from sphere; (b) equatorial streamlines around a sphere (x–y) plane (Cox *et al.*, 1968).

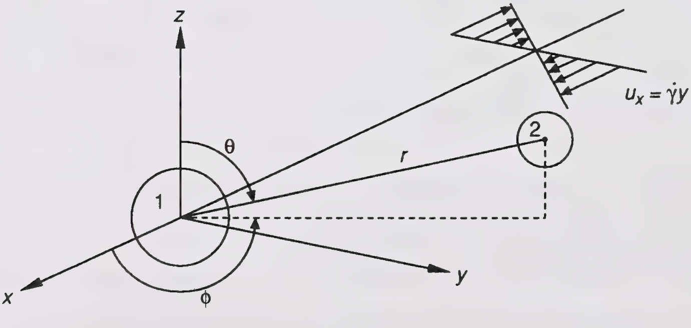

Figure 10-10. Coordinates for trajectory equations for two spheres in a simple shear flow.

The relative trajectories of sphere 2 with respect to sphere 1 are given by

$$\frac{dr}{dt} = \dot{\gamma} r \left(1 - \mathcal{A}\right) \sin^2\theta \ \sin\phi \ \cos\phi \tag{10-77a}$$

$$\frac{d\theta}{dt} = \dot{\gamma} \left(1 - \mathcal{B}\right) \sin\theta \ \cos\theta \ \sin\phi \ \cos\phi \tag{10-77b}$$

and

$$\frac{d\phi}{dt} = -\dot{\gamma}\left[\sin^2\phi + \frac{1}{2}\mathcal{B}\left(\cos^2\phi - \sin^2\phi\right)\right] \tag{10-77c}$$

where t is time. Coefficients $\mathcal{A}$ and $\mathcal{B}$ are functions of radial distance r and size ratio a_1/a_2. They are tabulated in Table 10-3 for equal-sized spheres ($a_1 = a_2$) with R ($= r/a$), where r is the separation distance between the spheres centres and a is the radius of the equal-sized spheres 1 and 2. $\mathcal{A}$ and $\mathcal{B}$ assume different values for unequal spheres.

Table 10-3. Values of $\mathcal{A}$, $\mathcal{B}$, and $\mathcal{C}$ for equal-sized spheres

R	$\mathcal{A}$	$\mathcal{B}$	$\mathcal{C}$
2.0000	1.0000	0.4060	0
2.0001	0.9996	0.3213	0.0004
2.0025	0.9900	0.2762	0.0098
2.0100	0.9619	0.2461	0.0374
2.0401	0.8679	0.1996	0.1310
2.0907	0.7505	0.1608	0.2510
2.1621	0.6313	0.1275	0.3777
2.2553	0.5214	0.0988	0.5017
2.3709	0.4248	0.0748	0.6190
2.5103	0.3424	0.0553	0.7287
2.67498	0.2735	0.0399	0.8306
2.8662	0.2167	0.0281	0.9254
3.0862	0.1704	0.0193	1.0133
3.3370	0.1331	0.0130	1.0950
3.6213	0.1033	0.00856	1.1709
4.7048	0.0468	0.0023	1.3666
6.2149	0.0204	0.0006	1.5207
11.1139	0.0036	0.0000	1.7310
20.1353	0.0006	0.0000	1.8512

Taken from Zeichner and Schowalter (1979)

Figure 10-11 shows the equatorial trajectories for two spheres of radii a_1 and a_2. It is clear that the trajectories are similar to the case around a sphere in simple shear as is shown in Figure 10-9. The flow is characterized by open and closed trajectories. In the absence of the Brownian motion and external forces, two spheres approaching each other from infinity are unable to penetrate the region of closed trajectories and hence they are unable to approach each other closer than distance d_{min} where d_{min} is the minimum distance of approach of two spheres on the limiting trajectory (van de Ven, 1989). For equal-sized spheres, $d_{min}/a = 4.2 \times 10^{-5}$ (Arp and Mason, 1977) and for $a_2/a_1 = 0$, *i.e.*, a single sphere, $d_{min}/a_1 = 0.16$ (Cox *et al.*, 1968). It becomes clear, then, that when the hydrodynamic interactions are taken into consideration, no coagulation takes place between two particles under a simple shear flow in the absence of the Brownian motion and dispersion (attractive) forces. This is in contrast to Smoluchowski's analysis. In order for coagulation to occur under a simple shear flow, an attraction force needs to be present between the particles.

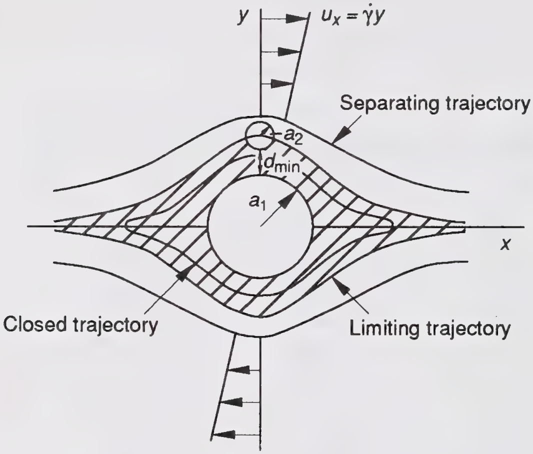

Figure 10-11. Equatorial trajectories of two spheres in a simple shear (schematic). The solid lines are the relative trajectories of a sphere of radius a_2 with respect to a reference sphere of radius a_1. Two kinds of trajectories exist: separating (or open) and closed ones, separated by a limiting trajectory. The shaded area is the region of closed trajectories (van de Ven, 1989).

We consider now the case of coagulation of two equal-sized spheres in laminar shear flow under the influence of interaction forces. Eq. (10-77a) can be regarded as a force balance along the line between sphere centres where the hydrodynamic force acts on the spheres; *i.e.*,

$$\text{Force} = (6\pi a\mu)\left(\frac{dr}{dt}\right)$$

For the case of a non-zero interaction force, Eq. (10-77a) becomes

$$(10\text{-}78) \qquad 6\pi a\mu \, \frac{dr}{dt} = 6\pi a\mu \left[\dot{\gamma} r \, (1 - \mathcal{A}) \, \sin^2\theta \, \sin\phi \, \cos\phi\right] + C\,(r/a) \sum_{\substack{\text{Interaction forces} \\ \text{in } r\text{-direction}}}$$

The implicit assumption made in writing Eq. (10-78) is that the interaction forces act only along the line of centres and are balanced by the component of the hydrodynamic force in that direction, so that the net force on each sphere is zero and there is no additional torque (van de Ven and Mason, 1976). Function $C(r/a)$ is a correction parameter to Stokes law due to the presence of a second sphere.

When the interaction forces are due to the London–van der Waals (attractive) and to electrostatic (repulsive) forces, one can write

The London–van der Waals force is given by

$$(10\text{-}79a) \quad F_A(r) = -\frac{d\phi_A}{dr}$$

where for the case of unretarded dispersion potential ϕ_A between two equal-sized spheres, it can be given by

$$\phi_A = -\frac{A}{6}\left[\frac{2}{R^2 - 4} + \frac{2}{R^2} + ln\left(\frac{R^2 - 4}{R^2}\right)\right]$$

with $R = \frac{r}{a}$

In dimensionless form, Eq. (10-79a) becomes

$$(10\text{-}79b) \quad f_A(R) = \frac{a}{A}F_A(r) = -\frac{1}{A}\frac{d\phi_A}{dR}$$

The electrostatic repulsive force between the two spheres is given by

$$(10\text{-}80a) \quad F_R(r) = -\frac{d\phi_R}{dr}$$

where for a constant low surface potential, the electrostatic potential ϕ_R for two equal-sized spheres is given by Eq. (3-124) as

$$\phi_R = 2\pi\varepsilon\varepsilon_o\,\psi_s^2 a\ ln\left[1 + \exp\left(-\kappa a\,(\mathrm{R} - 2)\right)\right]$$

In dimensionless form, Eq. (10-80a) becomes

$$(10\text{-}80\text{b})\qquad f_R = -\frac{1}{4\pi\varepsilon\varepsilon_o\psi_s^2 a}\,\frac{d\phi_R}{dR}$$

leading to

$$f_R = \frac{1}{4\pi\varepsilon\varepsilon_o\,\psi_s^2}\,F_R(R)$$

Making use of Eqs. (10-79b) and (10-80b), Eq. (10-78) becomes

$$(10\text{-}81)\qquad \frac{dr}{dt} = \left[\dot{\gamma} r\,(1-\mathcal{A})\sin^2\theta\,\sin\phi\,\cos\phi\right] + \frac{C(R)}{6\pi a\mu}\left[4\pi\varepsilon\varepsilon_o\,\psi_s^2 f_R(R) + \frac{A}{a}f_A(R)\right]$$

Dimensionalizing the time t using $\dot{\gamma}$ as

$$\tau = t\,\dot{\gamma}$$

and making use of Eqs. (10-65b,c), Eq. (10-81) becomes in dimensionless form

$$(10\text{-}82\text{a})\qquad \frac{dR}{d\tau} = R\,(1-\mathcal{A})\,\sin^2\theta\,\sin\phi\,\cos\phi + \frac{C(R)}{N_f}\left(N_r f_R + f_A\right)$$

The corresponding trajectory equations represented by Eqs. (10-77b,c) become

$$(10\text{-}82\text{b})\qquad \frac{d\theta}{d\tau} = (1-\mathcal{B})\,\sin\theta\,\cos\theta\,\sin\phi\,\cos\phi$$

and

$$(10\text{-}82\text{c})\qquad \frac{d\phi}{d\tau} = -\left[\sin^2\phi + \frac{1}{2}\mathcal{B}\left(\cos^2\phi - \sin^2\phi\right)\right]$$

The function $C(R)$ is related to the parameter $G(h)$ given by Eq. (10-51) for the case of diffusion coefficient, where

$$(10\text{-}83)\qquad G(R) \cong \frac{2}{C(R)}$$

and

$$C(R) \cong \frac{4\left(3R^2 - 10R + 8\right)}{6R^2 - 11R} \tag{10-84}$$

where $R = r/a = 2 + h$.

Tabulation of $C(R)$ is given in Table 10-3. Various expressions for $\mathcal{A}$, $\mathcal{B}$, and C are given by Higashitani *et al.* (1982) and van de Ven and Mason (1976) for $R \rightarrow 2$ and $R \rightarrow \infty$.

Solution of the trajectory equations provides the trajectories of the colliding spheres. For the case of $N_r = 0$ (*i.e.*, absence of a repulsive force) and $N_f = 1$, Feke and Schowalter (1983) provide the trajectories at $z = 0$ plane (equatorial plane) as shown in Figure 10-12. There are three types of trajectories. The first type is an open trajectory initiated from downstream and extending to upstream infinity. Here, the two spheres do not coagulate. The second type of trajectory leads to coagulation. It crosses the x-axis and reverses direction prior to collision. This is shown by the shaded area of Figure 10-12. The third type of trajectory leads to coagulation before crossing the x-axis which is the plane of shear.

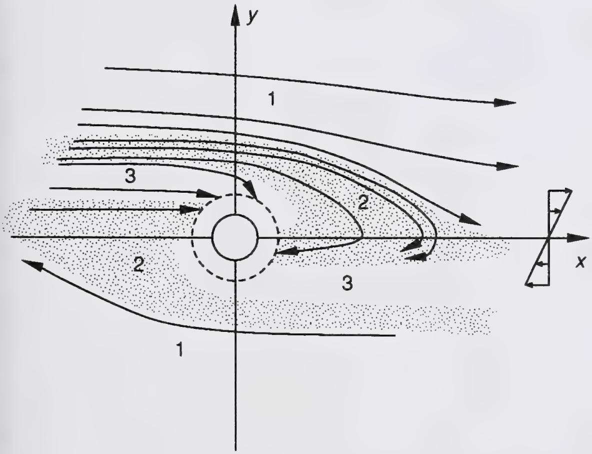

Figure 10-12. Trajectories in the $z = 0$ plane for two spheres in a simple shear flow, with $N_r = 0$ and $N_f = 1$: (1) open trajectories extending from upstream to downstream infinity; (2) trajectories leading to collision after crossing the plane of shear ($y = 0$) and reversing direction; (3) trajectories leading to collision prior to crossing the plane of shear (Feke and Schowalter, 1983) (reprinted by permission of Cambridge University Press).

Takamura *et al.* (1981) visualized the trajectories of shear-induced collisions between two equal-sized latex spheres for three cases: (a) repulsion is dominant, (b) weak attraction, and (c) strong attraction. Figure 10-13 shows the three cases. The two curves in each figure represent the projection on the xy-plane of the paths of the *centres* of the two spheres. At the origin is the exclusion sphere which cannot be penetrated by either colliding sphere. Figure 10-13a demonstrates the effect of a net repulsive force on the spheres trajectories. The spheres initially approach each other with their centres $\pm 0.15a$ off the x-axis. However, after they encounter each other, they recede with their centres $\pm 0.8a$ away from the x-axis.

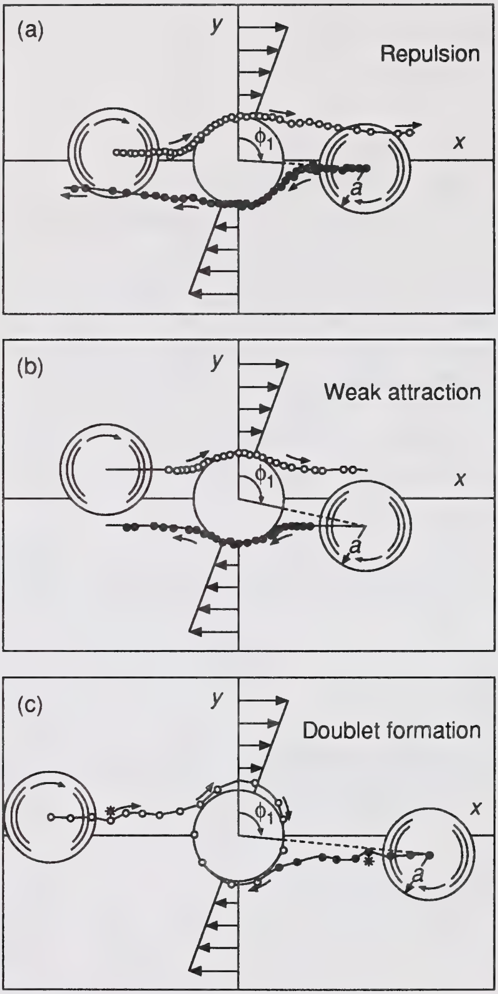

Figure 10-13. Trajectories of shear-induced collisions of 2.6 μm PS latex spheres in 50% aqueous glycerol showing the projection on the *xy*-plane of the paths of the centres of spheres from the midpoint between them. At the centre is the exclusion sphere which cannot be penetrated if the collision occurs in the *xy*-plane (Takamura *et al.*, 1981).

Figure 10-13b shows the case of a weak attraction upon increasing the KCl electrolyte concentration to 10 mM. The paths of approach and recession of the two spheres become almost a mirror image of each other. By further increasing the electrolyte concentration to 100 mM, the net force becomes attractive and a doublet is formed upon the spheres collision as is shown in Figure 10-13c.

To evaluate the coagulation rate, it is necessary to know the limiting trajectory within which all particles collide. A limiting trajectory for the case of two equal-sized spheres is defined as that which terminates at $\phi = 0$ with $r = 2a$ (see Figure 10-10). The area occupied by the limiting trajectories is usually evaluated by retracing backward in time the path of the particles. The limiting interception area is shown in Figure 10-14 by the shaded area. The corresponding limiting interception area for Smoluchowski's analysis is shown for comparison in Figure 10-15.

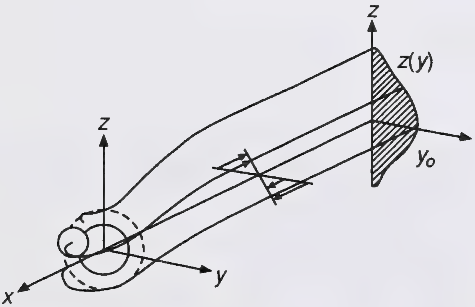

Figure 10-14. Trajectory of real systems (Higashitani *et al.*, 1982).

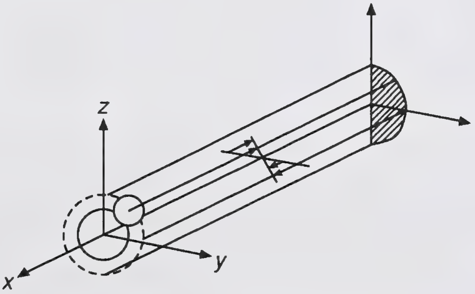

Figure 10-15. Trajectory of Smoluchowski model (Higashitani *et al.*, 1982).

The rate of coagulation between particles of equal-sized spheres per unit volume J is given by counting the number of particles crossing the interception area, where

$$J = 4n^2\dot{\gamma} \int_0^{y_o} yz(y)\, dy \tag{10-85}$$

where $z = z(y)$ is the function defining the boundary of the interception area and y_o is the y value of the boundary at $z = 0$. Recalling Smoluchowski's collision rate $J_{o,sh}$ defined as

$$J_{o,sh} = \frac{32}{3} a^3\dot{\gamma}n^2 \tag{10-86}$$

it is possible to define a stability ratio W as

$$W = \frac{J_{o,sh}}{J} \tag{10-87}$$

Large W values indicate a stable colloidal system. In some literature, the inverse of W is used and W^{-1} is called the shear coagulation coefficient. Figure 10-16 shows the stability ratio W as a function of N_f for the case of $N_r = 0$.

At small N_f values, W becomes less than unity, indicating a strong attractive London–van der Waals force. However, at large values of N_f, where the London–van der Waals force becomes weaker relative to the hydrodynamic force, W increases rapidly indicating a high hydrodynamic resistance for the approaching particles and a reduction in J.

The preceding interpretation of Figure 10-16 is to keep the hydrodynamic potential $6\pi a^3\dot{\gamma}\mu$ constant and the change in N_f is due to the Hamaker constant. The variation in A reflects changes in the attractive London–van der Waals forces. One can also use Figure 10-16 to examine the effect of increasing the flow strength $\dot{\gamma}$. Here A is kept constant. Recognizing that $\dot{\gamma}$ appears both in W and in N_f, a change in N_f from, say, 10^2 to 10^5 gives a corresponding change in W from ~5 to ~20. This means that J at $N_f = 10^5$ is ~250 times that at $N_f = 10^2$. Consequently, increasing $\dot{\gamma}$ by a factor of 10^3 has a profound effect on increasing the collision rate per unit volume.

Now let us study the effect of viscosity by keeping other parameters constant. N_f contains μ and W does not implicitly contain μ. Increasing N_f from 10^2 to 10^5 would give a corresponding change in J of $5/20 = 0.25$. This means that increasing the fluid viscosity by a factor of 10^3 only reduces J by a factor of 4.

The integration of the trajectory Eq. (10-82) for different N_r and N_f produces stability diagrams (van de Ven and Mason, 1976; Zeichner and Schowalter, 1977). A typical stability plot is shown in Figure 10-17. It should be recalled that for a given fluid viscosity, particle radius, medium dielectric constant, and Hamaker constant, one obtains $N_r \propto \psi_s^2 \propto$

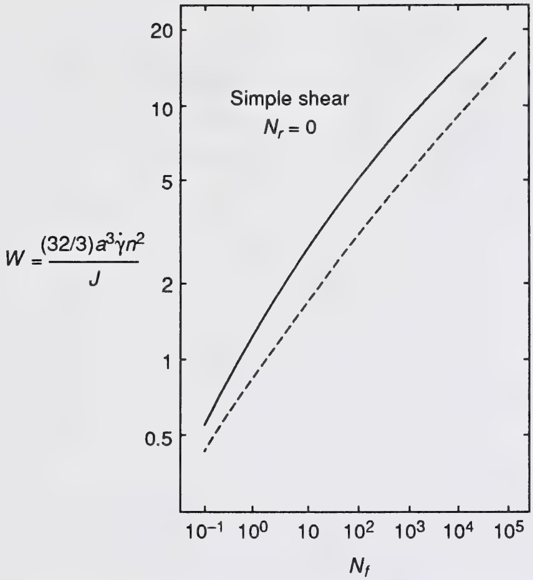

Figure 10-16. Comparison of stability ratios W for flow-induced coagulation $Pe = \infty$ using unretarded potential. -----, trajectory analysis of Zeichner and Schowalter (1977); —— (Feke and Schowalter, 1983) (reprinted by permission of Cambridge University Press).

(repulsion force) and $N_f \propto \dot{\gamma} \propto$ (flow strength). Consequently, $\sqrt{N_r}$ represents changes in the surface potential ψ_s and N_f represents the strength of the flow field. From an experimenter's point of view, ψ_s is controlled by the ionic strength and pH of the electrolyte solution.

The stability diagram shown in Figure 10-17 is divided into three regions. In region 1, coagulation occurs in the primary minimum. In region 2, coagulation occurs in the secondary minimum, and finally in region 3, no coagulation occurs (Zeichner and Schowalter, 1977). For example, if one is to start with a sol under no shear containing spherical particles with, say, $N_r = 20$, then upon subjecting the sol to increasing shear, doublets coagulating in the primary minimum would be formed. Increasing N_f beyond 5×10^3 would cause the doublet to deflocculate. For $N_r = 100$, if a sol is sheared then doublets would form at the secondary minimum. A further increase in the rate of shear would deflocculate the doublets out of the secondary minimum. Increasing the shear rate further would cause the particles to coagulate into the primary minimum. At still higher shear rates, doublets would deflocculate out of the primary minimum. If one is to decrease the shear rate, the dispersed sol will again coagulate into the primary minimum. Further lowering of the shear rate will not, however, cause deflocculation or a shift to secondary minimum flocculation.

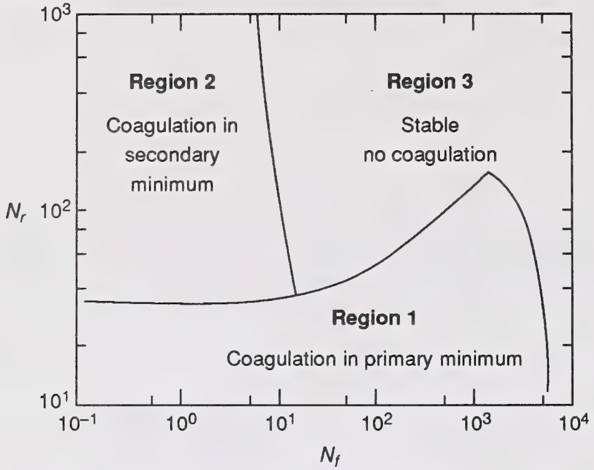

Region 1 – primary minimum coagulation
Region 2 – secondary minimum coagulation
Region 3 – stable

(Calculated for unretarded attraction, constant surface potential, $\kappa a = 100$ and $d_{min}/a = 2.004$).

Figure 10-17. Stability plane for shear flow (Zeichner and Schowalter, 1977).

The boundaries of the various regions shift with κa as shown in Figure 10-18. This type of a stability diagram is very important in the formation of emulsions and in the process of demulsification under shear. In all cases discussed above, the Brownian motion was not considered and we dealt with cases corresponding to large *Pe*.

Figure 10-17 is useful in interpreting many industrial processes where colloidal systems are of concern. For example, Yan and Masliyah (1993) found that for solids stabilized oil-in-water emulsions, it is possible to demulsify such emulsions by the addition of fresh oil under mixing action. The mixing action breaks down the added fresh oil into large oil droplets which act as scavengers to the solids-coated oil emulsion droplets. Here coagulation occurs in the primary minimum and hence scavenging takes place. In this process, the mixing action, *i.e.*, the shear rate, is very important. Very high mixing rates were found to be detrimental to the scavenging process because the added fresh oil would form a stable emulsion at large N_f values.

Another example is in the processing of oil sands and the recovery of bitumen. Oil sands containing bitumen are diluted with hot water in the presence of NaOH and are slurried in a rotational drum. After the liberation of the bitumen from the sand grains, it becomes desirable to avoid the coagulation of the liberated bitumen with the fines (or clays) in the

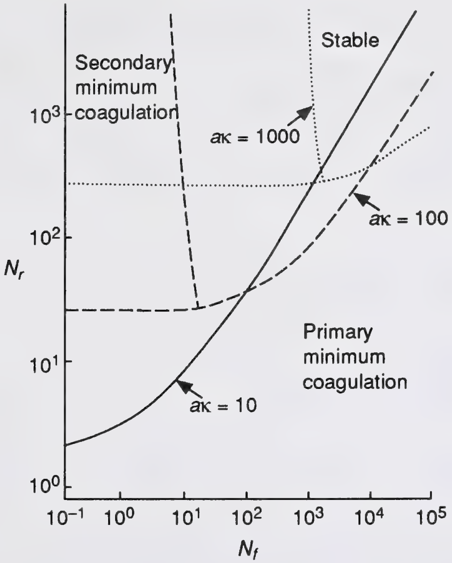

Figure 10-18. Stability diagram for doublet formation in a simple shear flow with $Pe = \infty$, with a constant-potential boundary condition and the non-retarded Hamaker form for the attraction force (Zeichner and Schowalter, 1977).

slurry. Proper N_r and N_f values should be maintained so that the slurrying operation occurs in region 3. This depends on the amount of NaOH added and the degree of mixing in the rotating conditioning drum.

For cases of intermediate Pe values, the combined effects of the Brownian diffusion on shear-induced coagulation of colloidal dispersions are dealt with by Feke and Schowalter (1985). The protocol is to combine the analysis made for the Brownian and shear coagulation. Figure 10-19 shows the rate of doublet formation normalized with $J_{o,Br}$. Two regions are given, one for $Pe \ll 1$ and $Pe \gg 1$. No solution was provided for the intermediate region. Figure 10-19 indicates that in the region of $Pe \ll 1$, increasing $\dot{\gamma}$ (all other parameters being constant) has little effect on the collision rate per unit volume J. This situation is similar to the classical mass transfer process in the absence of external forces. In such a situation, the dimensionless mass transfer group, the Sherwood number Sh is given by

$$Sh = b_1 + b_2 Pe \qquad \text{for } Pe < 1 \tag{10-88}$$

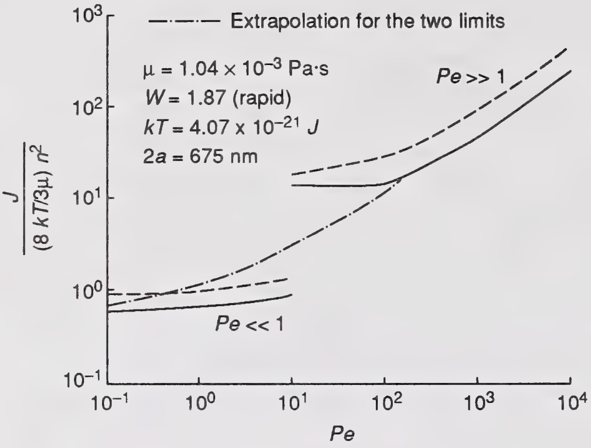

Figure 10-19. Rate of doublet formation for spheres as a function of *Pe*, showing the results from the perturbation expansions in the $Pe << 1$ and $Pe >> 1$ limits for $A/kT = 2$ (——) and 20 (----) and no repulsion ($N_r = 0$) (Feke and Schowalter, 1985).

where constants b_1 and b_2 are of the order of unity. Here *Sh* is a weak function of *Pe*. For the case of $Pe >> 1$, J increases rapidly with changes in the flow strength as characterized by $\dot{\gamma}$ in a similar fashion as for Figure 10-16.

The analysis of the preceding sections clearly indicates the complexity of the particle–particle coagulation process where the Brownian motion, hydrodynamic forces and interaction forces due to electrostatic and dispersion can play a major role. Experimental studies tend to confirm the theoretical analysis for rapid coagulation. However, deviation from theory occurs for slow coagulation where appreciable repulsive forces are present (Zeichner and Schowalter, 1979; Kihira *et al.*, 1992).

10.3 NOMENCLATURE

$\mathcal{A},\mathcal{B},\mathcal{C}$	flow functions, dimensionless
a, a_1, a_2	particle radius, m
A	Hamaker constant, J
C_A	dimensionless parameter describing the relative importance of dispersion and hydrodynamic potentials (or forces), $A/36\pi\mu a^3\dot{\gamma}$

C_R	dimensionless parameter describing the relative importance of electrostatic and hydrodynamic forces, $2\varepsilon\varepsilon_o\psi_s^2/3a^2\mu\dot{\gamma}$
$d_{\parallel}$	correction factor for the diffusion coefficient for motion parallel to the surface of the spheres, dimensionless
$d_{\perp}$	correction factor for the diffusion coefficient for motion normal to the surface of the spheres, dimensionless
D	particle diffusion coefficient, m^2/s
$\underline{\underline{D}}$	particle diffusion coefficient tensor, m^2/s
D_∞	particle diffusion coefficient at infinite dilution, m^2/s
D_i,D_j	diffusion coefficient of particles i and j, respectively, m^2/s
f	friction coefficient, Eq. (10-6), Ns/m
$f_A(R)$	dimensionless dispersion potential
$f_R(R)$	dimensionless electrostatic potential
$f(x)$	dimensionless function for the dispersion potential, Eq. 10-59
$F(r)$	interaction force function, N
$g(X,\kappa a)$	dimensionless function for the electrostatic potential
h	dimensionless gap between two surfaces, $h = R - 2$
i,j,k	particle species
J_{ij}	collision rate (frequency) per unit volume, $m^{-3}\ s^{-1}$
$J_{o,Br}$	Smoluchowski collision rate per unit volume due to Brownian diffusion, $8kTn^2/3\mu$, $m^{-3}s^{-1}$
$J_{o,sh}$	Smoluchowski collision rate per unit volume due to simple shear, $(32/3)a^3\dot{\gamma}n^2$, $m^{-3}s^{-1}$
k	Boltzmann constant, J/K
K	function defined by Eq. 10-36, m^3/s
m	mass of a particle, kg
n	number of particles per unit volume (number concentration), m^{-3}
n_∞	number concentration of particles at time zero, m^{-3}
n_i,n_j,n_k	number concentration of particle species i, j, and k, respectively, m^{-3}
$n_{i\infty}$,$n_{j\infty}$, $n_{k\infty}$	number concentration of particle species i, j, and k in the undisturbed state, respectively, m^{-3}

N_A	dimensionless parameter describing the relative importance of the dispersion potential and Brownian motion, A/kT
N_f	dimensionless parameter describing the relative importance of the hydrodynamic and dispersion potentials (or forces), $6\pi a^3\dot{\gamma}\mu/A$
N_i	total number of released particles per unit area at time zero and $x = 0$, m^{-2}
N_0	value of N_{tot} at time zero, m^{-3}
N_r	dimensionless parameter describing the relative importance of electrostatic and dispersion potentials (or forces), $4\pi\varepsilon\varepsilon_o a\psi_s^2/A$
N_R	dimensionless parameter describing the relative importance of the electrostatic potential and Brownian motion, $4\pi\varepsilon\varepsilon_o a\psi_s^2/kT$
N_{tot}	total number of particles per unit volume (number of concentrations), m^{-3}
Pe	Peclet number, a measure of convection to diffusional transport, dimensionless
r	radial position; dimensional centre-to-centre distance between two spheres, m
R	dimensionless centre-to-centre distance between two spheres, r/a
t	time, s
t_{Br}	characteristic half-time for flocculation due to Brownian diffusion, $\pi\mu\, a^3/\alpha_p kT$, s, Eqs. (10-41a) and (10-41b); $\pi\mu\, a^3W/\alpha_p kT$, Eq. (10-55)
t_{sh}	characteristic half-time for flocculation due to shear, $\pi/4\dot{\gamma}\alpha_p$, s, Eq. 10-75
T	absolute temperature, K
u_x	fluid velocity in x-direction, m/s
U	dimensionless fluid velocity, Eq. 10-61b
v	particle velocity, m/s
v_i, v_j, v_k	volume of particle species $i, j,$ and $k,$ respectively, m^3
W	stability ratio, dimensionless
x	Cartesian coordinate, m
X	dimensionless distance or coordinate, x/a
α_p	volume fraction of particles, dimensionless
β	function relating to f/m, Eq. (10-7); collision frequency function, m^3/s
β_{ij}	collision frequency function pertaining to particles i and j, m^3/s

$\dot{\gamma}$	shear rate, s^{-1}
ε	dielectric constant of a medium, dimensionless
ε_o	permittivity of vacuum, C/Vm
θ	spherical coordinate
κ	inverse Debye length, m^{-1}
μ	fluid viscosity, Pa s
τ	dimensionless time, $t\dot{\gamma}$
ϕ	spherical coordinate
ϕ	interaction potential, J
ϕ_A	dispersion potential, normally assumed to be attractive, J
ϕ_R	electrostatic potential, normally assumed to be repulsive, J
ψ_s	surface potential, V

10.4 REFERENCES

Arp, P.A. and Mason, S.G. (1977), *The Kinetics of Flowing Dispersion. VIII. Doublets of Rigid Spheres (theoretical),* J. Colloid Interface Sci., **61**, 21–43.

Batchelor, G.K. and Green, J.T. (1972), *The Hydrodynamic Interaction of Two Small Freely-Moving Spheres in a Linear Flow Field,* J. Fluid Mechanics, **56**, 375–400.

Brenner, H. (1961), *The Slow Motion of a Sphere Through a Viscous Fluid Towards a Plane Surface,* Chem. Eng. Sci., **16**, 242–51.

Cox, R.G., Zia, I.Y.Z., and Mason, S.G. (1968), *Particle Motions in Sheared Suspensions. XXV. Streamlines Around Cylinders and Spheres,* J. Colloid Interface Sci., **27**, 7–18.

Derjaguin, B.V. and Landau, L. (1941), *Theory of the Stability of Strongly Charged Lyophobic Sols and the Adhesion of Strongly Charged Particles in Solutions of Electrolytes,* Acta Physicochim. URSS, **14**, 633–62.

Derjaguin, B.V. and Muller, V.M. (1967), *Slow Coagulation of Hydrophobic Colloids,* Dokl. Akad. Nauk. SSSR, **176**, 738–41.

Feke, D.L. and Schowalter, W.R. (1983), *The Effect of Brownian Diffusion on Shear-Induced Coagulation of Colloidal Dispersion,* J. Fluid Mechanics, **133**, 17–35.

Feke, D.L. and Schowalter, W.R. (1985), *The Influence of Brownian Diffusion on Binary Flow-Induced Collision Rates in Colloidal Dispersion,* J. Colloid Interface Sci., **106**, 203–14.

Friedlander, S.K. (1977), *Smoke, Dust and Haze: Fundamentals of Aerosol Behavior,* John Wiley and Sons, New York.

Fuchs, N. (1934), Z. Phys., **89**, 736–43.

Kao, S.V., Cox, R.G., and Mason, S.G. (1977), *Streamlines Around Single Spheres and Trajectories of Pairs of Spheres in Two-Dimensional Creeping Flow*, Chem. Eng. Sci., **32**, 1505–15.

Kihira, H., Ryde, N., and Matijevic, E. (1992), *Kinetics of Heterocoagulation I. A Comparison of Theory and Experimen*t, Colloids and Surfaces, **64**, 317–24.

Kim, S. and Mifflin, R.T. (1985), *The Resistance and Mobility Functions of Two Equal Spheres in Low Reynolds Number Flow*, Phys. Fluids, **28**, 2033–45.

Higashitani, K. and Matsuno, Y. (1979), *Rapid Brownian Coagulation of Colloidal Dispersions,* J. Chem. Eng. Japan, **12**, 460–65.

Higashitani, K., Ogawa, R., Hosokawa, G., and Matsuno, Y. (1982), J. Chem. Eng. Japan, **15**, 299–304.

Honig, E.P., Roebersen, G.J., and Wiersema, P.H. (1971), *Effect of Hydrodynamic Interaction on the Coagulation Rate of Hydrophobic Colloids,* J. Colloid Interface Sci., **36**, 97–109.

Lichtenbelt, J.W.Th., Pathmananoharan, C., and Wiersema, P.H. (1974), *Rapid Coagulation of Polystyrene Latex in a Stopped Flow Spectrophotometer*, J. Colloid Interface Sci., **49**, 281–85.

Lin, C.J., Lee, K.J., and Sather, N.F. (1970), *Slow Motion of Two Spheres in a Shear Field,* J. Fluid Mechanics, **43**, 35–47.

Lips, A. and Willis, W.E. (1973), *Low Angle Scattering Technique for the Study of Coagulation*, J. Chem. Soc. Faraday Trans. *I*, **69**, 1226–36.

Mathews, B.A. and Rhodes, C.T. (1970), *Studies of the Coagulation Kinetics of Mixed Suspensions*, J. Colloid Interface Sci., **32**, 332–38.

Probstein, R.F. (1989), *Physicochemical Hydrodynamics*, Butterworths, Boston.

Russel, W.B., Saville, D.A., and Schowalter, W.R. (1989), *Colloidal Dispersions*, Cambridge University Press, Cambridge.

Smoluchowski, M. von (1917), Z. Phys. Chem., **92**, 129–68.

Spielman, L.A. (1970), *Viscous Interactions in Brownian Coagulation*, J. Colloid Interface Sci., **33**, 562–71.

Spielman, L.A. (1977), *Particle Capture from Low-Speed Laminar Flows*, Ann. Review of Fluid Mechanics, **9**, 297–319.

Takamura, K., Goldsmith, H.L., and Mason, S.G. (1981), *The Microrheology of Colloidal Dispersions XII. Trajectories of Orthokinetic Pair-Collisions of Latex Spheres in a Simple Electrolyte,* J. Colloid Interface Sci., **82**, 175–89.

van de Ven, Theo G.M. (1989), *Colloidal Hydrodynamics*, Academic Press, London.

van de Ven, Theo G.M. and Mason, S.G. (1976), *The Microrheology of Colloidal Dispersion. IV. Pairs of Interacting Spheres in a Shear Flow*, J. Colloid Interface Sci., **57**, 505–16.

Verwey, E.J.W. and Overbeek, J.Th.G. (1948), *Theory of the Stability of Lyophobic Colloids*, Elsevier, Amsterdam.

Yan, Y. and Masliyah, J. (1993), *Solids-Stabilized Oil-in-Water Emulsion: Scavenging of Emulsion Droplets by Fresh Oil Addition,* Colloids and Surfaces, **75**, 123–32.

Zeichner, G.R. and Schowalter, W.R. (1977), *Use of Trajectory Analysis to Study Stability of Colloidal Dispersions in Flow Fields*, AIChEJ, **23**, 243–54.

Zeichner, G.R. and Schowalter, W.R. (1979), *Effects of Hydrodynamic and Colloidal Forces on the Coagulation of Dispersions*, J. Colloid Interface Sci., **71**, 237–53.

DEPOSITION OF COLLOIDAL PARTICLES

11

11.1 GENERAL

In Chapter 10 we discussed particle–particle interaction under Brownian motion and field forces. A stability ratio *W* was derived to assess the stability of a colloidal system. The cases considered were concerned with particles of similar size and consequently the analysis was of interest in studying the stability of colloidal systems under Brownian motion, shear and interparticle forces such as the London–van der Waals attractive and electrostatic repulsive forces.

In this chapter we shall deal with a small particle-large surface interaction. The small particle is of colloidal size that is much smaller than the collector with which it is interacting. The large surface can be a cylindrical fibre in a filter mat, a granular particle in a packed bed or simply a surface within the colloidal system, *e.g.*, a container's wall. Various deposition configurations are shown in Figure 11-1. We shall deal only with the process of deposition rather than with the process of detachment. The latter case is more complicated to analyze as the depth of the energy minimum in which a particle is captured is usually not known. However, the study of detachment itself can provide information regarding the strength of the forces between a particle and a surface (van de Ven, 1989).

There are two approaches to the study of particle deposition. The first method is the Eulerian approach where the distribution of particles is evaluated in space. In the absence of colloidal forces and for infinitesimal particle size, the Eulerian approach becomes that of the study of heat or mass transfer from submerged objects in a flowing stream. To this end, the generalized convection-diffusion equation is solved for the diffusing colloidal particles subject to the appropriate boundary conditions. The second method is the Lagrangian approach. Here attention is focused on a single particle trajectory which is described by Newton's laws of motion. The particle path is followed and the particle trajectories determine the collision or capture efficiency between the colloidal particle and the larger collector particle. The forces associated with Newton's laws are deterministic in nature and consequently most of the literature studies employing the Lagrangian approach usually do not consider the Brownian motion and hence the diffusion of the particles. However, it is possible to include the Brownian motion in the analysis and both approaches should, in principle, yield similar results (van de Ven, 1989).

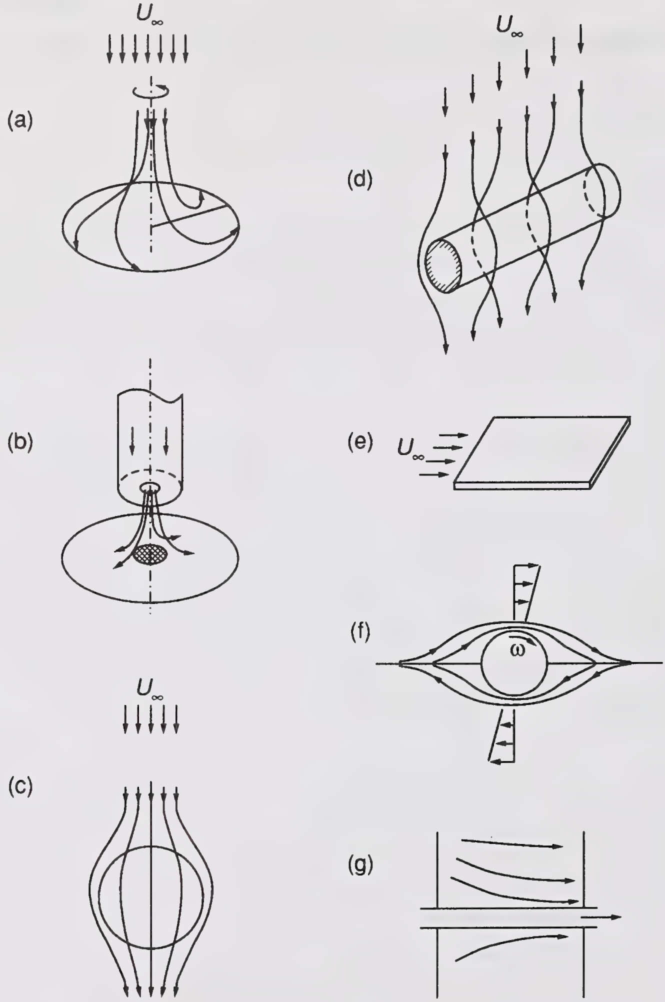

Figure 11-1. Various deposition geometries: (a) rotating disc; (b) impinging jet; (c) flow over a sphere; (d) cross flow over a cylinder; (e) flow along a flat plate; (f) sphere in shear flow; and (g) flow parallel to a cylinder (Adamczyk, 1989a,b).

11.2 CLASSICAL DEPOSITION MECHANISMS

Deposition of particles onto surfaces occurs due to several interparticle forces. However, in limiting cases it is possible to distinguish between the various modes of particle deposition.

The various modes can be classified as follows:

11.2.1 Brownian Diffusion: Classical Convection-Diffusion Transport

Submicron particles undergo Brownian motion which enhances their deposition during flow past the surface of a collector. The governing transport equation is given by the convection-diffusion equation as

$$\vec{u} \cdot \vec{\nabla} c = D_{\infty} \nabla^2 c \tag{11-1}$$

where $\vec{u}$ is the fluid velocity
c is the particle concentration and
D_{∞} is the particle diffusion coefficient given by the Stokes–Einstein equation as

$$D_{\infty} = \frac{kT}{6\pi\mu a} \tag{11-2}$$

This analysis treats the particles as diffusing non-interaction points with D_{∞} being a constant. The particle hydrodynamic velocity is the same as the fluid velocity. The solution of the Navier–Stokes equation provides the fluid velocity $\vec{u}$.

The mass transfer rate is related to the flow Reynolds and Schmidt numbers. In the limit of creeping flow, the mass transfer is related to the flow Peclet number Pe which is the product of the Reynolds and Schmidt numbers.

In general for $Pe \ll 1$, the dimensionless mass transfer group as presented by the Sherwood number is of the order Pe. On the other hand, when $Pe \gg 1$, the Sherwood number becomes of the order $Pe^{1/3}$. Here Pe is the flow Peclet number defined as LU_{∞}/D_{∞} where L and U_{∞} are the characteristic length and fluid velocity, respectively.

11.2.2 Interception Deposition

Capture by interception assumes that the particles have a finite size and they are non-interacting and non-diffusing. The centre of a particle follows exactly the undisturbed fluid streamline past the collector. When the particle touches the collector, capture or deposition takes place. Capture by pure interception ignores the increased hydrodynamic resistance between the particles and the collector upon approach. Figure 11-2 shows capture by interception of a spherical particle by a spherical collector. Particles located above the limiting trajectory or streamline will not intercept the collector. Particles located below the limiting trajectory will intercept the collector.

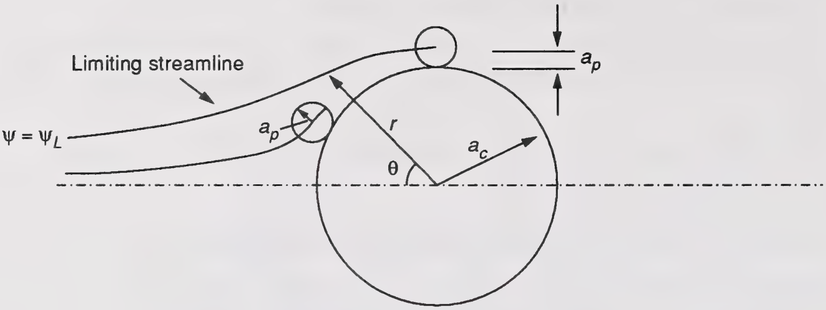

Figure 11-2. Capture due to interception by a spherical collector.

As the particles follow the flow streamline, it is possible to evaluate the flux of particles that intercept a collector from the knowledge of the flow stream function. For the case of a spherical collector, the flow stream function, under creeping flow conditions, is given by

$$\psi = \frac{1}{2} U_\infty \left(r^2 - \frac{3}{2} a_c r + \frac{a_c^3}{2r} \right) \sin^2\theta \tag{11-3}$$

The spherical coordinates are shown in Figure 11-2 together with the streamlines which are the locus of a constant ψ-value. The volumetric flow rate between any streamline and the collector axis is given, by definition, as $2\pi\psi$. A particle is considered to be captured or intercepted by the collector when its centre is within one particle radius from the collector surface. Consequently, all particles within such a limiting streamline are captured. The limiting streamline for the special case of interception deposition is given by setting $r = a_p + a_c$ and $\theta = \pi/2$; hence

$$\psi_L = \frac{1}{2} U_\infty \left[\left(a_p + a_c\right)^2 - \frac{3}{2} a_c \left(a_p + a_c\right) + \frac{a_c^3}{2} \left(\frac{1}{a_p + a_c} \right) \right] \tag{11-4}$$

The total flux of the captured particles is given by $2\pi\psi_L n_\infty$. Capture efficiency is defined by the ratio of the actual captured particles to the idealized capture given by the area swept by the collector $\pi a_c^2 U_\infty n_\infty$. The capture efficiency is then given by

$$\eta_I = \frac{2\pi\psi_L n_\infty}{\pi a_c^2 U_\infty n_\infty} = \frac{2\psi_L}{a_c^2 U_\infty} \tag{11-5a}$$

Making use of Eq. (11-4), the capture efficiency becomes

$$\eta_I = \frac{1}{a_c^2}\left[\left(a_p + a_c\right)^2 - \frac{3}{2}\, a_c \left(a_p + a_c\right) + \frac{a_c^3}{2}\left(\frac{1}{a_p + a_c}\right)\right] \tag{11-5b}$$

For the case of $a_p/a_c \ll 1$, the above expression reduces to

$$\eta_I = \frac{3}{2}\left(\frac{a_p}{a_c}\right)^2 \tag{11-6}$$

The interception capture efficiency η_I is normally used as a means to assess other modes of capture. For the case of flows with high Reynolds number, the capture efficiency due to a spherical collector is given by Weber and Paddock (1983) as

$$\eta_I = \frac{3}{2}\left(\frac{a_p}{a_c}\right)^2\left[1 + \frac{\left(\frac{3}{8}\right) Re}{1 + 0.367\ Re^{0.56}}\right] \qquad 0 < Re \leq 150 \tag{11-7}$$

where $Re = U_\infty\, a_c\, \rho/\mu$.

For the case of creeping flow in a packed bed of spherical collectors, the single collector efficiency is modified as

$$\eta_I = \frac{3}{2}\left(\frac{a_p}{a_c}\right)^2 A_{sph} \tag{11-8}$$

where A_{sph} is a dimensionless parameter that expresses the modification of the stream function due to the presence of other collector particles (Spielman, 1977; Neale and Masliyah, 1975). This type of approach has been quite successful in the modelling of capture by pure interception and under colloidal forces in a packed bed or a filter mat. For Happel's cell model simulating flow through a packed bed of spheres, the dimensionless function A_{sph} is given by

$$A_{sph} = \frac{2\left(1 - \alpha_c^{5/3}\right)}{2 - 3\alpha_c^{1/3} + 3\alpha_c^{5/3} - 2\alpha_c^2} \tag{11-9}$$

where α_c is the collector volume fraction. Note when $\alpha_c \to 0$, A_{sph} becomes unity.

The collection efficiency for a single collector can be applied to evaluate the decrease in the particle number concentration through a packed bed or a filter mat. Assume a packed bed having n_c spherical collectors per unit volume of the bed. Consider an element of thickness dx within the packed bed. A particle number balance on the differential thickness dx provides

$$\left[U_\infty n A_b\right] - \left[U_\infty n A_b + U_\infty A_b \frac{dn}{dx}\,dx\right] - \left(n_c A_b dx\right)\left(\pi a_c^2 U_\infty n\right)\eta = 0 \tag{11-10}$$

where U_∞ is the fluid velocity away from the collector surface
A_b is the bed cross-sectional area and
n is the particle number concentration at distance x along the bed.

The differential element is shown in Figure 11-3. The above balance equation reduces to

$$\frac{dn}{dx} = -\pi a_c^2 n_c \eta n \tag{11-11}$$

The number of collectors per unit volume, n_c, is given by

$$n_c = \frac{\alpha_c}{\frac{4\pi}{3} a_c^3} \tag{11-12}$$

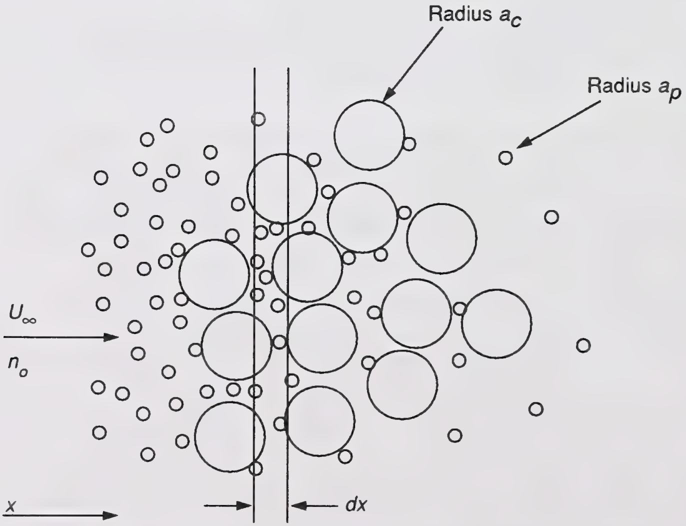

Figure 11-3. Particle deposition in a packed bed of spherical particles.

Combining Eqs. (11-11) and (11-12) leads to

$$\frac{dn}{dx} = -\left[\frac{3\alpha_c\eta}{4a_c}\right] n \tag{11-13}$$

A filter coefficient is normally defined as

$$\lambda = \frac{3\alpha_c\eta}{4a_c} \tag{11-14}$$

Making use of the filter coefficient definition, we obtain

$$\frac{dn}{dx} = -\lambda n \tag{11-15}$$

For an incoming suspended particle number concentration of n_o (at $x = 0$), Eq. (11-15) can be integrated to give

$$n = n_o \exp(-\lambda x) \tag{11-16}$$

Eq. (11-16) indicates that the decay in the number concentration is exponential and that the filter coefficient λ can be considered as a characteristic penetration depth. The collision efficient η can be determined for cases other than pure interception as will be shown in later sections.

11.2.3 Inertial Deposition

When suspended non-interacting particles do not follow the flow streamlines due to their inertia, their capture by a collector is termed inertial deposition. For particles of less than 10 μm in liquids, inertial deposition is not important. However, inertial deposition in gases can be very significant (Friedlander, 1977). Figure 11-4 shows inertial deposition of a spherical particle onto a cylindrical collector.

Newton's second law can be used to write a force balance for a particle in a flow field. It is given as

$$m_p \frac{d^2\vec{x}}{dt^2} = 6\pi\mu a_p \left(\vec{u} - \frac{d\vec{x}}{dt}\right) \tag{11-17}$$

where m_p is the mass of the particle for $\rho_p \gg \rho$.

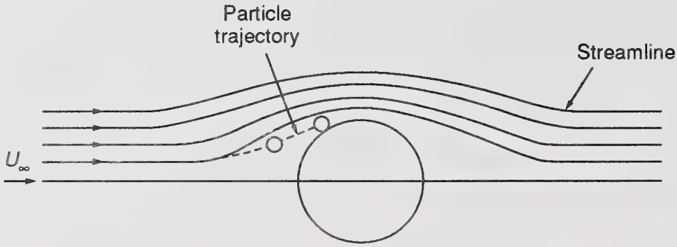

Figure 11-4. Inertial impaction of a spherical particle on a cylindrical fibre.

The term on the left side of Eq. (11-17) is the particle acceleration; the term on the right side is the drag on the particle. Here Stokes drag is used because the particle Reynolds number is assumed to be small. The term $\vec{u}$ is the fluid velocity vector and $\vec{x}$ is the particle position vector. Procedures to solve Eq. (11-17) are given by Michael and Norey (1969), Griffin and Meisen (1973), and Masliyah and Duff (1975).

Dimensionalization of Eq. (11-17) leads to

$$St \frac{d^2\vec{X}}{d\tau^2} = \vec{u}^* - \frac{d\vec{X}}{d\tau} \tag{11-18}$$

where

$$\tau = \frac{t}{\left(\frac{a_c}{U_\infty}\right)} \tag{11-19a}$$

$$\vec{X} = \frac{\vec{x}}{a_c} \tag{11-19b}$$

$$\vec{u}^* = \frac{\vec{u}}{U_\infty} \tag{11-19c}$$

and

$$St = \frac{2}{9}\left(\frac{a_p}{a_c}\right)^2 \left(\frac{\rho_p}{\rho}\right)\left(\frac{\rho\, a_c\, U_\infty}{\mu}\right) \tag{11-19d}$$

Here ρ and ρ_p are the fluid and particle densities, respectively. *St* is the Stokes number which is a measure of the particle inertia with respect to viscous forces. Variation of the collection efficiency η with the Stokes number is shown in Figure 11-5. The flow field used is that of a potential flow over a sphere given by

$$\psi = \frac{1}{2} U_\infty r^2 \left[1 - \left(\frac{a_c}{r} \right)^3 \right] \sin^2\theta$$

The collection efficiency increases with increasing Stokes number where the particle inertia becomes important.

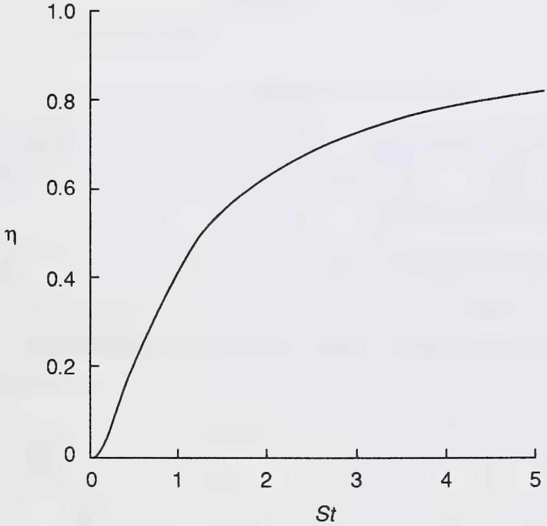

Figure 11-5. Efficiency due to inertial capture by a spherical collector using potential flow velocity (Michael and Norey, 1969) (reprinted by permission of Cambridge University Press).

In a colloidal system, capture can occur due to the combination of Brownian motion, hydrodynamic interaction, and the presence of interparticle forces such as the London–van der Waals and electrostatic forces. In this chapter we shall deal with both the Lagrangian and the Eulerian approaches taking into consideration the hydrodynamic and interparticle forces.

11.3 EULERIAN APPROACH

The generalized convection-diffusion equation which governs particle transfer due to a flow field characterized by a velocity vector $\vec{u}$ is given by

$$\frac{\partial n}{\partial t} + \vec{\nabla} \cdot \vec{j} = Q \tag{11-20}$$

where

$$\vec{j} = \vec{v}n - \underline{\underline{D}} \cdot \vec{\nabla} n + \frac{n}{kT} \underline{\underline{D}} \cdot \vec{F} \tag{11-21}$$

where $\vec{j}$ is the flux of the particles (particles per unit time and unit area)

n is the local particle number concentration

$\underline{\underline{D}}$ is the diffusion coefficient tensor

$\vec{F}$ is the force experienced by the particle

$\vec{v}$ is the particle hydrodynamic velocity, *i.e.*, the particle velocity that is induced by the fluid motion

T is the absolute temperature

k is the Boltzmann constant and

Q is a source term.

For a particle of a finite size, the hydrodynamic particle velocity is not equal to the fluid velocity. For a point particle size, however, *i.e.*, an ion, one can equate $\vec{v}$ with the fluid velocity $\vec{u}$.

The reason for the introduction of the diffusion coefficient tensor rather than simply using a scalar quantity is that the particle diffusion coefficient is a function of the particle position relative to a surface. This was illustrated by Honig *et al.* (1971) expression for the diffusion coefficient variation with gap width between two spherical particles. For the case of a spherical particle (1) diffusing near another spherical particle (2), one can write the diffusion coefficient tensor (van de Ven, 1989) as

$$\underline{\underline{D}} = (D_1 + D_2)_\infty \begin{pmatrix} d_{\parallel} & 0 \\ 0 & d_{\perp} \end{pmatrix} \tag{11-22}$$

where $(D_1 + D_2)_\infty$ is the diffusion coefficient of the diffusing spherical particles in an infinite medium given by the Stokes–Einstein equation. The terms $d_{\parallel}$ and $d_{\perp}$ are correction factors due to the finite gap width between the two spheres. They are both functions of the ratio of the spheres radii and the separation gap width. $d_{\|}$ refers to correction parallel to the surfaces and $d_{\perp}$ refers to correction normal to the surfaces of the spheres, *i.e.*, along the line connecting the centres of the spheres. For the case of equal-sized spheres, $d_{\perp} = 1/G(h)$ as was given by Eq. (10-51). For the case of a spherical colloidal particle of radius a and a very large sphere, *i.e.*, a flat surface, Eq. (11-22) becomes

$$\underline{\underline{D}} = D_{\infty} \begin{pmatrix} d_{\|} & 0 \\ 0 & d_{\perp} \end{pmatrix} \tag{11-23}$$

It should be noted, however, that $d_{\|}$ and $d_{\perp}$ of Eq. (11-23) are different from those of Eq. (11-22) because $d_{\|}$ and $d_{\perp}$ are functions of the spheres radii. Both $d_{\|}$ and $d_{\perp}$ approach zero as the gap width $h \rightarrow 0$. For small h

$$d_{\perp} = 2h \qquad \text{for } a_1 = a_2$$

and

$$d_{\perp} = h \qquad \text{for } a_2 \rightarrow \infty$$

$d_{\|}$ is proportional to $1/ln\ h$. As the dimensionless gap width becomes large, $d_{\|} \rightarrow 1$ and $d_{\perp} \rightarrow 1$ (van de Ven, 1989; Batchelor, 1976; Happel and Brenner, 1965).

The velocity of the fluid $\vec{u}$ is usually evaluated from the solution of the Navier–Stokes equation in the absence of the dispersed particles. To this end, the analysis becomes limited to a very dilute dispersed phase. The required hydrodynamic velocity of the particle $\vec{v}$ is related to the fluid velocity $\vec{u}$ by making corrections due to the presence of the collector surface.

For a given problem, the forces and the flow configuration are first identified. The flux $\vec{j}$ is determined and solution to Eq. (11-20) is then obtained. Various situations will be presented to illustrate the use of the Eulerian approach.

11.3.1 Deposition Due to Brownian Diffusion Without External Forces: Spherical Collector

Here we shall deal with the classical case of deposition onto a spherical collector due to Brownian diffusion alone in the absence of any other forces. The diffusing particles are considered to be of submicron size with their hydrodynamic velocity identical to the fluid velocity. With the radius a_p being very small point particles, the colloidal forces are taken to be zero and the diffusion coefficient is constant. For steady-state conditions, with $Q = \vec{F} = 0$ and for a constant diffusion coefficient, combining Eqs. (11-20) and (11-21) leads to

$$\vec{\nabla} \cdot \left[n\vec{u} - D_{\infty}\vec{\nabla} n \right] = 0 \tag{11-24}$$

Recognizing that $\vec{\nabla} \cdot \vec{u} = 0$ for an incompressible fluid, the above equation becomes

$$\vec{u} \cdot \vec{\nabla} n - D_\infty \nabla^2 n = 0 \tag{11-25}$$

Eq. (11-25) in spherical coordinates becomes

$$u_r \frac{\partial n}{\partial r} + \frac{u_\theta}{r} \frac{\partial n}{\partial \theta} = D_\infty \left[\frac{1}{r^2} \frac{\partial}{\partial r} \left(r^2 \frac{\partial n}{\partial r} \right) + \frac{1}{r^2 \sin\theta} \frac{\partial}{\partial \theta} \left(\sin\theta \frac{\partial n}{\partial \theta} \right) \right] \tag{11-26}$$

For Stokes flow about an isolated sphere (in the limit of a very small Reynolds number), the flow velocities in the radial and angular-directions are given by Bird *et al.* (1960) as:

$$u_r = -U_\infty \cos\theta \left[1 - \frac{3}{2} \frac{a_c}{r} + \frac{1}{2} \frac{a_c^3}{r^3} \right] \tag{11-27a}$$

and

$$u_\theta = U_\infty \sin\theta \left[1 - \frac{3}{4} \frac{a_c}{r} - \frac{1}{4} \frac{a_c^3}{r^3} \right] \tag{11-27b}$$

For large Peclet numbers, the variation in the concentration is much higher in the r-direction than that in the θ-direction and one can rewrite Eq. (11-26) as

$$u_r \frac{\partial n}{\partial r} + \frac{u_\theta}{r} \frac{\partial n}{\partial \theta} = D_\infty \left[\frac{\partial^2 n}{\partial r^2} + \frac{2}{r} \frac{\partial n}{\partial r} \right] \tag{11-28}$$

The flow and the coordinate system is shown in Figure 11-6. Assuming a perfect sink at the spherical collector surface, the boundary conditions become

(11-29a) symmetry at $\theta = 0, \pi$ for all r

(11-29b) $n = 0$ at $r = a_c$ for all θ

and

(11-29c) $n \rightarrow n_\infty$ at $r \rightarrow \infty$ for all θ

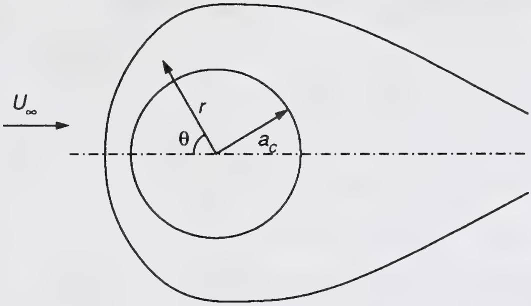

Figure 11-6. Diffusion boundary layer about a spherical particle collector.

Here n_∞ is the bulk value of n at a large distance from the spherical collector. A solution to Eq. (11-28) is given by Masliyah and Epstein (1973) and other solutions are cited by Clift *et al.* (1978). However, simplification in the solution can be made by assuming that the diffusion process is limited to a region very close to the surface and hence the velocity profile needs to be true only close to the spherical collector. Consequently, the velocity components are approximated by

$$\text{(11-30a)} \quad u_r = -\frac{3}{2}\left(\frac{y}{a_c}\right)^2 U_\infty \cos\theta$$

and

$$\text{(11-30b)} \quad u_\theta = \frac{3}{2}\left(\frac{y}{a_c}\right) U_\infty \sin\theta$$

where

$$\text{(11-30c)} \quad \frac{r}{a_c} = 1 + \frac{y}{a_c}$$

The above velocity expressions are valid close to the collector surface. Levich (1962) obtained a similar solution to Eqs. (11-28) to (11-30). At the collector surface, the flux $j_\perp$ is given by

$$\text{(11-31a)} \quad -j_\perp = j_r = -D \left.\frac{\partial n}{\partial r}\right)_{\text{surface}} \quad , \text{m}^{-2}\text{s}^{-1}$$

and the total rate of particles diffusing to the surface is given by

$$(11\text{-}31b)\quad \int_S j_\perp \, dS = 2\pi a_c^2 \int_o^\pi j_\perp \sin\theta \; d\theta$$

where $j_\perp$ is the flux normal to the collector surface and

S is the spherical collector surface area.

The local Sherwood number characterizing the mass transfer is given as

$$(11\text{-}32a)\quad Sh(\theta) = \frac{a_c j_\perp}{D_\infty n_\infty}$$

where n_∞ is the particles (molecules) number concentration at a large distance from the surface of the spherical collector. The average Sherwood number is defined as

$$(11\text{-}32b)\quad Sh = \frac{1}{S} \int_S Sh(\theta) \; dS$$

The solution of Eq. (11-28) with the velocities defined by Eq. (11-30) subject to the boundary conditions of Eq. (11-29) provides the dimensionless mass transfer number:

$$(11\text{-}33)\quad Sh = 0.624\,(Sc\,Re)^{1/3} \qquad \text{for } Sc\,Re \gg 1$$

where the Schmidt number (ratio of momentum transfer to molecular diffusion) is given by

$$(11\text{-}34a)\quad Sc = \frac{(\mu/\rho)}{D_\infty}$$

and the Reynolds number (ratio of inertial to viscous forces) is given by

$$(11\text{-}34b)\quad Re = a_c \rho \, U_\infty/\mu$$

Eq. (11-33) is usually referred to as the Lighthill–Levich or simply the Levich equation. The product of Sc and Re is normally called the Peclet number and it is given by

$$(11\text{-}34c)\quad Pe = Sc\,Re = \frac{a_c\,U_\infty}{D_\infty}$$

Acrivos and Goddard (1965) give a first-order correction to Eq. (11-33) as

$$Sh = 0.624\,(Sc\,Re)^{1/3} + 0.46 \qquad Pe \gg 1 \tag{11-35}$$

For the case of small Peclet numbers, solution of the complete convection-diffusion equation for the case of creeping flow is given by Acrivos and Taylor (1962) as

$$Sh = 1 + \frac{Pe}{2} \qquad Pe \ll 1 \tag{11-36}$$

Eqs. (11-33), (11-35), and (11-36) were derived using creeping flow velocities ($Re \to 0$) about the spherical collector and the equations are identical to those given for classical mass transfer from spheres.

11.3.2 Deposition Due to Brownian Diffusion With External Forces: Stagnation Flow

Convenient techniques that are often used in experimental and theoretical studies for deposition of colloidal particles are those of rotating disks (Marshall and Kitchener, 1966; Hull and Kitchener, 1969; Prieve and Lin, 1980) and of stagnation flows due to impinging jets (Dabros and van de Ven, 1983; Boluk and van de Ven, 1989; Adamczyk *et al.*, 1989). Other geometries are discussed by Adamczyk (1989a,b).

In the previous section, diffusion due to Brownian motion was considered with the diffusing particles taken as "point" particles. In this section we shall discuss in detail the Eulerian approach to the study of finite size particle deposition in a stagnation flow due to an impinging jet. We shall take into account the relationship between the fluid and particle velocities, a variable diffusion coefficient, and interparticle forces.

Consider a fluid containing colloidal particles impinging on a flat plate as shown in Figure 11-7. Due to the axisymmetry of the flow, the velocity components in the angular direction are zero and the velocity field is given by the radial and the normal components, namely u_r and u_z, respectively. As the Schmidt number of the colloidal system exceeds unity by one or two orders of magnitude, the diffusion boundary layer is much thinner than the hydrodynamic boundary layer. It is for this reason that the flow velocities need to be characterized close to the impingement region only. For flow near the stagnation region, the velocities of the fluid are given by

$$u_r = \alpha z r \tag{11-37}$$

and

$$u_z = -\alpha z^2 \tag{11-38}$$

The parameter α characterizes the intensity of the flow (Dabros and van de Ven, 1983). Here it is assumed that the presence of the particles does not alter the flow field.

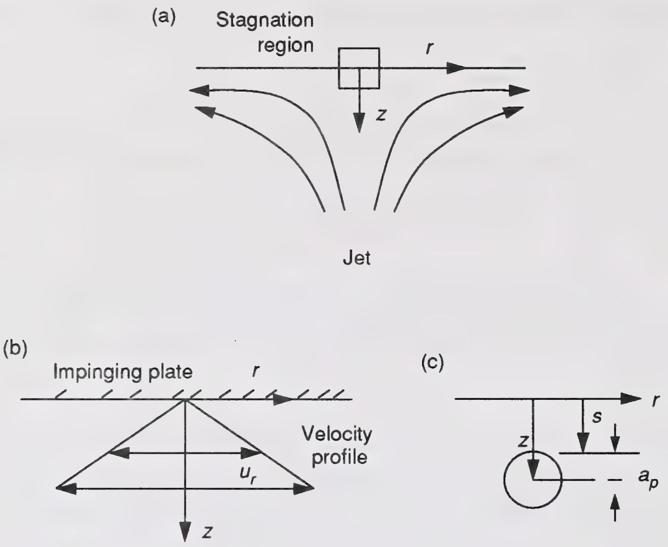

(a) overall flow geometry
(b) velocity profile at the stagnation region shown by the box in (a)
(c) position of a colloidal particle with respect to the impinging surface

Figure 11-7. Impinging jet geometry.

The movement of a particle entrained in the stagnation region of the flow is decomposed into normal (z-direction) and tangential (r-direction) components. The colloidal particle Reynolds number is assumed to be small enough that Stokes flow holds. Eq. (11-21) can be written as

$$(11\text{-}39) \quad j_r = v_r n - \left(D_{rr}\frac{\partial n}{\partial r} + D_{rz}\frac{\partial n}{\partial z}\right) + \frac{n}{kT}\left[D_{rr}F_r + D_{rz}F_z\right]$$

and

$$(11\text{-}40) \quad j_z = v_z n - \left(D_{zr}\frac{\partial n}{\partial r} + D_{zz}\frac{\partial n}{\partial z}\right) + \frac{n}{kT}\left[D_{zr}F_r + D_{zz}F_z\right]$$

The definition of a dot product of a tensor $\underline{\underline{T}}$ with a vector $\vec{A}$ is given below.◆

Recognizing from Eq. (11-22) that $D_{zr} = D_{rz} = 0$, we can write

$$j_r = v_r n - D_{rr}\frac{\partial n}{\partial r} + \frac{n}{kT} D_{rr} F_r \tag{11-41}$$

and

$$j_z = v_z n - D_{zz}\frac{\partial n}{\partial z} + \frac{n}{kT} D_{zz} F_z \tag{11-42}$$

where j_r and j_z are the fluxes in r- and z-directions, respectively.

Following Spielman and Fitzpatrick (1973), the relationships between the fluid and particle velocities and the local particle diffusion coefficients are given by

$$v_r = u_r f_3(h) \tag{11-43a}$$

$$v_z = u_z f_1(h) f_2(h) \tag{11-43b}$$

$$D_{rr} = D_\infty d_{||} = D_\infty f_4(h) \tag{11-43c}$$

and

$$D_{zz} = D_\infty d_\perp = D_\infty f_1(h) \tag{11-43d}$$

where f_1 to f_4 are the hydrodynamic universal (correction) functions relating the deviation from Stokes flow and the Stokes–Einstein relationship due to the presence of the collector wall. f_1 is given by Brenner (1961), f_2 is given by Goren (1970) and Goren and O'Neill (1971), and f_3 and f_4 are given by Goldman *et al.* (1967a,b). Asymptotic behaviours of f are listed in Table 11-1. Curve-fit expressions for f are given in Table 11-2. Figure 11-8 shows the variation of the functions with the dimensionless gap h, where

$$\frac{z}{a_p} = h + 1 \tag{11-44}$$

◆ The dot product of a tensor $\underline{\underline{T}}$ with a vector $\vec{A}$ is given by

$$\begin{aligned}\underline{\underline{T}} \cdot \vec{A} &= (T_{xx}A_x + T_{xy}A_y + T_{xz}A_z)\,\vec{i}_x \\ &+ (T_{yx}A_x + T_{yy}A_y + T_{yz}A_z)\,\vec{i}_y \\ &+ (T_{zx}A_x + T_{zy}A_y + T_{zz}A_z)\,\vec{i}_z\end{aligned}$$

Table 11-1. Asymptotic expressions for the universal hydrodynamic functions for a spherical particle near a flat solid surface (Spielman and Fitzpatrick, 1973)

Function	$h \to 0$	$h \to \infty$
$f_1(h)$	h	$1 - \frac{9}{8(h+1)}$
$f_2(h)$	3.23	$\left[1 - \frac{9}{8(h+1)}\right]^{-1}$
$f_3(h)$	$\frac{0.7431}{0.63736 - 0.2 \ln h}$	$1 - \frac{5}{16(h+1)^{-3}}$

Table 11-2. Curve fit for the universal functions f_i

i	a	b	c	d	e
1	0.92667	−0.3990	0.14869	−0.6010	1.2015
2	0.56954	1.362	1.3596	0.8764	0.5250
3	0.150	−0.3752	3.906	−0.625	3.105
4	1.2643	−1.23122	0.2734	0.8189	0.1750

$$f_i = 1.0 + b_i \exp(-c_i h) + d_i \exp(-e_i h^{a_i})$$

It should be noted that the correction factors f_1 to f_4 and $d_{\|}$ and $d_{\perp}$ are for the geometry of a sphere and a solid plane as applicable to the problem at hand.

Making use of Eq. (11-43), the flux Eqs. (11-41) and (11-42) become

$$j_r = u_r f_3 n - D_\infty f_4 \frac{\partial n}{\partial r} + \frac{n}{kT} D_\infty f_4 F_r \tag{11-45}$$

and

$$j_z = u_z f_1 f_2 n - D_\infty f_1 \frac{\partial n}{\partial z} + \frac{n D_\infty}{kT} f_1 F_z \tag{11-46}$$

where D_∞ is given by the Stokes–Einstein equation.

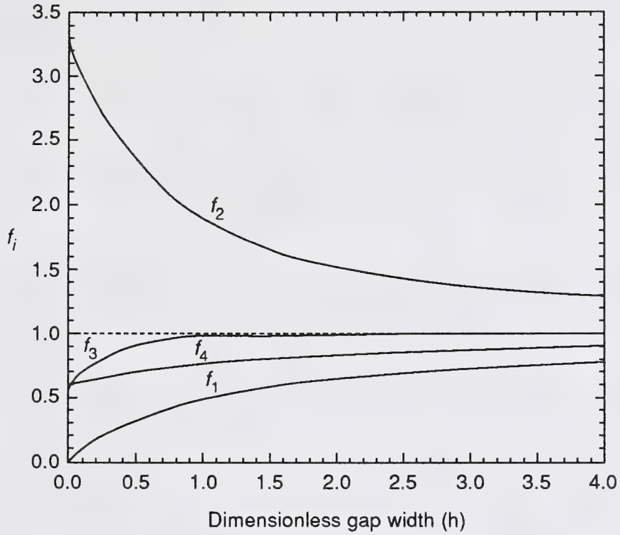

Figure 11-8. Universal hydrodynamic correction factors for diffusion and particle motion near a plane for the case of a sphere.

The z-direction component of the force F_z is composed of gravitational force, London–van der Waals force, and electrostatic (electric double-layer) force. F_z is given by

$$F_z = F_{gz} + F_A + F_R \tag{11-47}$$

Here it is assumed that the colloidal forces act normal to the surface of the collector. The r-direction component of the force is that due to gravity alone:

$$F_r = F_{gr} \tag{11-48}$$

For a horizontal deposition plate, F_r is zero.

For steady-state conditions and a zero source term, Eq. (11-20) in cylindrical coordinates becomes

$$\frac{1}{r}\frac{\partial}{\partial r}\left(rj_r\right) + \frac{\partial j_z}{\partial z} = 0 \tag{11-49}$$

From Eqs. (11-45) and (11-46), the flux conservation Eq. (11-20) becomes

$$(11\text{-}50)\quad \frac{1}{r}\frac{\partial}{\partial r}\left[\left(u_r f_3 n - D_\infty f_4 \frac{\partial n}{\partial r} + \frac{n}{kT} D_\infty f_4 F_r\right) r\right] + \frac{\partial}{\partial z}\left[u_z f_1 f_2 n - D_\infty f_1 \frac{\partial n}{\partial z} + \frac{n}{kT} D_\infty f_1 F_z\right] = 0$$

Eq. (11-50) is the convection-diffusion equation for the transport process in the presence of external forces. This equation was derived for a stagnation flow configuration and is also applicable to other axisymmetric deposition configurations such as a rotating disc.

The elements that make up the forces F_r and F_z are discussed below.

The gravitational force is given by

$$(11\text{-}51a)\quad F_{gr} = \frac{4\pi}{3} a_p^3\, \Delta\rho g \sin\theta$$

and

$$(11\text{-}51b)\quad F_{gz} = \frac{4\pi}{3} a_p^3\, \Delta\rho g \cos\theta$$

where $\Delta\rho$ is the density difference between the particle and the fluid. The inclination angle θ is between the z-axis and the vertical.

Retarded London–van der Waals dispersion force (Suzuki *et al.*, 1969) between a sphere and a plane is given by

$$(11\text{-}52)\quad F_A = -\frac{\bar{\lambda}\left(\bar{\lambda} + 22.232\, h\right) A}{6\, h^2 \left(\bar{\lambda} + 11.116\, h\right)^2 a_p}$$

where $\bar{\lambda} = \lambda/a_p$ is a dimensionless parameter accounting for retardation with λ being the London wavelength usually taken as 10^{-7} m (100 nm). A is the Hamaker constant ($\equiv A_{123}$).

The electric double-layer force expression is given by Hogg *et al.* (1966) as

$$(11\text{-}53)\quad F_R = 4\pi\varepsilon\varepsilon_o \kappa a_p \zeta_p \zeta_c \left[\frac{\exp\left(-\kappa a_p h\right)}{1 \pm \exp\left(-\kappa a_p h\right)} \mp \frac{\left(\zeta_c - \zeta_p\right)^2}{2\,\zeta_c \zeta_p} \cdot \frac{\exp\left(-2\,\kappa a_p h\right)}{\left\{1 - \exp\left(-2\,\kappa a_p h\right)\right\}}\right]$$

The upper and lower signs in Eq. (11-53) correspond to constant surface potential and constant surface charge, respectively.

The following dimensionless groups are defined as:

$$\text{Gravitational parameter} = \frac{\text{gravitational force}}{\text{Brownian motion force}} = Gr$$

$$(11\text{-}54a) \quad Gr = \frac{2}{9}\frac{\Delta\rho g a_p^3}{\mu D_\infty}$$

$$\text{Double-layer parameter} = \frac{\text{electrostatic force}}{\text{Brownian motion force}} = Dl$$

$$(11\text{-}54b) \quad Dl = \frac{4\pi\,\varepsilon\varepsilon_o\, a_p\, \zeta_p\, \zeta_c}{kT}$$

A second double-layer parameter *Da* is defined as

$$(11\text{-}54c) \quad Da = \frac{\left(\zeta_c - \zeta_p\right)^2}{2\,\zeta_c\,\zeta_p}$$

Da parameter accounts for the asymmetry of the electric double layers. For $\zeta_p = \zeta_c$, *Da* becomes zero.

Normalizing the forces by (kT/a_p), neglecting radial derivatives, and setting $\theta = 0$, Eq. (11-50) becomes

$$(11\text{-}55) \quad \frac{d}{dh}\left[\frac{1}{2}Pe f_1 f_2 n\,(1+h)^2 + f_1\frac{dn}{dh} - n f_1 F_z^*\right] - Pe f_3\,(1+h)\,n = 0$$

where

$$(11\text{-}56) \quad F_z^* = -Ad\,\frac{\bar{\lambda}\left(\bar{\lambda} + 22.232\,h\right)}{h^2\left(\bar{\lambda} + 11.116\,h\right)^2}$$

$$+ (Dl)\left(\kappa a_p\right)\left[\frac{\exp\left(-\kappa a_p h\right)}{1 \pm \exp\left(-\kappa a_p h\right)} \mp Da\left\{\frac{\exp\left(-2\kappa a_p h\right)}{1 - \exp\left(-2\kappa a_p h\right)}\right\}\right] + Gr$$

where

$$Pe = \frac{2\,a_p^3\,\alpha}{D_\infty} \tag{11-57}$$

and

$$Ad = \frac{A}{6\,kT} \tag{11-58}$$

Ad is a measure of the relative strengths of London–van der Waals force to the Brownian motion force. It is usually referred to as the adhesion number or parameter. The parameters that influence particle deposition on smooth surfaces are κa, $\overline{\lambda}$, *Ad, Dl, Da, Gr,* and *Pe.*

Although the above analysis was derived for stagnation flow, it is valid for any flow configuration having velocities of the form given by Eqs. (11-37) and (11-38). Therefore by using an appropriate *Pe* definition, the analysis for the various flow geometries become similar. For the case of an impinging jet, the flow strength α is given by

$$\alpha = \overline{\alpha}\,(Re)\,\frac{Re\,\upsilon}{R_{jet}^3}$$

where $\overline{\alpha}\,(Re) = \beta\,Re^{1/2}$, and β is of order unity (Dabros and van de Ven, 1987). R_{jet} is the jet tube radius and υ is the kinetic viscosity. The Reynolds number *Re* is given by

$$Re = \frac{U_\infty R_{jet}}{\upsilon} \tag{11-59}$$

where U_∞ is the average exit velocity of the jet. Various definitions of Peclet number for other geometries are given by van de Ven (1989).

The boundary conditions of Eq. (11-55) are

$$n \longrightarrow n_\infty \qquad \text{at} \quad h \longrightarrow \infty \tag{11-60a}$$

and

$$n \longrightarrow 0 \qquad \text{at} \quad h = \delta_m / a_p \tag{11-60b}$$

where δ_m is identified with the distance of the primary energy minimum. The solution of Eq. (11-55) subject to Eq. (11-60) can be expected to yield an upper limit to the flux towards the collector for a given energy of interaction between the particle and surface and for given hydrodynamic conditions (Dabros and van de Ven, 1983,1987). The boundary condition (Eq. (11-60b)) assumes that all particles arriving close to the collector surface are irreversibly captured in an infinite-depth energy sink and disappear from the system (Adamczyk, 1989a). In most studies δ_m/a_p is taken as zero or as a fixed small value, say 10^{-3} (Prieve and Lin, 1980).

The local Sherwood number is defined as

$$Sh_l = -j_{zw} \frac{a_p}{D_\infty n_\infty} = j_\perp \frac{a_p}{D_\infty n_\infty} \tag{11-61a}$$

where j_{zw} is the flux in the z-direction at the surface of the collector (*i.e.*, at $z = a + \delta_m$). The average Sherwood number is given by

$$Sh = \frac{1}{S} \int_s Sh_l \, dS \tag{11-61b}$$

where Sh is the average Sherwood number and S is the deposition surface area. j_{zw} is evaluated using Eq. (11-46) once the distribution of n is known. Numerical techniques are normally employed in solving Eq. (11-55), thus providing the variation of n with h.

Transport equations similar to Eq. (11-55) are given by Prieve and Ruckenstein (1974) for the case of a spherical collector; Prieve and Lin (1980), Rajagopalan and Kim (1981), and Clint *et al.* (1973) for the case of a rotating disc; Dabros and van de Ven (1983,1987) and Boluk and van de Ven (1989) for the case of an impinging jet; Adamczyk and van de Ven (1981a) for the case of parallel plates channel; and Adamczyk and van de Ven (1981b) for the case of cylindrical collectors. General discussions on the kinetics of particle accumulation on collectors is given by Adamczyk *et al.* (1984), Adamczyk and van de Ven (1984), and Adamczyk *et al.* (1992).

Solutions of the transport equations such as Eq. (11-55) provide values for the Sherwood number Sh and a knowledge of how the various parameters, *e.g.*, Pe, Dl, Da, and Ad affect mass transport.

In this section, detailed analysis was given for the impinging jet geometry. Mass transfer analysis, *i.e.*, particle deposition for other geometries, is very similar. The effect of the various parameters on the dimensionless mass transfer Sh will be given below. Table 11-3 gives the definitions of the Reynolds, Peclet, and Sherwood numbers for the various geometries. van de Ven (1989) provides tabulation of the velocity components near the surface of the various geometries.

For the case of Brownian particles with negligible London–van der Waals and electric double-layer forces, the stagnation flow Sherwood number is given by Levich's type equation as

$$Sh = 0.616\, Pe^{1/3} \tag{11-62}$$

with $Pe \gg 1$ and $Dl = Ad = Gr = 0$.

Table 11-3. Definition of Reynolds, Peclet, and Sherwood numbers for various deposition geometries

Collector geometry	Reynolds number	Peclet number	Sherwood number
Spherical collector	$\frac{a_c \rho U_\infty}{\mu}$	$\frac{a_c U_\infty}{D_\infty}$	$\frac{1}{S}\int_S \left(\frac{a_c j_\perp}{D_\infty n_\infty}\right) dS$
Cylindrical collector	$\frac{a_c \rho U_\infty}{\mu}$	$\frac{a_c U_\infty}{D_\infty}$	$\frac{1}{S}\int_S \left(\frac{a_c j_\perp}{D_\infty n_\infty}\right) dS$
Impinging jet	$\frac{U_\infty R_{jet} \rho}{\mu}$	$\frac{2 a_p^3 \alpha}{D_\infty}$	$\frac{1}{S}\int_S \left(\frac{a_p j_\perp}{D_\infty n_\infty}\right) dS$
Rotating disc	$a_p^3 \left(\frac{\omega}{\upsilon}\right)^{3/2}$	$\frac{1.02\, \omega^{3/2} a_p^3}{\upsilon^{1/2} D_\infty}$	$\frac{1}{S}\int_S \left(\frac{a_p j_\perp}{D_\infty n_\infty}\right) dS$

Pe and *Sh* are defined by Eqs. (11-57) and (11-61b), respectively. Sherwood number variation is similar to that obtained for mass transfer of point particles towards a spherical collector as given by Eq. (11-33).

For a spherical collector, again for negligible external forces, the effect of a finite particle size on the mass transfer (deposition) is shown in Figure 11-9. Here the Sherwood number is given for the transport of particles of finite size to the surface of a spherical collector. The Levich equation, which is valid for $a_p/a_c \rightarrow 0$ and when a diffusion boundary layer exists ($Pe \gg 1$), is plotted for comparison. Deviation from the Levich equation occurs when the diffusion boundary layer thickness is not small compared to the collector radius. This occurs at low values of *Pe*. Also deviation from the Levich equation becomes apparent when the particle size becomes large as compared with the diffusion boundary layer thickness. This situation occurs at high values of *Pe*.

For the case of a spherical collector under no-flow conditions, *i.e.*, $Pe = 0$, the effect of London–van der Waals forces on the Sherwood number is shown in Figure 11-10 for finite sized particles. It is clear from Figure 11-10 that when a_c/a_p becomes large, $Sh \rightarrow 1$ irrespective of the values of A/kT which are a measure of the attractive dispersion force. However, for smaller values of a_c/a_p, the dispersion force has a large influence on the Sherwood number which is a measure of the deposition (Prieve and Ruckenstein, 1974). The limit of $Sh \rightarrow 1$ as $Pe \rightarrow 0$ is that of pure diffusion of infinitesimal particles.

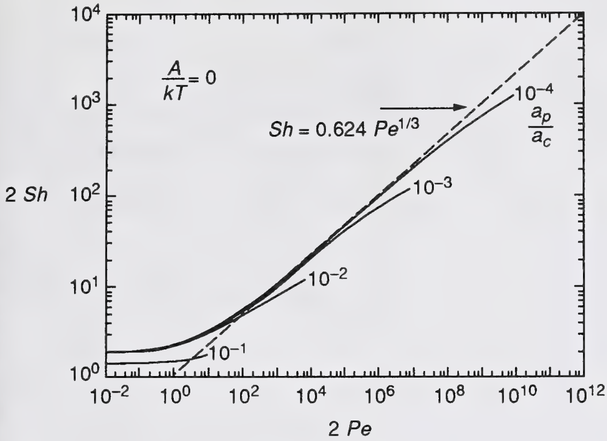

Figure 11-9. Sherwood numbers computed for the convection-diffusion of particles of finite size to the surface of a spherical collector by neglecting interaction forces. The dashed line is for the Levich equation which is valid when a diffusion boundary layer exists and the particles are infinitesimal (Prieve and Ruckenstein, 1974).

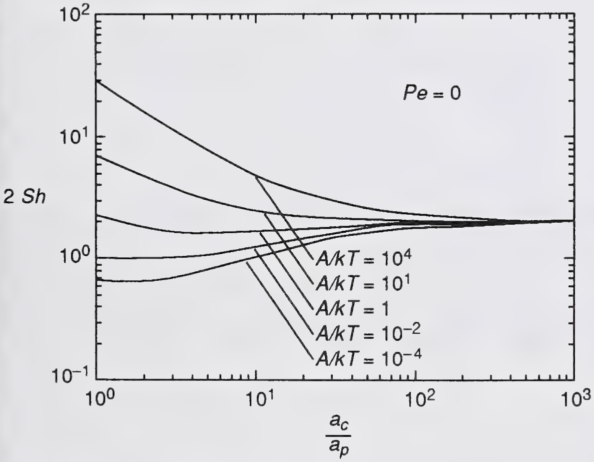

Figure 11-10. Sherwood numbers for the transport of finite sized particles through a stagnant fluid to a spherical collector under the action of diffusion and dispersion forces (Prieve and Ruckenstein, 1974).

Again, for the case of a spherical collector, the effect of the London–van der Waals forces on the deposition in the absence of other forces was studied by Prieve and Ruckenstein (1974). They evaluated the Sherwood number as a function of the Peclet number for different values of a_p/a_c. Figure 11-11 shows the case of $a_p/a_c = 10^{-4}$. The Levich Eq. (11-33) is shown for comparison. At low values of Peclet number, *Sh* becomes insensitive to *A*/*kT*. This is because the deposition is diffusion-controlled. At higher values of *Pe*, the Sherwood number becomes more dependent on *A*/*kT*. This is due to the fact that the diffusion boundary layer becomes very thin and offers little resistance to mass transfer, consequently the dispersion force plays a more important role in the mass transfer process. The reasons for the deviation from the Levich equation at very small and large *Pe* are similar to those advanced for Figure 11-9.

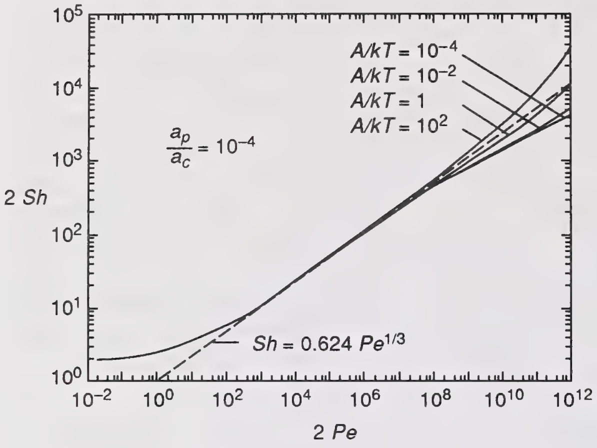

Figure 11-11. Sherwood numbers computed for the transport of finite particles to a spherical collector under the combined diffusion and dispersion forces (Prieve and Ruckenstein, 1974).

Similar plots for the case of a rotating disc are given by Prieve and Lin (1980). For large values of *Pe* and *(A/kT)/Pe*, the deposition Sherwood number in the absence of electrostatic and gravity forces is given by

$$Sh = 0.55\,(A/kT)^{1/3}\,Pe^{2/3}$$

Prieve and Ruckenstein (1974) gave an approximate plot indicating the regions where dispersion or convection-diffusion is rate controlling for the case of a spherical collector. Figure 11-12 identifies the regions in which either London–van der Waals or diffusion may be neglected when calculating the deposition rate. When the diffusion boundary layer is thin, the dispersion forces control the deposition rate. On the other hand,

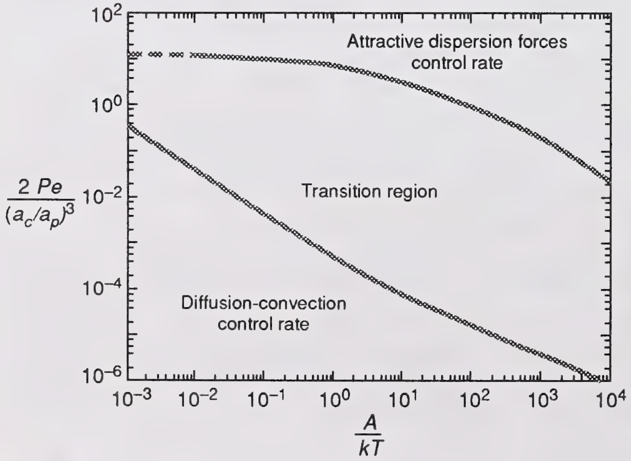

Figure 11-12. Regions of capture mechanism and controlling rate for the case of a spherical collector for $a_c/a_p > 10^3$ in the absence of electrostatic forces (Prieve and Ruckenstein, 1974).

when the diffusion boundary layer is thick, the convection-diffusion process controls the deposition rate.

For a spherical collector, the effect of gravitational forces upon the rate of deposition is shown in Figure 11-13 in the absence of an electric double-layer force. The effect of gravitational force is substantial at lower values of *Pe*.

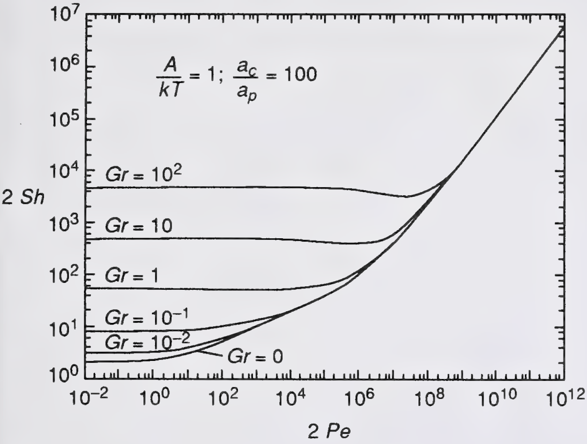

Figure 11-13. Effect of gravitational forces upon the rate of deposition for a given radius ratio for the case of spherical collectors in the absence of electrostatic force (Prieve and Ruckenstein, 1974).

In the limit of $Gr \gg 1$, the rate of particle deposition becomes

$\pi a_c^2 v_t n_\infty$, particles/unit time

where v_t is the Stokes terminal velocity of the particles given by

$$v_t = \frac{2 g \Delta\rho a_p^2}{9\mu} \tag{11-63}$$

The deposition Sherwood number is then given by

$$Sh = \left(\frac{\pi a_c^2 v_t n_\infty}{4\pi a_c^2}\right) \frac{a_c}{D_\infty n_\infty} \tag{11-64}$$

leading to

$$Sh = \frac{1}{4}\left(\frac{a_c}{a_p}\right) Gr \tag{11-65}$$

where the gravitational number is defined by Eq. (11-54a). The flat regions of the curves of Figure 11-13 are given by Eq. (11-65).

For the case of a stagnation flow collector, *e.g.*, an impinging jet, Dabros and van de Ven (1983) gave the variation of Sherwood number with the double-layer parameter *Dl* for various Reynolds numbers *Re*. A negative *Dl* number means that the particle and the collector have opposite signs for their surface (zeta) potentials. It is clear from Figure 11-14 that a critical *Dl* value exists. Beyond the critical *Dl* value the deposition rate is suddenly reduced by several orders of magnitude. By increasing the value of *Dl*, the energy barrier increases and the height of the energy barrier becomes the rate-determining factor. This type of sudden drop in *Sh* with *Dl* is characteristic of all collectors and also of coagulation of colloidal particles (van de Ven, 1989). Figure 11-14 also shows that changing the Reynolds number from 10 to 30 has the effect of increasing *Sh* when deposition occurs, but has an insignificant effect when the deposition rate is small. Other examples for the effect of *Dl* are given by Adamczyk (1989a,b).

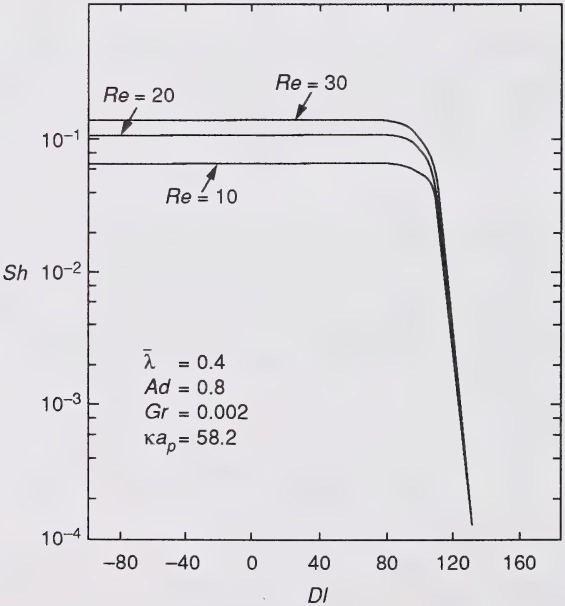

Figure 11-14. Calculated values of the Sherwood number as a function of the double layer parameter *Dl* (Dabros and van de Ven, 1983).

The question of whether adding the individual process rates produces the total effective mass transfer rate was addressed by Prieve and Ruckenstein (1974). They showed that there is good agreement between the exact solution of the transport equation and that obtained from the summation of the individual contributions to the deposition rate from each mechanism. For the case of a spherical collector with $a_c/a_p = 10^4$, and $A/kT = 10^4$ individual contributions due to gravity, Brownian motion (diffusion) and dispersion forces were summed and compared with the exact solution that considers these effects simultaneously. The comparison between the two approaches is shown in Figure 11-15. The open circles are given by the exact solution and the solid line is from the addition of individual contributions. The agreement between the two approaches is fairly good. However, there is no theoretical basis for concluding that the concept of additivity should hold under other physical parameters. It should be recognized that the comparison is made for $A/kT = 10^4$ which gives a rather large vlaue for A.

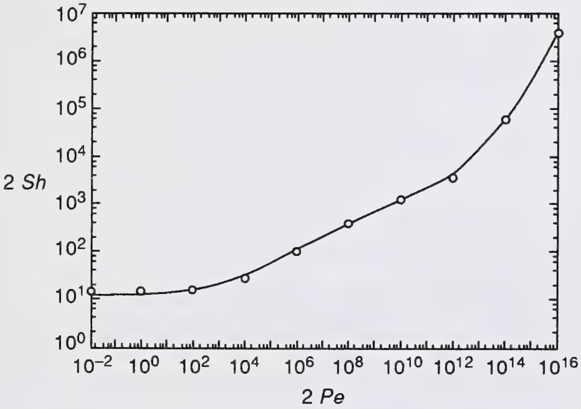

Figure 11-15. Adequacy of the additivity rule for $a_c/a_p = 10^4$ and $A/kT = 10^4$. The curve represents results obtained by summing individual contributions from gravitational force, Brownian motion, and London force. Open circles were obtained from simultaneously considering all effects (Prieve and Ruckenstein, 1974).

11.4 LAGRANGIAN APPROACH

In the previous section, we dealt with the deposition of particles having a finite Peclet number by solving the generalized convection-diffusion equation. Here we shall deal with particle capture (or deposition) in the absence of Brownian motion and hence diffusion, *i.e.*, $Pe \gg 1$. The special case of particles capture by a spherical collector will be treated in detail.

11.4.1 Particle Collisions on a Spherical Collector: With the Presence of External Forces

The case of particles capture by a spherical collector is of industrial importance in flotation columns where air bubbles are used as collectors of small mineral particles and in filtration using a packed bed.

In the Lagrangian approach, the flow field about the collector is assumed to be undisturbed by the presence of the colloidal particle. The fluid flow near the collector is deduced from the general expression of the flow and it is decomposed into a normal component and a tangential component with respect to the collector surface. A force balance on the colloidal particle is made in the directions normal and tangential to the collector surface. From the force balance equations, the angular variation of the gap between the colloidal particle and the surface is obtained and the balance equations provide the basis for the evaluation of the deposition efficiency.

When the spherical collector is small, it is possible to neglect the fluid inertia and the flow field is given by the Stokes solution. The undisturbed axisymmetric flow field close to a spherical collector is given by

$$\psi = \frac{3}{4} A_{sph} U_\infty (r - a_c)^2 \sin^2\theta \tag{11-66}$$

where ψ is the stream function
U_∞ is the undisturbed fluid velocity
a_c is the collector radius
r is the radial coordinates and
A_{sph} is a dimensionless parameter characterizing the flow model used to account for the presence of other collectors.

For an isolated spherical collector, $A_{sph} = 1$. For example, using Happel's model (1958) for a packed bed of spherical particles, A_{sph} is given by

$$A_{sph} = \frac{2\left(1 - \alpha_c^{5/3}\right)}{2 - 3\,\alpha_c^{1/3} + 3\,\alpha_c^{5/3} - 2\,\alpha_c^2}$$

where α_p is the solids bed volume fraction.

Figure 11-16 shows the flow geometry together with the collector and the colloidal particle.

The fluid velocity components are related to the stream function as

$$u_r = -\frac{1}{r^2 \sin\theta} \frac{\partial\psi}{\partial\theta} \tag{11-67a}$$

and

$$u_\theta = \frac{1}{r \sin\theta} \frac{\partial\psi}{\partial r} \tag{11-67b}$$

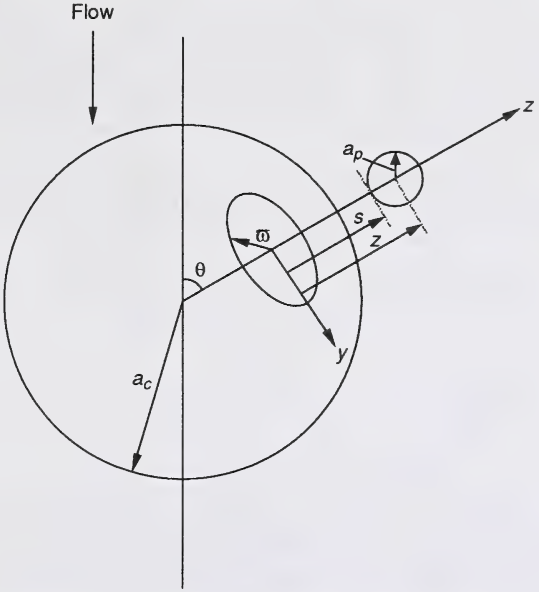

Figure 11-16. Flow geometry of a colloidal particle in the proximity of a larger spherical collector.

Following the approach of Spielman and Fitzpatrick (1973), it is possible to define a system of local cylindrical coordinates ϖ and z whose origin is on the collector surface with $r = a_c$ and θ. Here θ is the angle corresponding to the centre position of the colloidal particle to be captured. With this coordinate system, the origin of the coordinates changes position as the entrained particle moves around the collector. The fluid flow near the collector in the new cylindrical coordinates is given by

$$\vec{u} = \vec{u}_{st} + \vec{u}_{sh} \tag{11-68}$$

where

$$\vec{u}_{st} = \frac{3\, A_{sph}\, U_\infty \cos\theta}{2\, a_c^2}\left[\varpi z \vec{i}_{\varpi} - z^2 \vec{i}_z\right] \tag{11-69a}$$

and

$$\vec{u}_{sh} = \frac{3\, A_{sph}\, U_\infty \sin\theta}{2\, a_c}\, z \vec{i}_y \tag{11-69b}$$

$\vec{i}_y$, $\vec{i}_{\varpi}$, $\vec{i}_z$ are unit vectors in the y, ϖ, and z-directions, respectively.

The velocity vector $\vec{u}_{st}$ represents an axisymmetric stagnation flow at $\varpi = 0$, whereas $\vec{u}_{sh}$ represents a shear flow parallel to the collector surface. Locally, one can think of the entrained colloidal particle as being subjected to a stagnation flow and a shear flow as described by Eq. (11-69). Both $\vec{u}_{st}$ and $\vec{u}_{sh}$ represent the undisturbed fluid flow velocities about the collector sphere in the absence of the colloidal particle.

The entrained particle velocity is decomposed separately into flow fields corresponding to its normal and tangential velocities. This is allowed as the flow equation is linear and the method of superposition can be used (Happel and Brenner, 1965).

The particle normal velocity *ds*/*dt* under the influence of a total normal force F_n is given by

$$\frac{ds}{dt} = \frac{F_n f_1}{\left(6\pi\mu a_p\right)} \tag{11-70}$$

where F_n is the total force acting on the entrained particle normal to the collector surface. This is shown in Figure 11-17. Here f_1 is the hydrodynamic universal correction factor given by Brenner (1961). It relates to the additional retardation in the translation velocity of the colloidal particle in a stagnant fluid towards a flat surface under the influence of a force F_n. Here s is the dimensional separation distance given by

$$s = z - a_p \tag{11-71}$$

The total force acting on the entrained particle normal to the collector surface is the sum of the electric double-layer, London–van der Waals, gravitational, and hydrodynamic forces. The normal force F_n is given by

$$F_n = F_A + F_R + F_{gz} + F_{Hyd} \tag{11-72}$$

The electric double-layer force between a spherical particle and a plane is given by Eq. (11-53), that due to dispersion is given by Eq. (11-52) and that due to gravity is given by

$$F_{gz} = -\frac{4\pi}{3} a_p^3 \, \Delta\rho \, g \cos\theta \tag{11-73}$$

The hydrodynamic force is due to the fluid stagnation flow and it is given by

$$F_{Hyd} = \left[-\frac{3\left(s + a_p\right)^2 A_{sph}\, U_\infty \cos\theta}{2\, a_c^2} \right] \left[6\pi\mu\, a_p \right] f_2 \tag{11-74}$$

where the term in the first square brackets of Eq. (11-74) represents the *z*-directed fluid velocity as given by Eq. (11-69a).

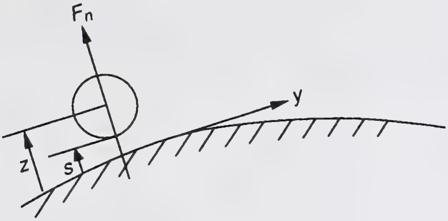

(a) Particle moving under applied force

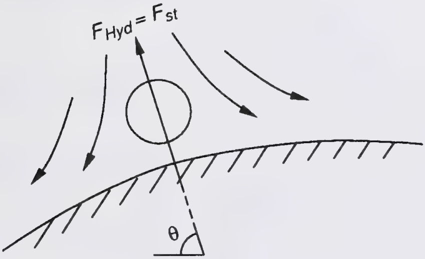

(b) Stationary particle

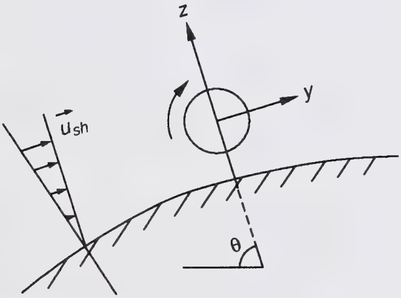

(c) Freely moving particle

Figure 11-17. Resolution of the fluid velocity into stagnation and shear type flows.

To simplify the analysis we shall use the non-retarded expression for the London–van der Waals potential and assume that the collector and the particle to have nearly the same value for the zeta potential. This will allow the dropping of the second term in Eq. (11-53). Letting $h = s/a_p$, Eq. (11-70) when combined with the constitutive expressions for the normal force components, yields

$$\text{(11-75)} \quad \left(\frac{dh}{dt}\right)\left[\frac{6\pi\mu a_p^2}{f_1}\right] = -\frac{2\,A}{3\,a_p\,(h+2)^2\,h^2} + 4\pi\varepsilon\varepsilon_o\kappa a_p\,\zeta_p\zeta_c\left[\frac{\exp\left(-\kappa a_p h\right)}{1 \pm \exp\left(-\kappa a_p h\right)}\right]$$

$$- \frac{4\pi}{3}\,a_p^3\,\Delta\rho\,g\cos\theta - \left(6\pi\mu a_p^3 f_2\right)\left[\frac{3\,(h+1)^2\,A_{sph}\,U_\infty\cos\theta}{2\,a_c^2}\right]$$

The above equation relates the variation of the separation distance h with time to the various flow conditions and physical properties of the system.

The motion of the entrained colloidal particle parallel to the collector (y-direction) is composed of two parts. The first part is the free rotation and translation due to the fluid shear velocity $\vec{u}_{sh}$. The particle velocity due to the fluid shear velocity is given by

$$\text{(11-76a)} \quad v_{py\,1} = \left[\frac{3\,A_{sph}\,U_\infty\,(s+a)\,\sin\theta}{2\,a_c}\right] f_3$$

The quantity in the square brackets of Eq. (11-76a) is the shear velocity given by Eq. (11-69b). The second part of the y-direction velocity of the particle corresponds to the free rotation and translation of the particle under the external force of gravity and it is given by

$$\text{(11-76b)} \quad v_{py\,2} \cong \left[\frac{f_4}{6\pi\mu\,a_p}\right]\left[\frac{4\pi\,a_p^3\,\Delta\rho\,g\,\sin\theta}{3}\right]$$

The functions f_3 and f_4 are given by Goldman *et al.* (1967a,b).

The resultant particle velocity in the y-direction is given by combining Eqs. (11-76a) and (11-76b) leading to

$$\text{(11-76c)} \quad a_c\,\frac{d\theta}{dt} = \frac{3\,a_p\,A_{sph}\,U_\infty\,(h+1)\,\sin\theta}{2\,a_c} f_3 + \frac{2\,a_p^2\,\Delta\rho\,g\,\sin\theta}{9\mu} f_4$$

The trajectory equation for the entrained particle can be obtained by eliminating the time from Eqs. (11-75) and (11-76c). The trajectory equation is given by

$$\frac{1}{f_1}\left[\frac{3}{2}(h+1)f_3 + N_G\left(\frac{a_p}{a_c}\right)f_4\right]\sin\theta\,\frac{dh}{d\theta} = -\frac{N_A}{h^2(h+2)^2} + N_A N_\zeta\,\kappa a_p\left[\frac{\exp\left(-\kappa a_p h\right)}{1\pm\exp\left(-\kappa a_p h\right)}\right] - \left[\frac{3}{2}f_2(h+1)^2 + N_G\right]\cos\theta \tag{11-77}$$

where N_A is the attraction number defined as

$$N_A = \frac{A\,a_c^2}{9\pi\mu\,a_p^4\,U_\infty A_{sph}} \tag{11-78a}$$

N_ζ is the electrostatic (repulsion) number defined as

$$N_\zeta = \frac{6\pi\,\varepsilon\varepsilon_o\,\zeta_c\zeta_p\,a_p}{A} \tag{11-78b}$$

and N_G is a dimensionless gravity number defined as

$$N_G = \frac{2\,\Delta\rho g\,a_c^2}{9\mu\,U_\infty A_{sph}} \tag{11-78c}$$

In the previous section when dealing with the deposition rate due to an impinging jet, the Brownian motion was taken into consideration. Consequently, the gravitational *Gr*, double layer *Dl,* and adhesion parameter *Ad,* were defined relative to the Brownian motion thermal energy *kT*. As the diffusion mechanism is not considered here, the gravitational N_G, electrostatic N_ζ, and the attraction number N_A, cannot be defined relative to *kT*. Consequently, even though these dimensionless numbers represent the strength of the forces to which they are named, their bases are different.

The electrostatic repulsion number N_ζ represents the ratio of electrostatic repulsive to London–van der Waals attractive forces. The gravitational number N_G represents the ratio of gravitational force to the viscous force modified by $(a_c/a_p)^2$. Similarly, the attraction number N_A represents the ratio of the dispersion attraction force to the viscous force modified by $(a_c/a_p)^2$.

Spielman and Fitzpatrick (1973) in their analysis of colloidal deposition on spherical collectors neglected the terms $N_G\ (a_p/a_c)$ and further assumed negligible electrostatic repulsion forces, *i.e.*, $N_\zeta = 0$. On the other hand Spielman and Cukor (1973) assumed $N_G = 0$ but incorporated electric double-layer repulsion in their analysis.

Figure 11-18 shows the paths of a colloidal particle near a spherical collector. Three types of particle trajectories are shown. Particle trajectory *a* leads to a collision. Trajectory *b* is the limiting trajectory separating a collision trajectory from a non-collision trajectory. Trajectory *c* is a non-collision trajectory. All particles within the stream tube *T* would lead to a collision. The capture efficiency is given by Eq. (11-5a) as

$$\eta = \frac{2\,\psi_L}{a_c^2\,U_\infty} \tag{11-79}$$

For the case of $(a_p/a_c) \ll 1$, the stream function for the flow over a spherical collector is given by

$$\psi \approx \frac{3}{4} A_{sph}\, a_c^2\, U_\infty \left(\frac{a_p}{a_c}\right)^2 (h+1)^2 \sin^2\theta$$

and the collision efficiency becomes

$$\eta = \frac{3\,A_{sph}}{2}\left(\frac{a_p}{a_c}\right)^2 \lim_{\theta\to 0}\left[(h+1)^2 \sin^2\theta\right] \tag{11-80}$$

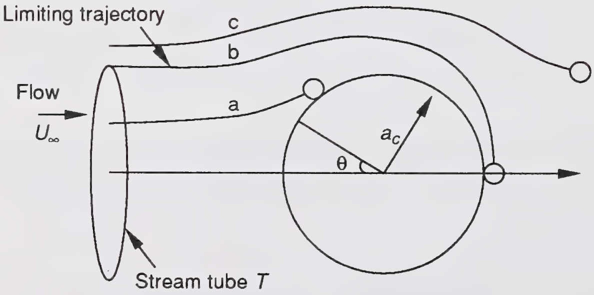

Figure 11-18. Paths of a colloidal particle: trajectory *a* leads to a collision, trajectory *b* is the limiting trajectory, and trajectory *c* leads to no collision.

Solution of Eq. (11-77) by backward integration from $\theta = \pi$ and $h = 0$ to large values of h with $\theta \to 0$ would then, in principle, determine the limit of $(h+1)^2 \sin^2\theta$. Hence, the collision efficiency can be determined. In practice, however, there is an infinite attraction ($N_A \neq 0$) at $\theta = \pi$ and $h = 0$. Spielman and Fitzpatrick (1973) discussed the details of the initial condition necessary in order to be able to proceed with the backward integration of Eq. (11-77).

It should be recalled here that capture by pure interception for the case of a spherical collector is given by Eq. (11-6)

$$\eta_I = \frac{3}{2} A_{sph} \left(\frac{a_p}{a_c} \right)^2$$

where, for an isolated spherical particle, $A_{sph} = 1$.

In the limit of a very large attraction number N_A and in the absence of gravitational and electrostatic repulsion forces, Spielman and Goren (1970,1971) used limiting expressions for the hydrodynamic universal functions and obtained an analytical expression for the collision efficiency for a spherical collector as

$$\text{(11-81a)} \quad \eta = \left[\frac{3}{2} A_{sph} \left(\frac{a_p}{a_c} \right)^2 \right] \left(\frac{4}{3} \right) \left[\frac{9}{5} N_A \right]^{1/3}$$

for $N_A \gg 1$, with $N_G = N_\zeta = 0$.

The term appearing in the first square brackets of Eq. (11-81a) is the pure interception capture efficiency for a spherical collector. Consequently, Eq. (11-81a) can be written as

$$\text{(11-81b)} \quad \frac{\eta}{\eta_I} = \frac{4}{3} \left[\frac{9}{5} N_A \right]^{1/3}$$

Clearly, for $N_A \gg 1$, η/η_I becomes larger than unity. The enhancement in the collection efficiency is due to the presence of the London–van der Waals attractive force.

Similarly, Spielman and Goren (1970) obtained a limiting expression for the case of a cylindrical collector:

$$\text{(11-82)} \quad \eta = \left[2\, A_{cyl} \left(\frac{a_p}{a_c} \right)^2 \right] \left(\frac{3\pi}{4} N_A \right)^{1/3}$$

for $N_A \gg 1$, $N_G = N_\zeta = 0$.

Here the term in the square brackets is the pure interception efficiency for a cylindrical collector. The hydrodynamic flow parameter A_{cyl} is given by

Isolated cylinder (Lamb's solution)

$$(11\text{-}83a) \quad A_{cyl} = \frac{1}{2}\left[2.0 - ln\left(\frac{2\rho\, a_c\, U_\infty}{\mu}\right)\right]^{-1}$$

Fibre mat (Happel, 1959; Guzy *et al.*, 1983; Adamczyk and van de Ven, 1981b)

$$(11\text{-}83b) \quad A_{cyl} = -\left[ln\, \alpha_p + \frac{(1-\alpha^2)}{(1+\alpha^2)}\right]^{-1} \qquad \text{Happel's model}$$

The stream function for flow past a cylinder for the case of $a_p << a_c$ is defined as

$$(11\text{-}83c) \quad \psi = 2\, A_{cyl}\, U_\infty (r - a_c)^2 \, \frac{\sin\theta}{a_c}$$

Eq. (11-83c) is valid for $Re \lesssim 0.5$. For the case of a cylindrical collector, a_c becomes the radius of the cylinder. The attraction number for the case of the cylinder becomes

$$N_A = \frac{A\, a_c^2}{9\, \pi\mu\, a_p^4\, U_\infty A_{cyl}}$$

and the ratio of the deposition efficiency to that of the interception efficiency for $N_A >> 1$ becomes for the case of a cylindrical collector

$$\frac{\eta}{\eta_I} = \left[\frac{3\pi}{4}\, N_A\right]^{1/3}$$

Once again, η/η_I becomes larger than unity for $N_A >> 1$.

For a spherical collector with $N_\zeta = 0$, the variation of the ratio of the capture efficiency to that due to pure interception as obtained by the numerical solution of Eq. (11-77) is shown in Figure 11-19. As would be expected, for a given value of the gravitational group N_G, the capture efficiency ratio increases with the attraction number N_A. For a fixed N_A, the capture efficiency ratio increases with increasing gravitational number N_G. The asymptotic solution given by Eq. (11-81b) for $N_\zeta = N_G = 0$ is also shown in Figure 11-19. Good agreement between the numerical and the asymptotic solution is evident for $N_A >> 1$. Such a good agreement indicates that the separation distance s does not need to be very large compared to a_p before the hydrodynamic interactions become weak (Probstein, 1989).

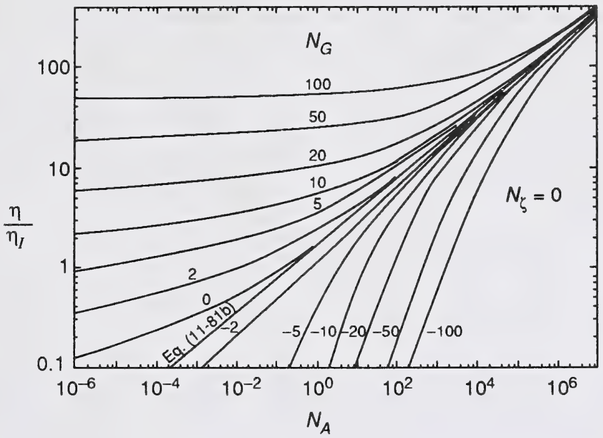

Figure 11-19. Variation of normalized capture efficiency for a spherical collector with attraction number N_A (Spielman and Fitzpatrick, 1973).

For a cylindrical collector, Figure 11-20 shows the variation of the ratio of the capture efficiency to that of pure interception computed using an equation corresponding to Eq. (11-77) (Spielman and Fitzpatrick, 1973). The asymptotic solution given by Eq. (11-82) for $N_A \gg 1$, $N_G = N_\zeta = 0$ is also shown on Figure 11-20. Good agreement is once again present for $N_A > 1$ between the two solutions.

In the absence of gravitational force $N_G = 0$, Spielman and Cukor (1973) numerically solved the trajectory equation for the case of a spherical collector for both constant potential and constant charge cases. Here the solution is governed by the double-layer inverse length κa, the attraction (adhesion) number N_A, and the repulsion number N_ζ. The analysis is made using an unretarded dispersion potential. The expression for the repulsive double layer is restricted to $|\zeta_c \sim \zeta_p| < 0.05$ V and $\kappa a_p > 10$. A typical potential energy of interaction is shown in Figure 11-21.

Depending on the values of κa_p, N_A, and N_ζ, four possible modes of capture are predicted. For the case of $\kappa a \gg 1$ and constant charge, Figure 11-22 shows the four modes of capture. In zone I, where no capture is possible, the particles are unable to surmount the repulsive energy barrier as shown in Figure 11-21. Here all particles escape capture. In zone II, capture occurs at the primary minimum. In this region, $N_\zeta/\kappa a_p$ is small indicating a weak repulsive energy barrier. In zone III, capture occurs at the secondary minimum. Here, no approaching particles are carried over the repulsive energy barrier. The secondary minimum is sufficiently deep to prevent some particles from escaping. In zone IV, a small region is present where combined capture by the primary and secondary minima occurs (Spielman, 1977).

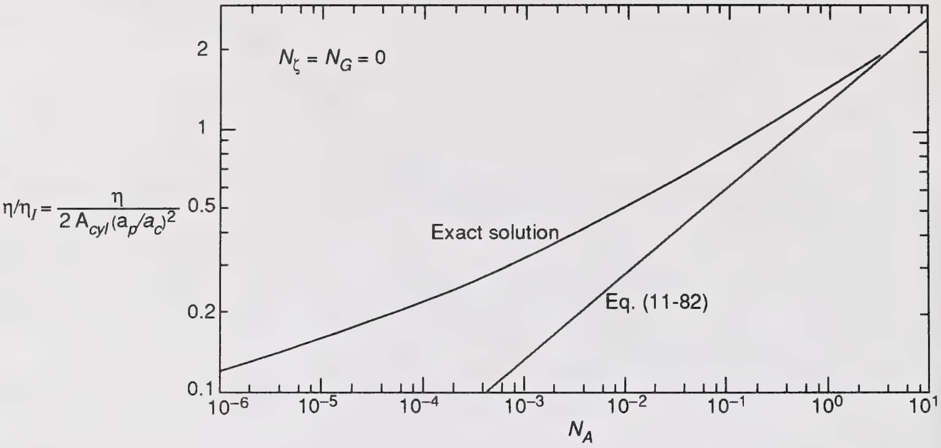

Figure 11-20. Normalized capture efficiency *versus* attraction number for capture of neutrally buoyant particles by a cylinder. Hydrodynamic interactions and van der Waals attraction are incorporated (Spielman and Fitzpatrick, 1973).

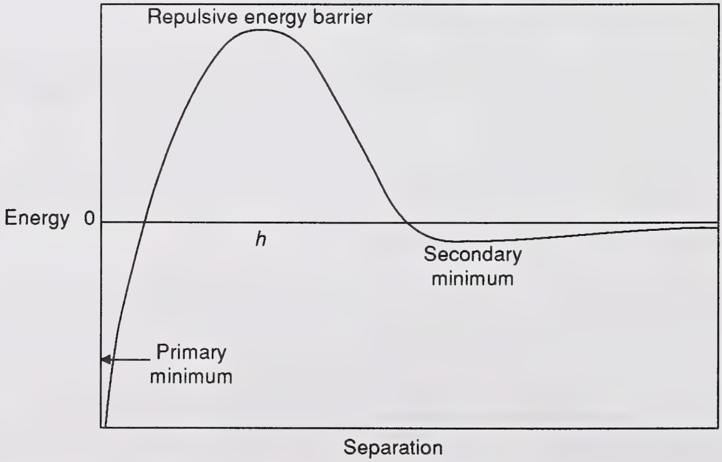

Figure 11-21. Variation of combined London–van der Waals attraction and electric double-layer repulsion potentials with separation distance between a colloidal particle and a collector.

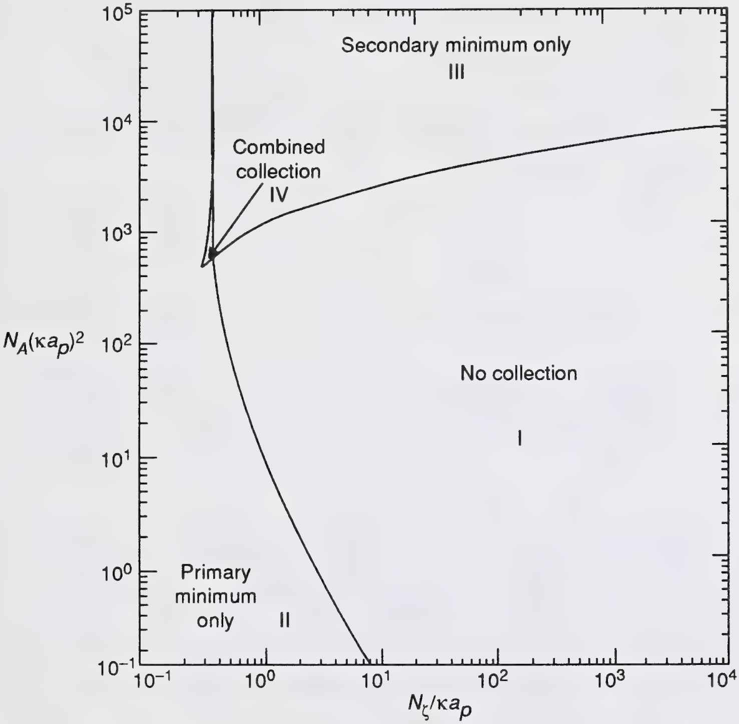

Figure 11-22. Modes of capture of non-diffusing particles by a spherical collector at constant surface charge with $\kappa a_p \gg 1$. Hydrodynamic interactions, London–van de Waals attraction, and double-layer repulsion are incorporated (Spielman and Cukor, 1973).

The effect of the dimensionless inverse Debye length κa_p on the location of the four zones is shown in Figure 11-23 for the case of constant surface charge and in Figure 11-24 for the case of constant surface potential.

Figure 11-25 illustrates the variation of the capture efficiency (normalized with the pure interception capture efficiency) with the attraction number at fixed repulsion numbers. Recall that the repulsion number N_ζ represents the ratio of repulsive to attractive forces. In other words for a constant non-zero value of N_ζ, the attractive and repulsive forces are fixed. Consequently, for a given system, a change in N_A is derived from changes in the flow velocity U_∞. At $N_\zeta = 0$, the capture efficiency increases with N_A as a consequence of increasing the attractive forces. A high capture efficiency can be achieved either by increasing the value of the Hamaker constant or decreasing the flow velocity. All the curves for non-zero N_ζ values give a lower capture efficiency. This is to be expected due to the presence of a repulsive force. Consider now a given value of N_ζ, say $N_\zeta = 200$ for the constant charge case. For a given system, N_ζ fixes the strengths of the repulsive and

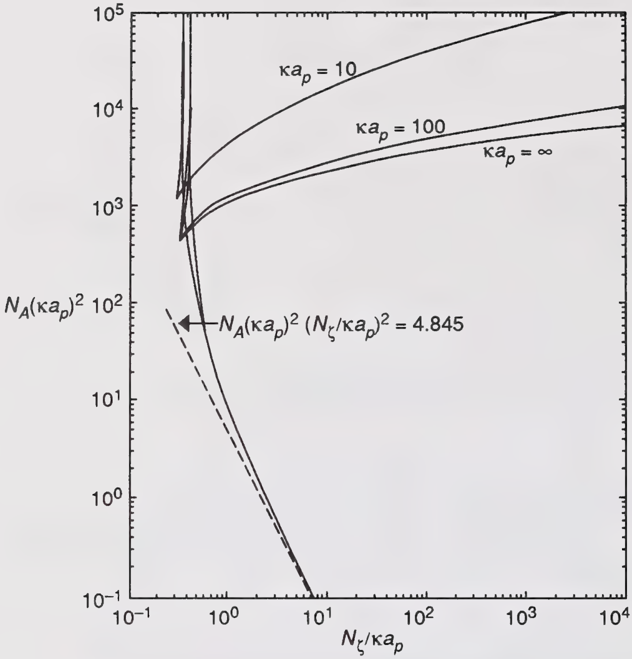

Figure 11-23. Regions of capture modes for non-diffusing particles by a spherical collector at constant surface charge for selected values of κa (Spielman and Cukor, 1973).

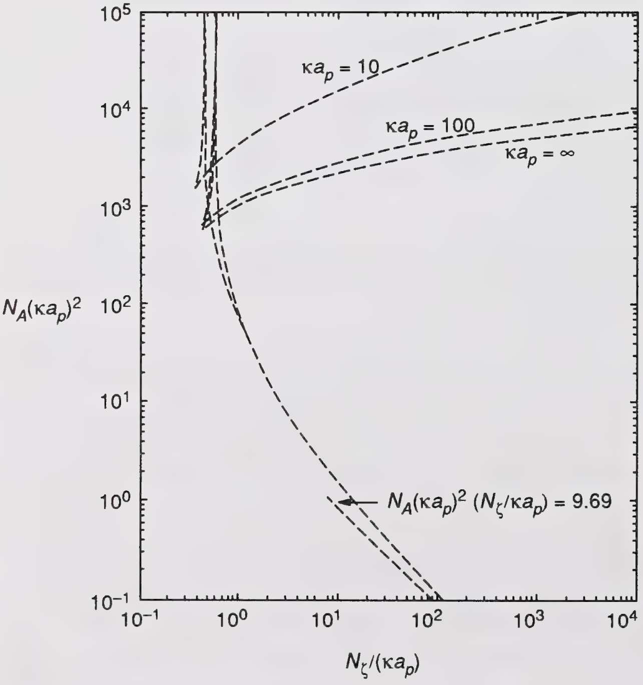

Figure 11-24. Regions of capture modes for non-diffusing particles by a spherical collector at constant potential for selected values of κa_p (Spielman and Cukor, 1973).

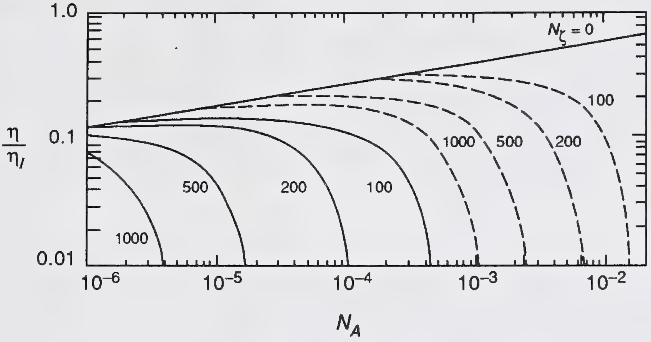

Figure 11-25. Normalized efficiency *versus* attraction number at fixed selected repulsion numbers and $\kappa a_p = 10$ for the spherical collector: —— constant charge; ---- constant potential (Spielman and Cukor, 1973).

attractive forces. Hence a change in N_A can be attributed to a change in the fluid velocity which may be capable of propelling a particle over the repulsive energy barrier to be captured at the collector surface. Indeed, for $N_\zeta = 200$, the capture efficiency is just below that for $N_\zeta = 0$ at $N_A < 10^{-5}$. However, as N_A increases, it leads to a weaker flow which may not be able to push particles over the repulsive energy barrier. Consequently, increasing N_A leads to a lower capture and, finally, when N_A is sufficiently large, no capture occurs.

11.5 RELATIONSHIP BETWEEN DEPOSITION EFFICIENCY AND SHERWOOD NUMBER

The deposition rates were reported in terms of Sherwood numbers when the analysis was made using the Eulerian approach. However, capture efficiency was used when dealing with the Lagrangian approach. The Sherwood numbers for the case of the spherical collector reported in the previous section can be cast in terms of the capture efficiency. The establishment of a relationship between the capture efficiency and the Sherwood number for the case of a spherical collector is given below.

Recall that the average Sherwood number was defined (see Table 11-3) as

$$Sh = \frac{1}{S} \int_S \left(\frac{j_\perp a_c}{D_\infty n_\infty} \right) dS = \frac{a_c}{S\, D_\infty n_\infty} \int_S j_\perp \, dS \tag{11-84}$$

The integral $\int_S j_\perp \, dS$ is given by

$$\int_S j_\perp \, dS = 2\pi \, \psi_L \, n_\infty \tag{11-85}$$

where $2\pi\ \psi_L\ n_\infty$ represents the total flux of the particles. Here ψ_L represents the limiting stream function for a given capture mechanism.

Combining Eqs. (11-84) and (11-85) leads to

$$(11\text{-}86)\qquad Sh = \left(\frac{a_c}{S\ D_\infty\ n_\infty}\right)\left(2\pi\ \psi_L\ n_\infty\right)$$

From the definition of the capture efficiency for the case of a spherical collector as given by Eq. (11-5a) and by setting $S = 4\pi\ a_c^2$, Eq. (11-86) becomes

$$Sh = \left(\frac{a_c}{4\pi\ a_c^2\ D_\infty\ n_\infty}\right)\left(\eta\pi\ a_c^2\ U_\infty\ n_\infty\right)$$

leading to

$$(11\text{-}87)\qquad Sh = \frac{\eta\ Pe}{4}$$

where $Pe = a_c\ U_\infty / D_\infty$ for a spherical collector. Eq. (11-87) relates the Sherwood number of a spherical collector to its capture efficiency.

The equivalent expression for the case of a cylindrical collector is given as

$$Sh = \frac{\eta\ Pe}{\pi}$$

11.6. EXPERIMENTAL VERIFICATIONS

In the previous sections we discussed the theoretical development of the deposition of colloidal particles on a surface. The mass transfer rate was given by dimensionless groups, either in terms of a collection efficiency η or in terms of a Sherwood number *Sh*. For the case of a spherical collector, the relationship between η and *Sh* was derived and it is given by Eq. (11-87).

For the case of deposition in a stagnation flow, spinning disc, and channel flow, the theoretical descriptions of the flow field are well established. On the other hand, for the case of flow in a packed bed or in a fibre mat, the flow field is deduced using approximate flow models. Consequently, any disagreement between the experimental and theoretical deposition rates in the case of a well-defined flow geometry can only be attributed to the manner by which interparticle forces are modelled. Hence, experimental data from well-defined flow geometries are valuable for establishing the validity of the DLVO theory.

Hull and Kitchener (1969) studied the deposition of polystyrene particles ($a_p = 0.154 \times 10^{-6}$ m) onto a rotating disc under laminar flow conditions. In their first set of deposition experiments, the surface of the rotating disc was covered with polyvinylpyridine copolymer film giving a zeta potential of 0.072 V. The polystyrene particles zeta potential was −0.070 V. For this case of opposite signs in the zeta potential, the experimentally measured deposition rate was very close to that given by the Levich theory, where

$$j_\perp = 0.62\, D_\infty^{2/3} \left(\frac{\rho}{\mu}\right)^{1/6} \omega^{1/2}\, n_\infty \tag{11-88}$$

The Levich equation represents the case where the deposition process is purely mass-transfer controlled in the absence of interparticle forces. The agreement of the experimental results with the Levich theory is not surprising as, for the system studied, the adhesion number Ad is of order 10^{-1} and the double-layer number Dl is negative. For the case of a stagnation flow, Figure 11-14 showed that when Dl is small or negative, the Sherwood number for a given flow Reynolds number is not sensitive to Dl variation. Eq. (11-88) gives

$$\frac{j_\perp}{n_\infty\, \omega^{1/2}} = 0.62\, D_\infty^{2/3} \left(\frac{\rho}{\mu}\right)^{1/6} \tag{11-89}$$

The right side of Eq. (11-89) is a constant for a given system. Making use of the definitions given in Table 11-3, Eq. (11-89) leads to

$$\frac{Sh}{Re^{1/3}} = 0.62\, Sc^{1/3} \tag{11-90}$$

In this case, the local and the average Sherwood numbers are the same.

For negative and small values of Dl, the curves of Figure 11-14 conform to the relationship given by Eq. (11-90) and in turn to Eq. (11-89). According to Hull and Kitchener experimental measurements for the case of opposite signs in zeta potential, the particles flux is given as

$$\frac{j_\perp}{n_\infty\, \omega^{1/2}} = 7.59 \times 10^{-8}\ \mathrm{m/s}^{1/2}$$

whereas the Levich theory gives 7.66×10^{-8} m/s$^{1/2}$. The agreement between the experimental measurements and the Levich theory is excellent.

Hull and Kitchener carried out further experimental tests where the zeta potential of the surface of the rotating disc is rendered negative by coating the disc surface with Formvar. Here both the particles and the disc surface have the same signs for the zeta potential. In this case, there is an electrostatic repulsion between the polystyrene particles and the disc surface. The experimental results showed poor agreement with the deposition theory which takes into account the dispersion and electrostatic forces.

Clint *et al.* (1973) carried out similar experiments to those conducted by Hull and Kitchener. Clint *et al.* regulated the zeta potential of the polystyrene particles ($a_p = 0.214 \times 10^{-6}$ m) and the rotating disc surface by the addition of $Ba(NO_3)_2$. The zeta potential of the particles varied from about –0.025 to –0.012 V and the deposition surface zeta potential from –0.005 to –0.007 V by changing the electrolyte concentration from 5 to 20 mol/m^3, respectively.

When Clint *et al.* accounted for the formation of doublets and triplets within the bulk suspension for the case of high electrolyte concentration, they were able to obtain reasonable agreement with the deposition theory where dispersion and electrostatic forces are accounted for. However, poor agreement with theory was obtained at low electrolyte concentrations where the repulsive forces are strongest. Clint *et al.* pointed out that the deposition rate was very sensitive to the value used for the zeta potential of the deposition surface. Changing ζ_c from –0.0061 to –0.0062 V had the effect of changing the deposition rate by 16%. The change in ζ_c corresponds to 0.1 mV which is well within experimental error for a zeta potential measurement.

Bowen and Epstein (1979) carried out deposition experiments from a flowing suspension of silica particles in a parallel-plates channel. The deposition corresponding to their experimental Run II-2 is shown in Figure 11-26. Table 11-4 gives details of their experimental run. For this test, the silica particles and the deposition surface have opposite signs for the zeta potential. It is clear that the initial variation of the concentration of deposited particles with time is linear and the deposition rate declines with time. The experimental initial deposition rate was found to be 7.87×10^6 m^{-2} s^{-1}. The theoretical value as calculated by Adamczyk and van de Ven (1981b) is given as 7.63×10^6 m^{-2} s^{-1}. Again excellent agreement between the experimental and theoretical deposition rates exists. As in the case of the rotating disc deposition measurements, for the case of opposite signs for the zeta potential, the deposition rate is good in agreement with Levich-type analysis. In this case, the theoretical analysis was conducted by Levesque (1928); see Adamczyk and van de Ven (1981) and Bowen *et al.* (1976). The Levich-type local deposition rate in a channel is given by

$$(11\text{-}91) \quad j_\perp = \frac{n_\infty D_\infty}{b\,\Gamma(4/3)} \left[\frac{2}{(9\gamma)}\right]^{1/3}$$

where

$$(11\text{-}92\text{a}) \quad \gamma = \frac{(2 D_\infty x)}{\left(3 V_m b^2\right)}$$

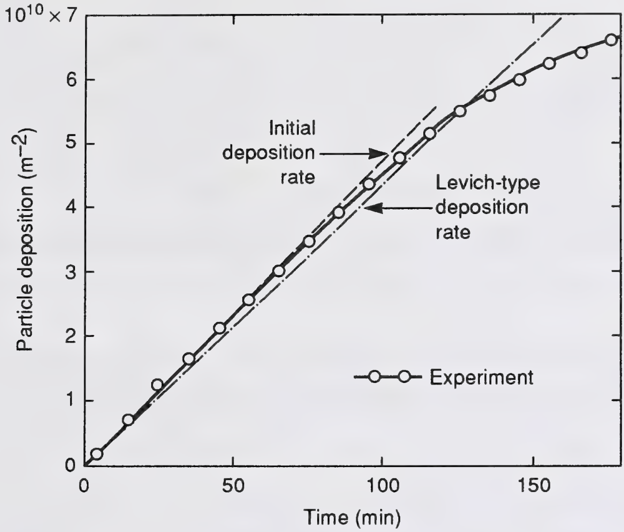

Figure 11-26. Deposition onto a positive 2VP/S substrate. Run II-2 (Bowen, 1978).

Table 11-4. Physical data for Run II-2 of Bowen (1978) and Bowen and Epstein (1979)

Silica particle radius, a_p	0.324×10^{-6} m
Zeta potential of particle, ζ_p	–0.075 V
Zeta potential of deposition surface, ζ_c	0.015 V
Temperature, T	298 K
Axial distance, x	0.125 m
Channel half-width, b	0.000426 m
Particle number concentration, n_∞	0.795×10^{14} m^{-3}
Average axial velocity, V_m	0.149 m/s
Counterion concentration	6.8×10^{-6} mol/L
Hamaker constant (assumed), A	10^{-21} J
Diffusion coefficient, D_∞	7.53×10^{-13} m^2/s
κa_p	2.77
$Dl = 4\pi\varepsilon\varepsilon_o a_p \zeta_p \zeta_p / kT$	–780
$Ad = A/6\,kT$	0.04
$Pe = 3\,V_m a_p^3 / 2\,b^2 D_\infty$	0.056
Channel Reynolds number, $4V_m b\rho/\mu$	284

and

$$D_\infty = \frac{kT}{6\pi\mu a_p} \qquad \text{(11-92b)}$$

V_m is the average velocity in the channel,
b is the channel half-width,
x is the axial downstream distance at which the deposition measurements are taken, and
$\Gamma(4/3)$ is Gamma function given as 0.893.

The Levich deposition rate is given as 7.22 × 10^6 $\mathrm{m^{-2}\ s^{-1}}$ which agrees quite well with the experimentally determined value. In dimensionless form, Eq. (11-91) is given by

$$Sh_l = \frac{a_p j_\perp}{n_\infty D_\infty} = 0.678 \left(\frac{Pe}{\bar{x}}\right)^{1/3} \qquad \text{(11-93)}$$

where

$$\bar{x} = \frac{x}{b} \qquad \text{(11-94a)}$$

The Peclet number is given after Adamczyk and van de Ven (1981a) as

$$Pe = \frac{3 V_m a_p^3}{2 b^2 D_\infty} \qquad \text{(11-94b)}$$

Similar to the previous studies with a rotating disc, poor agreement for deposition was obtained when the deposited channel wall had a zeta potential ζ_c of the same sign as the colloidal particles. ζ_c varied from –0.009 V to –0.046 V. The theoretical analysis predicted no deposition whereas experimentally significant deposition was observed.

In summary, when the electrostatic forces act as attractive forces, good agreement was observed between the theoretical analysis and the experimental measurements. Hence, the mass transfer is not much affected by either the attractive dispersion or the attractive electrostatic forces. In most cases, Levich-type analysis predicts the deposition rate quite adequately. However, when strong repulsive forces due to the electric double layer are present, large deviations between the theoretical analysis and the experimental measurements occur. There are many possible explanations for these discrepancies. As was indicated earlier, when electrostatic repulsive forces are present, the deposition rates become very sensitive to the exact value of the zeta potential used. Moreover, unlike an idealized surface, real surfaces have small-scale roughness elements and a non-uniform distribution of charge sites on the surface. The interaction between a given particle and a substrate is strongly dependent upon the nature of the local areas coming into contact (Bowen and Epstein, 1979). Kihira *et al.* (1992) were able to develop a mathematical model that accounts for the discreteness of the surface charge where it was assumed that it followed a Gaussian distribution with an assigned mean and a standard deviation. The mean Stern potential is assigned to the surface zeta potential. The standard deviation becomes a measure of the homogeneity of the surface charge. By adjusting the standard deviation of the surface potential, they were able to match their experimental coagulation stability ratio with their theoretical model. To this end a new theory of electric double layer interactions is required that can account for heterogeneities of the geometry and the charge distribution as applied to real surfaces.

For the case of deposition in packed beds, Spielman and Fitzpatrick (1973) conducted a very extensive experimental study for the deposition of latex particles in beds of glass spheres. The colloidal particles had a wide range of size with a_p being in the range of $0.36 - 11 \times 10^{-6}$ m and the collector size a_c being in the range of $0.065 - 0.36 \times 10^{-3}$ m. For the case of a negligible double-layer repulsion, *i.e.*, small N_ζ numbers and negligible gravity numbers N_G, they plotted the dimensionless filter coefficient λ/λ_I *versus* the attraction number N_A as shown in Figure 11-27. The filter coefficient λ is defined by Eq. (11-14) and the pure interception filter coefficient λ_I is given by

$$\lambda_I = \frac{9\,\alpha_c A_{sph}\, a_p^2}{8\, a_c^3} \tag{11-95}$$

The flow model correction factor A_{sph} used in the attraction number N_A is due to Happel (1958) and it is given by Eq. (11-9). The solid line on Figure 11-27 is from the solution of Eq. (11-77). Good agreement between the experimental and theoretical deposition results is evident even though to some extent the theoretical analysis is dependent on the choice of the flow model A_{sph}.

When repulsion forces are not negligible, considerable scatter in η/η_I *versus* N_A plot was observed and the data could not be correlated with the repulsion number N_ζ.

The effect of sedimentation on λ/λ_I is shown in Figure 11-28 for $N_G = 4.3$, 12.9, and 43.2. Curves for $N_G = 0$ are also shown for comparison purposes. The solid curves are due to theory, Eq. (11-77). It is clear that there is good agreement between the theory and the experimental data. The dashed lines give the dimensionless filter coefficient for the combined interception and gravity. They are given by

$$\frac{\lambda}{\lambda_I} = 1 + \frac{2}{3} N_G \qquad \text{for } N_G > -3/2 \tag{11-96}$$

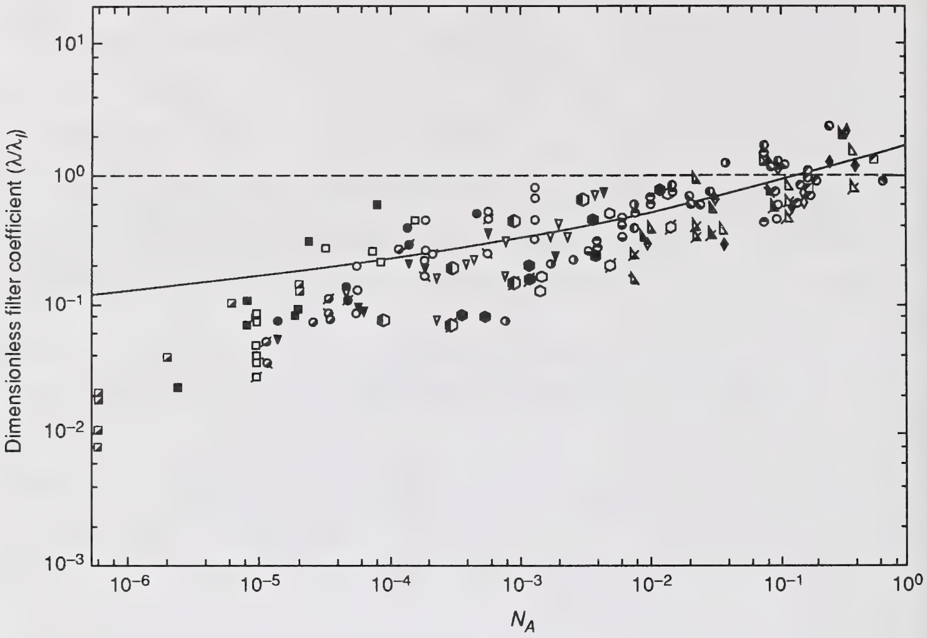

Figure 11-27. Variation of the dimensionless filter coefficient λ/λ_I with the attraction number for negligible repulsion and sedimentation. Solid line, theoretical analysis with $N_\zeta = N_G = 0$; dashed line with λ given by Eq. (11-95) (Spielman and Fitzpatrick, 1973).

The development of the above equation does not include the hydrodynamic interaction between a colloidal particle and the collector surface. At higher N_G numbers, the exact solution and that given by Eq. (11-96) become closer.

Vaidyanathan and Tien (1988) re-examined Fitzpatrick's (1972) data by incorporating non-uniform potentials in the trajectory analysis. The average collection efficiency is defined as

$$\bar{\eta} = \int_{-\infty}^{\infty} \int_{-\infty}^{\infty} f_p\left(\zeta_p\right) f_c\left(\zeta_c\right) \eta\left(\zeta_p, \zeta_c\right) d\zeta_p \, d\zeta_c \tag{11-97}$$

where $f_c(\zeta_c)$ and $f_p(\zeta_p)$ are probability density functions of the collector and particle zeta potential, respectively. $\eta(\zeta_p, \zeta_c)$ is the collection efficiency when the collector has a zeta potential ζ_c and the particles ζ_p. Figure 11-29 shows the filter coefficient variation with the ionic strength. The collector and particle zeta potentials are included in the plot. The agreement between the prediction of Vaidyanathan and Tien with the experimental data of Fitzpatrick (1972) for the filter coefficient λ is found to be reasonably good at the onset of unfavourable surface interactions but poor as the ionic concentrations decline further.

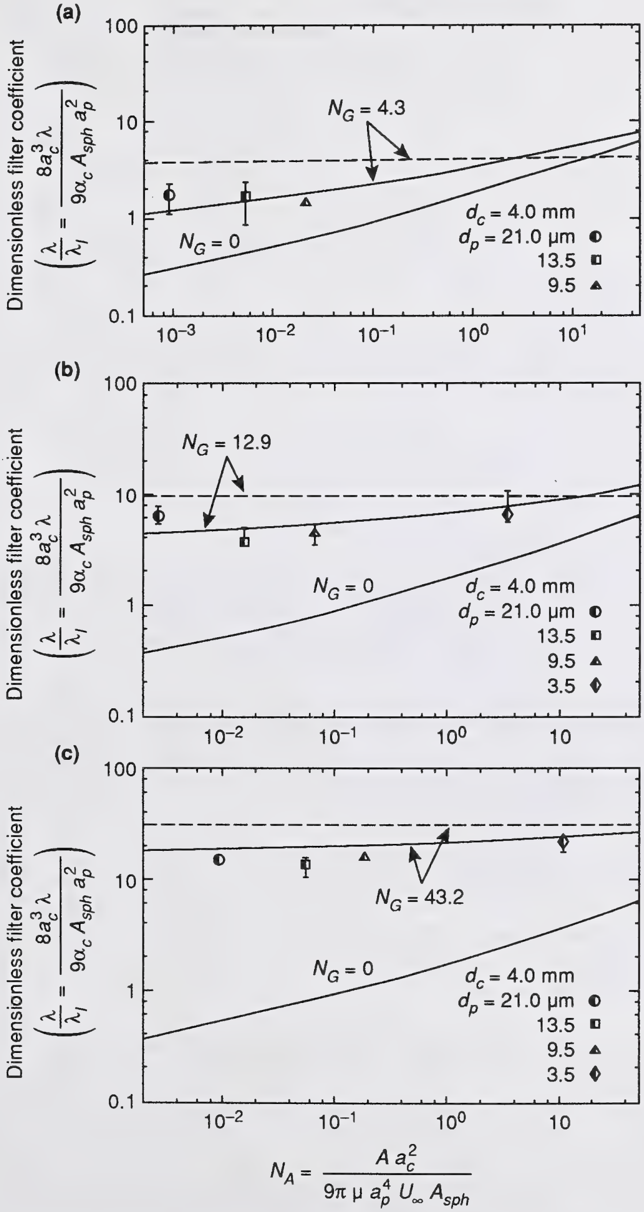

Figure 11-28. Variation of dimensionless filter coefficient with attraction number for different gravity numbers. Solid line, theoretical analysis; dashed line, Eq. (11-96) (Spielman and Fitzpatrick, 1973).

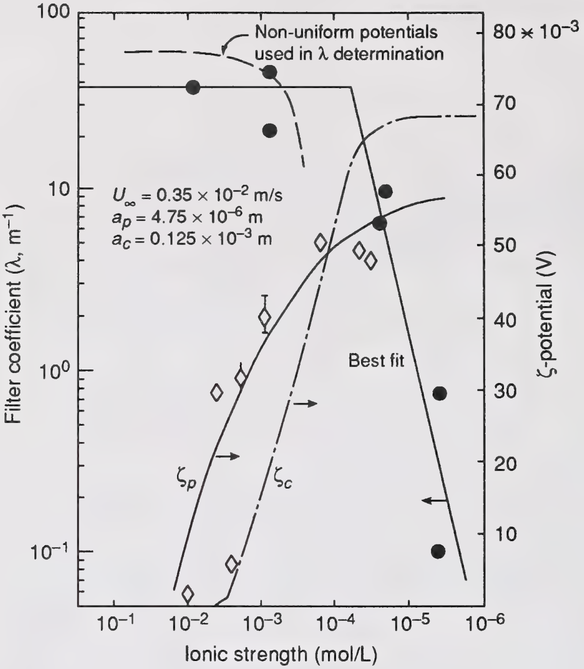

Figure 11-29. Filter coefficient variation with electrolyte ionic strength (Fitzpatrick and Spielman, 1973). Non-uniform potentials type solution from Vaidyanathan and Tien (1988).

Guzy *et al.* (1983) showed that particle retention on unconsolidated fibrous porous media depends on the flow model used in estimating the flow field within the porous bed. The various flow models, *e.g.*, the Happel, the Kuwabara, and the Brinkman cell models, lead to small but very significant differences in the streamlines near the collector surface. The differences are most pronounced for lower porosity beds of filters.

The sensitivity of the collision efficiency to the flow model and electric double-layer thickness is illustrated by Guzy *et al.* (1983). Figure 11-30 shows the sum of the London–van der Waals attractive force F_A and the electric double layer repulsive force F_R for $Dl = 100$, $Ad = 0.1$, and $\overline{\lambda} = 0.4$ with $Da = Gr = 0$. Plots for various κa_p are shown. It is of interest to discuss $\kappa a_p = 5$ and 50 (equally true for $\kappa a_p = 2$ and 57) as the maximum net repulsive force of $(F_A + F_R)$ is nearly the same but the maximum values occur at different separation gap values h. Due to the lubrication effects, the "attractive" hydrodynamic force is weaker near the collector surface than farther out. Thus, for an expanded double layer, $\kappa a_p = 5$, the hydrodynamic force is sufficient to move the particle through the energy barrier as opposed to the case of $\kappa a_p = 50$. A small change in the value of the normal velocity near

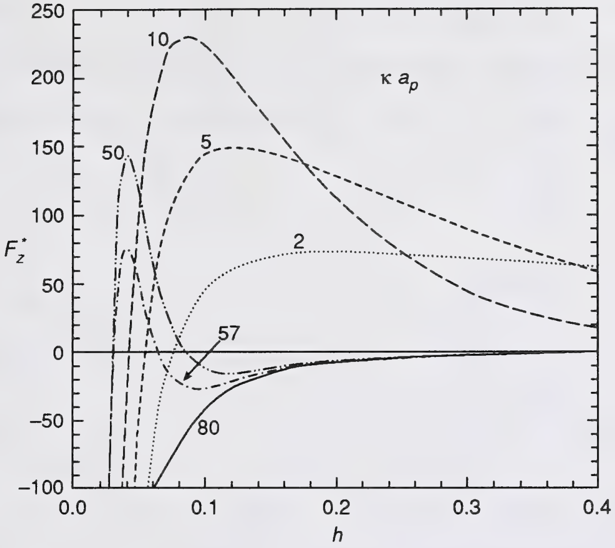

Figure 11-30. Variation of the sum of the electric double-layer and London–van der Waals dimensionless forces as given by Eq. (11-56) with the dimensionless gap length.

the collector surface (*i.e.*, the position of the streamline) can make a significant difference as to whether capture will occur or not. This is why the flow model is very important.

It is clear from the comparison between the experimental measurements and the theoretical analysis that there is much room for improvement in the DLVO theory as applied to real surfaces and in the flow models for deposition in filter beds (Hirtzel and Rajagopolan, 1985).

For a comprehensive treatise on granular filtration and deposition of particles, the reader is referred to Tien (1989).

11.7 SUMMARY OF DIMENSIONLESS GROUPS

11.7.1 Dimensionless Groups in the Flux Equation

(a) Double-layer parameter I, *Dl*

Measure of electrostatic to Brownian motion forces

$$Dl = \frac{4\pi\,\varepsilon\varepsilon_o\,a_p\,\zeta_p\,\zeta_c}{kT}$$

(b) Double-layer parameter II, *Da*

Measure of asymmetry of the electric double layer

$$Da = \frac{\left(\zeta_c - \zeta_p\right)^2}{2\,\zeta_c\,\zeta_p}$$

(c) Adhesion parameter, *Ad*

Measure of London–van der Waals to Brownian motion forces

$$Ad = \frac{A}{6\,kT}$$

(d) Retardation parameter, $\overline{\lambda}$

Measure of retardation due to the finite speed of light

$\overline{\lambda} = \lambda/a_p$ where $\lambda = 10^{-7}$ m

(e) Gravitational parameter, *Gr*

Measure of gravitational to Brownian motion forces

$$Gr = \frac{2}{9}\,\frac{\Delta\rho\, g\, a_p^3}{\mu\, D_\infty}$$

(f) Double-layer thickness parameter, κa_p

Measure of electric double-layer thickness

$$\kappa a_p = \left(\frac{2\, e^2 z\, n_\infty}{\varepsilon\varepsilon_o\, kT}\right)^{-1/2} a_p$$

Table 11-3 (p. 266) gives the definitions of the Reynolds, the Peclet, and the Sherwood numbers for the various geometries. For the case of a cylinder, the dimensionless groups in Table 11-3 are the same as for the case of a spherical collector with a_c being the cylindrical collector radius.

11.7.2 Dimensionless Groups in the Trajectory Equation

(a) Electrostatic number, N_ζ

Measure of electrostatic repulsion to London–van der Waals forces

$$N_\zeta = \frac{6\pi \, \varepsilon\varepsilon_o \, \zeta_c \zeta_p \, a_p}{A}$$

(b) Attraction number, N_A

Measure of London–van der Waals to viscous forces

$$N_A = \frac{A \, a_c^2}{9 \, \pi\mu \, a_p^4 \, U_\infty A_c}$$

where

$A_c \equiv A_{cyl}$ for a cylindrical collector

and

$A_c \equiv A_{sph}$ for a spherical collector

(c) Gravity number, N_G

Measure of gravitational to viscous forces

$$N_G = \frac{2 \, \Delta\rho \, g \, a_c^2}{9 \, \mu \, U_\infty A_c}$$

(d) Double-layer thickness parameter, κa_p

Measure of electric double-layer thickness

$$\kappa a_p = \left(\frac{2 \, e^2 z \; n_\infty}{\varepsilon\varepsilon_o \, kT} \right)^{-1/2} a_p$$

11.8 NOMENCLATURE

a	spherical particle radius, m
a_c	collector radius (spherical or cylindrical), m
a_p	colloidal particle radius, m
A	Hamaker constant, J
Ad	adhesion parameter, $A/6kT$
A_b	empty bed cross-sectional area, m^2
A_c	dimensionless flow parameter (= A_{cyl} or A_{sph})
A_{cyl}	dimensionless flow parameter accounting for the presence of cylindrical particles in a fibre mat, Eq. (11-83a,b)
A_{sph}	dimensionless flow parameter accounting for the presence of spherical particles in a suspension, Eq. (11-9)
c	particle concentration, m^{-3} or mol/m^3
d_c	spherical collector diameter, mm
d_p	colloidal particle diameter, µm
$d_{\|\|}$	correction factor for diffusion coefficient parallel to surfaces, dimensionless
$d_{\perp}$	correction factor for diffusion coefficient normal to surfaces, dimensionless
Da	double layer parameter due to potential asymmetry, $(\zeta_c - \zeta_p)^2/2\,\zeta_c\zeta_p$
D_l	double layer parameter, $4\pi\varepsilon\varepsilon_o a_p\zeta_p\zeta_c/kT$
D_{rr}	diffusion coefficient correction for parallel to surfaces, m^2/s
D_{rz}	diffusion coefficient correction for normal and tangential movements, m^2/s
D_{zz}	diffusion coefficient correction for normal to surfaces, m^2/s
$D_{1\infty}, D_{2\infty}$	particle diffusion coefficient in infinite dilution, m^2/s, $kT/6\pi\mu a$
$\underline{\underline{D}}$	diffusion coefficient tensor, m^2/s
f_1, f_2, f_3, f_4	universal hydrodynamic correction factors (Tables 11-1 and 11-2), dimensionless
F_r	force in r-direction, N
F_z	force in z-direction, N
F_z^*	dimensionless interparticle z-directed force
F_{hyd}	hydrodynamic forces, N

F_{gr}	gravitational force in r-direction, N
F_{gz}	gravitational force in z-direction, N
F_A	dispersion force (attractive), N
F_R	electrostatic (repulsion) force, N
$\vec{F}$	fluctuating force vector, N
g	gravitational acceleration, m/s^2
Gr	gravitational parameter, $2\Delta\rho g a_p^3/9\mu D_\infty$
h	dimensionless gap width, s/a_p
$\vec{i}$	unit vector
$\vec{j}$	particles flux vector, $m^{-2}\ s^{-1}$
j_r	particles flux in r-direction, $m^{-2}\ s^{-1}$
$j_\perp$	particles flux normal to the collector surface, $m^{-2}\ s^{-1}$
k	Boltzmann constant, J/K
L	characteristic length, m
m_p	particle buoyant mass, kg
n	local number concentration, m^{-3}
n_c	number of collectors per unit volume, m^{-3}
n_o	number concentration of particles at bed inlet, m^{-3}
n_∞	number concentration of particles far from a collector, m^{-3}
N_A	attraction number, $A\, a_c^2/9\pi\mu\, a_p^4\, U_\infty A_{sph}$
N_G	gravity number, $2\Delta\rho g\, a_c^2/9\mu\, U_\infty\, A_{sph}$
N_ζ	electrostatic (repulsion) number, $6\pi\varepsilon\varepsilon_o\zeta_c\zeta_p a_p/A$
Pe	Peclet number, defined differently for the various geometries
Q	source term, $m^{-3}\ s^{-1}$
r	radial coordinate, m
Re	Reynolds number (see Table 11-3)
s	dimensional gap between two surfaces, $s = a_p h$
S	collector surface area, m^2
Sc	Schmidt number, $(\mu/\rho)/D_\infty$

Sh	average Sherwood number (see Table 11-3)
$Sh(\theta), Sh_l$	local Sherwood number
St	Stokes number, Eq. (11-19d)
t	time, s
T	absolute temperature, K
u_r	radial fluid velocity, m/s
u_z	normal fluid velocity, m/s
$\vec{u}$	fluid velocity vector, m/s
$\vec{u}*$	dimensionless fluid velocity vector
$\vec{u}_{st}$	stagnation fluid velocity vector, m/s
$\vec{u}_{sh}$	shear fluid velocity vector, m/s
U_∞	characteristic velocity, fluid velocity far from a collector, superficial velocity in a packed bed, m/s
v_r	radial component of particle velocity, m/s
v_t	terminal velocity of a free settling spherical particle, m/s
v_z	normal component of particle velocity, m/s
$\vec{v}$	particle velocity vector, m/s
V_m	average velocity in a channel, m/s
x	Cartesian coordinate, distance along a channel, m
$\vec{x}$	direction vector, m
$\vec{X}$	dimensionless direction vector, Eq. (11-19b)

α	impinging jet flow coefficient, m^{-1} s^{-1}
α_c	volume fraction of particles
$\overline{\alpha}$	dimensionless impinging jet flow coefficient
ε	dielectric constant
ε_o	permittivity of vacuum, C/Vm
ζ_c	collector zeta potential, V
ζ_p	colloidal particle zeta potential, V
η	collection efficiency

η_I	pure interception collection efficiency
θ	angular coordinate
κ	inverse Debye length, m^{-1}
λ	filter coefficient, Eq. (11-14), dimensionless
λ	London wavelength, of order of 10^{-7} m
$\bar{\lambda}$	dimensionless London wavelength, λ/a_p
μ	fluid viscosity, Pa s
υ	kinematic viscosity, m^2/s
ρ	fluid density, kg/m^3
ρ_p	particle density, kg/m^3
ψ	stream function, m^3/s for flow over a spherical particle; m^2/s for flow over a cylinder
ψ_L	limiting stream function defining a particular collection mode
ω	angular velocity of a spinning disc, s^{-1}
ϖ	local radial coordinate, m
$\vec{\nabla}$	del operator, m^{-1}
∇^2	Laplacian operator, m^{-2}

11.9 REFERENCES

Acrivos, A. and Goddard, J.D. (1965), *Asymptotic Expansions for Laminar Forced-Convection Heat and Mass Transfer*, J. Fluid Mechanics, **23**, 273–91.

Acrivos, A. and Taylor, T. (1962), *Heat and Mass Transfer from Single Spheres in Stokes Flow*, Phys. Fluids, **5**, 387–94.

Adamczyk, Z. (1989a), *Particle Transfer and Deposition from Flowing Colloid Suspensions*, Colloids and Surfaces, **35**, 283–308.

Adamczyk, Z. (1989b), *Particle Deposition from Flowing Suspensions*, Colloids and Surfaces, **39**, 1–37.

Adamczyk, Z., Dabros, T., Czamecki, J., and van de Ven, T.G.M. (1984), *Kinetics of Particle Accumulation at Collectors Surfaces. II. Exact Numerical Solutions*, J. Colloid Interface Sci., **97**, 91–104.

Adamczyk, Z., Siwek, B., and Zembala, M. (1992), *Reversible and Irreversible Adsorption of Particles on Homogeneous Surfaces*, Colloids and Surfaces, **62**,. 119–30.

Adamczyk, Z., Siwek, B., Zembala, M., and Warszynski, P. (1989), *Enhanced Deposition of Particles Under Attractive Double-Layer Forces*, J. Colloid Interface Sci., **130**, 578–87.

Adamczyk, Z. and van de Ven, T.G.M. (1981a), *Deposition of Particles Under External Forces in Laminar Flow Through Parallel-Plate and Cylindrical Channels*, J. Colloid Interface Sci., **80**, 340–57.

Adamczyk, Z. and van de Ven, T.G.M. (1981b), *Deposition of Brownian Particles onto Cylindrical Collectors*, J. Colloid Interface Sci., **84**, 497–518.

Adamczyk, Z. and van de Ven, T.G.M. (1984), *Kinetics of Particle Accumulation at Collector Surfaces. II. Approximate Analytical Solutions,* J. Colloid Interface Sci., **97**, 68–90.

Batchelor, G.K. (1976), *An Introduction to Fluid Dynamics*, Cambridge University Press, Cambridge.

Bird, R.B., Stewart, W.E., and Lightfoot, E.N. (1960), *Transport Phenomena*, John Wiley & Sons, New York.

Boluk, M.Y. and van de Ven, T.G.M. (1989), *Kinetics of Electrostatically Controlled Deposition of Colloidal Particles on Solid Surfaces in Stagnation Point Flow,* PCH Physicochemical Hydrodynamics, **11**, 113–27.

Bowen, B.D. (1978), *Fine Particle Deposition in Smooth Channels*, PhD Thesis, University of British Columbia, Vancouver, British Columbia, Canada.

Bowen, B.D. and Epstein, N. (1979), *Fine Particle Deposition in Smooth Parallel-Plate Channels*, J. Colloid Interface Sci., **72**, 81–97.

Bowen, B.D., Levine, S., and Epstein, N. (1976), *Fine Particle Deposition in Laminar Flow Through Parallel-Plate and Cylindrical Channels*, J. Colloid Interface Sci., **55**, 375–90.

Brenner, H. (1961), *The Slow Motion of a Sphere Through a Viscous Fluid Towards a Plane Surface*, Chem. Eng. Sci., **16**, 242–51.

Clift, R., Grace, J.R., and Weber, M.E. (1978), *Bubbles, Drops and Particles*, Academic Press, London.

Clint, G.E., Clint, J.H., Corkill, J.M., and Walker, T. (1973), *Deposition of Latex Particles on a Planar Surface*, J. Colloid Interface Sci., **44**, 121–32.

Dabros, T. and van de Ven, T.G.M. (1983), *A Direct Method for Studying Particle Deposition onto Solid Surfaces*, Colloid Polymer Sci., **261**, 694–707.

Dabros, T. and van de Ven, T.G.M. (1987), *Deposition of Latex Particles on Glass Surfaces in an Impinging Jet*, PCH Physicochemical Hydrodynamics, **8**, 161–72.

Fitzpatrick, J.A. (1972), *Mechanisms for Particle Capture in Water Filtration*, PhD Dissertation, Division of Engineering and Applied Physics, Harvard University, Cambridge, MA.

Fitzpatrick, J.A. and Spielman, L.A. (1973), *Filtration of Aqueous Latex Suspensions Through Beds of Glass Spheres,* J. Colloids Interface Sci., **43**, 350–69.

Friedlander, S.K. (1977), *Smoke, Dust and Haze*, John Wiley and Sons, New York.

Goldman, A.J., Cox, R.G., and Brenner, H. (1967a), *Slow Viscous Motion of a Sphere Parallel to a Plane Wall: I. Motion Through a Quiescent Fluid*, Chem. Eng. Sci., **22**, 637–51.

Goldman, A.J., Cox, R.G., and Brenner, M. (1967b), *Slow Viscous Motion of a Sphere Parallel to a Plane Wall: II Couette Flow*, Chem. Eng. Sci., **22**, 653–60.

Goren, S.L. (1970), *The Normal Force Exerted by Creeping Flow on a Small Sphere Touching a Plane*, J. Fluid Mechanics, **41**, 619–25.

Goren, S.L. and O'Neill, M.E. (1971), *On the Hydrodynamic Resistance to a Particle of a Dilute Suspension When in the Neighbourhood of a Large Obstacle*, Chem. Eng. Sci., **26**, 325–38.

Griffin, F.O. and Meisen, A. (1973), *Impaction of Spherical Particles on Cylinders at Moderate Reynolds Numbers*, Chem. Eng. Sci., **28**, 2155–64.

Guzy, C.J., Bonano, E.J. and Davis, E.J. (1983), *The Analysis of Flow and Colloidal Particle Retention in Fibrous Porous Media*, J. Colloid Interface Sci., **95**, 523–43.

Happel, J. (1958), *Viscous Flow in Multiparticle Systems*, AIChEJ, 4, 197–201.

Happel, J. (1959), *Viscous Flow Relative to Arrays of Cylinders*, AIChEJ, 5, 174–77.

Happel, J. and Brenner, H. (1965), *Low Reynolds Number Hydrodynamics*, Prentice-Hall, Englewood Cliffs, N.J.

Hirtzel, C.S. and Rajagopalan, R. (1985), *Colloidal Phenomena, Advanced Topics*, Noyes Pub., N.J.

Hogg, R., Healy, T.W., and Fuerstenau, D.W. (1966), *Mutual Coagulation of Colloidal Dispersions*, Trans. Faraday Soc., **62**, 1638–51.

Honig, E.P., Roeberson, G.J., and Wiersema, P.H. (1971), *Effect of Hydrodynamic Interaction on the Coagulation Rate of Hydrophobic Colloids*, J. Colloid Interface Sci., **36**, 97–109.

Hull, M. and Kitchener, J.A. (1969), *Interaction of Spherical Colloidal Particles with Planar Surfaces*, Trans. Faraday Soc., **65**, 3093–104.

Kihira, H., Ryde, N., and Matijevic, E. (1992), *Kinetics of Heterocoagulation. Part 2: The Effect of Discreteness of Surface Charge*, J. Chem. Soc. Faraday Trans., **88**, 2379–86.

Levesque, M. (1928), Ann. Mines, **13**, 201.

Levich, V.G. (1962), *Physicochemical Hydrodynamics*, Prentice-Hall, Englewood Cliffs, N.J.

Marshall, J.K. and Kitchener, J.A. (1966), *The Deposition of Colloidal Particles on Smooth Solids*, J. Colloid Interface Sci., **22**, 342–51.

Masliyah, J.K. and Duff, A. (1975), *Impingement of Spherical Particles on Elliptical Cylinders*, Aerosol Sci., 6, 31–43.

Masliyah, J.H. and Epstein, N. (1973), *Numerical Solution of Heat and Mass Transfer from Spheroids in Steady Axisymmetric Flow,* Progress in Heat and Mass Transfer, **6**, 613–32.

Michael, D.M. and Norey, P.W. (1969), *Particle Collision Efficiencies for a Sphere*, J. Fluid Mechanics, **37**, 565–75.

Neale, G. and Masliyah, J.H. (1975), *Flow Perpendicular to Mats of Randomly Arranged Cylindrical Fibers (Importance of Cell Models)*, AIChEJ, **21**, 805–7.

Prieve, D.C. and Lin, M.M.J. (1980), *Adsorption of Brownian Hydrosols onto Rotating Disc Aided by Uniform Applied Force*, J. Colloid Interface Sci., **76**, 32–47.

Prieve, D.C. and Ruckenstein, E. (1974), *Effect of London Forces Upon the Rate of Deposition of Brownian Particles*, AIChEJ, **20**, 1178–87.

Probstein, R.F. (1989), *Physicochemical Hydrodynamics*, Butterworths, Boston.

Rajagopalan, R. and Kim, J.S. (1981), *Adsorption of Brownian Particles in the Presence of Potential Barriers: Effect of Different Modes of Double-Layer Interaction,* J. Colloid Interface Sci., **83**, 428–48.

Spielman, L.A. (1977), *Particle Capture from Low-Speed Laminar Flows,* Annual Review of Fluid Mechanics, **9**, 297–319.

Spielman, L.A. and Cukor, P.M (1973), *Deposition of Non-Brownian Particles Under Colloidal Forces*, J. Colloid Interface Sci., **43**, 51–65.

Spielman, L.A. and Fitzpatrick, J.A. (1973), *Theory for Particle Collection Under London and Gravity Forces*, J. Colloid Interface Sci., **42**, 607–23.

Spielman, L.A. and Goren, S.L. (1970), *Capture of Small Particles by London Forces from Low-Speed Liquid Flows*, Environmental Sci. and Tech., **4**, 135–40. See corrections in **5**, 254 (1971).

Tien, C. (1989), *Granular Filtration of Aerosols and Hydrosols*, Butterworths, Boston.

Suzuki, A., Ho, N.F.H., and Higuchi, W.I. (1969), *Predictions of the Particle Size Distribution Changes in Emulsions and Suspensions by Digital Computation*, J. Colloid Interface Sci., **29**, 552–64.

van de Ven, Theo, G.M. (1989), *Colloidal Hydrodynamics*, Academic Press, London.

Vaidyanathan, R. and Tien, C. (1988), *Hydrosol Deposition in Granular Beds*, Chem. Eng. Sci., **43**, 289–302.

Weber, M.E. and Paddock, D. (1983), *Interceptional and Gravitational Collision Efficiencies for Single Collectors at Intermediate Reynolds Numbers*, J. Colloid Interface Sci., **94**, 328–35.

ELECTROKINETIC APPLICATIONS 12

12.1 GENERAL

We shall consider in this chapter some selected applications of electrokinetic transport phenomena to illustrate the influence of the electric double layer and dispersion forces on the transport of ions, charged particles, and liquids. Electrokinetic transport phenomena play an important role in many industrial processes, waste water treatment, and biological and physiological functions.

12.2 ELECTROKINETIC SALT REJECTION IN POROUS MEDIA

Clays, various porous solids, and membranes (*e.g.*, cellophane) have the property of partially rejecting salt when a saline solution filters through. In other words, the salt concentration in the filtrate is lower than that in the saline solution upstream of a porous packed bed or a membrane. In order to conserve the salt mass balance, the porous solid acts as a filter by not allowing the salt to pass through. The physical mechanism of salt rejection in a charged capillary can be modelled using electrokinetic principles. The surface charge gives rise to a potential field which extends a distance comparable to the inverse Debye length into the capillary pore. Salt rejection analysis for the idealized single circular pore can be extended to the actual porous medium. It should be recognized that salt rejection in a capillary is a reverse osmosis phenomenon where flow of a liquid occurs from high to low salt concentrations. Such a flow occurs under the influence of an imposed pressure gradient. The term hyperfiltration is also used for the salt rejection phenomenon to be discussed in this section.

Jacazio *et al.* (1972) give an excellent account of the salt rejection phenomenon in a circular capillary. Their analysis is presented here to demonstrate the application of electrokinetic principles. As in the case of electroosmosis, the total electric potential $\Phi(x)$ is assumed to be a linear combination of the induced potential $\phi(x)$ and the electric double-layer potential $\psi(r,x)$:

$$\Phi(x,r) = \phi(x) + \psi(x,r) \tag{12-1}$$

Boltzmann equilibrium is assumed, *viz.*

$$c_{\pm}(x,r) = f_{\pm}(x) \exp\left[\mp \overline{\psi}(x,r)\right] \tag{12-2}$$

where $\overline{\psi} = zF\psi/RT$ and $f_{\pm}(x)$ is a function related to the ionic concentration.

For the case where the inverse Debye length is very small compared to the capillary radius, the potential in the central core of the capillary depends only on the axial direction x leading to

$$f_{\pm}(x) = c(x) \tag{12-3}$$

and Eq. (12-2) becomes

$$c_{\pm}(x,r) = c(x) \exp\left[\mp \overline{\psi}(x,r)\right] \tag{12-4}$$

The Poisson equation in cylindrical coordinates is given by

$$\frac{1}{r}\frac{\partial}{\partial r}\left(r\frac{\partial \Phi}{\partial r}\right) + \frac{\partial^2 \Phi}{\partial x^2} = -\frac{\rho^{(f)}}{\varepsilon\varepsilon_o} \tag{12-5}$$

leading to

$$\lambda^2 \frac{1}{R}\frac{\partial}{\partial R}\left(R\frac{\partial \overline{\psi}}{\partial R}\right) = \sinh \overline{\psi} \tag{12-6}$$

where

$$\frac{\partial^2 \overline{\psi}}{\partial x^2} \ll \frac{\partial^2 \overline{\psi}}{\partial r^2} \tag{12-7a}$$

$$\frac{\partial^2 \phi}{\partial x^2} = 0 \tag{12-7b}$$

$$R = \frac{r}{a} \tag{12-7c}$$

$$\lambda = \frac{\lambda_D}{a} \tag{12-7d}$$

and

$$\text{(12-7e)} \qquad \lambda_D = \left(\frac{\varepsilon \varepsilon_o RT}{2 z^2 F^2 c(x)} \right)^{1/2}$$

Eq. (12-6) can be solved subject to the boundary conditions

$\overline{\psi}(x,r) = \overline{\psi}(x,r)$ at $R = 1$ (capillary wall)

and

$\frac{\partial \overline{\psi}}{\partial R} = 0$ at $R = 0$ (axis of symmetry)

It should be noted that the Debye length λ_D is a function of the axial position. The solution of Eq. (12-6) reflects λ axial variation. For a given axial position, the solution of Eq. (12-6) provides the radial distribution of the potential $\overline{\psi}(x,r)$. Jacazio *et al.* (1972) assumed that the fluid flow within the capillary is given by the Poiseuille relation as

$$u_x(r) = 2V(1 - R^2)$$

where V is the average fluid velocity and $u_x(r)$ is the axial fluid velocity at a radial position r.

Jacazio *et al.* (1972) made use of the axial ionic flux and the fact that at any axial location, the total current is zero, to arrive at the axial ionic concentration equation:

$$\text{(12-8)} \qquad \left(\frac{H}{Pe} \right) \frac{d\bar{c}}{d\bar{x}} - \bar{c} = -\bar{c}_2 G$$

where $\bar{x} = x/L$, dimensionless axial distance
$Pe = VL/D_\infty$, flow Peclet number
$\bar{c} = c(x)/c_1$, dimensionless axial concentration.

c_1 is the feed salt concentration and L is the capillary length. The exit salt concentration c_2 is given by

$$\text{(12-9)} \qquad c_2 = \frac{J_s}{(2\pi a^2 V)}$$

J_s is the total flux of the dissociated salt molecules, mol/s. The salt rejection coefficient is defined as

$$(12\text{-}10) \qquad Rej = 1 - \frac{c_2}{c_1}$$

Rej is equal to unity for complete salt rejection by the capillary tube and zero for no rejection.

The coefficients *H* and *G* of Eq. (12-8) are functions of the radial position $\overline{\psi}$ and λ. The initial condition for Eq. (12-8) is $\bar{c} = 1$ at $\bar{x} = 0$. The evaluation of *Rej* is obtained by the simultaneous solution of Eqs. (12-6) and (12-8). Solution details are provided by Jacazio *et al.* It is clear from Eq. (12-8) that salt rejection is a function of the surface charge, Peclet number and Debye length. Usually, the Debye length at the capillary inlet is specified.

The salt rejection coefficient for a cylindrical pore as a function of the Peclet number for different values of wall potential is shown in Figure 12-1. Here λ_1 represents λ value evaluated using the bulk feed concentration c_1. Clearly, the salt rejection increases with an increasing Peclet number and becomes constant as $Pe \rightarrow \infty$. At small *Pe*, diffusion is dominant with the result that there is a lower rejection. At large values of *Pe*, convection is dominant and salt rejection is increased. At a fixed *Pe* value, the rejection increases for higher surface potentials.

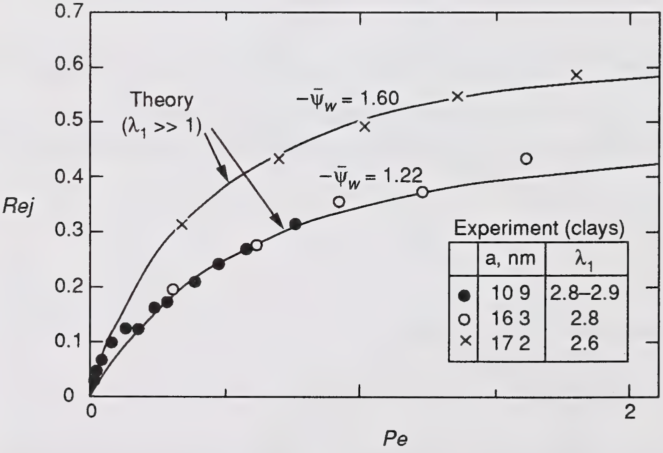

Figure 12-1. Salt rejection coefficient of a cylindrical pore with a constant surface potential for a large Debye length as a function of the Peclet number, and comparison with experiments on compacted clays (Jacazio *et al.*, 1972) (reprinted by permission of American Chemical Society).

For $Pe \gg 1$, Figure 12-2 shows the variation of salt rejection with the inlet Debye length λ_1. The salt rejection coefficient approaches zero as the Debye length approaches zero. As salt rejection takes place entirely within the Debye sheath, a small λ_1 would

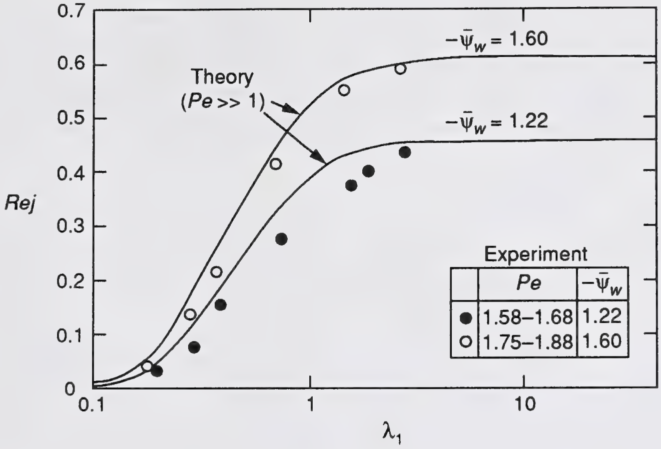

Figure 12-2. Salt rejection coefficient of a cylindrical pore with a constant surface potential for a large Peclet number as a function of the Debye ratio, and comparison with experiments on compacted clays (Jacazio *et al.*, 1972) (reprinted by permission of American Chemical Society).

indicate that nearly the entire pore has $\bar{\psi} = 0$ and the electric double layer is confined to an area close to the capillary surface. Consequently, no salt rejection is expected to occur. For larger λ_1 values, the electric double layer extends to the entire capillary pore and rejection is enhanced. Clearly, Figure 12-2 indicates that higher salt rejection is expected for a saline feed having low salt concentrations.

The experimental results with clays and cellophane agree quite well with the capillary model put forward by Jacazio *et al.* as is shown in Figures 12-1 and 12-2.

12.3 ELECTROOSMOTIC CONTROL OF HAZARDOUS WASTES

Electroosmosis phenomenon was described in details in Chapter 6. Electroosmosis entails the migration of a liquid through a porous charged surface under the influence of an applied electric field. Electroosmosis has been used for the dewatering and consolidation of soils, mine tailings, and waste sludges.

As fluid flow occurs due to an applied electric field, appropriate placement of electrodes would direct the fluid flow in a controlled manner. Consequently, it is possible to direct the flow of specially injected fluids or in-situ fluids in a fashion that would divert groundwater from a spill site, direct a chemical sealant toward a waste site, or dewater the region surrounding a hazardous waste area. The various modes of electroosmotic control of hazardous wastes are given below. They are detailed by Renaud and Probstein (1987).

A case of water drainage close to a hazardous waste site is shown in Figure 12-3. Here, the groundwater level is lowered under the waste site by implanting anode electrodes around the waste area. The cathode electrodes are located further away from the waste site. For a negatively charged porous medium, the salt bearing groundwater flows from the anode to the cathode, thus lowering the groundwater level in the immediate vicinity of the waste site (see Figure 5-1).

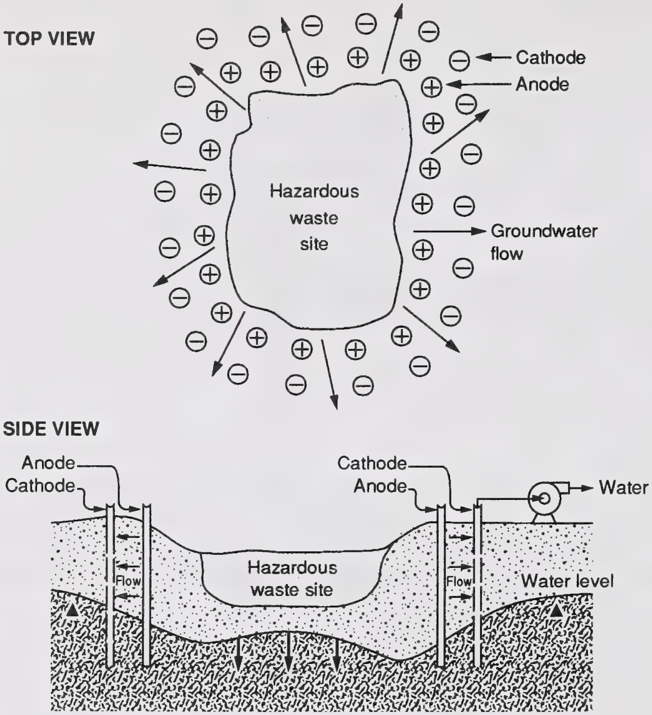

Figure 12-3. Soil dewatering close to a contaminated site (Renaud and Probstein, 1987).

Figure 12-4 shows that chemical sealants injected at the anode electrodes can be directed away from the hazardous waste and thus can isolate the waste site from the groundwater flow.

Renaud and Probstein discussed in detail the case where groundwater flow toward a contaminated waste site is controlled and directed away from the contaminated area. This control is achieved by creating an adverse pressure gradient surrounding the waste site by the appropriate placements of the electrodes as is shown in Figure 12-5. Renaud and Probstein showed that an adverse pressure gradient of 1 m H_2O/m can easily be maintained through the use of the applied electrical potential.

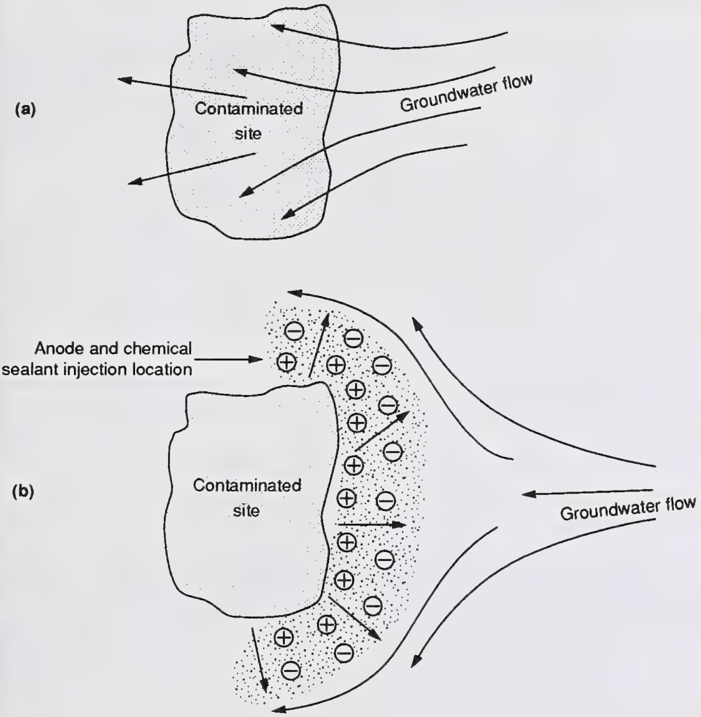

Figure 12-4. Chemical sealant controlled injection: (a) groundwater flow prior to sealant injection and (b) groundwater flow after sealant injection (Renaud and Probstein, 1987).

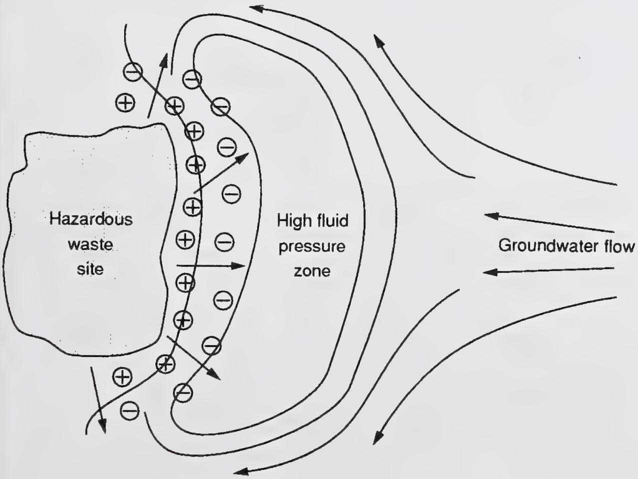

Figure 12-5. Contours of constant pressure near a waste site due to the placement of electrodes (adapted from Renaud and Probstein, 1987).

12.4 IONTOPHORETIC DELIVERY OF DRUGS

Transdermal (skin) delivery of drugs has gained increasing importance in recent years since this route of drug administration bypasses gastrointestinal degradation and hepatic (liver) metabolism. Iontophoresis, a process which causes an increase in the migration of ionic species into the skin or tissue under a gradient of electrical potential, is used to enhance the penetration of charged molecules (Liu *et al.*, 1988). Thus iontophoresis involves the transfer of ions or charged molecules (*e.g.*, insulin, pilocarpine) into the body by an electric field. Ions with a positive charge are driven into the skin at the anode and those with a negative charge at the cathode (Banga and Chien, 1988). Reviews discussing iontophoresis are given by Harris (1967) and Banga and Chien (1988). To a large extent, iontophoresis is similar to electrophoresis where with iontophoresis one deals with the transport of ions rather than colloidal particles.

Skin manifests a large impedance to charged molecules which are transmitted through the skin under an applied electric field. The stratum corneum (outer skin layer) is the least conductive layer of the skin. Skin also has hair follicles and sweat ducts that can provide a possible pathway for the migration and diffusion of ions across the skin (Chien, 1982). Under the application of an electric field, ionic species can penetrate the skin *via* the hair follicles and sweat ducts which are referred to as "shunt" (Siddiqui *et al.*, 1985, 1987).

Liu *et al.* (1988) discussed the electrical properties of the stratum corneum. They indicated that the stratum corneum has two important properties that affect iontophoresis. First, stratum corneum can be polarized by a direct electric field (dc). Secondly, its impedance changes with the frequency of the applied electric field, *i.e.*, an electric field alternating between zero and a positive value with a given waveform. Consequently, the skin can be represented by an equivalent electric analogue as shown in Figure 12-6.

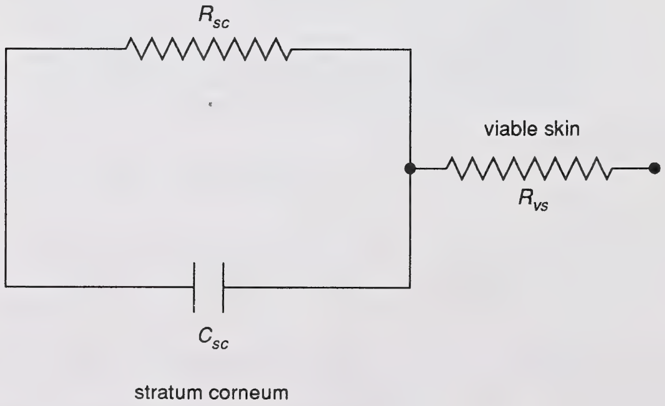

Figure 12-6. Equivalent circuit of skin impedance where R_{vs} and R_{sc} are the resistors for the viable skin and stratum corneum, respectively. C_{sc} is the capacitance for the stratum corneum (Liu *et al.*, 1988).

The stratum corneum is represented by a combination of resistive and a capacitive components which is a function of the pulse frequency. Yamamoto and Yamamoto (1976,1978) found that the impedance of human skin decreases with the increase in the pulse frequency. The viable skin is represented by pure resistance R_{vs}, which does not change with the pulse frequency.

From the above characteristics of the stratum corneum it becomes clear that when a direct electric field is utilized to enhance penetration of charged molecules, electrochemical polarization becomes established in the skin. The induced polarization operates against the applied electrical field and reduces the current density. As pointed out by Liu *et al.*, the polarization of the stratum corneum is similar to the charging of a capacitor C_{sc} shown in Figure 12-6 with an initial current i. The input current decays exponentially across the stratum corneum when a constant dc voltage is applied. As a current is due to the ionic movement within the skin, it becomes clear that the movement of the ionic species through the skin is expected to decay when a dc voltage is applied.

To avoid polarization of the stratum corneum, a pulse dc voltage is normally used in the application of iontophoresis. This pulse mode is a dc voltage that periodically alternates "on" and "off" for the applied voltage. When the voltage is "on," the charged molecules penetrate the skin while the stratum corneum is being polarized. During the "off" period, no ionic penetration takes place and the stratum corneum becomes depolarized. The manner by which the "on" and "off" cycles are administered controls the rate of the ionic species penetration into the skin.

Iontophoretic delivery of insulin to diabetic rats was investigated by Liu *et al.* (1988). The effectiveness of insulin delivery was monitored by measurement of the blood glucose. The lowering of the blood glucose is indicative of the insulin delivery. Figure 12-7 shows the variation of the blood glucose level with time due to the application of simple dc voltage and pulse dc voltage. The experiments were conducted on diabetic hairless rats. The

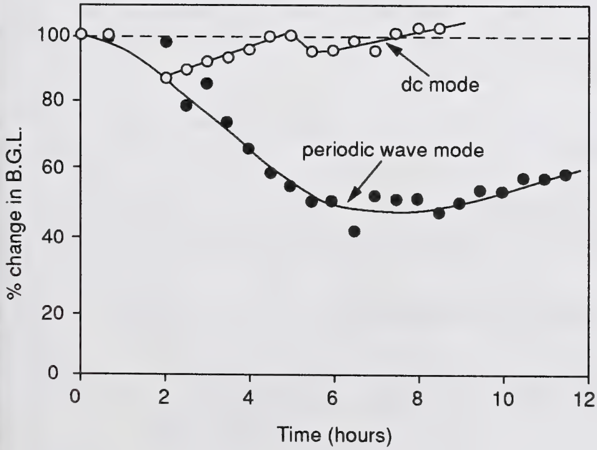

Figure 12-7. Effect of delivery mode on blood glucose levels (BGL) in diabetic hairless rats treated with transdermal periodic iontophoretic system at 2 mA (0.33 mA/cm^2) for 40 min: ○, simple dc; ●, pulse dc (2000 Hz) (Liu *et al.*, 1988).

dc voltage mode gave a slight initial change in the blood glucose level (BGL); however, little change in BGL occurred after four hours. This is due to the polarization of the stratum corneum. However, pulsed dc voltage shows excellent penetration of insulin into the rat's blood stream.

An electrokinetic model has been proposed by Schwendeman *et al.* (1992) to simulate iontophoresis.

12.5 FLOTATION OF OIL DROPLETS AND FINE PARTICLES

Rising air bubbles have been used in the mineral dressing industries to float valuable minerals from solid suspensions. As a bubble rises within the solids suspension, the fine solid particles are separated by adhering to the bubble's surface. Such a separation technique has been shown to be quite effective in removing oil droplets from oil wastewaters (Hung, 1978; Van Ham *et al.*, 1983; Pal and Masliyah, 1990).

In order to analyse the deposition process between an air bubble and an oil droplet or a solid particle, it becomes necessary to measure the zeta potentials of the air bubbles, solid particles, and oil droplets. To this end, Okada and Akagi (1987) developed an apparatus to measure the zeta potential of air bubbles. Figure 12-8 shows a schematic diagram of the experimental setup of Okada and Akagi (1987). The apparatus is of the microelectrophoresis type and the zeta potential is determined by measuring the electrophoretic velocity of the bubbles. The measuring system consists of a microscope, an electrophoresis cell, and a video camera attached to a recorder and a monitor. The air bubbles were generated by releasing the pressure of water containing dissolved air. The bubble size was 20–40 μm.

The experimental results for the air bubbles zeta potential are shown in Figure 12-9 for the case of aqueous cationic surfactant cetyltrimethylammonium bromide (CTAB) solution (5×10^{-5} mol/L) containing 0.5 vol% ethanol.

Clearly, the zeta potential of the air bubbles is a strong function of the ionic strength of the solution. This is similar for the case of the zeta potential dependence on ionic strength for liquids and solid surfaces.

Okada *et al.* (1988) carried out further zeta potential measurements on heavy oil ($a_p = 1.4 \times 10^{-6}$ m) and air bubbles in an anionic surfactant (sodium dodecyl sulphate (SDS) 1×10^{-4} mol/L) in the presence of different electrolytes (Figure 12-10). The zeta potentials are both a function of the electrolyte type and concentration. Yoon and Yordan (1986) gave extensive measurements of bubble zeta potentials and the effect of various surfactants.

Okada *et al.* (1990a,b) carried out flotation experiments for oil droplets. They measured the flotation efficiently η_T where

$$\eta_T = 1 - \frac{c_f}{c_i} \tag{12-11}$$

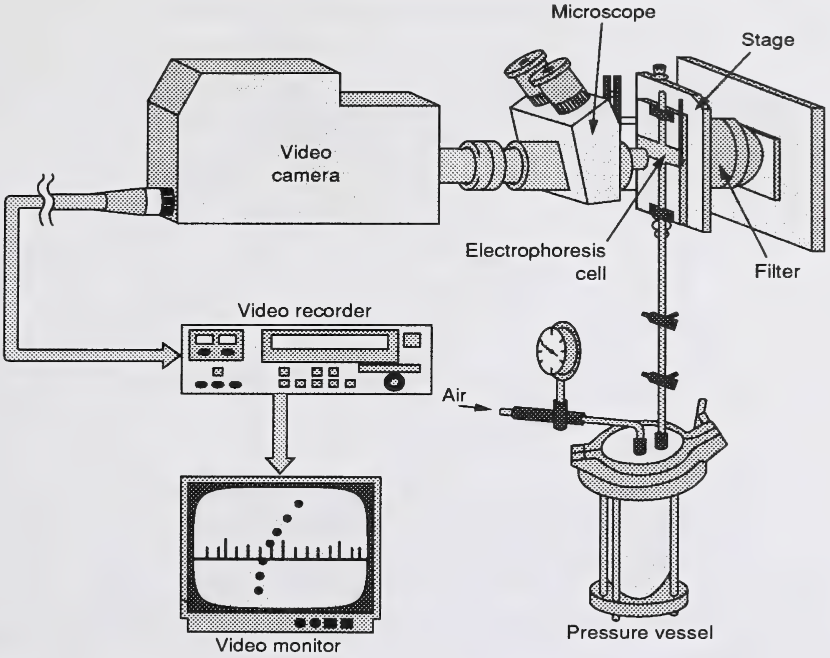

Figure 12-8. Schematic diagram of experimental apparatus used to measure zeta potential of air bubbles (Okada and Akagi, 1987).

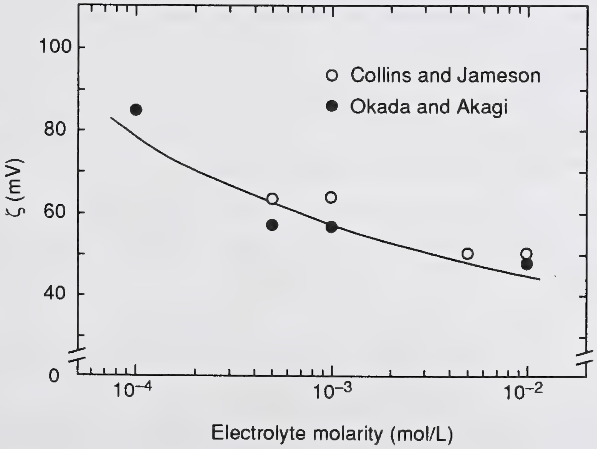

Figure 12-9. Effect of concentration of Na_2SO_4 electrolyte on the zeta potential of an air bubble at 25°C (Okada and Akagi, 1987),

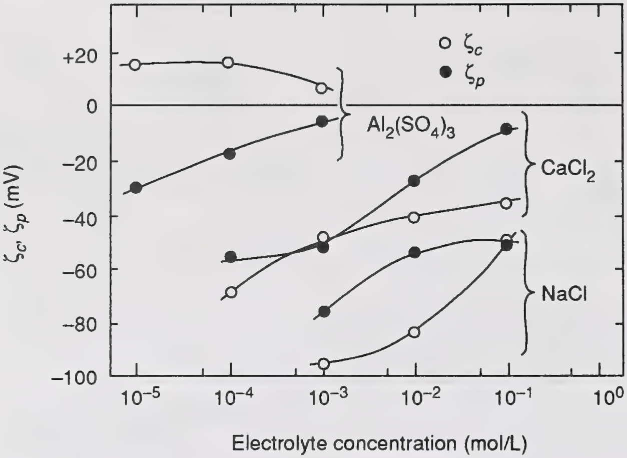

Figure 12-10. Variation of the zeta potential of air bubbles ζ_c and oil droplets ζ_p with electrolyte molarity (Okada *et al.*, 1988).

c_i and c_f are the initial and final oil droplets concentrations, respectively, in the flotation experiments, mg/L.

Okada *et al.* (1990a,b) also carried out a trajectory analysis similar to that of Section 11.4.1. For the case of flotation of oil droplets, they found that maximum flotability was achieved when the value of the dimensionless adhesion number $m = 4\pi\varepsilon\varepsilon_o\zeta_p\zeta_c/\kappa A$ was in the range of $m < 1.0$. Their dimensionless adhesion number is related to the electrostatic repulsion number N_ζ, which is defined by Eq. (11-78b). Figure 12-11 shows a comparison between the calculated collection efficiency using Eq. (11-77) and the experimentally measured values. The particles employed were polystyrene latex spheres with $a_p = 1.47 \times 10^{-6}$ m. Clearly, the zeta potentials of the particles and air bubbles play a crucial role in the collection efficiency. Fair agreement is evident between the theory and experiment.

From the above, the application of the DLVO theory coupled with the hydrodynamic interaction can be effectively used to study particle flotation in a systematic manner that can be very useful in optimizing solids and oil droplets collection in an industrial environment.

12.6 RHEOLOGY OF COLLOIDAL SYSTEMS

The rheology of a colloidal system is a very important property that influences the usage of the system in an industrial environment. In many situations, it is possible to alter the rheological behaviour of a colloidal suspension by changing the electrolyte concentration of the continuous aqueous phase or by anchoring long-chain polymers to the surface of the colloidal particles in the suspension.

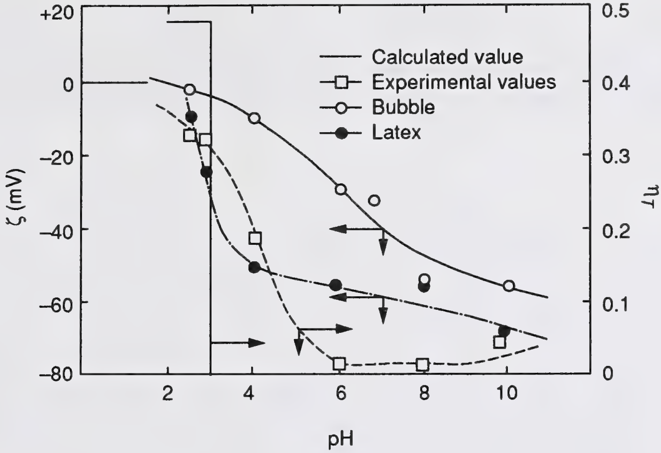

Figure 12-11. Comparison of calculated and experimental values of η_T, and effect of the zeta potentials of the bubble and particles on η_T in polyoxyethylene 23-lauryl ether solution (1×10^{-5} mol/L) with change of pH. The diameters of the bubbles and particles were 29.7 and 2.95 μm, respectively (Okada *et al.*, 1990b).

12.6.1 Historical Background

When a fluid is subjected to a simple shear, the shear stress τ required to produce a shear rate $\dot{\gamma}$ is given by

$$\tau = \mu(\dot{\gamma})\,\dot{\gamma} \tag{12-12}$$

The coefficient $\mu(\dot{\gamma})$ is known as the apparent viscosity of the fluid. When $\mu(\dot{\gamma})$ is independent of the shear rate, one can write

$$\tau = \mu\dot{\gamma} \tag{12-13}$$

where μ is a constant. Fluids obeying the formulation of Eq. (12-13) are known as Newtonian fluids. Water and simple organic liquids are Newtonian fluids.

Krieger and Eguiluz (1976) gave a tabulation of the dimensionless groups that control the rheology of a colloidal system under the influence of Brownian, viscous, and electrostatic forces. In the limiting case of negligible inertial effects and at steady state, the relative viscosity μ_r of a colloidal system is given by

(12-14) $\mu_r = \mu_s/\mu_c = f(\alpha_p, \tau_r, q_r, \kappa a_p)$

where μ_s and μ_c are the viscosities of the colloidal suspension and the continuous phase, respectively. α_p is the colloidal particles volume fraction. The dimensionless groups are τ_r, q_r, and κa_p where

$$\tau_r = \frac{\tau a_p^3}{kT} = \frac{\dot\gamma \mu_c a_p^3}{kT}$$ reduced shear stress

$$q_r = \frac{n_\infty e}{Nq}$$ charge ratio

and

$$\kappa a_p = \left[\frac{2 z^2 e^2 n_\infty}{\varepsilon\varepsilon_o kT}\right]^{1/2} a_p$$ dimensionless inverse Debye length for a $(z{:}z)$ electrolyte

It is possible to define a flow Peclet number Pe' as

$$Pe' = \frac{\dot\gamma a_p^2}{D_\infty}$$

Making use of the Stokes–Einstein relationship for the particle diffusion coefficient D_∞, *i.e.*,

$$D_\infty = \frac{kT}{6\pi a_p \mu_c}$$

the Peclet number becomes

$$Pe' = \frac{6\pi \dot\gamma \mu_c a_p^3}{kT} = 6\pi \tau_r$$

Rescaling Pe' one can write $Pe = \tau_r$. In some literature, the flow Peclet number Pe' is used in lieu of the reduced shear τ_r.

In the absence of electrostatic forces, the relative suspension viscosity becomes

$$\mu_r = f(\alpha_p, Pe)$$

Here, the viscosity of a suspension is affected only by the viscous forces, the Brownian motion, and the excluded volume of the particles. In such circumstances, the system is referred to as a "hard sphere model." In the limit of infinite dilution, *i.e.*, $\alpha_p \rightarrow 0$, the relative viscosity of a colloidal system becomes a function of the volume fraction only.

12.6.2 Hard Sphere Model

This is the case where only the viscous and Brownian motion forces are present. The relative viscosity is expected to depend only on the particles volume fraction and the flow Peclet number *Pe*. At a fixed volume fraction α_p, it is expected that rheological data for different particle sizes and for continuous phase viscosities μ_c collapse together when μ_r is plotted against *Pe*. This is indeed the case as is shown in Figure 12-12. The plot is an S-shaped curve characteristic of uncharged particles. For given continuous medium viscosity, temperature, and particle size, the plot of Figure 12-12 indicates that the relative viscosity of a colloidal suspension is a function of the shear rate $\dot{\gamma}$ and hence, by definition, exhibits non-Newtonian behaviour. In general, due to the Brownian diffusion, the relative viscosity of a suspension of colloidal particles can exhibit non-Newtonian characteristics. At low Peclet numbers, the Brownian motion dominates. However, at high Peclet numbers, the shearing force becomes dominant.

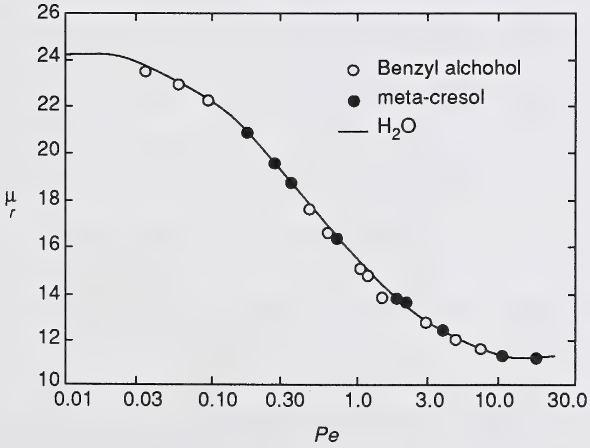

Figure 12-12. Relative viscosities *versus* Peclet number for $\alpha_p = 0.5$ monodispersions of polystyrene spheres of various sizes in different media (Krieger, 1972).

In both limiting cases, the colloidal suspension exhibits Newtonian characteristics. deKruif *et al.* (1986) gave the limiting values for the suspension viscosities as

$$(12\text{-}15)\quad \mu_0/\mu_c = \left(1 - \frac{\alpha_p}{0.63}\right)^{-2}$$

and

$$(12\text{-}16)\quad \mu_\infty/\mu_c = \left(1 - \frac{\alpha_p}{0.71}\right)^{-2}$$

where μ_0 and μ_∞ are the limiting viscosities at $Pe \to 0$ and $Pe \to \infty$, respectively. For a given colloidal system, μ_0 and μ_∞ correspond to $\dot{\gamma} \to 0$ (low shear rate) and $\dot{\gamma} \to \infty$ (high shear rate), respectively. The S-shaped curve can be cast (Krieger, 1972) as

$$(12\text{-}17)\quad \mu_r = \mu_0 + \frac{\left(\mu_0 - \mu_\infty\right)}{(1 + 2.32\, Pe)}$$

In the limit of infinite dilution, Einstein's result for the relative viscosity is given as

$$(12\text{-}18)\quad \mu_r = 1 + [\eta]\,\alpha_p + O\left(\alpha_p^2\right)$$

where $[\eta]$ is the intrinsic viscosity and has a value of 5/2 for the case of hard spheres. In the limit of $\alpha_p \to 0$, there should be no dependence of the relative viscosity on the flow Peclet number.

Batchelor (1977) extended Einstein's relationship for $Pe \ll 1$ to give

$$(12\text{-}19)\quad \mu_r = 1 + \left(\frac{5}{2}\right)\alpha_p + 6.2\,\alpha_p^2 + O\left(\alpha_p^3\right)$$

Figure 12-13 shows plots for Eqs. (12-15) to (12-19). It can be observed that the Einstein and Batchelor equations are only valid for $\alpha_p \lesssim 0.05$.

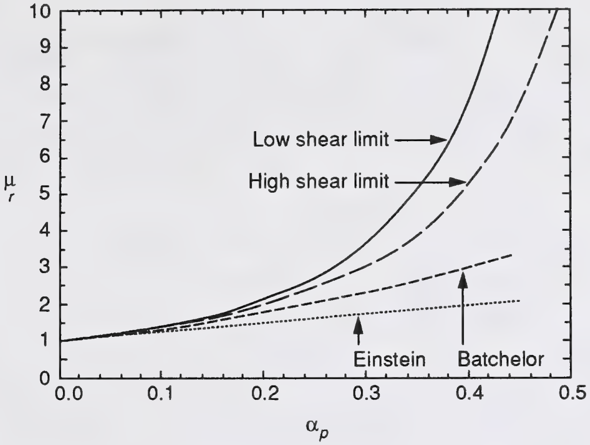

Figure 12-13. Variation of the relative viscosity of a colloidal suspension with the particles volume fraction. Hard sphere model.

12.6.3 Electroviscous Effects

Three distinct effects of the electrical charge on colloidal suspension rheology have been identified (Watterson and White, 1981). The first is known as the primary electroviscous effect. It arises from the distortion of the diffuse part of the electric double layer due to shear. The second is known as the secondary electroviscous effect. It arises from interparticle interactions which modify the particle trajectories and give rise to an increase in the effective particles excluded volume. The third is known as tertiary electroviscous effect. It is due to the expansion and contraction of the stabilizing polymer chains on the particle surface due to changes in the electrolyte concentrations (Hirtzel and Rajagopalan, 1985; Stein, 1985).

For dilute systems, the first electroviscous effect is more significant than the second effect as it influences the coefficient of $O(\alpha_p)$ in Eq. (12-19). The second electroviscous effect influences the coefficient of $O(\alpha_p^2)$ of Eq. (12-19). Consequently, the second electroviscous effect becomes significant for non-dilute colloidal suspensions (Russel, 1980).

The primary electroviscous effect was first identified by von Smoluchowski as being due to an enhanced energy dissipation rate caused by the interaction of the diffuse part of the electric double layer with the flow field. For a dilute system, in the presence of an electric double layer, the coefficient of α_p becomes

$$[\eta] = \left(\frac{5}{2}\right)[1 + E] \tag{12-20}$$

where $[1 + E]$ is the augmentation factor due to the presence of the electric double layer.

Watterson and White (1981) gave a plot of $[1 + E]$ as influenced by the dimensionless zeta potential $(e\zeta/kT)$ of the particles and inverse Debye length κa_p. Their plot is shown in Figure 12-14. For $\kappa a_p > 10$, *i.e.*, a thin electric double layer, the term $(1 + E)$ does not exceed 1.05 for $(e\zeta/kT)$ as high as 4 indicating little change in $[\eta]$ due to the first electroviscous effect. However, when the electric double layer is thick, *i.e.*, $\kappa a_p \ll 1$, the term $(1 + E)$ becomes appreciably greater than unity and the primary electroviscous effect becomes significant.

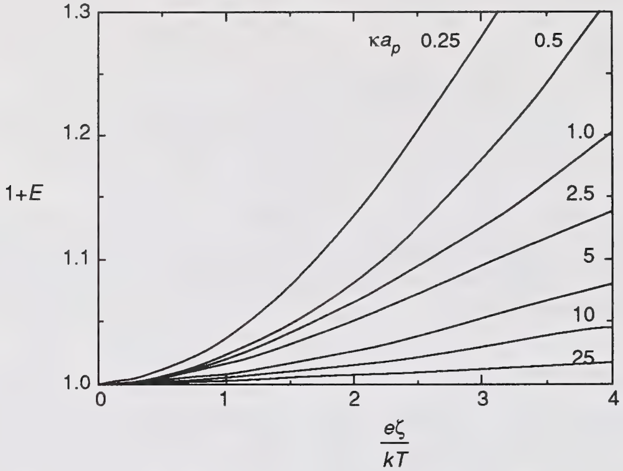

Figure 12-14. The primary electroviscous effect as a function of the electrokinetic potential in a (1:1) electrolyte solution (Watterson and White, 1981).

For non-dilute colloidal suspensions, the secondary electroviscous effect becomes significant where the probability of particle–particle interaction increases. Although in non-dilute colloidal systems both the primary and secondary electroviscous effects are present, the secondary effect becomes dominant at increasing particle concentrations. It is for this reason that one assumes that deviation from the hard sphere model at high concentrations is due to the secondary electroviscous effects.

Figure 12-15 shows variations of the relative viscosity of polystyrene latex with the continuous phase counterions concentration at different flow Peclet numbers for $\alpha_p = 0.509$. At high Pe, say $Pe = 100$, the relative viscosity is not sensitive to the variation of the electrolyte concentration. Here, the viscous forces are dominant. However, at lower Pe values, there is a sharp increase in the relative viscosity of the colloidal suspension with decreasing electrolyte concentration where κa_p is smaller and the effect of the electric double layer extends further away from the particle surface. For all values of Pe, there is a distinct minimum in the μ_r corresponding to an electrolyte concentration c_{min} that is independent of Pe. Electrolyte concentrations greater than c_{min} correspond to the flocculation of the colloidal system where the repulsive force becomes weaker with the addition of electrolytes.

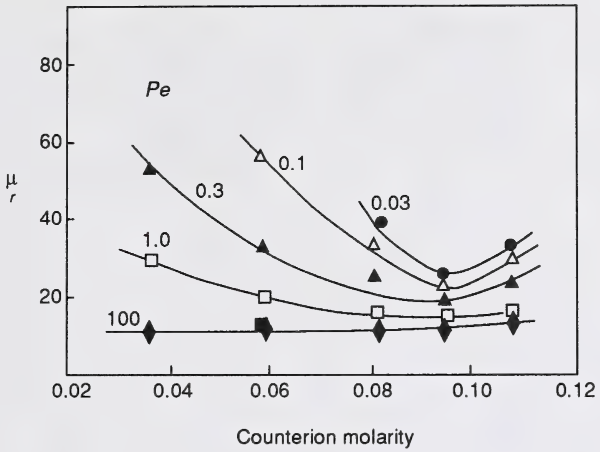

Figure 12-15. Effect of electrolyte molarity on the relative viscosity of monodisperse polystyrene latex, $a_p = 96 \times 10^{-9}$ m, $\alpha_p = 0.509$, pH = 2.7 with 2% anionic and 98% monoionic surfactants (Krieger, 1972).

Variation of the relative viscosity with the flow Peclet number is shown in Figure 12-16 for polystyrene latex particles, $\alpha_p = 0.4$ at different HCl concentrations ranging from 0 to 0.1 M. All curves tend to approach a common horizontal asymptote with an increasing *Pe* where the electroviscous forces are negligible in comparison to the viscous forces. According to Eq. (12-16) the asymptotic value is 5.25. At low *Pe* numbers (or shear stress), the viscosity of the deionized latex climbs as though approaching a vertical asymptote which is indicative of a yield stress. The apparent yield stress decreases with the addition of an electrolyte. At high electrolyte concentrations, there is no indication of a vertical asymptote and there is no possibility of a yield stress being present (Krieger and Eguiluz, 1976). The plot of Figure 12-16 suggests that the secondary electroviscous effects are extremely important in modifying the rheological behaviour of a colloidal suspension where the relative viscosity at a given *Pe* value can vary by several orders of magnitude.

A similar plot for polystyrene latex at $\alpha_p = 0.4$ is shown in Figure 12-17 where additions of K_2SO_4 and HCl are made. The Debye length has the same value when the concentration of HCl is double that of K_2SO_4. Figure 12-17 indicates that for given κa_p, the data collapse together onto one curve. The variation of the particles surface charge at the various HCL and K_2SO_4 concentrations was not reported.

The rheological behaviour of latex particles sterically stabilized by a polymer has been investigated by Willey and Moscosko (1978) and Liang *et al.* (1992). A plot of the relative viscosity of sterically stabilized monodisperse suspensions is given in Figure 12-18. For a given colloidal suspension, the relative viscosity increased sharply as the particles volume fraction approached its maximum packing value, a case similar to the hard sphere

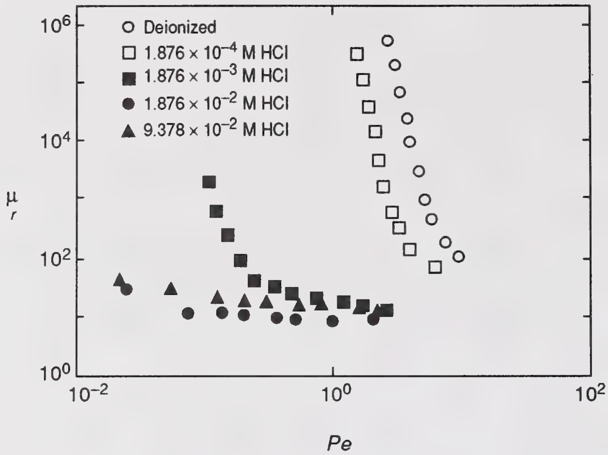

Figure 12-16. Variation of the relative viscosity of polystyrene latex ($a_p = 0.11 \times 10^{-6}$ m) at $\alpha_p = 0.4$ for various HCl concentrations (Krieger and Eguiluz, 1976).

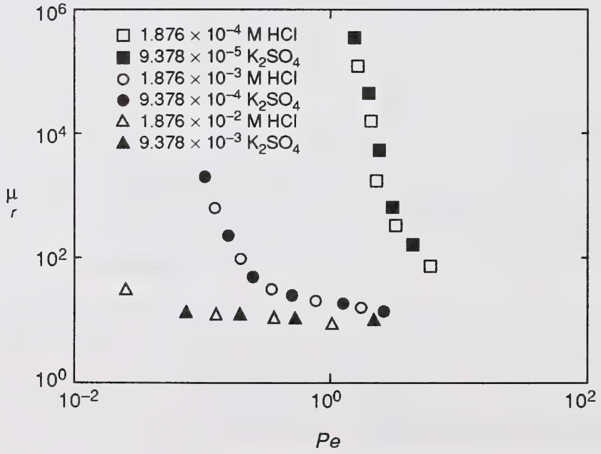

Figure 12-17. Effect on the relative viscosity due to different electrolytes at the same inverse Debye length (Krieger and Eguiluz, 1976).

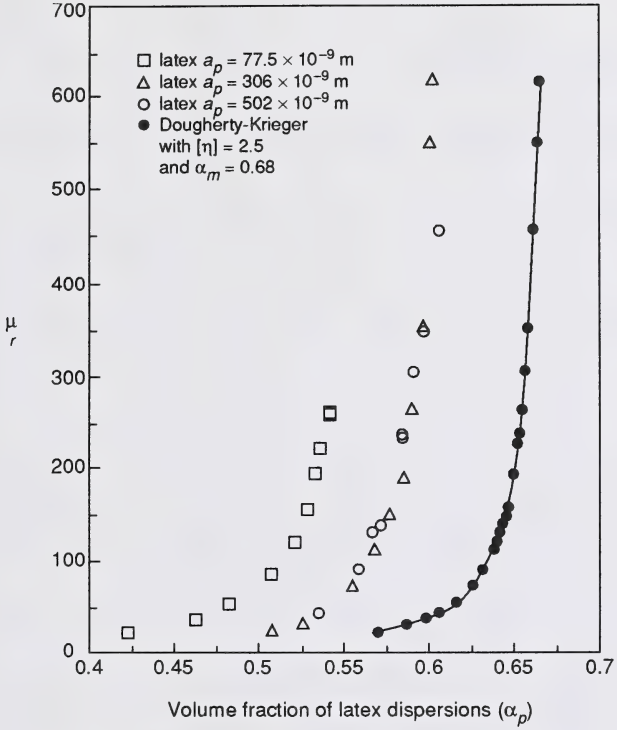

Figure 12-18. Relative viscosity *versus* volume fraction of polystyrene latex dispersions for various particle sizes (Liang *et al.*, 1992).

model. The relative viscosity data could be correlated using Dougherty and Krieger-type equation (Krieger, 1972) that was derived for a hard sphere model. The relative viscosity is given by

$$\mu_r = \left(1 - \frac{\alpha_p}{\alpha_m}\right)^{-[\eta]\alpha_m} \tag{12-21}$$

where α_m is the particles maximum packing volume fraction. It should be recognized that due to the attached polymeric chains at the colloidal particle surface, the volume fraction α_p is simply a nominal value. The effective volume fraction of the dispersed phase is given by

$$\alpha_{eff} = \alpha_p \left[1 + \left(\frac{\delta}{a_p} \right) \right]^3 \tag{12-22}$$

where δ is the polymeric chain length. δ is a function of the volume concentration α_p and shear rate $\dot{\gamma}$.

The relative viscosity data at $\alpha_p = 0.2$ of Willey and Macosko are plotted *versus* *Pe* in Figure 12-19 for a different PVC plastisol particle size and solvent quality. The collapse of the data onto a single curve would suggest that the PVC plastisols behave as an ideal colloidal suspension of rigid spheres subject to Brownian diffusion and they are little affected by the repulsive forces. The limiting relative viscosity value at $Pe \rightarrow 0$ is about 300. Comparison with the prediction from Eq. (12-15) indicates that a much greater effective volume fraction is operative than the nominal value of $\alpha_p = 0.2$ (Russel, 1980).

The rheology of a colloidal system is clearly a strong function of the operative colloidal forces. By altering the relative magnitude of these forces, it is possible to obtain the desired rheological characteristic. It is for this reason, among others, that colloidal suspensions have found many applications in paints, dyestuffs, and pharmaceutical and pesticidal formulations.

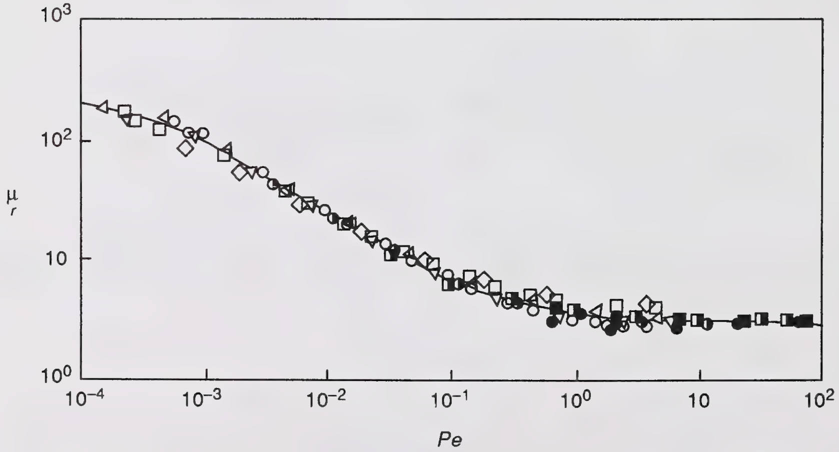

Figure 12-19. Relative viscosity of sterically stabilized PVC plastisols at α_p = 0.2 for different particle sizes and solvents (Willey and Macosko, 1978).

12.7 BITUMEN EXTRACTION FROM OIL SANDS

The total oil sands deposits in Alberta, Canada are estimated at 2×10^{11} m^3 of bitumen and the largest single deposit, in the Athabasca area, is estimated at 1.4×10^{11} m^3. Presently, there are two commercial plants that recover bitumen from oil sands in Alberta. Bitumen can be thought of as being a very viscous oil embedded within a sand matrix. The viscosity of bitumen at room temperature exceeds 10^3 Pa s. The bitumen content varies from 7 to 15% by weight for low and high grade deposits, respectively. The sand grains particle size varies from 300 μm to 0.1 μm. In the Athabasca deposit, the sand fraction with a size smaller than 44 μm increases with decreasing bitumen content in the oil sand (Camp, 1977).

The commercial process for bitumen recovery from oil sands uses the Clark hot water process that was developed in the 1920s (Clark and Pasternak, 1932). The hot water process consists of the following steps (Takamura, 1982):

1. The mined oil sands are agitated in a rotating drum (digester) in hot water with a small amount of added caustic to maintain a slurry pH in the range of 8 to 8.5. In the digester, the bitumen is physically separated from the sand grains. The digested slurry is composed of mineral solids, bitumen droplets attached to entrained air, and the suspending electrolyte solution.

2. The dispersed phases in the digested slurry are allowed to separate in settling vessels. The bitumen with its attached air is allowed to rise to the top of the settler constituting the primary bitumen recovery. The sand grains settle to the bottom of the settling vessels to form a dense slurry which is subsequently pumped to a tailings pond. Fine particulate matter, *e.g.*, clays and small bitumen droplets are removed from the middle of the settling vessel. This stream is called the middlings stream.

3. The middlings stream is fed to flotation cells to recover the suspended bitumen using conventional froth flotation.

Figure 12-20 shows a schematic process chart of the Clark hot water process.

It is generally assumed that the hydrophilic nature, *i.e.*, water-wetness of the sand grains, is an essential condition of the successful use of the hot water process (Camp, 1976).

For a high-grade oil sands deposit, the connate water is about 2–3% by weight. It is believed that this water is present as a thin layer that covers the entire surface of each sand grain. The presence of the connate water layer is an essential feature for the suitability of the hot water process. Under favourable conditions of extraction temperature, electrolyte concentration, and zeta potentials of bitumen and sand grains, the bitumen can be separated from the sand grains in the rotating drum. In contrast, the Utah tar sands deposits are characterized by hydrophobic sand grains and the absence of connate water. It is for this reason that the heavy oil cannot be recovered from the Utah deposits using the Clark hot water process.

Given the nature of the bitumen extraction process used in the commercial oil sands plants, electrokinetic principles can be used to guide us to formulate a better

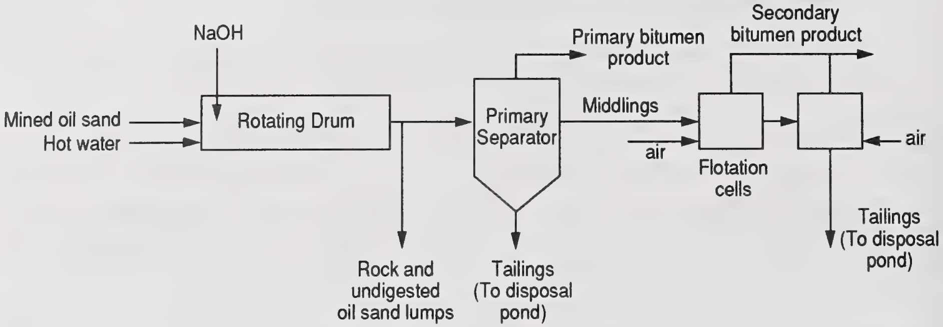
NaOH
Primary bitumen product
Secondary bitumen product
Mined oil sand
Hot water
Rotating Drum
Primary Separator
Middlings
air
Flotation cells
air
Tailings (To disposal pond)
Rock and undigested oil sand lumps
Tailings (To disposal pond)

Figure 12-20. Schematic process chart for the Clark hot water process.

understanding of the parameters that affect the bitumen recovery. To this end, the following topics will be discussed.

(a) Role of electrolyte concentration and type in the initiation of bitumen displacement from sand grains.

(b) Use of surface ionization models to predict bitumen and silica sand zeta potentials.

(c) Coagulation between bitumen, sand, and fines.

The following discussions are based on the studies conducted by Takamura and co-workers.

12.7.1 Initiation of Bitumen Displacement from Sand Grains

Simplified models of the structure of oil sand are shown in Figure 12-21. The earliest model is due to Cottrell who assumed that the sand grains are completely surrounded by a water film of a uniform thickness of about 10 nm. The clay minerals are assumed to be suspended in the water layer (Figure 12-21a). Dusseault and Morgenstern (1978) and Mossop (1980) refined the earlier model by assuming a grain-to-grain contact and by assuming that the clay minerals adhere directly to the sand grains. The presence of the thin connate water film surrounding the sand grain is due to the disjoining pressure within the connate water film. In other words, when two surfaces are pressed together in an electrolyte solution, the intervening electrolyte solution slowly thins out to leave an equilibrium film thickness (Blake, 1975). The liquid film behaves as though there is an excess pressure acting normal to the film and opposing further reduction in its thickness. The excess pressure or disjoining pressure is due to the electric double-layer repulsive force and the London–van der Waals attractive force (Takamura, 1982). In the case of oil sands, the two surfaces are the bitumen and the sand grain surfaces as shown in Figure 12-22. The disjoining pressure within the connate water layer is responsible for maintaining the presence of water layer through the millennium and also it plays a major role in the displacement of bitumen from the sand grains. The process of bitumen displacement is discussed below.

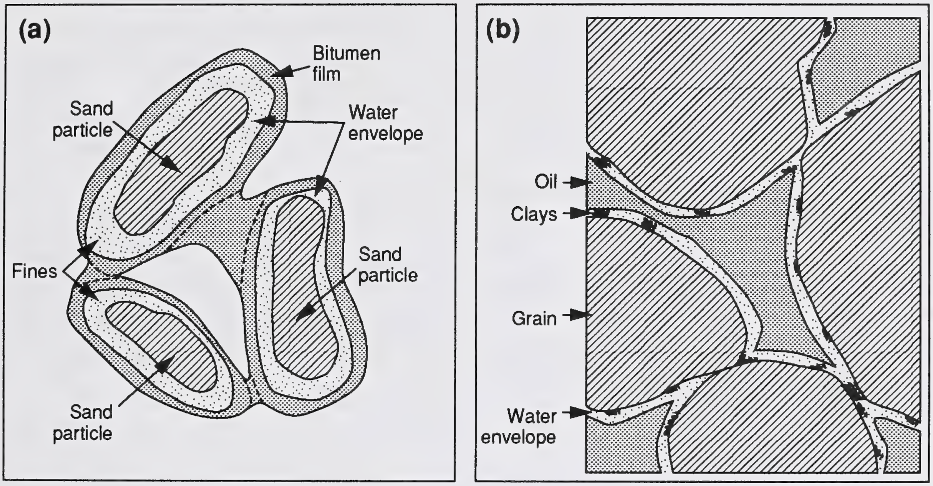

Figure 12-21. Schematic model structures of oil sands: (a) Cottrell, 1963 and (b) Mossop, 1980.

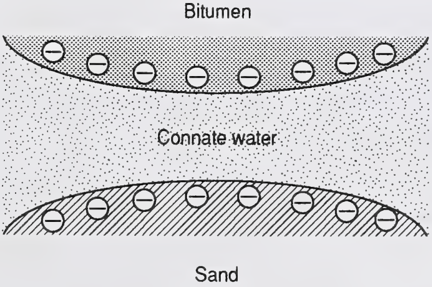

Figure 12-22. Schematic diagram showing the connate water separating the sand grain surface from the bitumen.

Takamura (1982) assumed that the disjoining pressure is given by

$$P = P_{rep}(h) + P_{att}(h) \tag{12-23}$$

The short range hydration forces are assumed to be negligible when h is less than a few nanometres (Israelachvili and Adams, 1978). The electric double-layer force per unit area for parallel plates having constant surface potentials is given by

$$P_{rep}(h) = n_\infty kT \frac{\left[2y_s y_b \cosh(\kappa h) - y_s^2 - y_b^2\right]}{\sinh^2(\kappa h)} \tag{12-24}$$

where y_b and y_s are the dimensionless zeta potentials of bitumen and sand, respectively. Here, it is assumed that the zeta potential and surface potential are the same. The dimensionless zeta potential is given by

$$y = \frac{ze\zeta}{kT} \tag{12-25}$$

κ is the inverse Debye length and it is given by

$$\kappa^2 = \frac{2\, e^2\, z^2\, n_\infty}{\varepsilon\varepsilon_o\, kT} \tag{12-26}$$

Expression (12-24) was derived in Section 3.8.

The retarded London–van der Waals attractive force per unit area between two parallel plates can be expressed as (Gregory, 1981)

$$P_{att}(h) = -A_{bms} \frac{(15.96\, h/\lambda + 2)}{12\pi h^3 (1 + 5.32\, h/\lambda)^2} \tag{12-27}$$

where A_{bms} is the Hamaker constant for the bitumen-electrolyte intervening medium-sand. λ is the London wavenumber taken as 100 nm. The individual Hamaker constants in vacuum are taken as $A_{bb} = 5.7 \times 10^{-20}$ J, $A_{ss} = 1.5 \times 10^{-20}$ J, and $A_{mm} = 3.7 \times 10^{-20}$ J for bitumen–bitumen, sand–sand, and the intervening medium, respectively.

The overall Hamaker constant A_{bms} can be evaluated using Eq. (9-19); *i.e.*

$$A_{bms} = (A_{ss} A_{bb})^{1/2} + (A_{mm} A_{mm})^{1/2} - (A_{mm} A_{ss})^{1/2} - (A_{mm} A_{bb})^{1/2}$$

However, Takamura and Chow (1983) made use of the Lifshitz theory and estimated A_{bms} as 1.0×10^{-20} J. The latter value was used in their calculation of the disjoining pressure. The composition of the connate water in the Athabasca oil sand is approximately that of a NaCl solution having a concentration range between 30 and 100 mM. However, small amounts of K^+, Ca^+, and Mg^{++} ions are also present.

The disjoining pressure between bitumen and sand is calculated by Takamura and co-workers at different conditions as shown in Figure 12-23. For the case of connate water with 0.1 M NaCl at pH = 5.6 and NaOH at pH = 11.5, repulsive forces exist. However, if NaOH is replaced by $CaCl_2$ at 0.01 M, an attractive disjoining pressure would result.

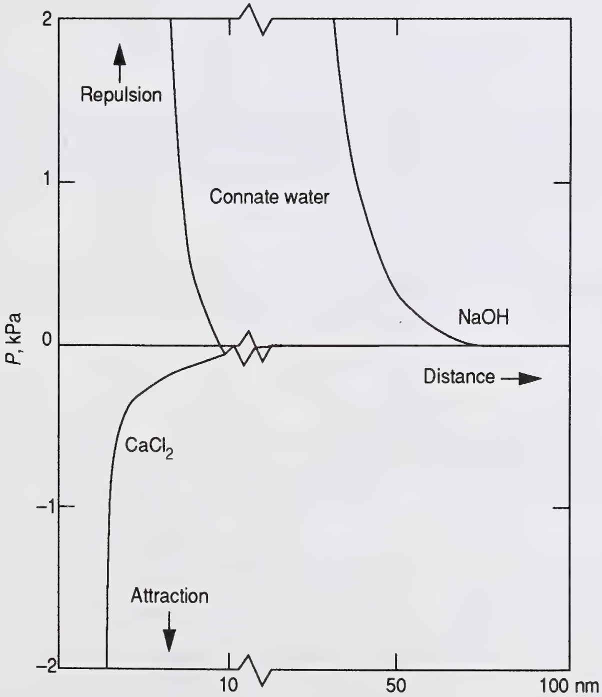

Figure 12-23. Calculated disjoining pressure between sand and bitumen surfaces with separation distance. Connate water having 0.1 M NaCl at pH 5.6, NaOH with pH 11.5, and $CaCl_2$ at 0.01 M (Takamura, 1982).

Takamura and co-workers suggested that the presence of the repulsive force is responsible for maintaining the existence of the connate water in the deposit through the millennia. Moreover, addition of NaOH in the processing of the oil sand is also important. In the rotating drum, the oil sand is agitated in hot water in the presence of NaOH. Under the shearing conditions within the slurry mixture in the rotating drum, the bitumen is sheared away from the sand grains. As the bitumen recedes from the sand grain, a repulsive force exists between the bitumen and the sand grain. Hence the bitumen can disengage completely from a sand grain resulting in a good separation between bitumen and mineral solids. Such a complete separation gives a high bitumen recovery. As the amount of NaOH affects the zeta potentials of the sand and bitumen and the Debye length, one would expect that bitumen recovery is a function of NaOH concentration. Experience from the commercial bitumen recovery plants gives similar conclusions.

For the case of 0.01 M $CaCl_2$, Figure 12-23 shows that for all separation values, attraction forces are present between the sand and the bitumen. This would indicate that disengagement between bitumen and sand cannot occur as bitumen would adhere to the sand grains. Indeed, it is well recognized in the oil sands industry that covalent ions are detrimental to bitumen recovery. A schematic illustration of bitumen disengagement behaviour for the case of NaOH and $CaCl_2$ is shown in Figure 12-24.

It is clear from the above discussion that the use of the DLVO theory is fairly helpful in the understanding of bitumen recovery. We now turn our attention to the use of ionization models to predict zeta potentials of bitumen and sand.

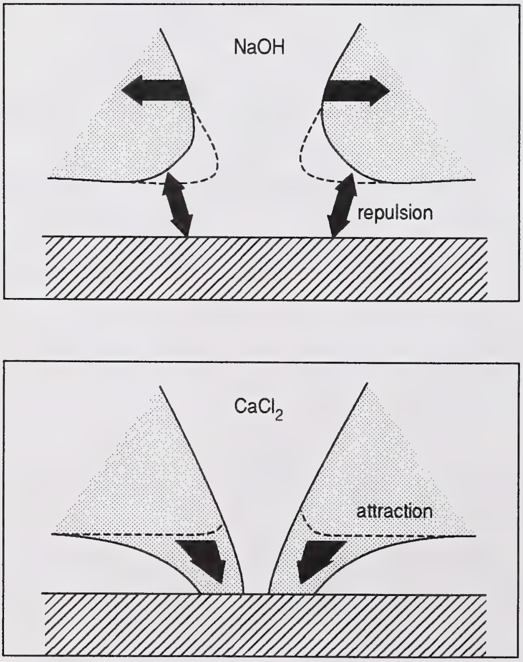

Figure 12-24. Schematic diagram showing (a) the receding of bitumen in an NaOH environment and (b) attachment of bitumen in $CaCl_2$ environment (Takamura, 1982).

12.7.2 Surface Ionization Models

Takamura and co-workers made use of surface ionization models to estimate the zeta potentials of bitumen and mineral solids. The values of zeta potentials can be used to estimate the interaction potential between bitumen–bitumen, bitumen–mineral solids, and mineral solids–mineral solids.

For the case of bitumen, the surface charge of the bitumen–water interface is derived from the dissociation of carboxyl groups (Takamura, 1985; Takamura and Chow, 1985).

$$RCOOH \rightleftharpoons RCOO^- + H^+$$

This is equivalent to Model II presented in Section 3.7.2. The $RCOO^-$ group is equivalent to the A^- group. The dissociation K_a is given by

$$K_a = \frac{[RCOO^-]_s \, [H^+]_o}{[RCOOH]_s} \tag{12-28}$$

$[\ ]_s$ denotes concentration at the surface within the bitumen phase and $[\ ]_o$ denotes concentration at the surface within the electrolyte solution. Following the analysis presented in Chapter 3, one can show that the surface charge density q_s is given by

$$q_s = \frac{-e\,[n]_s}{1 + \left[\frac{[H^+]_b}{K_a}\right] \exp\left(-\frac{e\,\psi_s}{kT}\right)} \tag{12-29}$$

This surface charge density must be balanced by the charge density within the electric double layer q_{dl} (see Eq. (3-70)):

$$q_{dl} = -\left[8\,\varepsilon\varepsilon_o\,kT\,n_\infty\right]^{1/2} \sinh\left(\frac{e\psi_s}{2\,kT}\right) \tag{12-30}$$

where n_∞ is the bulk counterions number concentration, m^{-3} and

$$q_s + q_{dl} = 0 \tag{12-31}$$

$[n]_s$ is the total surface ionizable groups concentration and $[H^+]_b$ is the hydronium ion concentration in the bulk solution. $[H^+]_b$ is related to the pH by

$$-\log_{10}\left\{\frac{[H^+]_b}{(1000\,N_a)}\right\} = \text{pH}$$

For given values of $[n]_s$ and K_a, Eqs. (12-29) to (12-31) can be solved simultaneously to evaluate the surface potential of the bitumen ψ_s, which is related to the zeta potential by

$$\text{(12-32)}\quad \zeta = \psi(x) = \frac{2kT}{ze}\, ln\, \frac{1 + \gamma_s \exp(-\kappa x)}{1 - \gamma_s \exp(-\kappa x)}$$

where

$$\text{(12-33a)}\quad \gamma_s = \frac{\exp\left(\frac{y_s}{2}\right) - 1}{\exp\left(\frac{y_s}{2}\right) + 1}$$

and

$$\text{(12-33b)}\quad y_s = \frac{ze\psi_s}{kT}$$

x is the location of the shear plane and it is taken as 0.6×10^{-9} m. Here, $\zeta = \psi\,(0.6 \times 10^{-9})$ and $\psi_s = \psi(0)$.

Measurements of the zeta potential for bitumen were carried out by Takamura and Chow (1985). They showed that the surface ionization model can represent the experimental zeta potential data for bitumen by setting $pK_a' = 4.5$, $[n]_s = 2.8 \times 10^{18}$ m^{-2}, and $x = 0.6 \times 10^{-9}$ m. Here K_a' is the value of K_a expressed in mol/L and K_a is given by m^{-3}.

The application of the ionizable surface groups model was also extended to the case of sand (silica). The silica surface becomes positively or negatively charged by one of the following surface dissociation reactions (Healy and White,1978; Takamura and Wallace, 1988):

$$\text{(12-34a)}\quad -SiOH_2^+ \rightleftharpoons -SiOH + H^+$$

and

$$\text{(12-34b)}\quad -SiOH \rightleftharpoons -SiO^- + H^+$$

The dissociation constants K_+ and K_- are defined as

$$K_+ = \frac{[SiOH]_s \, [H^+]_o}{[SiOH_2^+]_s} \tag{12-35a}$$

and

$$K_- = \frac{[SiO^-]_s \, [H^+]_o}{[SiOH]_s} \tag{12-35b}$$

The units of K_+ and K_- are m^{-3}.

The hydronium ion concentration $[H^+]_o$ is related to its bulk value by the Boltzmann distribution as given by Eq. (3-86). The surface charge density is given by

$$q_s = \frac{e[n]_s \left\{ \left([H^+]_b / K_+ \right) \exp(-y_s) - \left(K_- / [H^+]_b \right) \exp(y_s) \right\}}{1 + \left([H^+]_b / K_+ \right) \exp(-y_s) + \left(K_- / [H^+]_b \right) \exp(y_s)} \tag{12-36}$$

where the total surface density of the functional groups is given by

$$[n]_s = [\mathrm{SiOH}_2^+]_s + [\mathrm{SiOH}]_s + [\mathrm{SiO}^-]_s$$

For given values of K_-, K_+, and $[n]_s$ simultaneous solution of Eq. (12-36) with Eqs. (12-30) and (12-31) provide the surface potential ψ_s. Table 12-1 gives the best estimates of the adjustable parameters that gave the best fit with the measured zeta potential of sand (mineral solids) and fines (kaolinite) using experimental data from Takamura and his co-workers.

Figure 14-25 shows comparisons between the calculated (fitted) and measured zeta potentials of bitumen. The three-parameter model, *i.e.*, x, K_a, and $[n]_s$, is quite adequate in the prediction of the bitumen zeta potential. Figure 14-25 shows that the zeta potential of the bitumen is sensitive to pH, *i.e.*, to NaOH addition.

The variations of the zeta potentials for the cases of silica sand and fines (kaolinite) are shown in Figure 12-26. The parameter values of Table 12-1 are used. The zeta potentials of the mineral solids and bitumen are again sensitive to pH.

Table 12-1. Parameters used to calculate the zeta potential of bitumen, sand, and fines particles (Takamura and Wallace 1988)

Material	pK'_a	pK'_+	pK'_-	$[n]_s$, m^{-2}	x, m
Bitumen	4.5			2×10^{18}	0.6×10^{-9}
Sand		0.6	7.2	10^{18}	$-10^{-9} \log_{10} S$
Fines		5.0	7.0	10^{18}	$-10^{-9} \log_{10} S$

S is the concentration of Na$^+$ in mol/L.

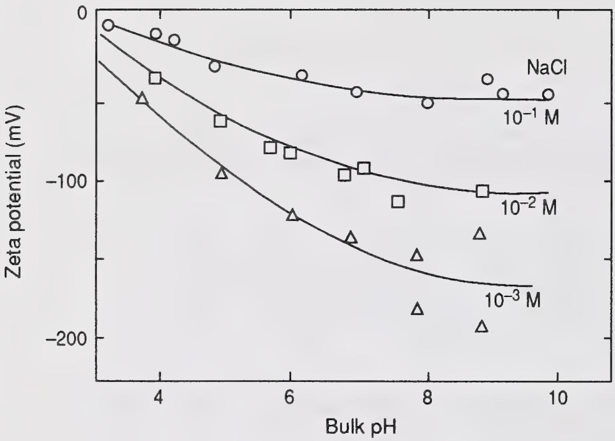

Figure 12-25. Variation of bitumen zeta potential at 25°C with bulk pH at different NaCl concentrations, solid lines, theory; symbols, experimental (Takamura and Isaacs, 1989).

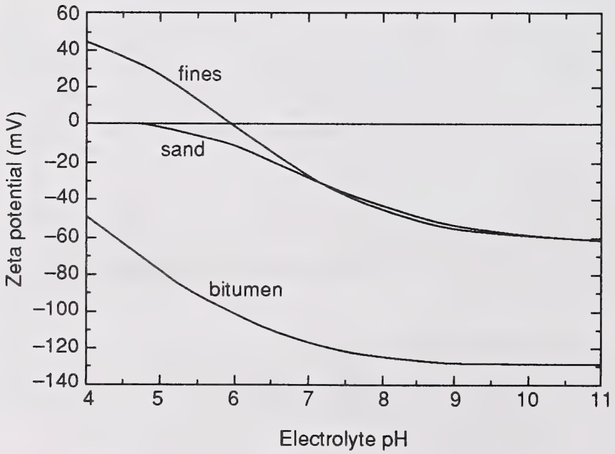

Figure 12-26. Variation of zeta potential with pH at 80°C with 0.01 M NaCl.

The use of the surface ionization model as a tool for predicting the zeta potentials of bitumen and mineral solids proved quite useful in the analysis of the interaction between the bitumen and mineral solids in the hot water process.

12.7.3 Bitumen Recovery

During the digestion step of the oil sand in the rotating drum, the bitumen separates from the sand grains and disperses in the digested slurry together with the fines mineral particles including clays and coarse sand (*e.g.*, silica). During the digestion step, the formation of large bitumen droplets is desirable as it increases their rise velocity and enhances their attachment to air bubbles. During the digestion stage, it is also desirable to minimize the coagulation of fines–fines, bitumen–fines, and bitumen–sand. Coagulation of fines–fines would increase the viscosity of the suspension (slurry) and consequently would slow down the separation between the bitumen droplets and the mineral solids. Attachment of bitumen droplets with fines and sand should also be minimized. Large aggregates of coagulated bitumen–fines or bitumen–sand do not float but rather settle together with the coarse sand and are not recovered in the hot water process. The coagulation analysis is presented below.

The total interaction potential for two spherical particles is considered to be the sum of the electric double-layer potential and the London–van der Waals potential (Takamura and Wallace, 1987,1988; Takamura and Isaacs, 1989). The Hogg *et al.* (1966) expression for the electrostatic potential can be used as given by Eq. (3-124). The retarded London–van der Waals potential for unequal spheres 1 and 2 is given by Gregory (1981) as

$$V_A = -A_{132} \frac{a_1 a_2}{6\left(a_1 + a_2\right) h} \left[1 - \frac{5.32\,h}{\lambda}\, ln\left(1 + \frac{\lambda}{5.32\,h}\right)\right]$$

where A_{132} is the overall Hamaker constant for particles 1 and 2 with the intervening medium being 3. a_1 and a_2 are the radii of particles 1 and 2, respectively. The zeta potentials of bitumen, sand, and fines are evaluated using the surface ionization models.

The plot of Figure 12-27 shows the three types of particle interactions, namely bitumen–bitumen, bitumen–fines, and fines–fines. When the maximum in the total energy is small, coagulation is to be expected. The value of the total potential at the primary maximum can be used as a criterion for a dispersion stability (Prieve and Ruckenstein, 1980). Takamura and co-workers used a value of 400 kT to distinguish between a stable and a coagulated dispersion. This value was selected based on batch extraction experiments. It should be recognized, however, that a value of 400 kT is fairly high as was pointed out by Czarnecki and Smith (1990). Nevertheless, the results given by Takamura and co-workers are quite useful in understanding the hot water process.

Figure 12-27 shows that at the same pH level but at different NaCl concentrations, the value of the primary maximum decreases with increasing levels of NaCl indicating that higher NaCl levels would lead to coagulation. In the commercial bitumen extraction process, increased values of NaCl in the mined oil sands lead to lower bitumen recovery.

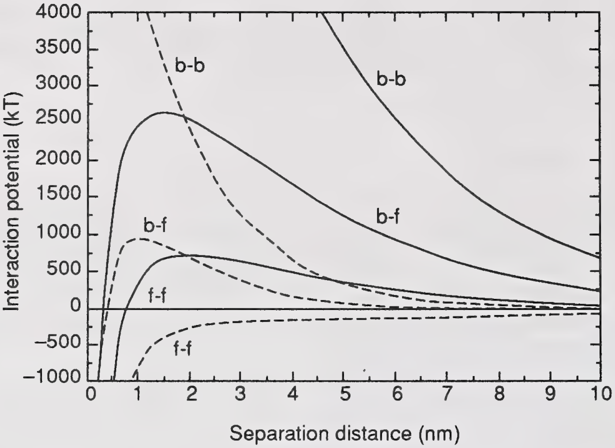

Figure 12-27. Variation of the interaction potential with the separation distance at 80°C for 5 μm particles at pH = 8: ——— 0.01 M NaCl; – – – 0.04 M NaCl

Figure 12-28 shows a stability diagram that was constructed using the 400 kT criterion for 5 μm diameter kaolinite particles. This plot suggests that hydroxyl ions and sodium ions play significant roles in the dispersion stability *via* the fines–fines interaction. The maximum tolerable level of sodium ions in the digestion stage is about 50 mM as indicated by Figure 12-28.

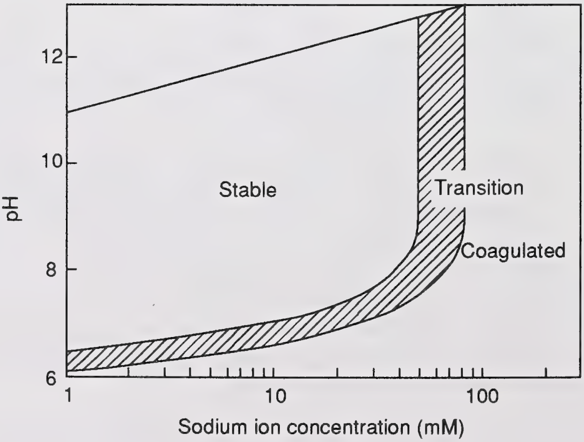

Figure 12-28. Stability diagram for 5 μm diameter kaolinite particles (Takamura and Wallace, 1988).

The studies of Takamura and his co-workers show that the DLVO theory can qualitatively describe the hot water process as employed for bitumen extraction. No data for the zeta potential are available for the air bubbles and consequently, it is not possible to analyse fines and bitumen flotation in the Clark hot water process.

Although discussions were centered on electrokinetic phenomena, surfactants present in the bitumen also play an important role in the bitumen recovery (Schramm *et al.*, 1984; Schramm and Smith, 1985). Surfactant effects were not addressed here.

12.8 NOMENCLATURE

a	capillary tube radius, m
a_p	particle radius, m
A	Hamaker constant, J
A_{bb}	Hamaker constant for bitumen in vacuum, J
A_{bms}	overall Hamaker constant for bitumen-medium-sand, J
A_{mm}	Hamaker constant for intervening medium in vacuum, J
A_{ss}	Hamaker constant for sand in vacuum, J
BGL	blood glucose level
c_f	final oil droplet concentration, mg/L
c_i	initial oil droplet concentration, mg/L
c_1	inlet ionic concentration, mol/m^3
c_2	outlet ionic concentration, mol/m^3
$\bar{c}$	dimensionless ionic concentration
$c(x)$	ionic concentration at an axial distance x along the capillary central axis
$c_\pm(x,r)$	ionic concentration, mol/m^3
C_{sc}	electric capacitance of the stratum corneum, F
D_∞	diffusion coefficient in infinite dilution, m^2/s
e	fundamental charge, C
F	Faraday constant, C/mol
J_s	total flux of dissociated salt, mol/s
k	Boltzmann constant, J/K
K_a	dissociation constant given as $K_a = 1000\,K'_a N_a$, m^{-3}

K_-	dissociation constant given as $K_- = 1000\, K'_-\, N_{a,}$ m^{-3}
K_+	dissociation constant given as $K_+ = 1000\, K'_+\, N_{a,}$ m^{-3}
K'_a	dissociation constant expressed as mol/L
K'_-	dissociation constant expressed as mol/L
K'_+	dissociation constant expressed as mol/L
L	capillary tube length, m
n_∞	bulk counterion concentration for (1:1) electrolyte, m^{-3}
n_∞	bulk ionic number concentration, m^{-3}
$[n]_s$	total ionizable surface groups density, m^{-2}
N	particle concentration, m^{-3}
N_a	Avogadro number, mol^{-1}
N_ζ	electrostatic repulsion number
P	disjoining pressure, Pa
Pe	flow Peclet number
$P_{att}(h)$	force per unit area due to attractive London–van der Waals interaction at a separation distance h, Pa
$P_{rep}(h)$	force per unit area due to electrostatic repulsion at a separation distance h, Pa
pK'	$-\log_{10} K'$
q	charge on particle, C
q_{dl}	charge density due to electric double layer, C/m^2
q_r	charge ratio, dimensionless
q_s	surface charge density, C/m^2
r	radial distance, m
R	dimensionless radial distance
Rej	salt rejection coefficient
R_{sc}	electrical resistance of the stratum corneum, Ω
R_{vs}	electrical resistance of viable skin, Ω
T	temperature, K
$u_x(r)$	local axial velocity, m/s
V	average fluid velocity, m/s

x	axial distance, m
x	location of shear plane, m
$\bar{x}$	dimensionless axial distance
y_s	dimensionless zeta potential for sand or at a surface
y_b	dimensionless zeta potential for bitumen or at a surface
z	valency
$[\ ]_b$	number bulk concentration, m^{-3}
$[\ ]_o$	number concentration at the surface within the electrolyte solution, m^{-3}
$[\ ]_s$	number concentration at the surface within the solid or bitumen phase, m^{-2}

α_m	volume fraction of particles at maximum packing
α_p	volume fraction of dispersed phase
$\dot{\gamma}$	shear rate, s^{-1}
δ	polymeric chain length, m
ε	dielectric constant, dimensionless
ε_o	permittivity of vacuum, C/mV
ζ_c	zeta potential of a collector (*e.g.*, air bubble), V
ζ_p	zeta potential of a particle (*e.g.*, bitumen or solid particle), V
η_T	flotation efficiency
$[\eta]$	intrinsic viscosity
κ	inverse Debye length, m^{-1}
λ	dimensionless Debye length, m
λ	London wave number, m
λ_D	Debye length, m
λ_1	dimensionless Debye length at capillary inlet
μ	fluid viscosity, Pa s
μ_c	continuous phase viscosity, Pa s
μ_0	limiting suspension viscosity at $\dot{\gamma} \to 0$
μ_r	relative suspension viscosity, μ_s/μ_c

μ_s	colloidal suspension viscosity, Pa s
μ_∞	limiting suspension viscosity at $\dot{\gamma} \rightarrow \infty$
$\rho^{(f)}$	free charge density, C/m^3
τ	shear stress, N/m^2
τ_r	reduced shear, dimensionless
$\phi(x)$	induced potential, V
$\Phi(x)$	total potential, V
$\psi(x)$	surface potential of bitumen or mineral solids at location x, V
$\psi(r,x)$	potential due to electric double layer, V
$\overline{\psi}(r,x)$	dimensionless potential due to electric double layer
ψ_s	surface potential of bitumen or mineral solids, V
$\overline{\psi}_w$	capillary wall potential, dimensionless

12.9 REFERENCES

Banga, A.K. and Chien, Y.W. (1988), *Iontophoretic Delivery of Drugs: Fundamentals, Developments and Biomedical Applications*, J. Controlled Release, **7**, 1–24.

Batchelor, G.K. (1977), *The Effect of Brownian Motion on the Bulk Stress in a Suspension of Spherical Particles*, J. Fluid Mechanics, **83**, 97–117.

Blake, T.D. (1975), *Investigation of Equilibrium Wetting Films on* n-*Alkanes on* α-*Alumina*, J. Chem. Soc. Faraday Trans. I, **71**, 192–208.

Camp, F.W. (1976), *The Tar Sands of Alberta, Canada*, Cameron Engineers Inc., Colorado, U.S.A.

Camp, F.W. (1977), *Processing Athabasca Tar Sands — Tailings Disposal*, Can J. Chem. Eng., **55**, 581–91.

Chien, Y.W. (1982), *Novel Drug Delivery Systems*, Marcel Dekker, New York.

Clark, K.A. and Pasternak, D.S. (1932), *Hot Water Separation of Bitumen from Alberta Bituminous Sand*, Ind. Eng. Chem., **34**, 1410–16.

Collins, G.L. and Jameson, G.J. (1977), *Double-Layer Effects in the Flotation of Fine Particles*, Chem. Eng. Sci., **32**, 239–46.

Cottrell, J.H. (1963), *in K.A. Clark Volume* (ed. Carrigy, M.), Alberta Research Council, Edmonton, Alberta, Canada.

Czarnecki, J. and Smith, R. (1990), *The Physical Chemistry of the Hot Water Process*, J. Can. Pet. Tech., **29** (November Supplement) 72–73. Reply by Wallace, D., Chow, R., and Takamura, K., 74–75.

deKruif, C.G., van Iersel, E.M.F., Vry, A., and Russel, W.B. (1986), *Hard Sphere Colloidal Dispersions: Viscosity as a Function of Shear Rate and Volume Fraction*, J. Chem. Phys., **83**, 4717–25.

Dusseault, M.B. and Morgenstern, N.R. (1978), *Shear Strength of Athabasca Oil Sands*, Can. Geotech. J., **15**, 216–38.

Gregory, J. (1981), *Approximate Expressions for Retarded van der Waals Interactions*, J. Colloid Interface Sci, **83**, 138–45.

Happel, J. (1958), *Viscous Flow in Multiparticle Systems*, AIChEJ, 4, 197–201.

Harris, R. (1967), *Iontophoresis*, in *Therapeutic Electricity and Ultraviolet Radiation* (ed. Licht, S.), Waverly Press, Baltimore, MD.

Healy, T.W. and White, L.R. (1978), *Ionizable Surface Group Models of Aqueous Interfaces*, Advances Colloid Interface Science, **9**, 303–45.

Hirtzel, C.S. and Rajagopalan, R. (1985), *Colloidal Phenomena. Advanced Topics*, Noyes Pub., N.J.

Hogg, R., Healy, T.W., and Fuerstenau, D.W. (1966), *Mutual Coagulation of Colloidal Dispersions*, Trans. Faraday Soc., **62**, 1638–51.

Hung, Y.T. (1978), *Evaluation of Flotation and Sedimentation in Treating Oil Refinery Wastes*, Proc. N.D. Acad. Sci., **30**, 51–63.

Israelachvili, J.N. and Adams, G.E. (1978), *Measurement of Forces Between Two Mica Surfaces in Aqueous Electrolyte Solution in Range 0–100 nm*, J. Chem. Soc. Faraday Trans. *I*, **74**, 975–1001.

Jacazio, G., Probstein, R.F., Sonin, A.A., and Yung, D. (1972), *Electrokinetic Salt Rejection in Hyperfiltration Through Porous Materials. Theory and Experiment*, J. Phys. Chem., **76**, 4015–23.

Krieger, I.M. (1972), *Rheology of Monodisperse Lattices*, Advances Colloid Interface Science, **3**, 111–36.

Krieger, I.M. and Eguiluz, M. (1976), *The Second Electroviscous Effect in Polymer Lattices*, Trans. Soc. of Rheology, **20**, 29–45.

Liang, W., Tadros, The. F., and Luckham, P.F. (1992), *Rheological Studies on Concentrated Polystyrene Latex Sterically Stabilized by Poly (ethylene oxide) Chains*, J. Colloid Interface Sci., **153**, 131–39.

Liu, J-C, Sun Y., Siddiqui, O., Chien, Y.W., Shi, W.-M., and Li, J. (1988), *Blood Glucose Control in Diabetic Rats by Transdermal Iontophoretic Delivery of Insulin*, Int. J. Pharmaceutics, **44**, 197–204.

Mossop, G.D. (1980), *Geology of the Athabasca Oil Sands*, Science, **207**, 145–52.

Okada, K. and Akagi, Y. (1987), *Method and Apparatus to Measure the ζ-Potential of Bubbles*, J. Chem. Eng. Japan, **20**, 11–15.

Okada, K., Akagi, Y., Kogure M., and Yoshioka, N. (1988), *Effect of Zeta Potentials of Oil Droplets and Bubbles on Flotation of Oil-in-Water Mixtures*, Can. J. Chem. Eng., **66**, 276–81.

Okada, K., Akagi, Y., Kogure M., and Yoshioka, N. (1990a), *Effect on Surface Charges of Bubbles and Fine Particles on Air Flotation Process*, Can. J. Chem. Eng., **68**, 393–99.

Okada, K., Akagi, Y., Kogure M., and Yoshioka, N. (1990b), *Analysis of Particle Trajectories of Small Particles in Flotation When the Particles and Bubbles are Both Charged*, Can. J. Chem. Eng., **68**, 614–21.

Pal, R. and Masliyah, J. (1990), *Oil Recovery from Oil in Water Emulsions Using a Flotation Column*, Can. J. Chem. Eng., **68**, 959–67.

Prieve, D.C. and Ruckenstein, E. (1980), *Role of Surface Chemistry in Primary and Secondary Coagulation and Heterocoagulation*, J. Colloid Interface Sci., **73**, 539–55.

Renaud, P.C. and Probstein, P.F. (1987), *Electroosmotic Control of Hazardous Wastes*, PCH Physico-Chemical Hydrodynamics, **9**, 345–60.

Russel, W.B. (1980), *Review of the Role of Colloidal Forces in the Rheology of Suspensions*, J. Rheology, **24**, 287–317.

Schramm, L.L., Smith, R.G., and Stone, J.A. (1984), *The Influence of Natural Surfactant Concentration on the Hot Water Process for Recovering Bitumen from the Athabasca Oil Sands*, AOSTRA J. Res., **1**, 5–13.

Schramm, L.L. and Smith, R.G. (1985), *Influence of Natural Surfactants on Interfacial Charges in the Hot Water Process for Recovering Bitumen from the Athabasca Oil Sands*, Colloids and Interfaces, **14**, 67–85.

Schwendeman, S.P., Amidon, G.L., Meyerhoff, M.E., and Levy, R.J. (1992), *Modulated Drug Release Using Iontophoresis Through Heterogeneous Cation-Exchange Membranes: Membrane Preparation and Influence of Resin Cross-Linkage*, Macromolecules, **25**, 2531–40.

Siddiqui, O., Roberts, M.S., and Polack, A.E. (1985), *The Effect of Iontophoresis and Vehicle pH on the In-Vitro Permeation on Lignocaine Through Human Stratum Corneum*, J. Pharm. Pharmacol., **37**, 732–35.

Siddiqui, O., Sun, Y., Liu, J.C., and Chien, Y.W. (1987), *Facilitated Transdermal Transport of Insulin*, J. Pharm Sci., **76**, 341–45.

Stein, H.N. (1985), *Rheological Behaviour of Suspensions*, **5**, 3–48. In Encyclopedia of Fluid Mechanics (ed. Cheremisinoff, N.P.), Gulf. Pub. Co.

Takamura, K. (1982), *Microscopic Structure of Athabasca Oil Sand*, Can. J. Chem. Eng., **60**, 538–45.

Takamura, K. (1985), *Physico-Chemical Characterization of Athabasca Oil Sand and Its Significance to Bitumen Recovery*, AOSTRA J. Research, **2**, 1–10.

Takamura, K. and Chow, R.S. (1983), *A Mechanism for Initiation of Bitumen Displacement from Oil Sand*, J. Can. Pet. Tech., **22**, 1–9.

Takamura, K. and Chow, R.S. (1985), *The Electric Properties of the Bitumen/Water Interface. Part II. Application of the Ionizable Surface-Group Model*, Colloids and Surfaces, **15**, 35–48.

Takamura, K. and Isaacs, E.E. (1989), *Interfacial Properties in Technical Handbook on Oil Sands, Bitumens and Heavy Oils* (eds. Hepler, L.G. and Hsi, C.), AOSTRA Tech. Pub. Series #6, Edmonton, Alberta, Canada.

Takamura, K. and Wallace, D. (1987), *Experimental and Theoretical Studies of the Hot Water Processability of Different Grades of Athabasca Oil Sand. Flocculation in Biotechnology and Separation Systems* (ed. Attia, Y.A.), 579–97.

Takamura, K. and Wallace, D. (1988), *The Physical Chemistry of the Hot Water Process*, J. Can. Pet. Tech., **27**, 98–106.

Van Ham, N.J.M., Behie, L.A., and Svrcek, W.Y. (1983), *The Effect of Air Distribution on the Induced Air Flotation of Fine Oil in Water Emulsions*, Can. J. Chem. Eng., **61**, 541–47.

Watterson, I.G. and White, L.R. (1981), *Primary Electroviscous Effect in Suspensions of Charged Spherical Particles*, J. Chem. Soc. Faraday Trans. *II*, **77**, 1115–28.

Willey, S.J. and Macosko, C.W. (1978), *Steady Shear Rheological Behavior of PVC Plastisols*, J. Rheology, **22**, 525–45.

Yamamoto, T. and Yamamoto, Y. (1976), *Electrical Properties of the Epidermal Stratum Corneum*, Med. Biol. Eng. Comp., **14**, 151–58.

Yamamoto, Y. and Yamamoto, T. (1978), *Dispersion and Correlation of the Parameters for Skin Impedance*, Med. Biol. Eng. Comp., **16**, 592–94.

Yoon, R-H. and Yordan, J.L. (1986), *Zeta-Potential Measurements on Microbubbles Generated Using Various Surfactants*, J. Colloid Interface Sci., **113**, 430–38.

AUTHOR INDEX

A

Abramson, H.A., 156, 158, 161
Acrivos, A., 257, 301
Adamczyk, Z., 244, 257, 265, 270, 280, 288, 290, 301–2
Adams, G.E., 189–91, 194, 330, 343
Akagi, Y., 314–15, 344
Amidon, G.L., 344
Anderson, J.L., 121–22
Arp, P.A., 226, 239
Atkinson, G., 87, 97

B

Babchin, A.J., 121–23, 161–62, 193
Banga, A.K., 312, 342
Batchelor, G.K., 223, 239, 253, 302, 320, 342
Behie, L.A., 345
Bell, G.M., 61, 68
Berg, J.C., 156, 162
Bird, R.B., 3–4, 71–72, 74, 97, 254, 302
Blake, T.D., 328, 342
Bohm, E., 20
Boluk, M.Y., 257, 265, 302
Bonano, E.J., 162, 303
Booth, F., 132, 161, 167–68, 171
Bowen, B.D., 288–89, 291, 302
Brenner, H., 211, 239, 253, 259, 274, 302–3

C

Camp, F.W., 327, 342
Chan, B.K., 61, 68
Chan, D.Y.C., 48, 56, 61, 68–69, 189, 194
Chien, T.W., 312, 342–44
Chow, R.S., 331, 333–34, 342, 345
Clark, K.A., 327–28, 339, 342
Clift, R., 255, 302
Clint, G.E., 265, 288, 302
Clint, J.H., 302
Collins, G.L., 342
Corkill, J.M., 302
Cottrell, J.H., 329, 342
Cox, R.G., 223–24, 226, 239–40, 303
Cukor, P.M., 278, 281, 283–85, 304
Czarnecki, J., 301, 337, 342

D

Dabros, T., 257, 264–65, 270, 301–2

Datta, R., 156, 161

Davis, E.J., 132, 154–58, 160, 162, 303

deKruif, C.G., 320, 343

Derjaguin, B.V., 57–58, 60, 69, 140, 161, 182, 198, 211, 239

Dorn, E., 101, 165, 171

Duff, A., 250, 304

Dukhin, S.S., 140, 161

Dusseault, M.B., 328, 343

E

Eguiluz, M., 323–24, 343

Elton, G.A.H., 119, 122

Epstein, N., 123, 171, 255, 288–89, 291, 302, 304

Everett, D.H., 20, 69

Eyges, L., 21, 69

F

Feke, D.L., 198, 215, 229, 233–36, 239

Feynman, R.P., 21, 69

Fink, A., 20

Fitzpatrick, J.A., 259–60, 273, 277–78, 281–82, 291–94, 302–4

Fowkes, F.M., 176, 194

Frank, N.H., 21, 70

Friedlander, S.K., 199, 201, 204, 207–8, 240, 249, 303

Fuchs, N., 198, 209, 239

Fuerstenau, D.W., 69, 303, 343

G

Goddard, J.D., 257, 301

Goldman, A.J., 259, 276, 303

Goldsmith, H.L., 240

Goren, S.L., 259, 279, 303–4

Gorin, M.H., 141, 161

Grace, J.R., 302

Green, J.T., 223, 239

Gregory, J., 57, 69, 178, 194, 330, 337, 343

Griffin, F.O., 250, 303

Gur, Y., 121, 123, 156, 161–62, 192–93

Guzman-Garcia, A.G., 123

Guzy, C.J., 156, 162, 280, 294, 303

H

Hamaker, H.C., 7, 173–77, 180–82, 189, 192–94, 212, 217, 232, 235–36, 262, 283, 289, 298, 330–31, 337, 339

Happel, J., 154, 162, 253, 272, 274, 280, 291, 303, 343

Harris, R., 312, 343

Haydon, D.A., 48, 69

Healy, T.W., 69–70, 303, 334, 343

Henry, D.C., 132–34, 137, 139–142, 144–45, 148, 150–51, 154, 156, 158–60, 162

Hiemenz, P.C., 2, 4, 41, 43, 69, 176, 180, 186, 188, 194

Higashitani, K., 216, 229, 231, 240

Higuchi, W.I., 304

Hill, R.F., 123, 193

Hirtzel, C.S., 295, 303, 321, 343

Ho, N.F.H., 59, 66, 304

Hogg, R., 57, 60–61, 69, 262, 303, 337, 343

Honig, E.P., 198, 211–12, 240, 252, 303

Hosokawa, G., 240

Hough, D.B., 181, 194

Hull, M., 257, 287–88, 303

Hung, Y.T., 314, 343

Hunter, R.J., 36, 48, 52, 69, 142, 150, 158, 162, 168, 171, 174, 178, 191, 194

I

Isaacs, E.E., 336–37, 345

Israelachvili, J.N., 32, 69, 188–91, 194, 330, 343

J

Jacazio, A., 121, 123, 305, 307–9, 343

Jameson, G.J., 342

Jirgensons, B., 14–15, 20

K

Kao, S.W., 223, 240

Keizer, A., 142, 162–63

Kihira, K., 57, 61, 69, 236, 240, 291, 303

Kim, J.S., 223, 240, 265, 304

Kitchener, J.A., 178, 195, 257, 287–88, 303

Kogure M., 344

Koh, W.H., 121–22

Kotamarthi, V.R., 156, 161

Kozak, M.W., 132, 154–58, 160, 162

Krieger, I.M., 317, 319–20, 323–25, 343

Kuwabara, S., 154, 156, 162, 168, 294

L

Landau, L., 182, 198, 239

Lee, K.J., 240

Leighton, R.B., 69

Levesque, M., 288, 303

Levich, V.G., 255–56, 265–67, 287, 290, 303

Levine, S., 57, 61, 68–69, 103, 115, 119–20, 123, 151–52, 154, 156, 159–60, 162, 168–71, 302

Levy, R.J., 344

Li, J., 82, 84–85, 87, 96, 188, 194, 291–92, 343

Liang, W., 323, 325, 343

Lichtenbelt, J.W.Th., 215, 240

Lide, D.R., 84–85

Lifshitz, E.M., 173–74, 194, 331

Lightfoot, E.N., 4, 97, 302

Lin, C.J., 223, 240

Lin, M.M.J., 257, 265, 268, 304
Lips, A., 215, 240
Liu, J.C., 312–13, 343–44
Loeb, A.L., 46, 48, 69, 163
Luckham, P.F., 343
Lyklema, J., 191, 195

M

Macosko, C.W., 326, 345
Mahanty, J., 178–79, 194
Marriott, J.R., 123
Marshall, J.K., 257, 303
Masliyah, J.H., 121–23, 234, 241, 243, 247, 250, 255, 304, 314, 344
Mason, S.G., 198, 226–27, 229, 232, 239–41
Mathews, B.A., 215, 240
Matijevic, E., 16, 20, 61, 69, 240, 303
Matsuno, Y., 216, 240
McCartney, L.N., 57, 61, 68–69
Meisen, A., 250, 303
Meyerhoff, M.E., 344
Michael, D.M., 250–51, 304
Mifflin, R.T., 223, 240
Miller, N.P., 156, 162
Möller, J.H.M., 150–52, 160, 162
Morgenstern, N.R., 328, 343
Morrison, F.A., 142, 150, 162–63
Morrison, I.D., 56, 58, 70, 173–74, 176–77, 194
Mossop, G.D., 328–29, 343
Moyer, L.S., 161
Muller, V.M., 211, 239

N

Neale, G., 28, 64, 69, 123, 151–52, 154, 156, 159–60, 162, 165, 171, 247, 304
Newman, J.S., 74, 81–82, 87–88, 97
Ninham, B.W., 173, 178–79, 194
Norey, P.W., 250–51, 304
Nyffenegger, R., 16, 20

O

O'Brien, R.W., 132, 145–47, 155–56, 162–63
O'Neill, M.E., 259, 303
Ogawa, R., 240
Ohshima, H., 57, 61, 70
Okada, K., 314–17, 344
Overbeek, J. Th., 17, 20, 57, 61, 69–70, 132, 162–63, 182, 186, 194, 198, 241

P

Paddock, D., 304

Pal, R., 314, 344

Parsegian, V.A., 173, 181–82, 194

Pashley, R.M., 189, 191, 194

Pasternak, D.S., 327, 342

Pathmananoharan, C., 215, 240

Perram, J.W., 69

Philip, J.R., 119, 123

Pintauro, P.N., 73, 97, 121, 123, 156, 163

Polack, A.E., 344

Prieve, D.C., 257, 265–71, 304, 337, 344

Probstein, R.F, 1–2, 4, 18, 20, 34, 56, 70, 76–77, 97, 123, 125, 163, 184, 194, 204, 207, 221, 240, 280, 304, 309–11, 343–44

Q

Quellet, C., 20

R

Rajagopalan, R., 265, 303–4, 321, 343

Ravina, I., 121, 123, 161–62, 193

Reed, L.D., 150, 163

Renaud, P.C., 344

Rhodes, C.T., 215, 240

Rice, C.L., 103, 117, 119–20, 123

Richmond, P., 189, 193

Ricka, J., 20

Roberts, M.S., 344

Roeberson, G.J., 303

Ross, S., 56, 58, 70, 173–74, 176–77, 194

Ruckenstein, E., 121, 123, 265–71, 304, 337, 343

Russel, W.B., 1–2, 4, 8–9, 20, 27, 29, 31, 40, 42, 48–49, 56–57, 70, 73, 79, 97, 143–44, 163, 174, 181, 187, 189, 194, 215, 240, 321, 326, 343–44

Ryde, N., 69, 240, 303

S

Sands, M., 69

Sasidhar, V., 121, 123

Sather, N.F., 240

Saville, D.A., 4, 20, 70, 97, 163, 194, 240

Schenkel, J.M., 178, 195

Schowalter, W.R, 4, 20, 70, 97, 163, 194, 198, 207, 215, 225, 229, 232–36, 239–41

Schramm, L.L., 339, 344

Schwendeman, S.P., 314, 344

Sengupta, M., 168, 171

Shaw, D.J., 61–63, 70, 99, 101, 112, 123, 132–33, 163, 184–85, 187–88, 195

Shi, W.-M., 343

Siddiqui, O., 312, 343–44

Siwek, B., 301–2

Slater, J.C., 21, 70

Smith, R.G., 337, 339, 342, 344

Smoluchowski, M. von, 132, 141, 150, 154–56, 158, 167–69, 171, 198, 203, 206, 211, 216, 219, 221–22, 226, 231–32, 237, 240, 321

Sonin, A.A., 123, 343

Sparnaay, M.J., 48, 57, 70

Spielman, L.A., 197–98, 211, 240, 247, 259–60, 273, 277–79, 281–85, 291–94, 303–4

Stein, H.N., 321, 344

Stern, O., 36, 61–63, 68, 70, 291

Stewart, W.E., 4, 97, 302

Stöber, W., 16, 20

Stone, J.A., 344

Straumanis, M.E., 14–15, 20

Sun Y., 343–44

Suzuki, A., 262, 304

Svrcek, W.Y., 345

T

Tabor, D., 189, 194–95

Tadros, The. F., 20, 343

Takamura, K., 48, 52, 70, 229–30, 241, 327–28, 330–39, 342, 345

Taylor, T., 257, 301

Tien, C., 292, 294–95, 304

V

Vaidyanathan, R., 292, 294, 304

van Blaaderen, A., 16, 20

van de Ven, T.G.M., 56, 58–59, 70, 198, 200–1, 211–12, 226–27, 229, 232, 240–41, 243, 252–53, 257, 264–65, 270, 280, 288, 290, 301–2, 304

Van der Drift, W.P.J.T., 142, 156, 162–63

van der Hoeven, P.H.C., 192, 195

Van Ham, N.J.M., 314, 345

van Iersel, E.M.F., 343

Van Os, G.A.J., 162

Verbrugge, M.W., 73, 97, 121, 123, 156, 163, 193

Verwey, E.J.W., 198, 241

Vrij, A., 16, 20

W

Walbridge, D.J., 12–13, 17, 20

Walker, T., 302

Wallace, D., 48, 52, 70, 334, 336–38, 342, 345

Warszynski, P., 302

Watterson, I.G., 321–22, 345

Weber, M.E., 247, 302, 304

Weiss, G.H., 181, 194

White, L.R., 16, 61, 69–70, 132, 145–47, 155–56, 163, 181, 190, 194, 321–22, 334, 343, 345

Whitehead, R., 103, 117, 119–20, 123

Wiersema, P.H., 69, 132, 163, 240, 303

Willey, S.J., 323, 326, 345
Willis, W.E., 215, 240
Winterton, R.M., 189, 195
Wooding, R.A., 119, 123

X

Xu, Z., 191, 195

Y

Yamamoto, T., 313, 345
Yamamoto, Y., 313, 345
Yan, Y., 234, 241
Yoon, R.-H., 191, 195, 314, 345
Yordan, J.L., 314, 345
Yoshioka, N., 344
Yung, E., 121, 343

Z

Zeichner, G.R., 198, 207, 225, 232–36, 241
Zembala, M., 301–2
Zia, I.Y.Z., 239

SUBJECT INDEX

A

adsorption, 35

aerosols, 197

agglomeration, *see* coagulation

arbitrary electrolyte, 64

associated colloids, 6

attraction potential, 175

Avogadro number, 2, 44, 65

B

biocolloids, 7

bitumen, 52, 234, 327–39

- displacement, 28
- dissociation constant, 333–35
- extraction, 327
- Hamaker constant 330–31
- interaction potential, 338
- recovery, 337
- surface ionization models, 333–35
- zeta potential, 336

blood glucose, 313–14

Boltzmann constant, 2

Boltzmann distribution, 33, 79–80

Boltzmann equilibrium, 33, 306

bond number, 12

Brownian

- coagulation, 203–9, 211, 213, 240
- diffusion, 204, 319, 326
- effect on viscosity, 316–19
- flocculation, 216
- force, 5, 7–9
- motion, 36, 198–203, 205–6, 211, 216, 226, 243, 277, 319, 342
- particles, 265

C

capacitance, 31

capture efficiency, 243, 278–83, 285–86

capture interception efficiency, 246–47

capture inertial efficiency, 251

cell model, 151–52, 156–59, 168, 247

cell models, 151, 156–57

- Happel, 154
- Kuwabara, 154, 156–57

characteristic time

- Brownian, 207
- shear, 223

charge

- capacity, 31
- conservation, 81, 88

    density 21, 37–38, 74, 105
    origin, 34, 48, 52
    point, 22, 26
chemical potential, 49, 88
Clark hot water process, 327–28
coagulation
    Brownian, 203–9, 216–19
    field force, 209–19, 223
    hydrodynamic, 223
    population balance, 203, 216, 222
    shear, 219–24, 232–35
cohesion work, 175–76
coions, 35, 62, 88
collectors, 243–44
collision frequency, 202
colloids
    association, 6
    biocolloids, 7
    classification, 6
    coagulation, 197
    deposition, 243
    disperse systems, 6
    macromolecular, 6
    multiple, 7
    preparation, 14
    purification, 17
    stability, 12
conductivity, 82–85, 91
    equivalent, 84
    molar, 82
conductors, 28
connate water, 327–29, 331–32
conservation of
    charge, 88
    current, 81, 88–89
    ionic mass, 76–79, 81, 89, 91, 252
    mass, 71, 89
    momentum, 71, 73, 89, 92–94
convection-diffusion equation, 72, 198, 243–45, 252
convection-diffusion-migration equation, 74–79, 252
counterions, 35, 186–88, 322, 333
creeping flow, 74, 89, 136, 153, 223, 240, 245–47, 257, 303
critical flocculation concentration, 186
cross product, 25
curl, 25
current density, 81, 89, 91
current flow, 100, 114, 117

D

Debye–Hückel approximation, 40, 64, 105, 126, 132–33
Debye length, 40, 43–44, 61, 64, 106, 125–26, 305–8, 318, 322–24, 332
deposition
    Brownian, 245, 253–71
    cell model, 294
    efficiency, 285

- Eulerian approach, 252–71
- experimental, 286–95
- geometries, 244, 265
- inertial, 249
- interception, 245
- Lagrangian approach, 271–85
- on cylinders, 279, 281
- on spheres, 267–69, 271–81, 283–85
- packed bed, 247–48, 272, 286, 292–95
- parallel plates, 288–91
- rotating disc, 287, 290
- stagnation flow, 257–66, 270, 286–87

Derjaguin approximation, 57–58, 60

diabetic, 313

dialysis, 17–8

dielectric constant, 30–32, 73, 191, 232

dielectric material, 28, 30, 191

diffuse double-layer, 35, 37, 45, 62–63

diffusion boundary layer, 255, 257, 266–69

diffusion coefficient, 77–78, 201, 211–15, 245, 252–53, 318

dimensionless groups in
- coagulation, 217–19
- electrophoresis, 143
- flux equation, 263–65, 295–96
- rheology, 317–18
- trajectory, 218–19, 297

dipoles, 29

disjoining pressure, 328, 330–31

dispersion forces, 173
- between flat plates, 179, 183
- between spheres, 178–79, 183, 227
- retarded potential, 178, 262, 330, 337
- between various geometrics, 178

dispersions, 6

dissociation constant, 50, 334–36

DLVO theory
- stabilization, 182–85, 191
- verification, 189–91, 286

Dorn effect, 101, 165

double-layer overlap, 56

double-layer thickness, *see* Debye length

drug delivery, 312

E

electric
- capacitance, 1, 31
- charge density, 21, 74
- conductance, 1
- conductivity, 82–85, 115, 117, 166
- double-layer, 35, 37, 45, 125–26
- force, 23, 73, 77–78, 138, 148–50, 165–66, 189–90, 261, 328–32
- neutrality, 36, 42, 64, 82, 88
- potential, 25, 30–1, 35–42, 45–9, 104, 126, 305–10
- potential difference, 1

- resistance, 1
- strength, 21, 27
- surface charge, 1, 21, 34–35

electric double-layer
- definition, 40, 64
- flat plates, 37
- spheres, 45

electrodialysis, 17–18

electrokinetic phenomenon, 99

electroosmosis, 99–100
- axial velocity, 108
- current flow, 114, 117
- electroviscous effect, 117
- flow, 109–10
- governing equations, 104–7
- high surface potential, 119
- Onsager principle, 117
- potential, 104
- pressure, 110, 117
- sinusoidal capillary, 121
- stationary surface, 113

electrophoresis, 100, 125
- boundary conditions, 142
- cylinders, 140–42
- dimensionless groups, 143
- Helmholtz–Smoluchowski, 130, 132
- Henry analysis, 133–40
- high surface potential, 145
- Hückel equation, 129
- improved solutions, 132, 145
- mobility, 129, 145–47, 150, 154
- particle concentration, 150–56
- particle conductivity, 140
- particle shape, 140
- relaxation effects, 132
- retardation, 132
- Smoluchowski equation, 132
- spheres, 140–42
- surface conductance, 132–33

electrophoretic mobility, 129, 154

electrostatic repulsion
- between charged plates, 52–57
- between charged spheres, 57
- Derjaguin approximation, 57
- HHF equation, 61
- potential, 60

electrostatic stabilization, 12, *see also* stabilization

electroviscous effects, 117, 321

elementary charge, 2

emulsions, 6–7, 14–15, 17, 234, 241, 304, 344–45

Eulerian approach, 243, 252–71

F

Faraday constant, 2, 65

filter coefficient, 249, 291–95

flocculation, 197–98, *see also* coagulation

flotation, 272, 314, 316, 327

flow
  capillary, 103
  impinging jet, 266
  packed bed flow, 247–48, 272, 286, 292–95
  parallel plates, 288–91
  rotating disc, 262, 266
  stagnation, 257, 262
force, 1, 5, 9
Fowkes equation, 176
free charge density, 37–38, 105
friction coefficient, 200

G

gas constant, 2, 65
Gaussian distribution, 199
Gibbs free energy, 14, 174
gold sols, 16
Gouy–Chapman model, 36, 64
  for flat plates, 37
  for spheres, 45
groundwater, 309

H

HHF equation, 61
Hamaker constant, 175–79
  effect of intervening medium, 180–82
  effective, 181–82
  various materials, 177
Hamaker model, 173
hard sphere model, 319, 325
hazardous wastes, 309
Helmholtz model, 36
Helmholtz–Smoluchowski equation, 109, 130, 132, 139
Henry
  function, 139, 140–41
  solution, 133–140
heterocoagulation, 57, 69, 240, 303, 344
hydronium ions, 50, 235
hydrosol, 197
hindered settling, 159
Hückel equation, 129, 158
hydration forces, 189, 191–92
hydrophobic forces, 191
hyperfiltration, *see* salt rejection

I

impinging jet, 257, 270
impurities, 17
inertial efficiency, 251
interception efficiency, 246–47
intrinsic viscosity, 320
inverse Debye length, 40, 43, 64, *see* also Debye length
ion exchange, 18
ion size, 188
ionic flux equation, 90
ionic strength
  effect on Debye length, 45, 64

  effect on stability, 13, 186–88, 191–92
  rheology, 323–24
  Schulze–Hardy rule, 186–88
iontophoretic delivery, 312–13
irrotational flow, 25

K

Krieger equation, 325

L

Lagrangian approach, 271–85
Langevin equation, 200
Laplace equation, 31
Levich equation, 265, 267, 287, 290
Lifshitz theory, 173
limiting streamline, 246
limiting trajectory, 245
London–van der Waals forces, 173, *see also* dispersion forces
London wavelength, 175

M

macromolecular colloids, 7
mass conservation, 71, 89
mass density, 75
mass fraction, 76
Maxwell equation, 21
  in a dielectric, 29
  in a vacuum, 21
membranes, 17–18, 305
mica surface, 191
mobility, 78–9, 145–47, 154
molar concentration, 65–66
molecular weight, 17
momentum equation, 53, 72–74, 89, 92–94
multiple colloids, 7

N

Navier–Stokes equation, 89, 107, 130
Nernst–Einstein equation, 78, 90
Nernst–Planck equation, 90
Newtonian fluid, 317
number concentration, 65–66, 202–4, 247–49, 253

O

Ohm Law, 82
oil sands, 327–39
Onsager principle, 117
orthokinetic flocculation, 197
osmotic pressure, 53–54

P

packed bed, 291–94
parallel plates, 288–90
particle
  coagulation, 197
  deposition, 243
  size, 8–12

 trajectory, 223–26
Peclet number, 218, 266, 290
perikinetic flocculation, 197
permeable membrane, 17
permittivity of vacuum, 2
pH, 34–5, 52, 191, 233, 317, 323, 327, 331, 333, 335–38, 344
physical constants, 1–3
Planck's constant, 2
point charge, 22–3
point of zero charge, 34
Poiseuille flow, 109
Poisson equation, 37, 52, 90, 104, 306
Poisson–Boltzmann equation, 39, 45, 64
polarization, 17, 28–29, 313
polarization dipole, 29, 67
polymer dispersions, 17
polymeric stabilization, 13
polymerization
 dispersion, 17
 emulsion, 17
 suspension, 17
potential determining ions, 49
potential energy curves, 182, 183–85
potential flow, 251
preparation of colloids
 condensation, 15
 dispersion, 14
pressure, 1
primary maximum, 184, 282

R

rapid coagulation, 197, 215
reduced shear, 318
relative viscosity, 318–20
retardation, 178, 185
reverse osmosis, 305
Reynolds number, 266
rheology, 316
rotating disc, 257, 286–88

S

salt rejection, 305–9
scale analysis, 9
Schmidt number, 245, 256–57
Schulze–Hardy rule, 186–88
secondary minimum, 185, 281
sedimentation
 effect on concentration, 168
 effect on deposition, 291–93
 potential, 101, 165
settling, 157
shear
 flow, 220, 223, 226, 234–35
 plane, 63
 rate, 317
Sherwood number, 235, 256, 265–66, 285
skin, 312
slow coagulation, 198

Smoluchowski equation in
  Brownian, 203, 211
  electroosmosis, 108
  electrophoresis, 132, 150
  electroviscous effect, 321
  sedimentation, 167
  shear, 219, 222
sols
  ferric hydroxide, 17
  gold, 16
  silver bromide, 16
  sulphur, 16
speed of light, 2, 178
stability diagram, 184, 233–35
stability ratio, 211, 214–15
stabilization
  DLVO theory, 182
  electrostatic, 12, 182
  non-aqueous, 13, 17, 192
  Schulze–Hardy rule, 186–88
  steric, 12, 197
stagnation flow, 257, 270
steric stabilization, 13
Stern
  plane, 61
  potential, 61
Stokes
  expression, 200
  number, 250
  terminal velocity, 269
Stokes–Einstein equation, 90, 201
stratum corneum, 312–14
stream function, 246, 251, 278
streaming potential, 100, 117
surface
  area, 10
  charge density, 21, 51, 56
  ionization, 34–35
  ionization models, 48, 333
  potential, 25, 54, 61, 63
  tension, 9, 11, 175–76, 219
surfactant, 35, 339
susceptibility, 30
symmetrical electrolyte, 64

T

trajectory equations, 225, 228

U

ultrafiltration, 17
universal hydrodynamic functions, 260

V

valence, 38–9, 145, 187–88
van der Waals forces, 173, *see also* dispersion forces
van't Hoff law, 54
vector operators, 3
verification, 189, 286

velocity
    mass average, 74
    molar average, 75
viscosity, *see* rheology

Z

zeta potential, 61
zeta potential of bubbles, 317

3 3286 50426 3670

COVER PHOTOGRAPH PROVIDED BY MR. SEAN SANDERS, DEPARTMENT OF CHEMICAL ENGINEERING, UNIVERSITY OF ALBERTA. IT SHOWS DEPOSITION OF COLLOIDAL BITUMEN DROPLETS ON A FLAT SURFACE.

PRINTED IN CANADA